



**SUPERCONDUCTOR
TECHNOLOGIES**

AD-A248 159



(2)

THE PROCESSING OF HIGH TEMPERATURE CERAMIC SUPERCONDUCTING DEVICES

Contract No.: N00014-88-C-0713

Principal Investigator: Dr. James H. Long, Jr.

ARPA Order No.: 06268

Contract Dates: 9-1-88 to 12-31-91

**DTIC
ELECTE
APR 01 1992
S D D**

FINAL REPORT

Volume 2

January 31, 1992

Submitted by Program Manager

James H. Long, Jr.

This document has been approved
for public release and sale; its
distribution is unlimited.

SUPERCONDUCTOR TECHNOLOGIES INC.

460 WARD DRIVE, SUITE F

SANTA BARBARA, CA 93111-2310

Phone (805) 683-7646

Fax (805) 683-8527

92 3 25 067

92-07621



THE VIEWS AND CONCLUSIONS CONTAINED IN THIS DOCUMENT ARE THOSE OF THE AUTHORS AND SHOULD NOT BE INTERPRETED AS NECESSARILY REPRESENTING THE OFFICIAL POLICIES, EITHER EXPRESSED OR IMPLIED, OF THE DEFENSE ADVANCED RESEARCH PROJECTS AGENCY OR THE U.S. GOVERNMENT.

**460 WARD DRIVE, SUITE F, SANTA BARBARA, CALIFORNIA 93111-2310
TELEPHONE (805) 683-7646 FAX (805) 683-8527**

BEI MOTION SYSTEMS COMPANY

STATUS REPORT FOR
LINEAR ACTUATOR PROTOTYPE

10 July 1989

Contract No.: N00014-88-C-0713-S-BEI-1

Contractor: BEI Motion Systems Company
2111 Palomar Airport Road Suite 250
Carlsbad, CA 92009

Principle Investigator: Mr. Jack Kimble
(619) 744-5671

REPORTING PERIOD ENDING JUNE 1989

Statement A per telecon
Dr. Wallace Smith
ONR/Code 1132
Arlington, VA 22217-5000
NWW 3/31/92

Accession For	
NTIS CRA&I	<input checked="checked" type="checkbox"/>
DTIC TAB	<input type="checkbox"/>
Unannounced	<input type="checkbox"/>
Justification	
By _____	
Distribution/	
Availability Codes	
Dist	Availability of Special
A-1	

I. PROGRAM SUMMARY

BEI Motion Systems Company has contracted to work with STI to design and specify planar coil suitable for linear actuator. If films are made with sufficient current densities, BEI will design a linear actuator or brushless DC motor system to incorporate planar coil.

II. PROGRAM STATUS

BEI has completed the preliminary evaluation on the planar coil and conductor requirements for the brushless DC motor. Results indicate that current density is adequate, however, there is not enough cross section of the conductor using the thin film approach. Preliminary design was based on two planar coils attached on each side of a central chill plate filled with liquid nitrogen. Evaluation was further performed on the output anticipated in thick film substrates 100 times thicker than the 1 micron thin film. Estimates with thick film substrates yielded .168 watts output which is still inefficient for DC brushless motor design. Thick film designs appear to be the correct approach to achieve a high conductor cross section enabling sufficient power levels to drive the actuator or motor. BEI evaluation has included detailed review and analyses of the following key areas: STI achievement of 10^5 amps per square centimeter of output in thin films; planar coil actuator design requirements including number of conductors and substrate size; and anticipated power output.

III. ACCOMPLISHMENTS

Progress was made with the contracted work statement. However, there were no firm accomplishments as thick films are not available for design consideration.

IV. PROBLEM AREAS

None experienced. A heightened level of attention needs to be given on thick film approaches to ensure continued progress.

V. CORRECTIVE ACTION

None.

VI. GOALS FOR NEXT REPORTING PERIOD

Continue low level research activity in accordance with approved funding levels for the planar coil design.

VII. FUNDING STATUS

a) Expended: \$11,547.56

THE PROCESSING OF HIGH TEMPERATURE CERAMIC SUPERCONDUCTING DEVICES

Contract No.: N00014-88-C-0713

Principal Investigator: Dr. James H. Long, Jr.

ARPA Order No.: 06268

Contract Dates: 9-1-88 to 12-31-91

FINAL REPORT

Volume 2

January 31, 1992

Submitted by Program Manager

James H. Long, Jr.

SUPERCONDUCTOR TECHNOLOGIES INC.

460 WARD DRIVE, SUITE F

SANTA BARBARA, CA 93111-2310

Phone (805) 683-7646

Fax (805) 683-8527

THE VIEWS AND CONCLUSIONS CONTAINED IN THIS DOCUMENT ARE THOSE OF THE AUTHORS AND SHOULD NOT BE INTERPRETED AS NECESSARILY REPRESENTING THE OFFICIAL POLICIES, EITHER EXPRESSED OR IMPLIED, OF THE DEFENSE ADVANCED RESEARCH PROJECTS AGENCY OR THE U.S. GOVERNMENT.



Superconducting Oscillator and Package Development

**Final Technical Report for
Contract No.: N00014-88-C-0713-S-AVT 1**

September 1991

Principal Investigator: A.P.S. Khanna

R & D STATUS REPORT

DARPA ORDER NO.:

PROGRAM CODE NO.:

CONTRACTOR : Avantek Inc.

CONTRACT NO. : N00014-88-C-0713-S-AVT-1

EFFECTIVE DATE OF CONTRACT: September 1, 1990

EXPIRATION DATE OF CONTRACT: August 31, 1991

PRINCIPAL INVESTIGATOR: Amarpal Khanna

TELEPHONE NO.: 408 943.4226

SHORT TITLE OF WORK: Superconductor Oscillator and Package
Investigation and Development

REPORTING PERIOD: JULY 1991 TO SEPTEMBER 91

o DESCRIPTION OF PROGRESS :

Attached Herewith

SUPERCONDUCTING OSCILLATOR (SCO) AND PACKAGE
INVESTIGATION AND DEVELOPMENT

R&D STATUS REPORT FOR THE PERIOD OF JULY 1991 TO SEPTEMBER 1991

DESCRIPTION OF PROGRESS:

Package Development:

Ten each of aluminum cases model SCP-1000 and stainless steel cases model SCP-2000 were assembled with RF feedthrus and 50 ohm thru line on alumina between the input and output ports. The thin film circuits were fabricated in Avantek. The internal dimensions of the aluminum package will accommodate a 1 cm square substrate and the SST package would accommodate a 1/4 by 1 in long substrate. The substrates are held in place with BeCu clamps and O-80 SST screws. The clamping arrangement is used to allow for mismatches in coefficient of expansion between the substrate and the metal packages. Standard SMA connectors are used with RF feedthrus soldered into place. RF connections to the substrate are accomplished with a gold ribbon wedge bonded to a contact pin. The contact pin engages the centerpin of the RF feedthru center conductor and exerts a constant loading to the center pin. This design technique precludes the need for any soldered connections inside the package. The lid is laser welded into place.

Experimental Method:

The ten cases of each type were welded and leak tested. Electrical measurements of S11 and S21 were then carried out using the network analyzer. The packages are mounted on a 1/4 inch aluminum or SST base plate. The packages are placed in an insulated box and liquid nitrogen poured into the box. Steady state temperature at 77 deg K is reached when gaseous nitrogen is no longer observed bubbling from the surface of the packages. It typically takes about 20 minutes to reach this condition. Temperature cycling of these cases from room to 77 deg K was carried out. A total of 75 cycles were completed in steps of 5, 5, 10, 30 and 25. The packages were tested for leakage as well as Rf (S11 and S21) performance at the end of each step. The results of the testing are summarized below. Detail data of the RF testing and leak testing at the end of 5, 10, 20, 50 and 75 cycles is attached as appendix 1. Copies of the documentation on the two cases SCP-1000 and SCP-2000 is enclosed as appendix 2.

# of Cycles	Number of units passed test			
	Stainless Steel RF	Steel Leak	Aluminum RF	Leak
Start	10	10	10	10
5	10	9	10	10
10	10	9	9	10
20	10	8	9	10
50	10	8	9	10
75	10	8	8	10

Out of 10 SST packages S/N 10 and S/N 7 failed fine leak test after 5 & 10 temperature tests respectively. All other parts passed the leak test up to 75 cycles. All SST packages passed the RF performance test up to 75 cycles. Final examination indicates the possibility of leak test failure due to poor soldering at RF feedthru.

Out of 10 aluminum packages S/N 002 and S/N 003 failed the RF performance test after 10 and 75 cycles respectively. All the packages passed the leak test up to 75 cycles. The units were cut open after the completion of the tests and the gold ribbons were found broken. The failure appears to be due to insufficient stress relief.

Superconductor Oscillator Design:

Investigations continued, on developing low phase noise oscillator using superconductor resonator. Main effort during this phase of development was on developing a series feedback integrated oscillator. Some experiments were conducted to conclude the parallel feedback investigation.

Parallel Feedback Superconductor Oscillator Design:

A bipolar amplifier was redesigned at 10 GHz using commercially available Si-Bipolar device NEC647. This device can provide a transmission gain of better than 6dB under matched conditions. The second prototype built provided >4dB of gain and was used as front end amplifier to the GaAs FET multistage amplifier. The phase noise using this amplifier was still about -100dBc/Hz at 10KHz from the carrier. Phase noise of better than -100dBc could not be achieved using the parallel feedback approach, it was decided to continue efforts on the series feedback integrated superconductor oscillator.

Series Feedback Integrated Superconductor oscillator:

The series feedback approach (figure 1) is a more commonly used configuration for designing oscillators and can be easily integrated with the superconductor resonator in the same compact package. The DC power required to generate 5 dBm at 10GHz is expected to be less than 50mw (3V,15ma). The resonator is a high Q notch filter at the desired oscillation frequency. The oscillation condition ($S_{11}' \times T_1 = 1$) is satisfied by choosing proper coupling of the resonator and the distance between the resonator and the transistor.

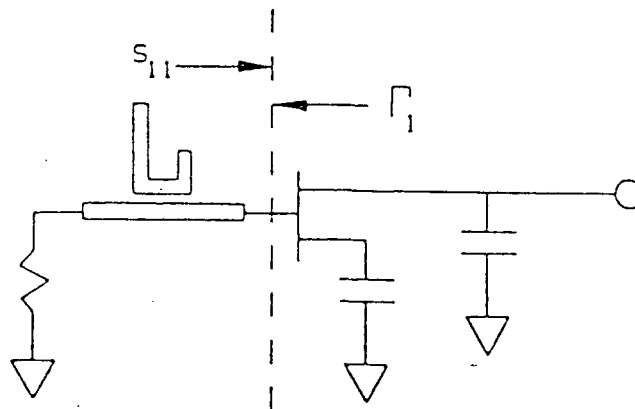


Fig.1 Series Feedback Superconductor Oscillator

CH1: A -M S + 4.06 dB
2.0 dB/ REF - .00 dB

CH1: A -M S + 4.06 dB
2.0 dB/ REF - .00 dB

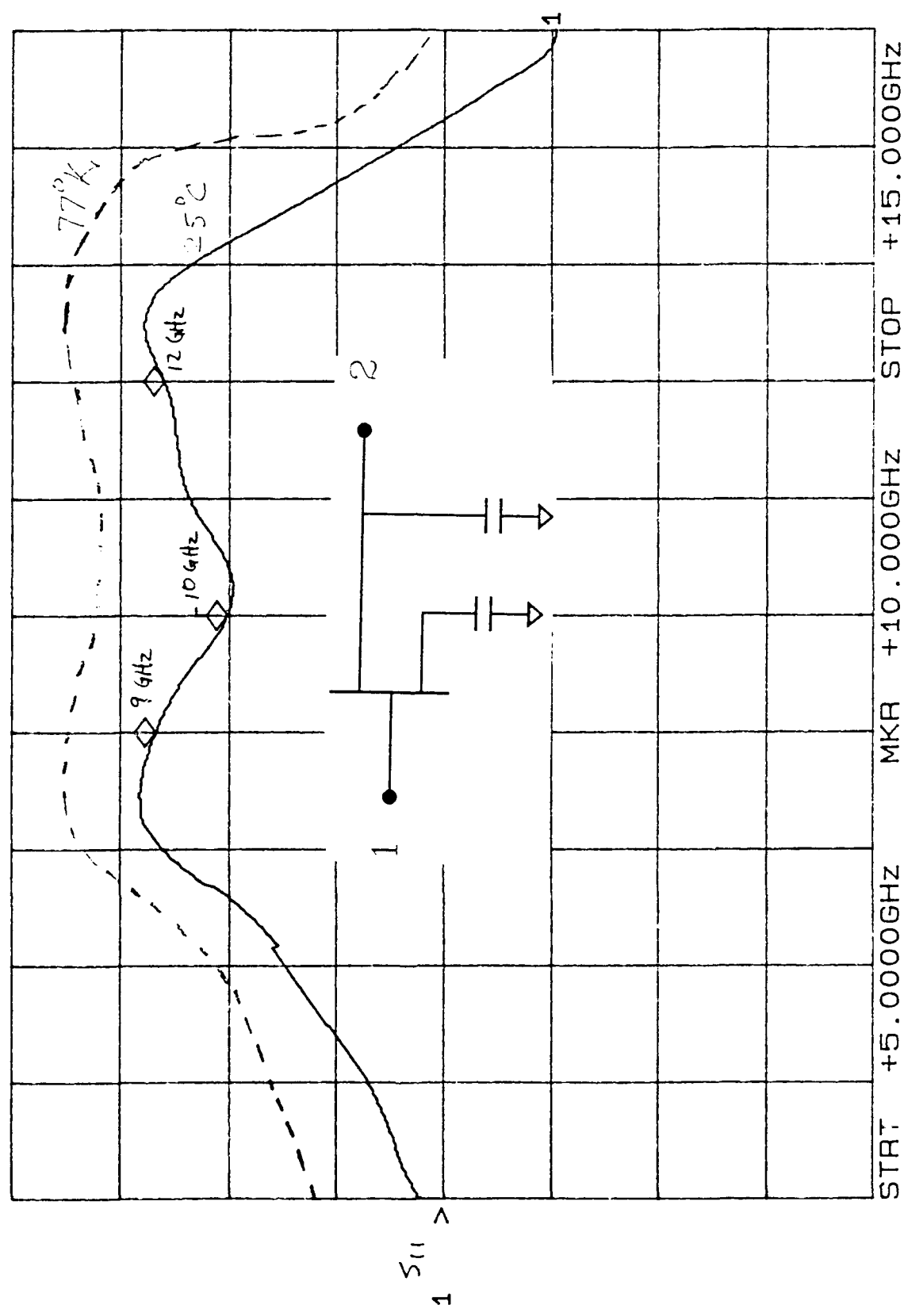


Fig.2 Negative Resistance of the active device at room and 77 deg K

CH2: B₀ - M + .15 dB
 1.0 dB/ REF - 15.13 dB

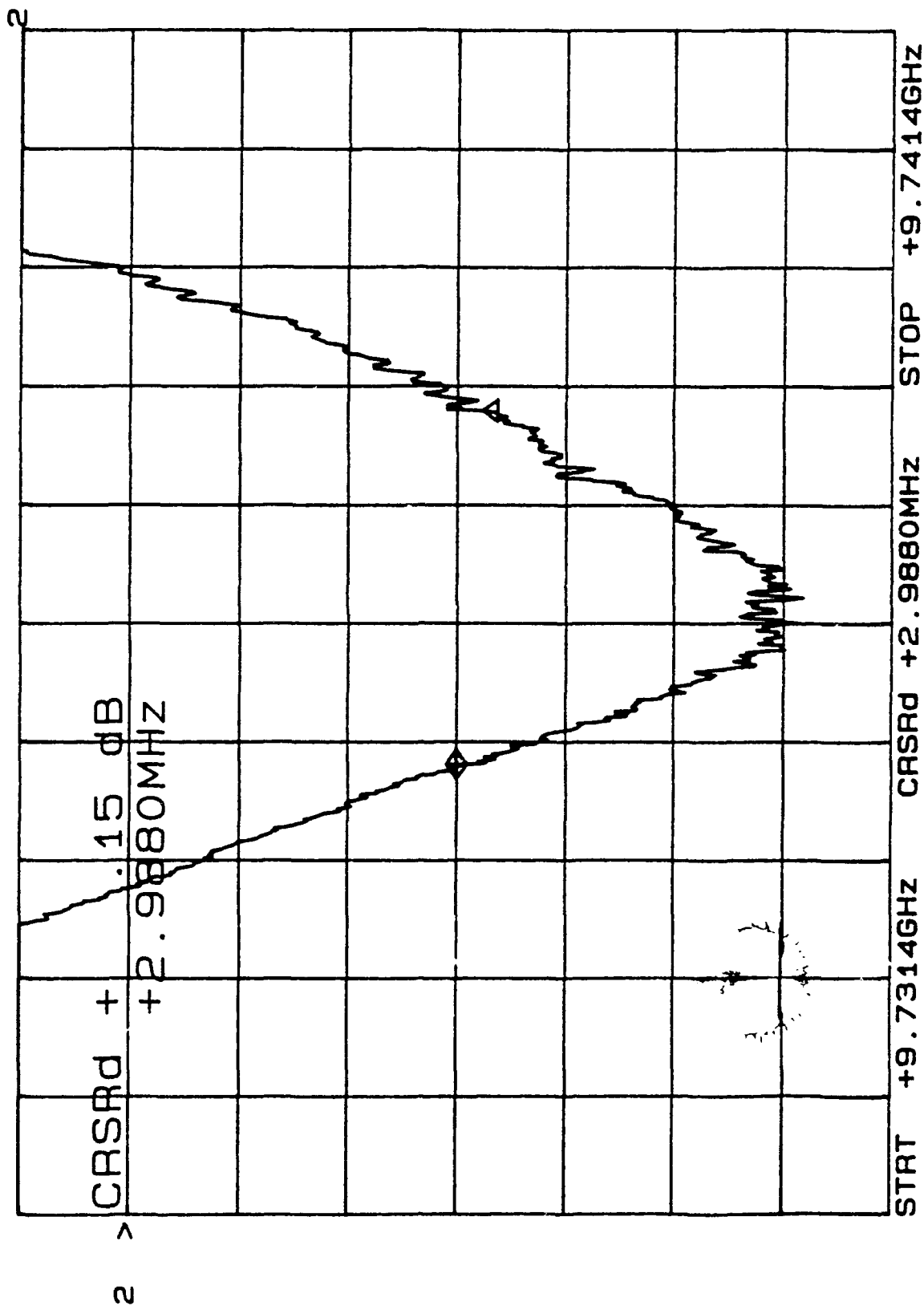


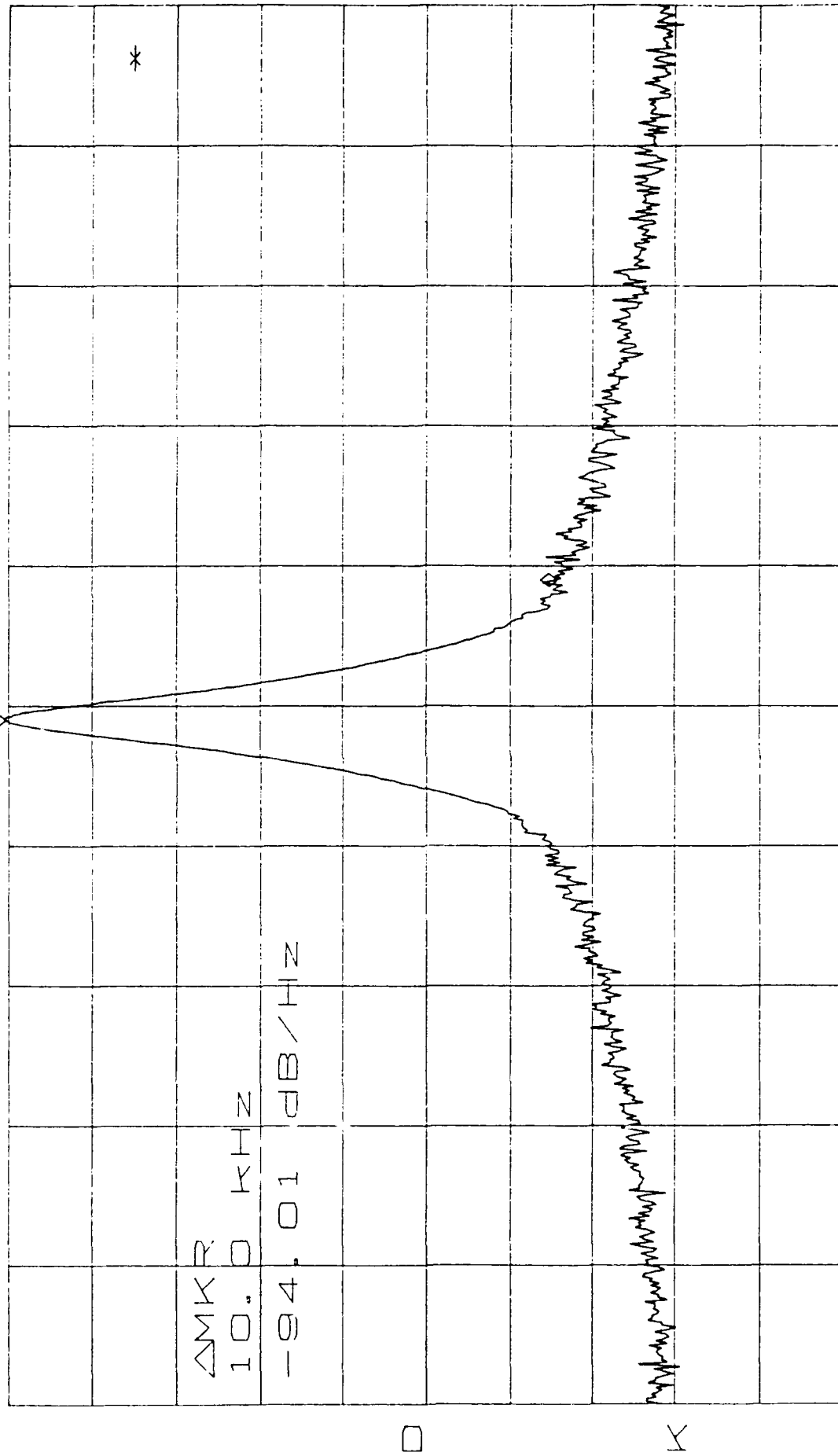
Fig.3 Superconductor Resonator Response at 77 deg K

ATTEN 20dB

RL 7.0dBm

$\Delta MKR -94.01 \text{ dB/Hz}$

10.0KHz



CENTER 9.74539056GHz SPAN 100.0KHz
RBW 1.0KHz *VBW 30Hz

Fig.4 Phase Noise of the series feedback Superconductor Oscillator

Generation of negative resistance:

In order to satisfy the oscillation condition ($S_{11}' \times T_1 > 1$) the reflection coefficient S_{11}' (figure 1) needs to be greater than $1/T_1$. Distributed capacitive feedback at the device source is used to generate the negative resistance ($S_{11}' > 1$) in the device. The device used is Avantek M125 GaAs FET. A linear CAD program was used to design the active circuit. Figure 2 shows the active device negative resistance at room and cold temperature. The S_{11}' increased by about 2dB from room to cold. The value of S_{11}' at cold should be one to two db greater than the T_1 of the resonator. Two negative resistance substrates are enclosed as part of the final report. These substrates can be used to build superconductor oscillators between 9 and 11 GHz.

High Q Superconductor Reflection Filter:

The superconductor reflection (notch) filter was designed and fabricated at STI. The resonator was tested for reflection coefficient and Q factor at 77 deg K. Typical resonance response is shown in figure 3. The $T_1 = -3$ dB and unloaded Quality factor of 3500 was measured at 9.7 GHz.

Series Feedback Superconductor Oscillator:

The superconductor resonator and the active negative resistance circuit were connected through a predetermined length of coaxial cable. The superconductor resonator was packaged in the standard STI package with SMA connectors. Active negative R circuit was assembled in an Avantek standard DSO case with 50 ohm lines connected to extend the circuit to the input and output connectors. The length at the input was adjusted to provide the necessary phase shift between the device and the resonator to satisfy the oscillation condition. Fig. 4 shows the phase noise of the series feedback oscillator at 9.7 GHz. Performance of this oscillator is shown in table II:

Table II

Frequency: 9.7 GHz
Power: 5 dBm
Pulling: .2 MHz @ 12 dB
Pushing: .1 MHz/V
Phase Noise: -95 dBc/Hz @ 10KHz
Bias: 5V, 20 mA

The oscillator discussed above provided important data that a reflection feedback oscillator can be successfully built. Reproducing the above design is difficult because the resonator and filter are in separate packages. The only packaged high Q notch filter available, stopped normal functioning and it was decided to continue work on an integrated oscillator by using the same package to accommodate active circuit as well as the superconductor resonator.

M125L

0.5 mA / 10 V

CH1

27073114

400

11/12/91

Power = 5 dBm

CTR 9.4772 GHz

SPAN 10 kHz/

RES BW 1 kHz

VF .1

REF -1 dBm

10 dB/

ATTEN 20 dB

SWP

AUTO

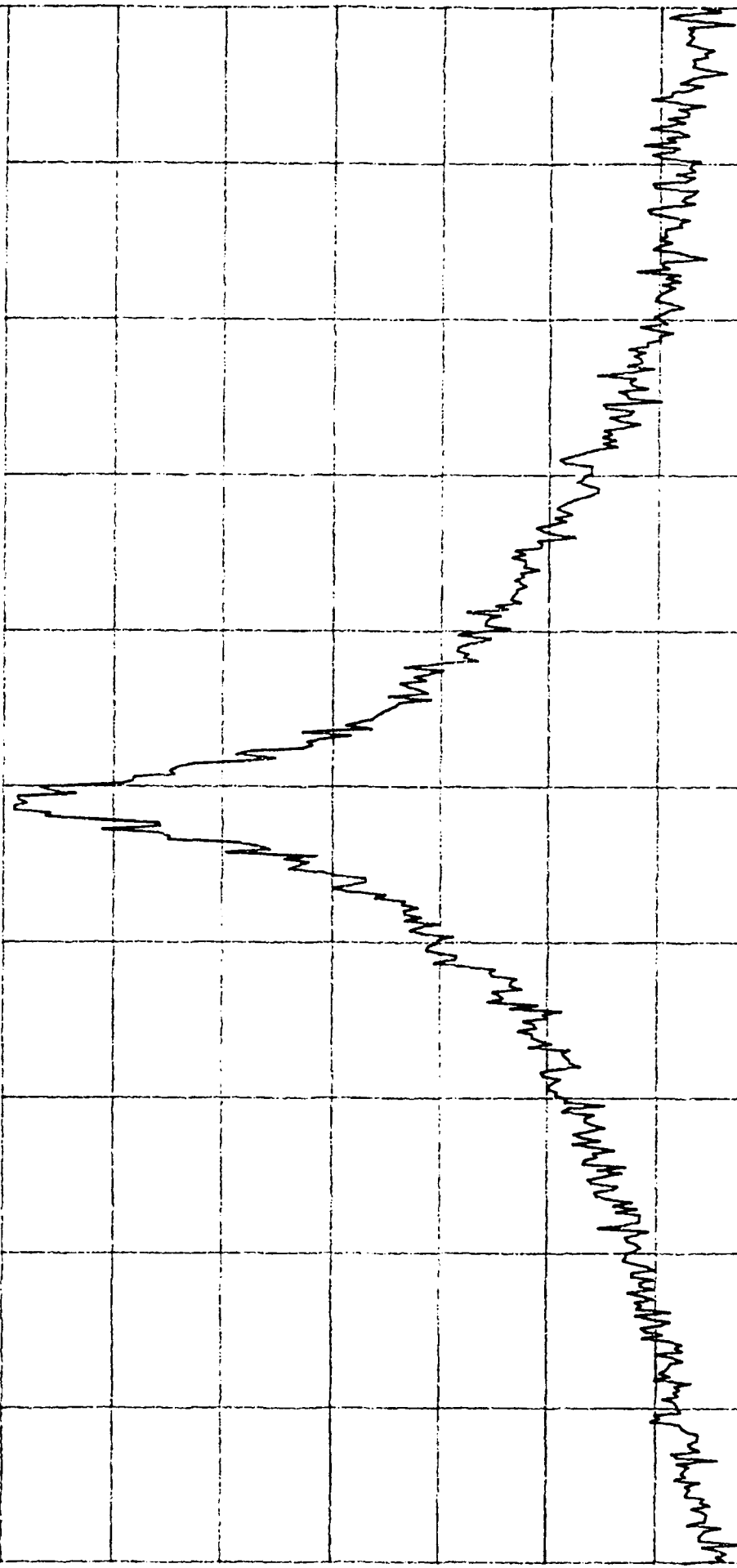


Fig.5 Phase Noise of Integrated Superconductor Oscillator. Scale: 10kHz/div

CTR 9.4759 GHz SPAN 20 kHz/ RES BW 1 kHz VF .1
REF -2 dBm 10 dB/ ATTN 20 dB SWP AUTO

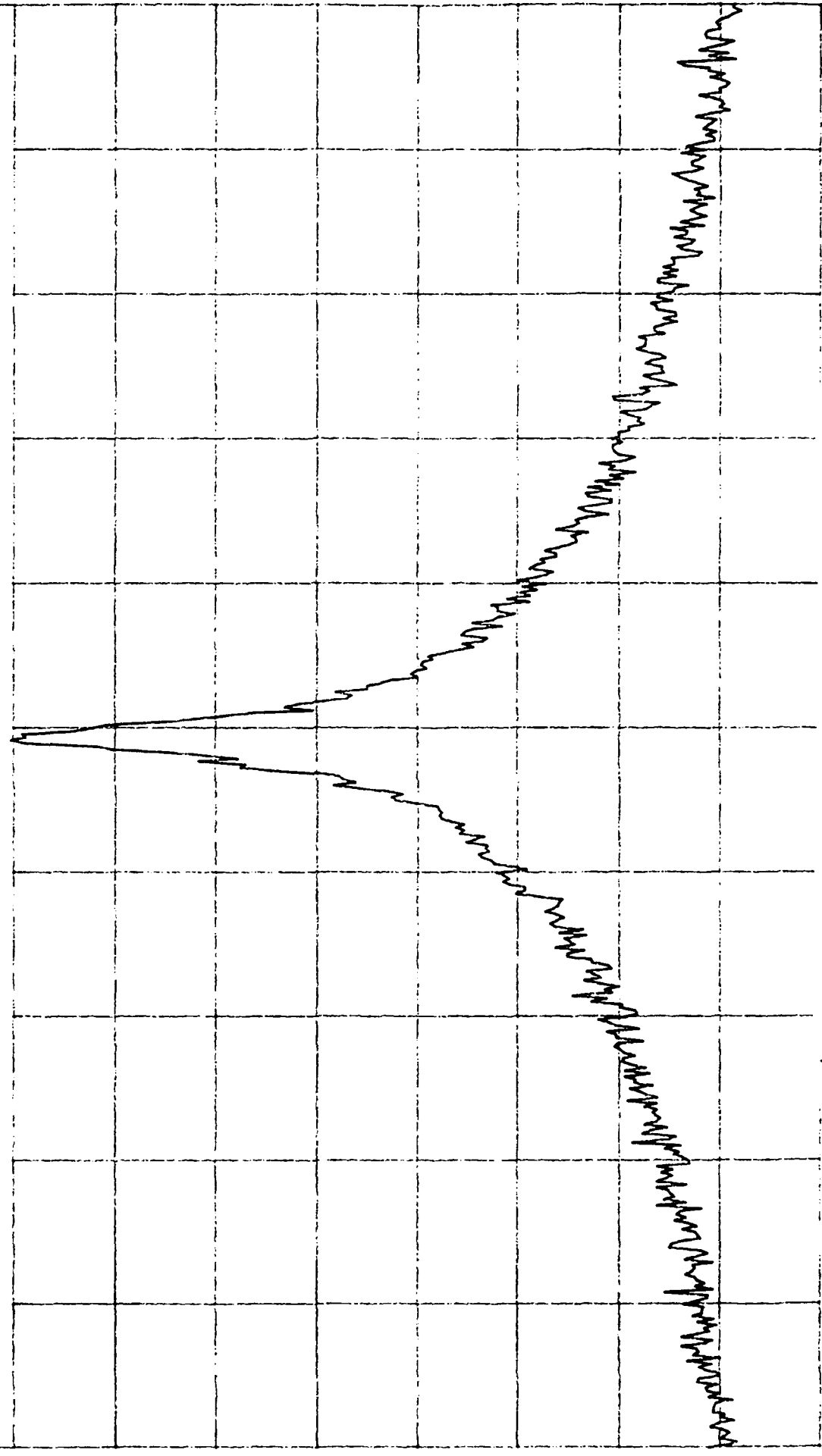


Fig. 6 Phase Noise of Integrated Superconductor Oscillator. Scale: 20KHz/div.

CR# # 2L / 073 / 74 #10
MISC
Pout 5 dBm
11/12/91

Integrated Oscillator:

Superconductor resonators were received from STI on substrates. The active circuit and a reflection filter were assembled in the same stainless steel case. The length of the 50 ohm line between the device and the resonator was adjusted to meet the phase part of the oscillation condition. The oscillator functioned at 9.47 GHz and had the following performance characteristics:

Frequency : 9.47 GHz
Power out: 5 dBm
Phase Noise: -82 dBc/Hz at 20KHz
Pulling into 12dBr: 5 MHz
Pushing : 1 MHz/V
Bias: 4V, 25 ma.

One integrated oscillator at 9.47 GHz is enclosed as part of this final progress report. Figure 5 and 6 represent the phase noise of the oscillator. The phase noise achieved was about 15 dB worse than the results achieved using the resonator (at 77 deg K) and the active circuit (at room temperature) in separate packages. The following seems to be the possible reasons for the relatively poor performance:

1. The radiation Q of the packaged resonator depends very strongly on the material and dimensions of the package. The package used for the integrated oscillator is not optimized for high Q.
2. Lower value of the loaded Q. The loaded Q in this case was much lower compared to when used in a separate package. As per the Quality factor measurements at STI, unloaded Q values of 3000 to 9000 were reported. The phase noise and frequency stability performance of the integrated oscillator indicates a much lower Q performance. This Q reduction may also be due to the losses between the resonator and the active device as well as the lossy interconnection between the superconductor resonator and the active circuit.

A gold microstrip GaAs FET oscillator was built on alumina substrate for comparison purposes. As shown in figure 7 the phase noise of the integrated superconductor oscillator is about 20 dB better than the microstrip resonator GaAs FET oscillator. More work needs to be done on improving the loaded quality factor of the superconductor resonators and optimization of package for better performance.

CTR 9.1845 GHz SPAN 20 KHz/ RES BW 1 KHz VF .1
REF -8 dBm 10 dB/ ATTN 10 dB SWP AUTO

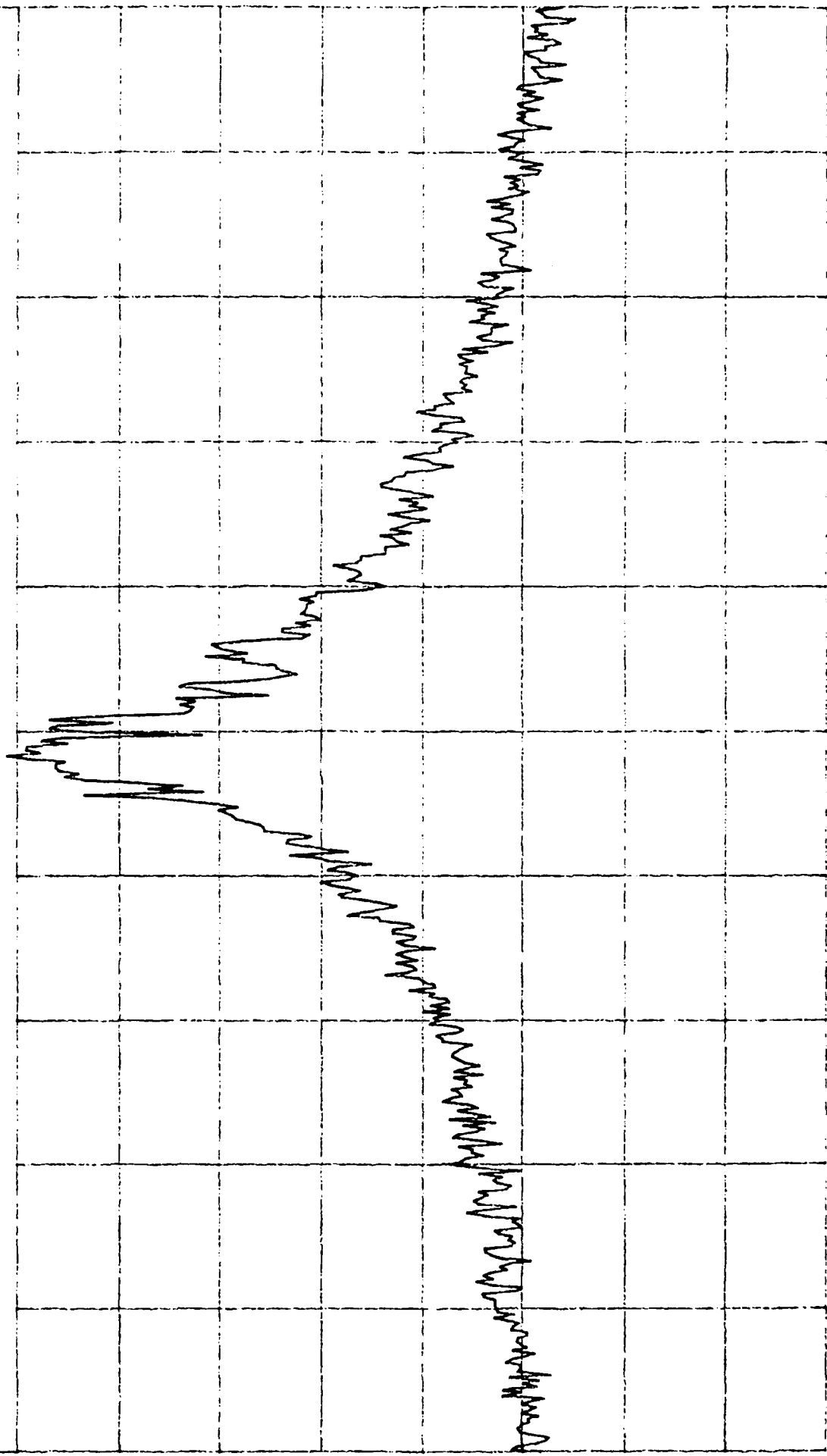


Fig. 7 Phase Noise of Gold Microstrip Resonator
Oscillator. Scale: 20KHz/div.

HARDWARE AS PART OF THE FINAL PROGRESS REPORT

1. 10 stainless steel packages used for temperature testing.
2. 10 aluminum packages used for temperature testing.
3. One integrated 9.47 GHz oscillator
4. Two 9-11 GHz negative resistance substrates

APPENDIX 1

TEMPERATURE CYCLE

TEST RESULTS



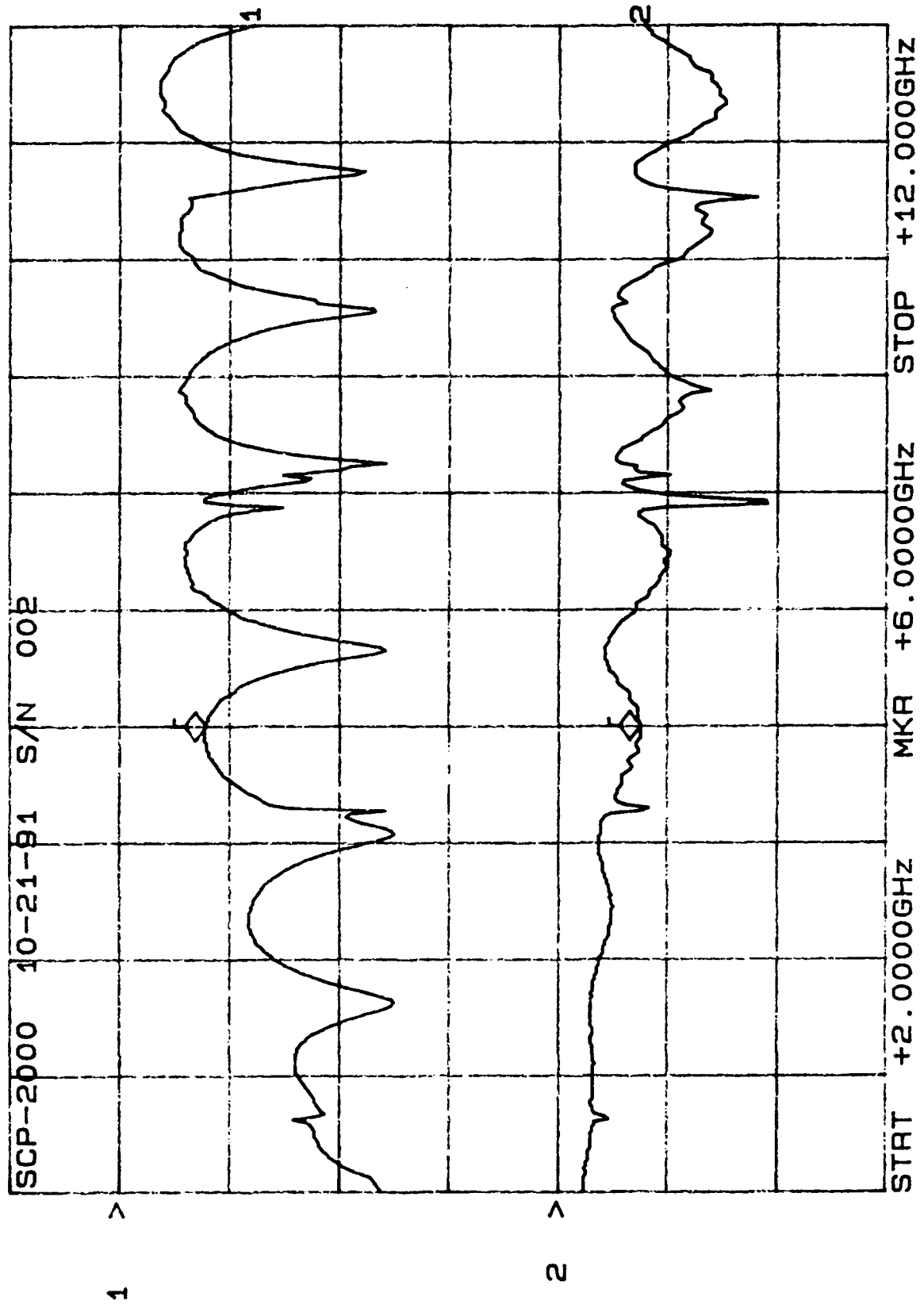
CERTIFIED TEST
DATA



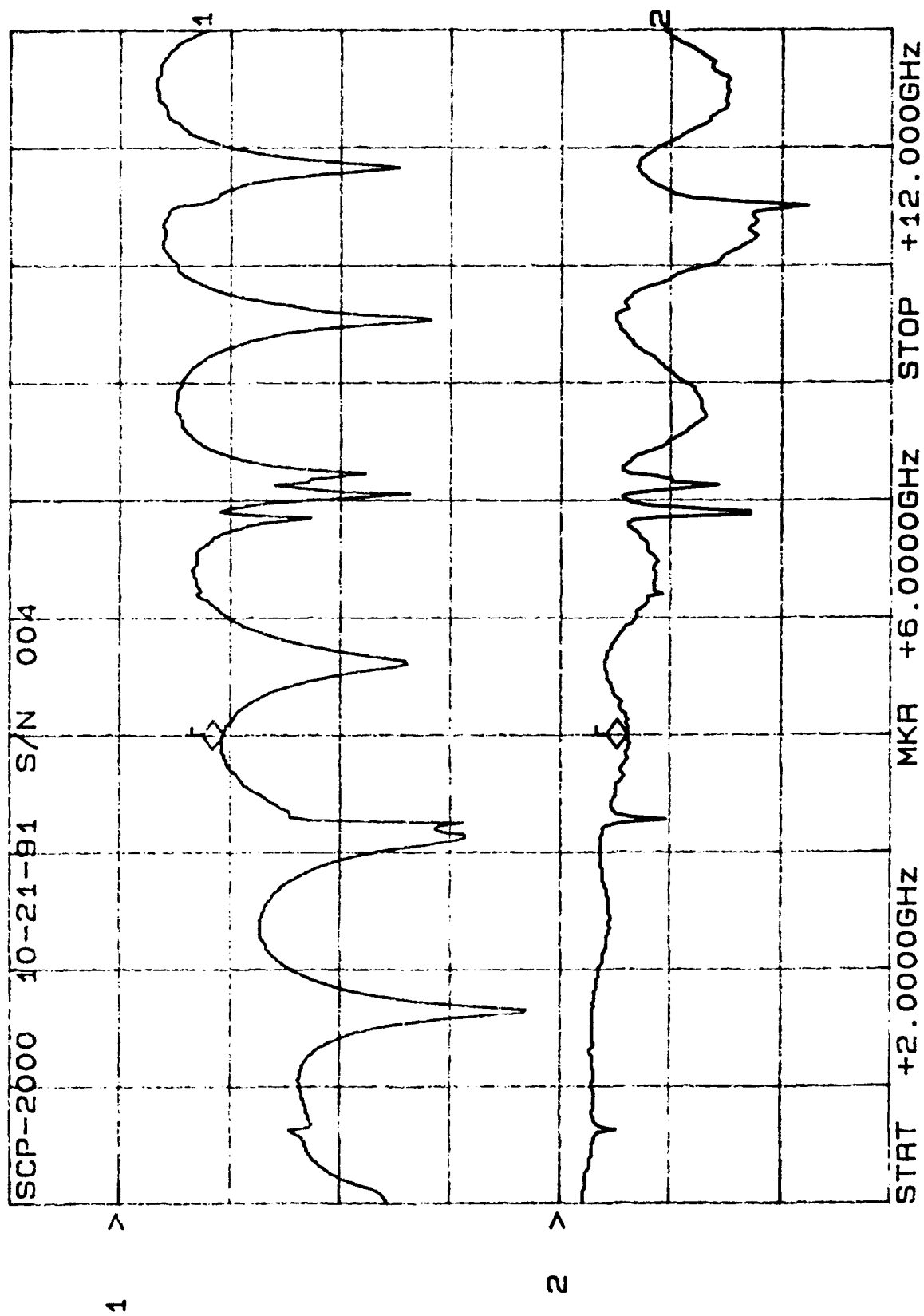
75 cycles

START DATE	CUSTOMER	QUALITY ACCPT
10-22-91	Eng	
COMPL DATE	TYPE OF TEST AVANTEK	WO/CSO TEST COND.
10-22-91	FINE LEAK TEST JI-32	SZ016205 A.
DEVICE TYPE	TEST REQUIREMENTS	BOMB PRESSURE AND DURATION
SLP-1000, 2000	MIL STD-883C METHOD 1014.8	
QTY START	QTY COMPL SENSITIVITY	2hrs @ 30psi
20	18 5×10^{-6} CC/SEC	
S/N LOT No.	LEAK RATE (CC/SEC)	PASS/FAIL DWELL TIME
001 SLP-2000	1×10^{-6}	PASS 10m
002		
003		
004		
005		
006		
007	10×10^{-6}	FAIL Leak @ Feed thru on Red Arrow.
008	1×10^{-6}	PASS
009		
010	15×10^{-6}	FAIL Leak @ Feed thru on Red Arrow.
001 SLP-1000	1×10^{-6}	PASS
002		
003		
004		
005		
006		
007		
008		
009		
010		

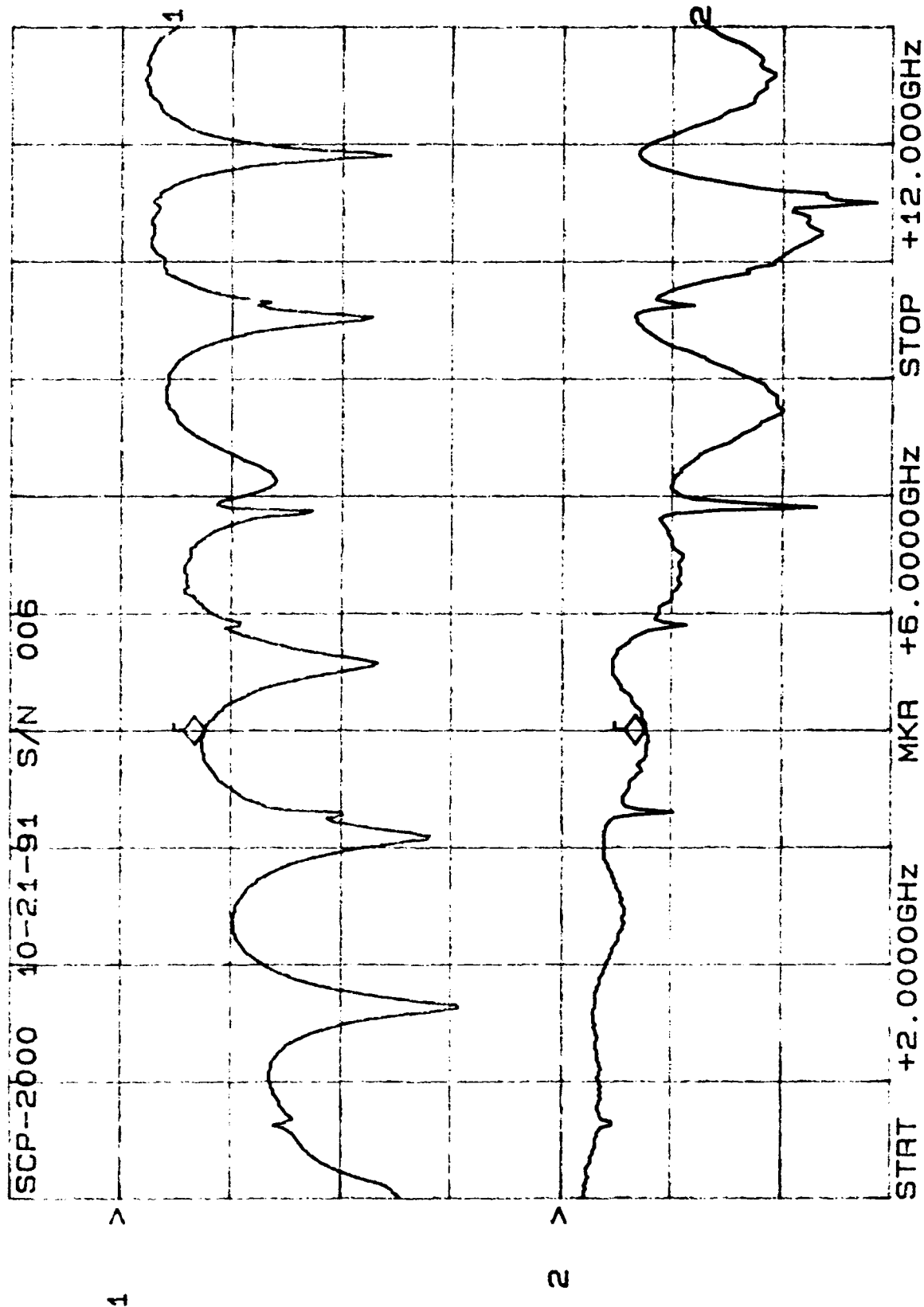
CH1: A -M REF = 7.77 dB CH2: B -M REF = 1.46 dB
 10.0 dB/ REF 2.0 dB/ REF + .00 dB



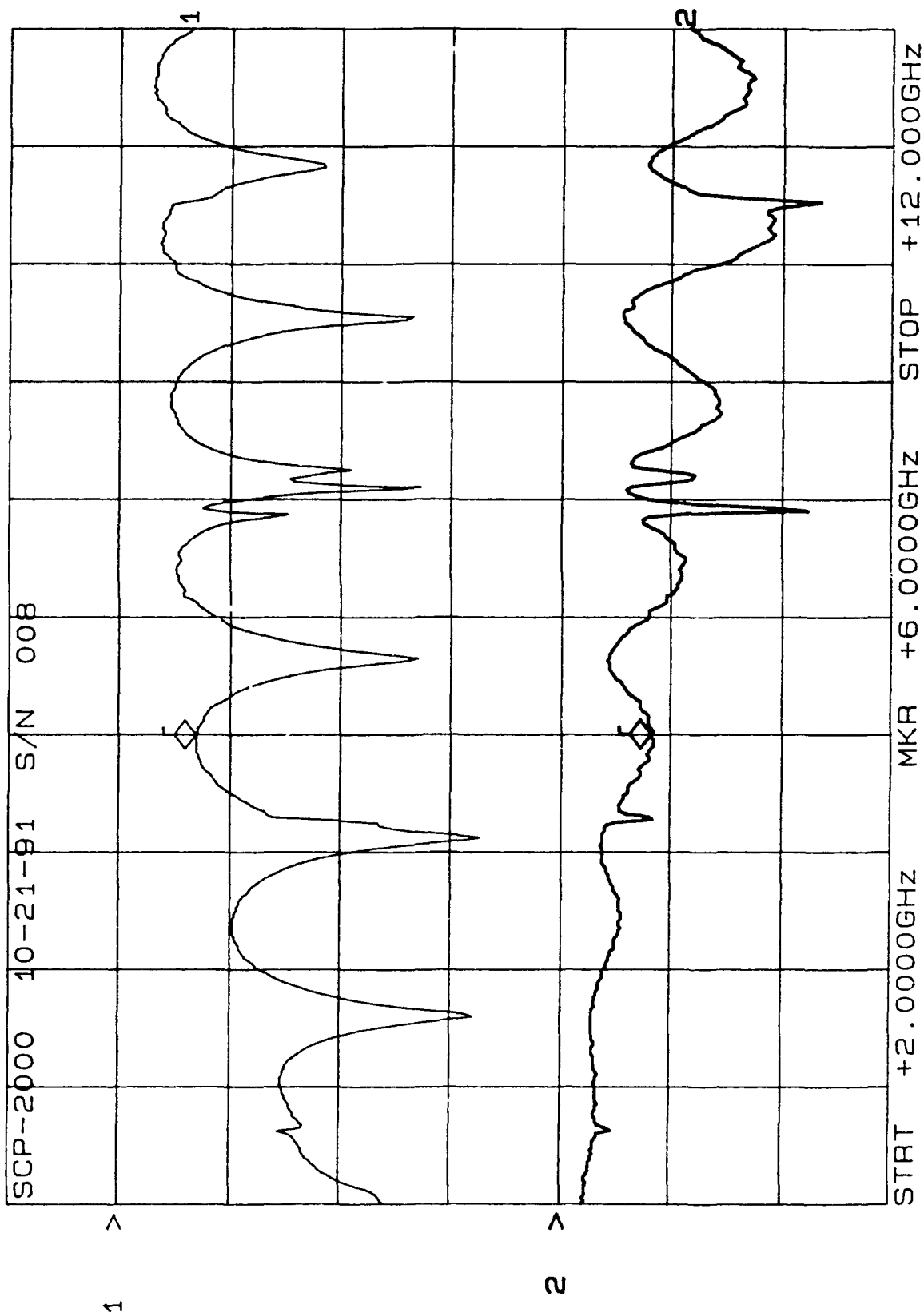
CH1: A -M REF - 9.28 dB CH2: B -M A - 1.21 dB
10.0 dB/ REF 2.0 dB/ REF + .00 dB



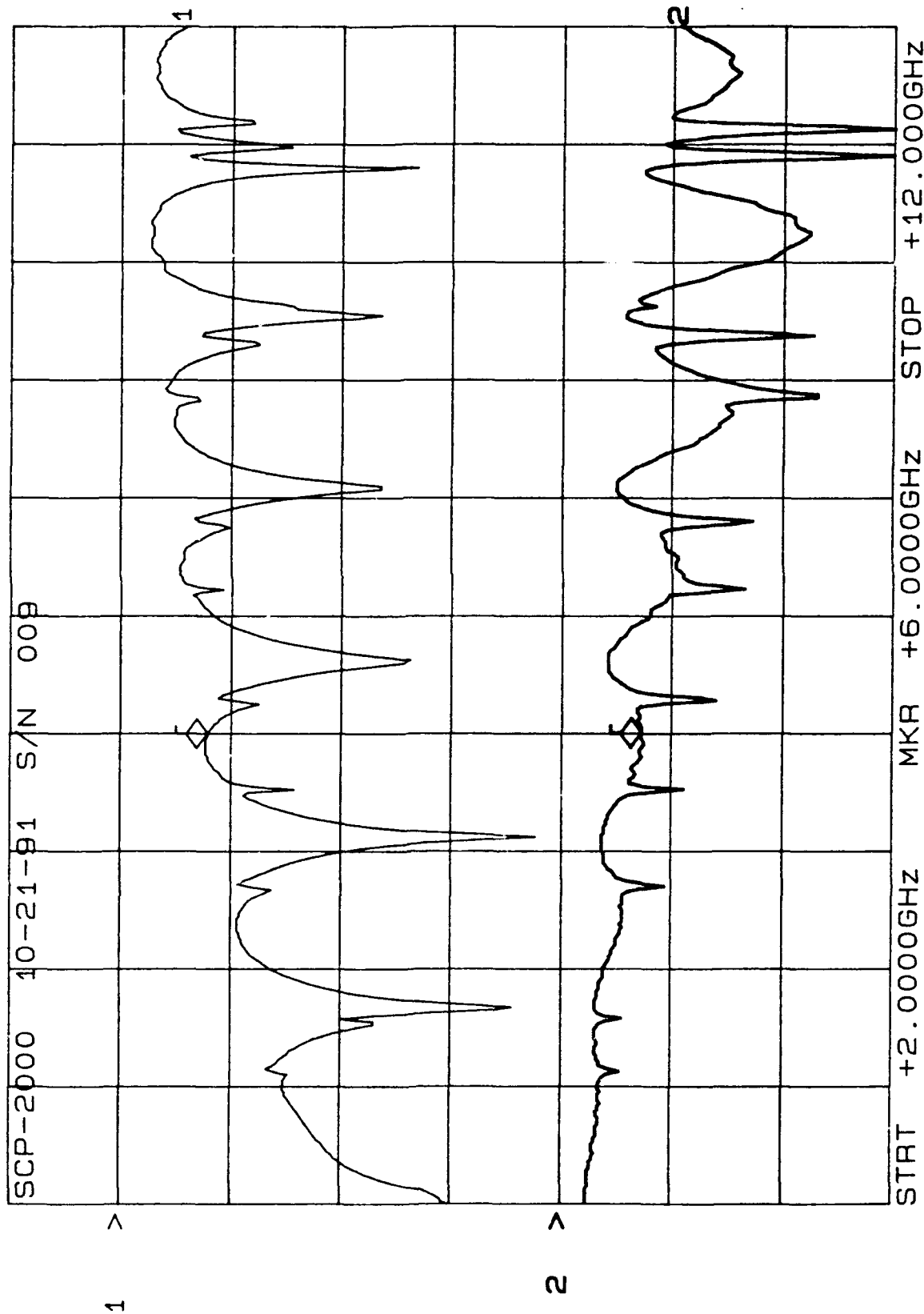
CH1: A -M REF - 7.56 dB CH2: B -M A - 1.52 dB
10.0 dB/ REF - .00 dB 2.0 dB/ REF + .00 dB



CH1: A -M - 6.89 dB CH2: B -M A - 1.65 dB
 10.0 dB/ REF - .00 dB 2.0 dB/ REF + .00 dB



CH1: A -M REF - 7.85 dB CH2: B -M A - 1.44 dB
 10.0 dB/ REF - .00 dB 2.0 dB/ REF + .00 dB



50 Cycles

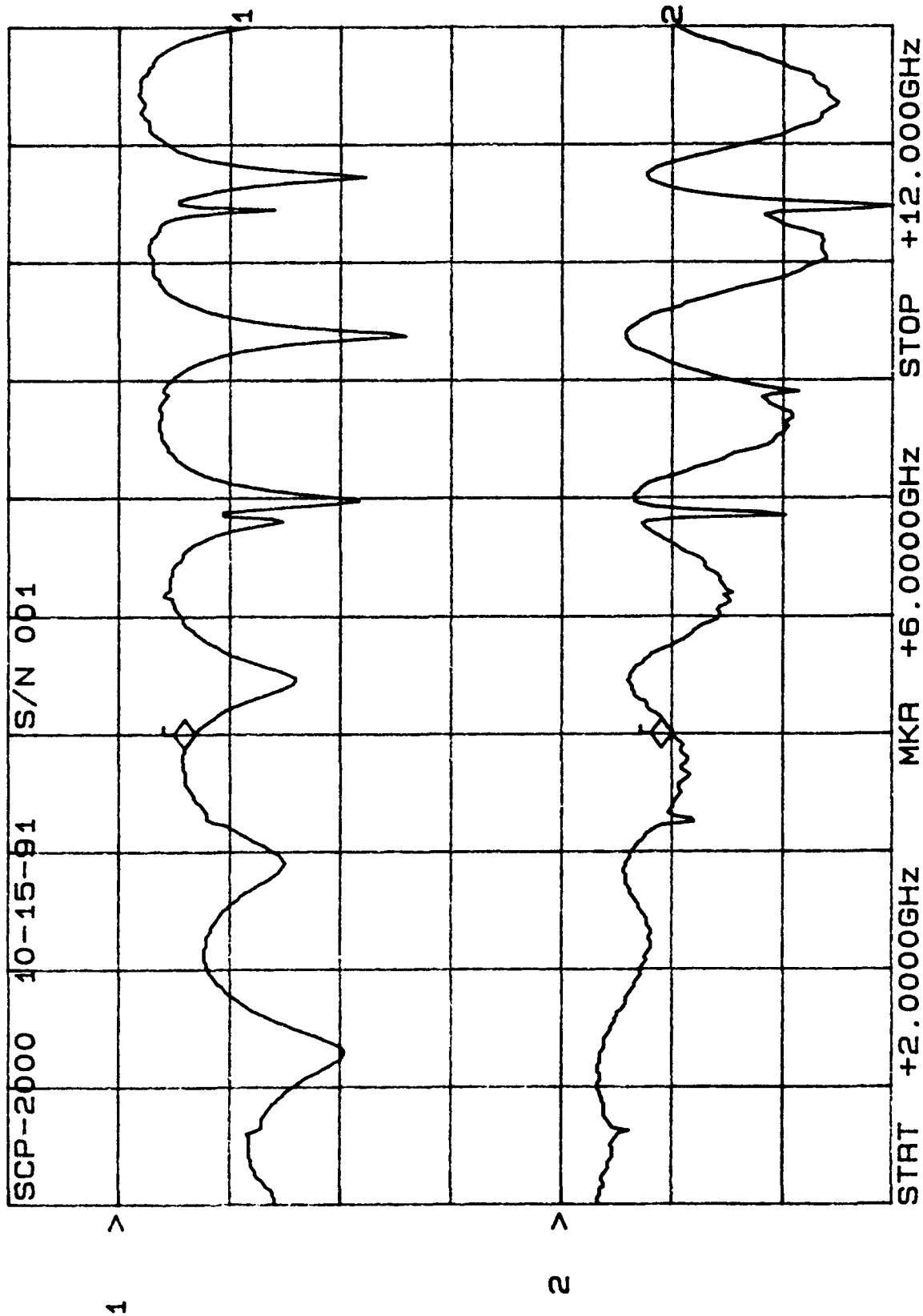


CERTIFIED TEST DATA

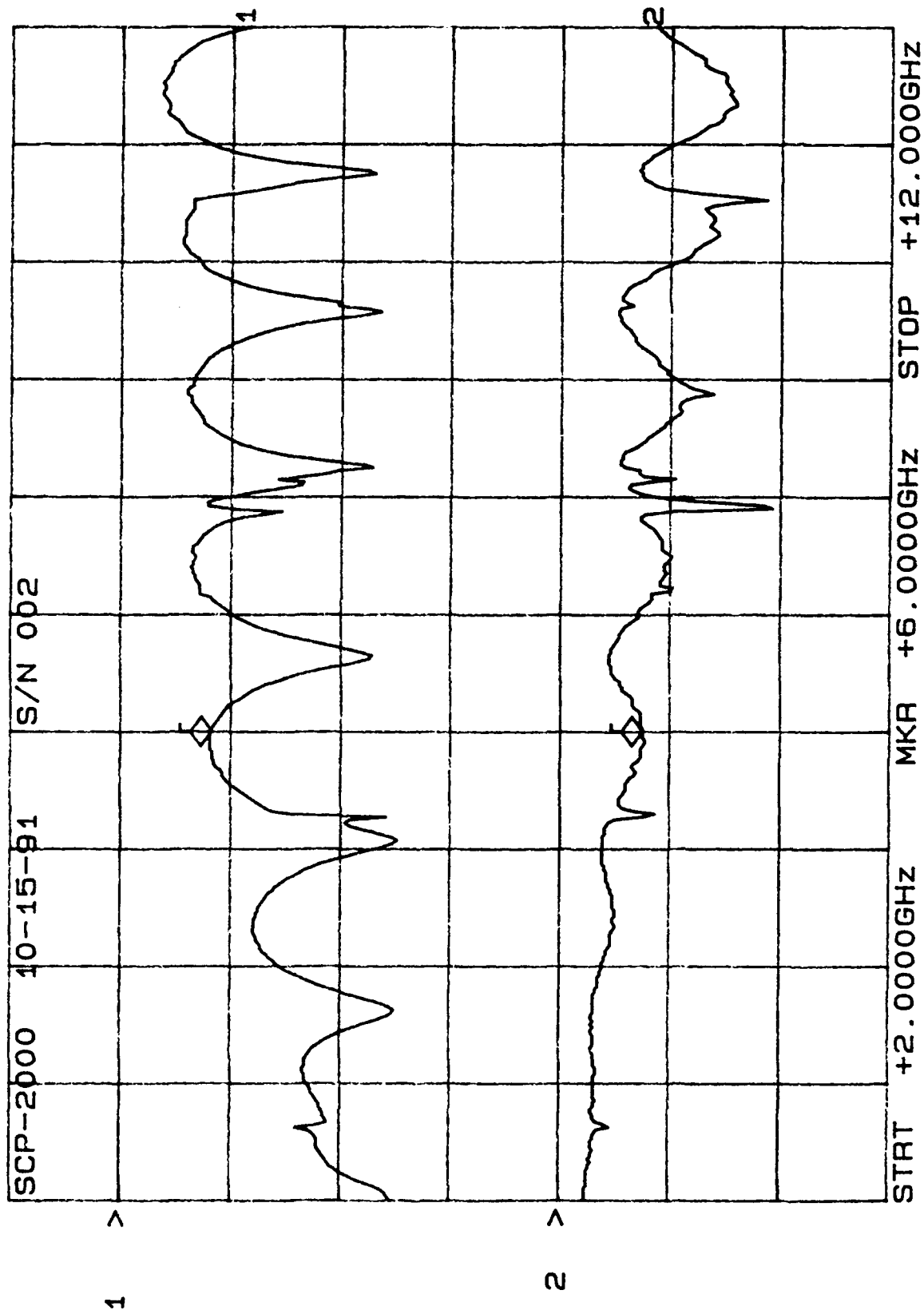
After 50 cycles

START DATE 10-16-91	CUSTOMER Stork	QUALITY ACCT E.L. ACCEPT 04	
COMPL DATE 10-16-91	TYPE OF TEST AVANTEK FINE LEAK TEST J1-32	WO/CSO TEST CONT SZ016205 A	
DEVICE TYPE SCP-2000 SCP-1000	TEST REQUIREMENTS MIL STD-883C METHOD 1014.8	BOMB PRESSURE AND DURATION	
QTY START 20	QTY COMPL SENSITIVITY 18 5×10^{-7} CC/SEC	2hrs @ 30psi	
(S/N) LOT No.	LEAK RATE (CC/SEC)	PASS/FAIL	DWELL TIME
SCP-2000 001	2×10^{-9}	PASS	15 min
002			
003			
004			
005			
006			
007	10×10^{-6}	FAIL	Leak @ Feed thru on Red Arrow
008	2×10^{-9}	PASS	
009	2×10^{-9}		
010	10×10^{-6}	FAIL	Leak @ Feed thru on Red Arrow
SCP-1000 001	2×10^{-9}	PASS	
002			
003			
004			
005			
006			
007			
008			
009			
010			

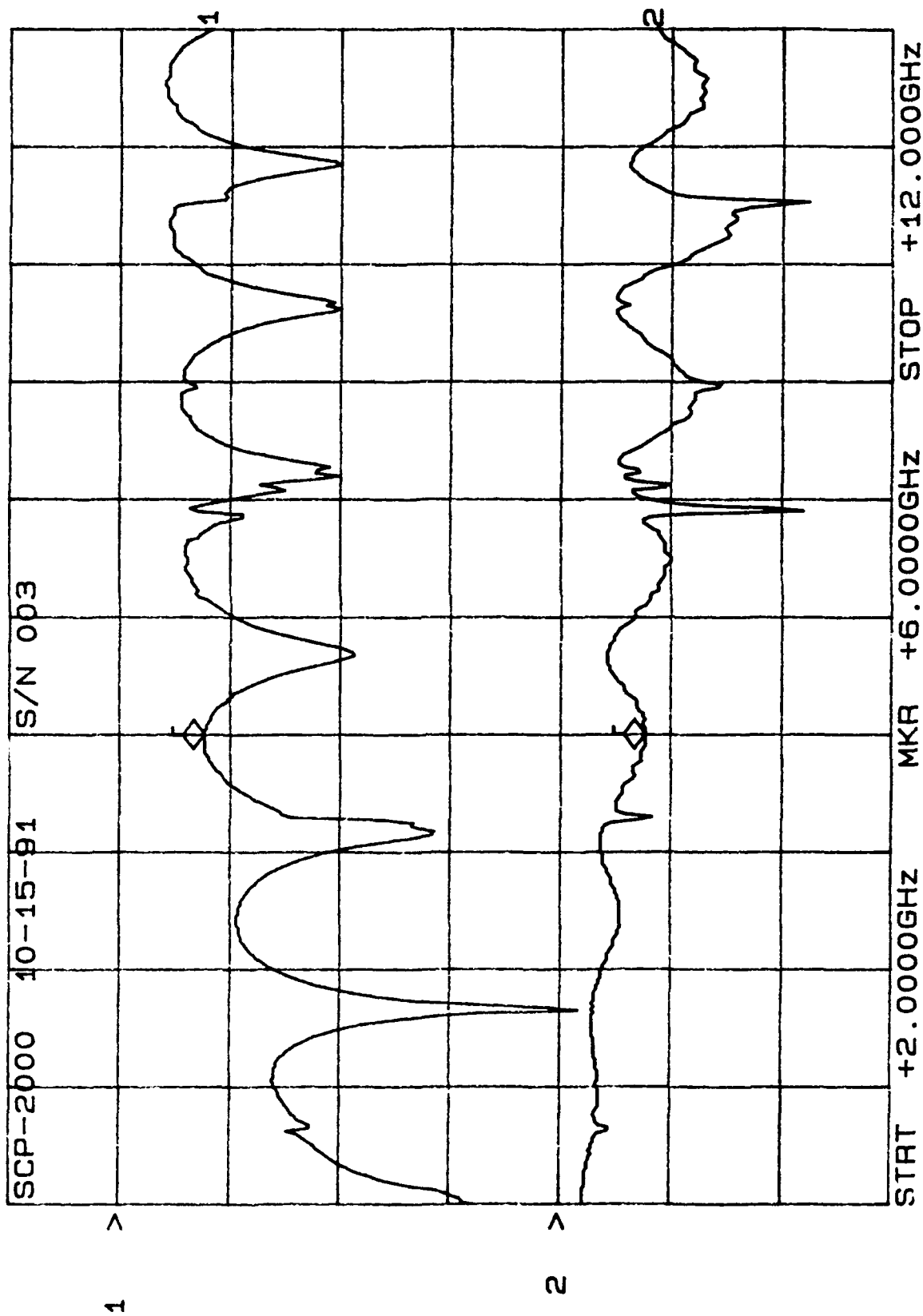
CH1: A -M - 6.79 dB CH2: B -M A - 1.99 dB
10.0 dB/ REF - .00 dB 2.0 dB/ REF + .00 dB



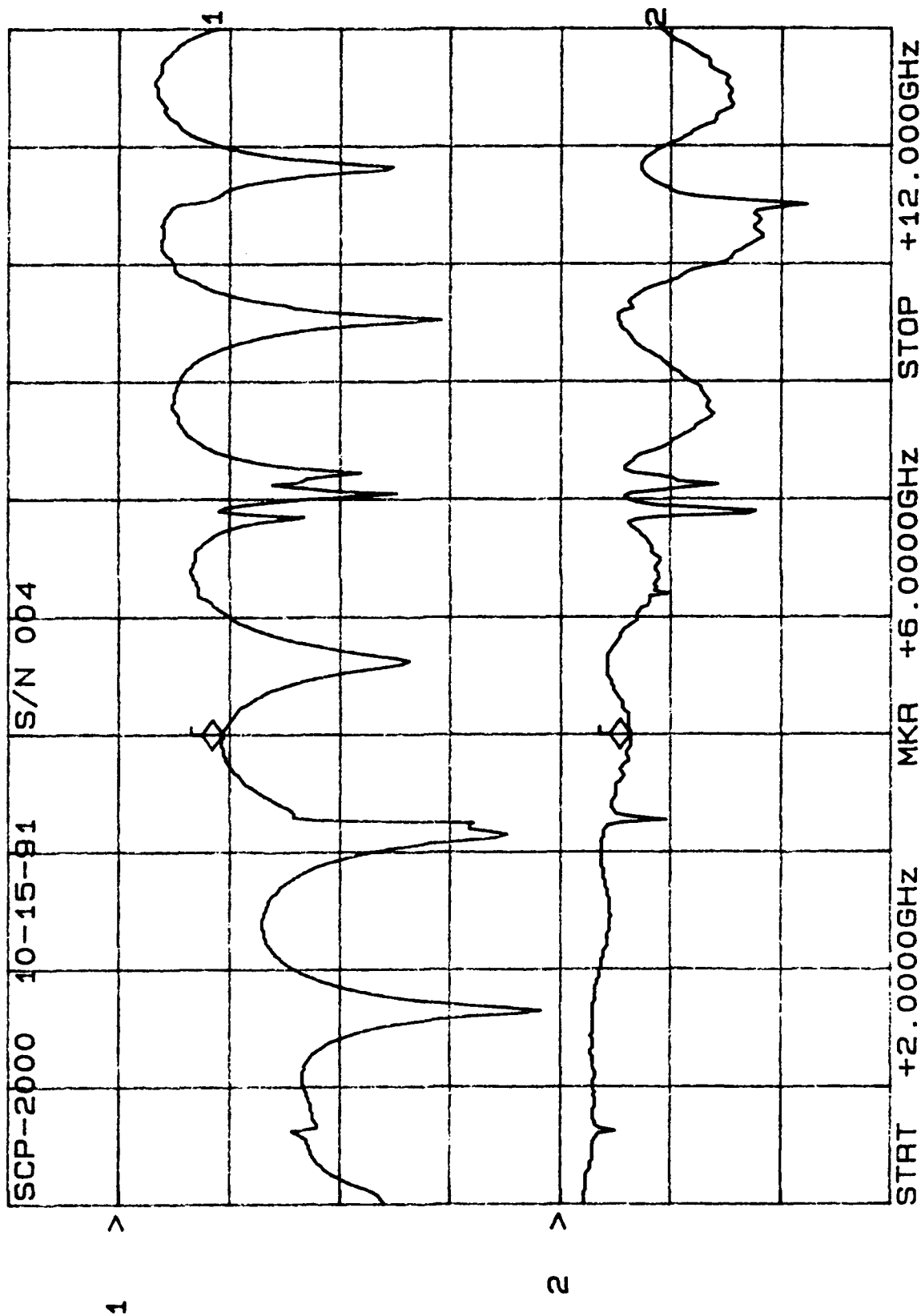
CH1: A -M - 8.17 dB CH2: B -M A - 1.48 dB
 10.0 dB/ REF - .00 dB 2.0 dB/ REF + .00 dB



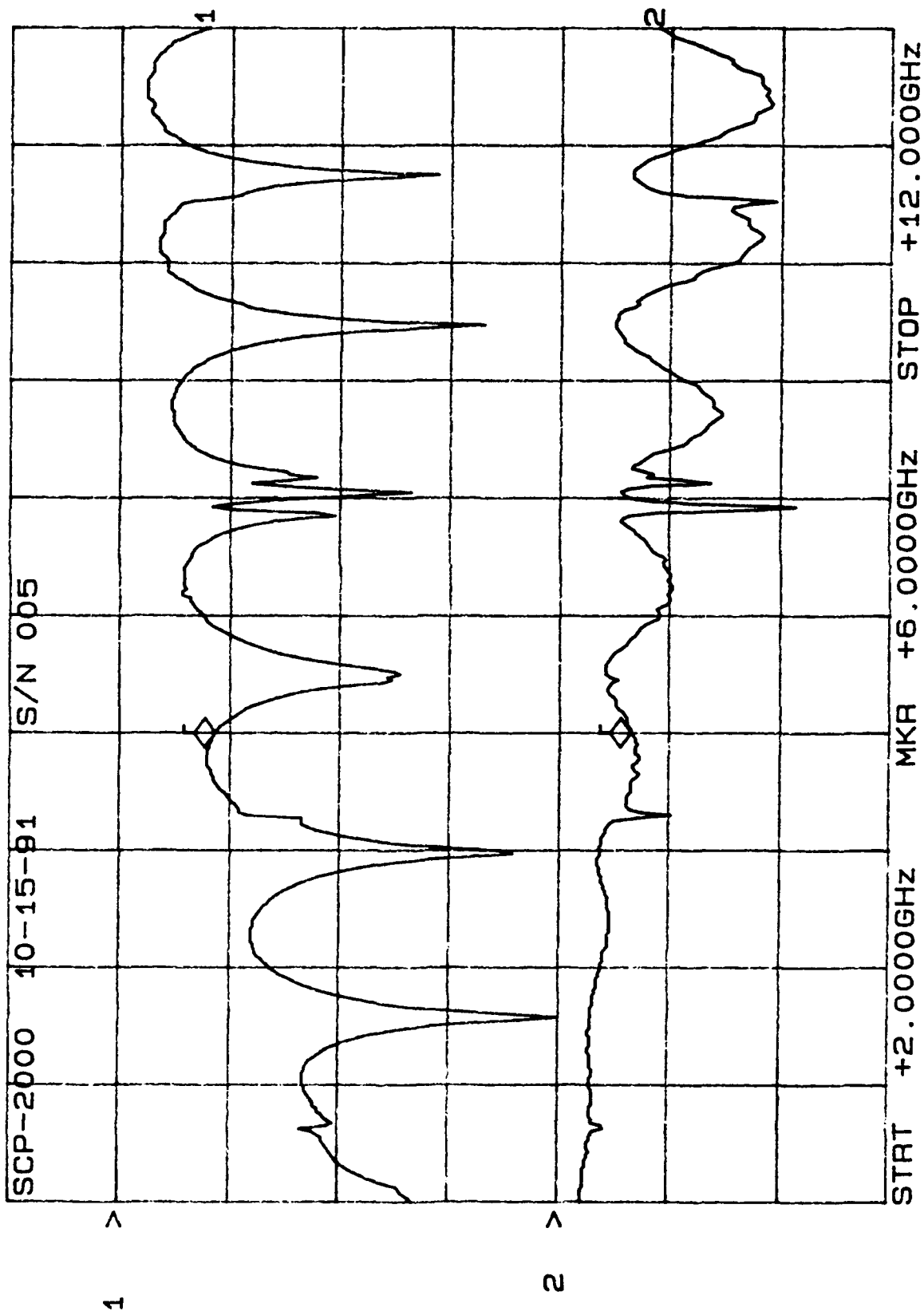
CH1: A -M REF - 7.58 dB CH2: B -M REF + 1.51 dB
 10.0 dB/ REF - .00 dB 2.0 dB/ REF + .00 dB



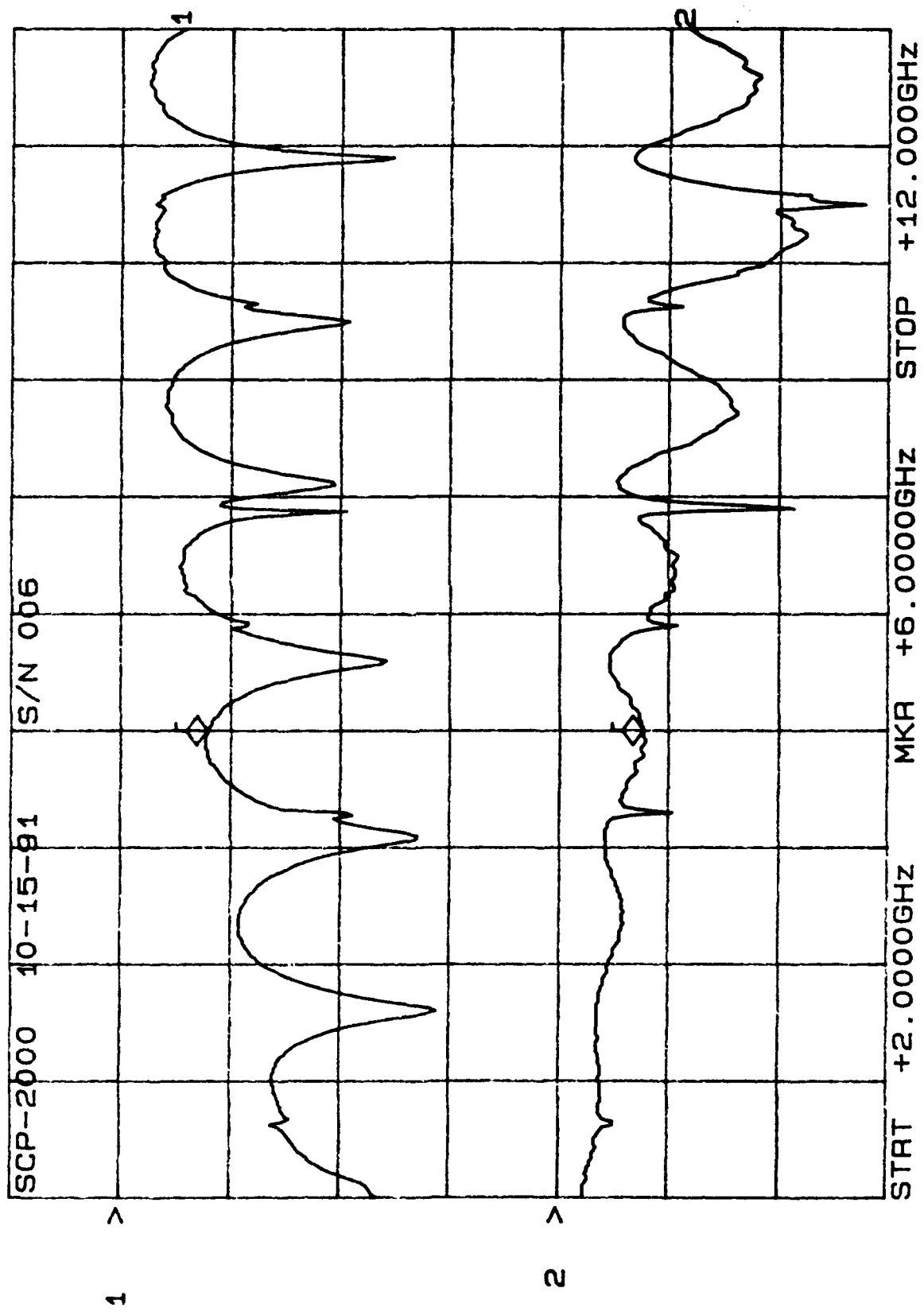
CH1: A -M REF - 9.32 dB CH2: B -M A - 1.23 dB
 10.0 dB/ REF - .00 dB 2.0 dB/ REF + .00 dB



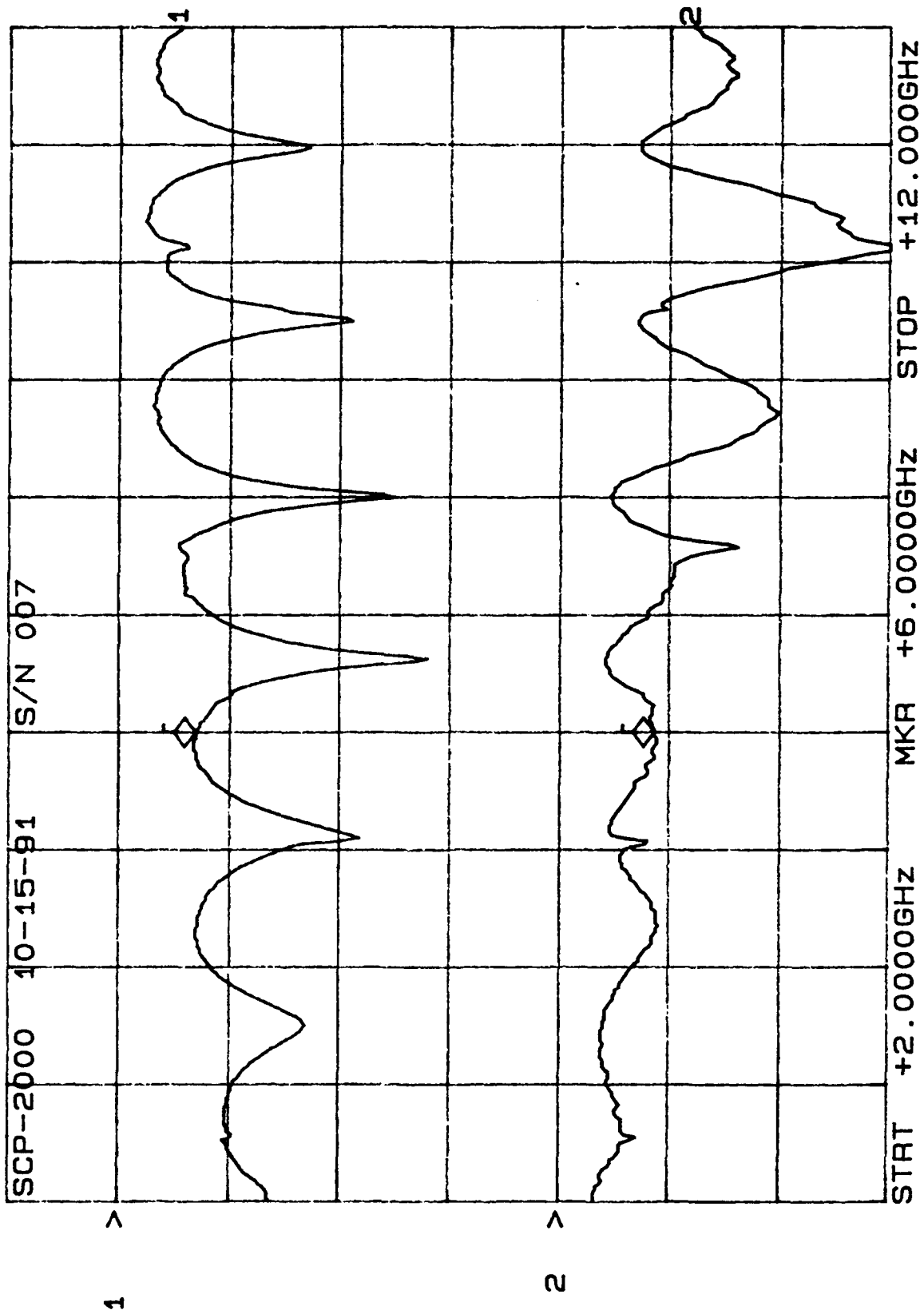
CH1: A -M - 8.58 dB CH2: B -M A - 1.30 dB
 10.0 dB/ REF - .00 dB 2.0 dB/ REF + .00 dB



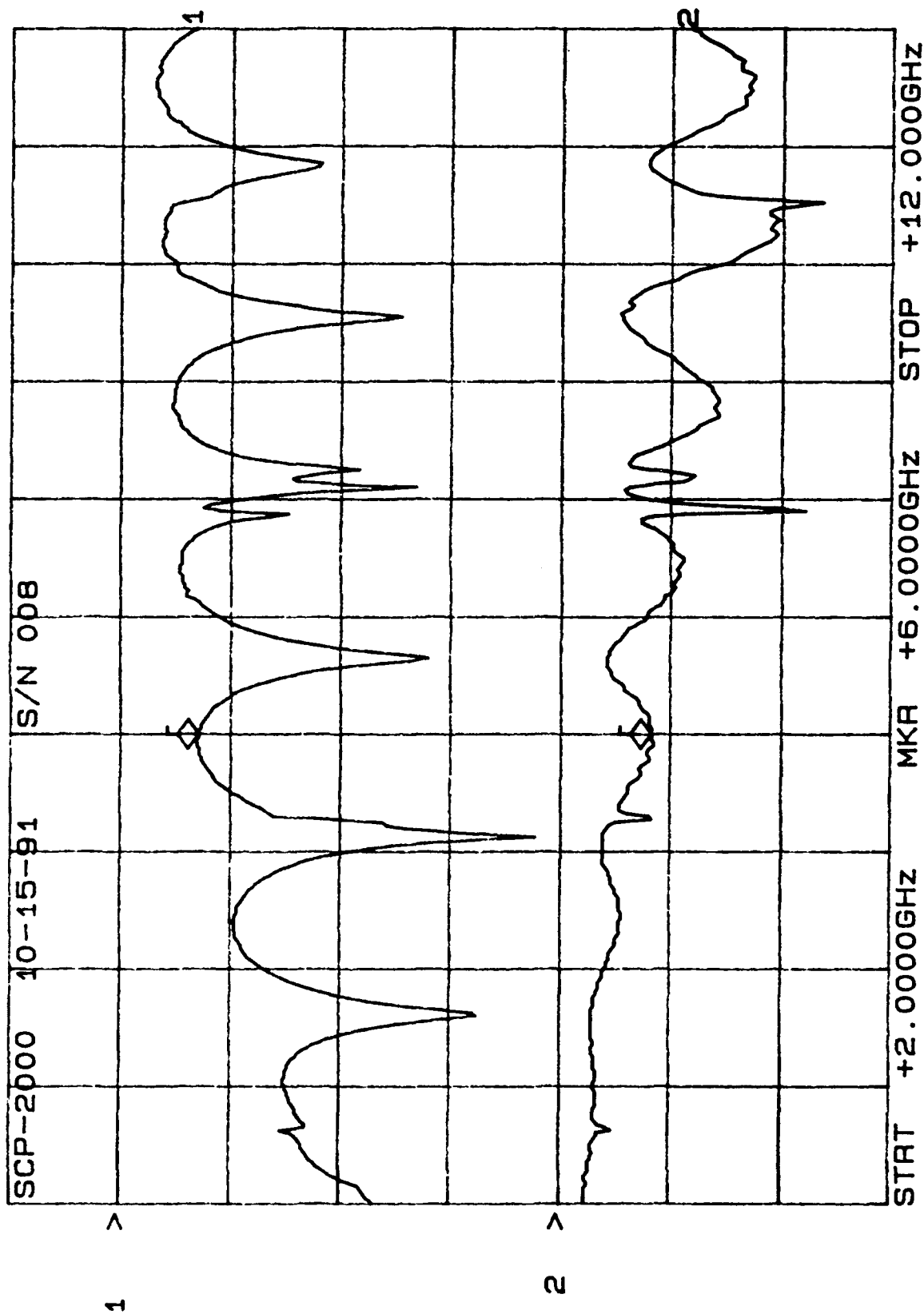
CH1: A -M REF - 7.86 dB CH2: B -M A - 1.51 dB
 10.0 dB/ REF - .00 dB 2.0 dB/ REF + .00 dB



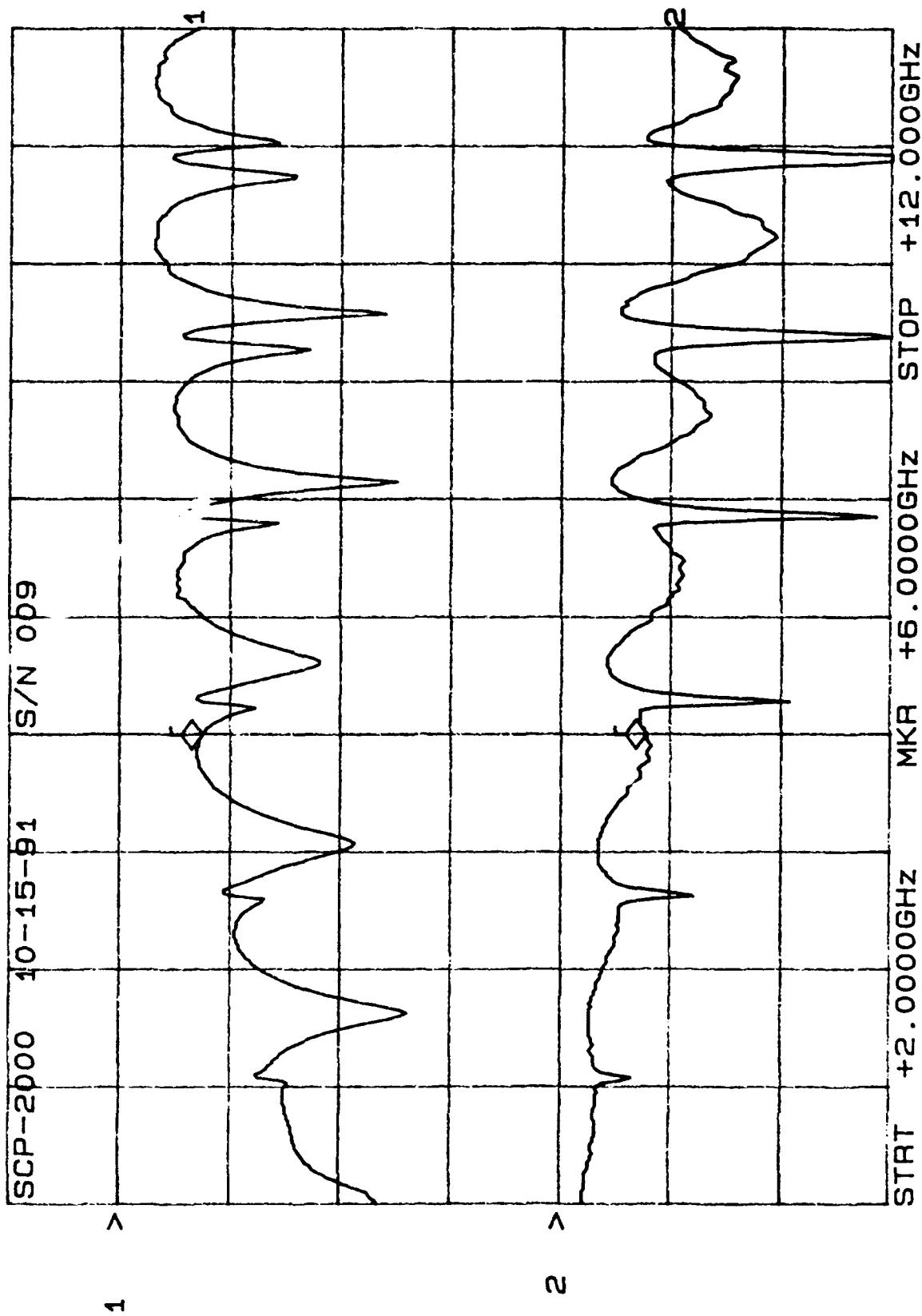
CH1: A -M - 6.90 dB CH2: B -M A - 1.71 dB
10.0 dB/ REF - .00 dB 2.0 dB/ REF + .00 dB



CH1: A -M REF - 7.00 dB CH2: B -M REF + 1.64 dB
 10.0 dB/ REF - .00 dB 2.0 dB/ REF + .00 dB

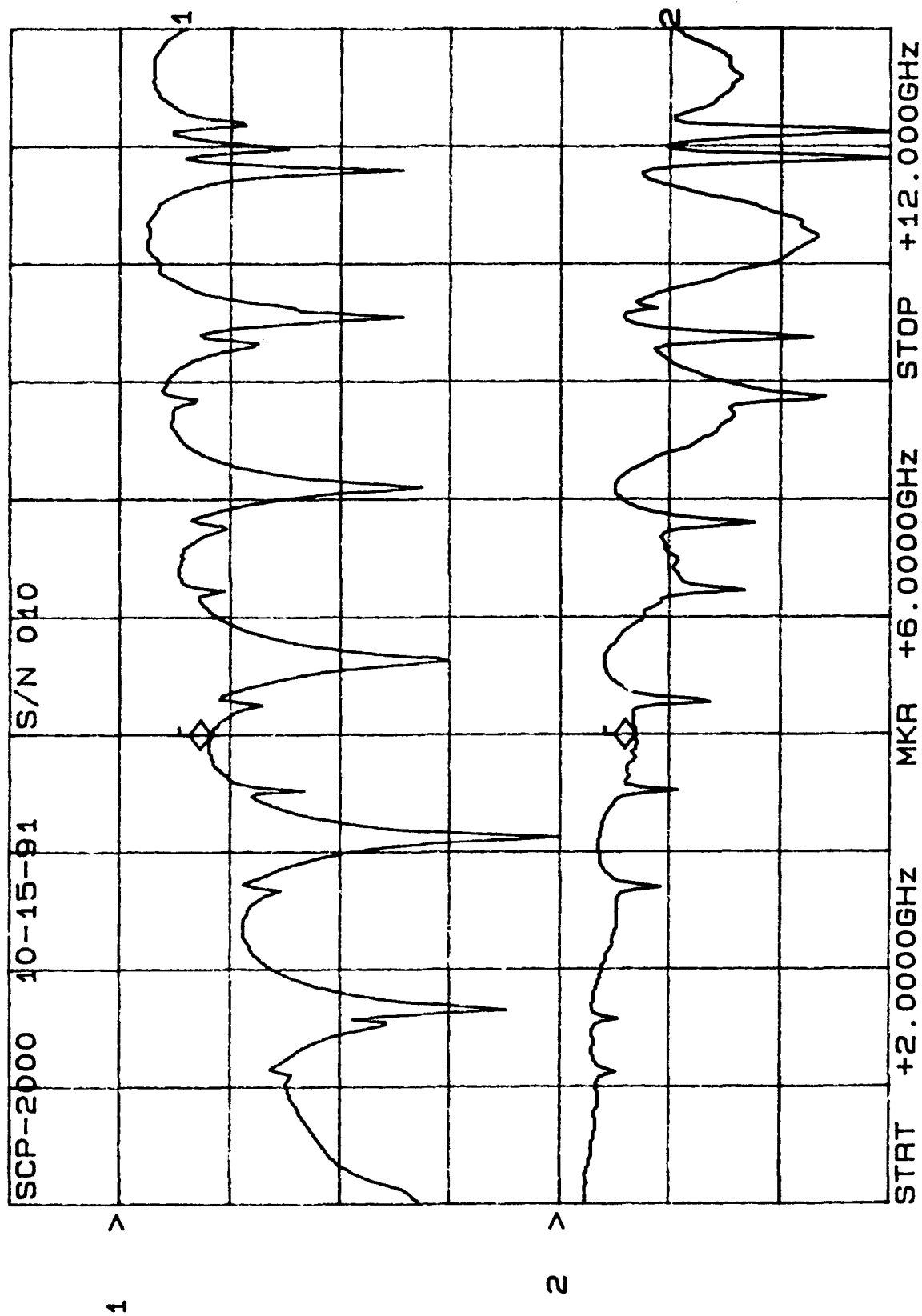


CH1: A -M REF = 7.42 dB CH2: B -M A - 1.54 dB
 10.0 dB/ REF = .00 dB 2.0 dB/ REF + .00 dB



After 50 cycles

CH1: A -M - 8.20 dB CH2: B -M A - 1.37 dB
10.0 dB/ REF - .00 dB 2.0 dB/ REF + .00 dB



20 Cycles

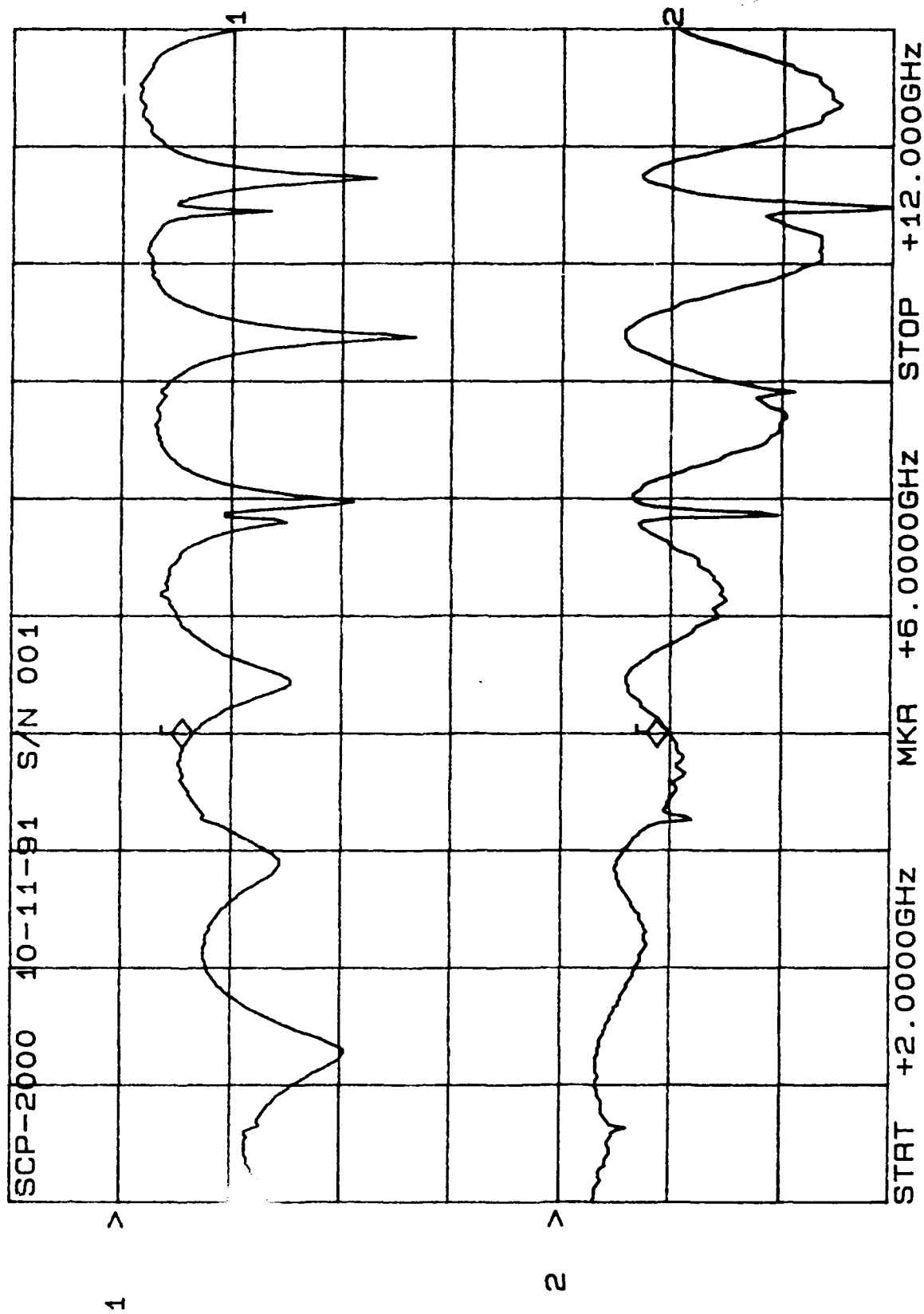


CERTIFIED TEST
DATA

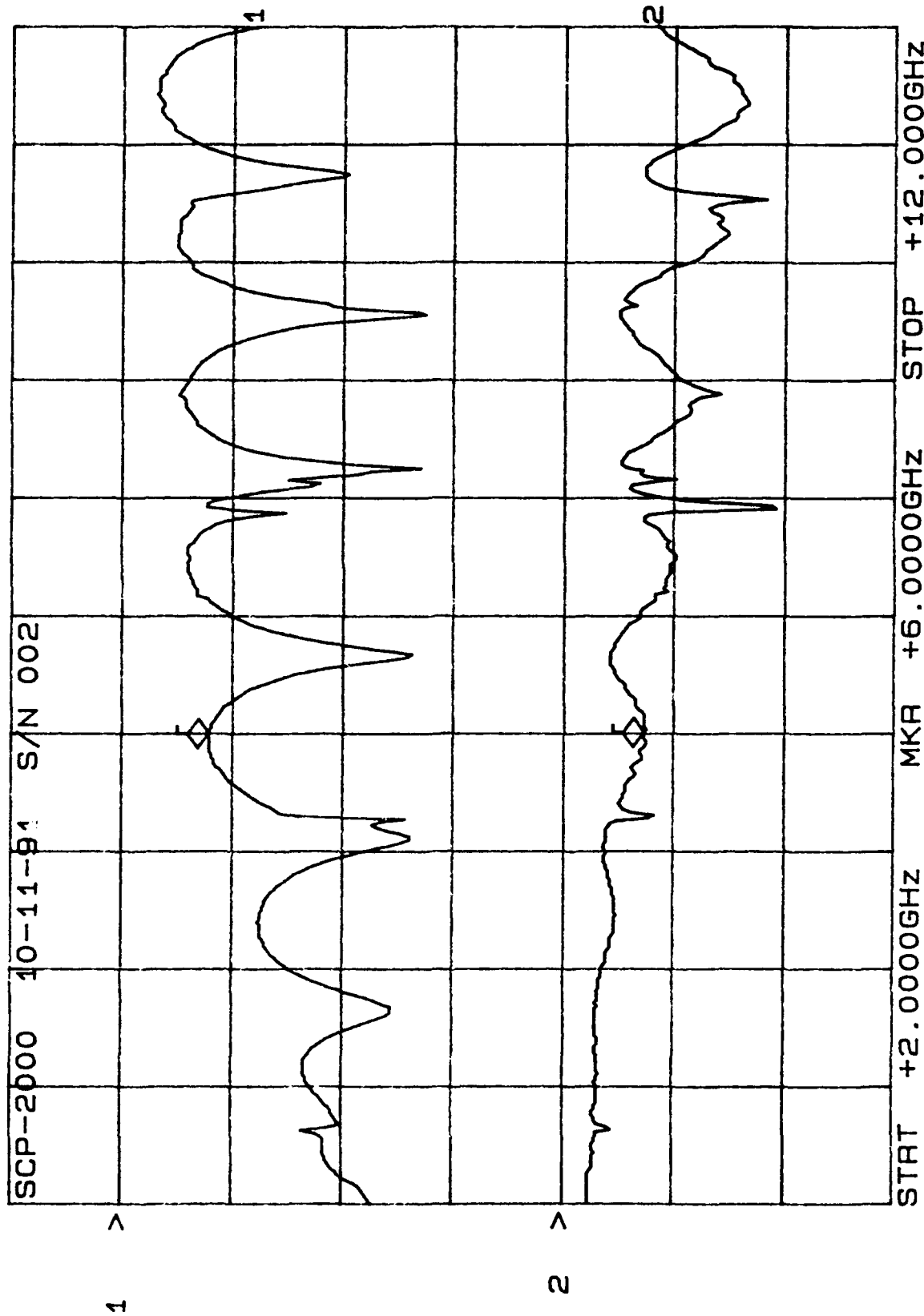
RECEIVED
02
ACCEPTED
02

WO/CSO TEST COND.
S-2016205 A
BOMB PRESSURE AND
DURATION
30 psi @ 2 hrs

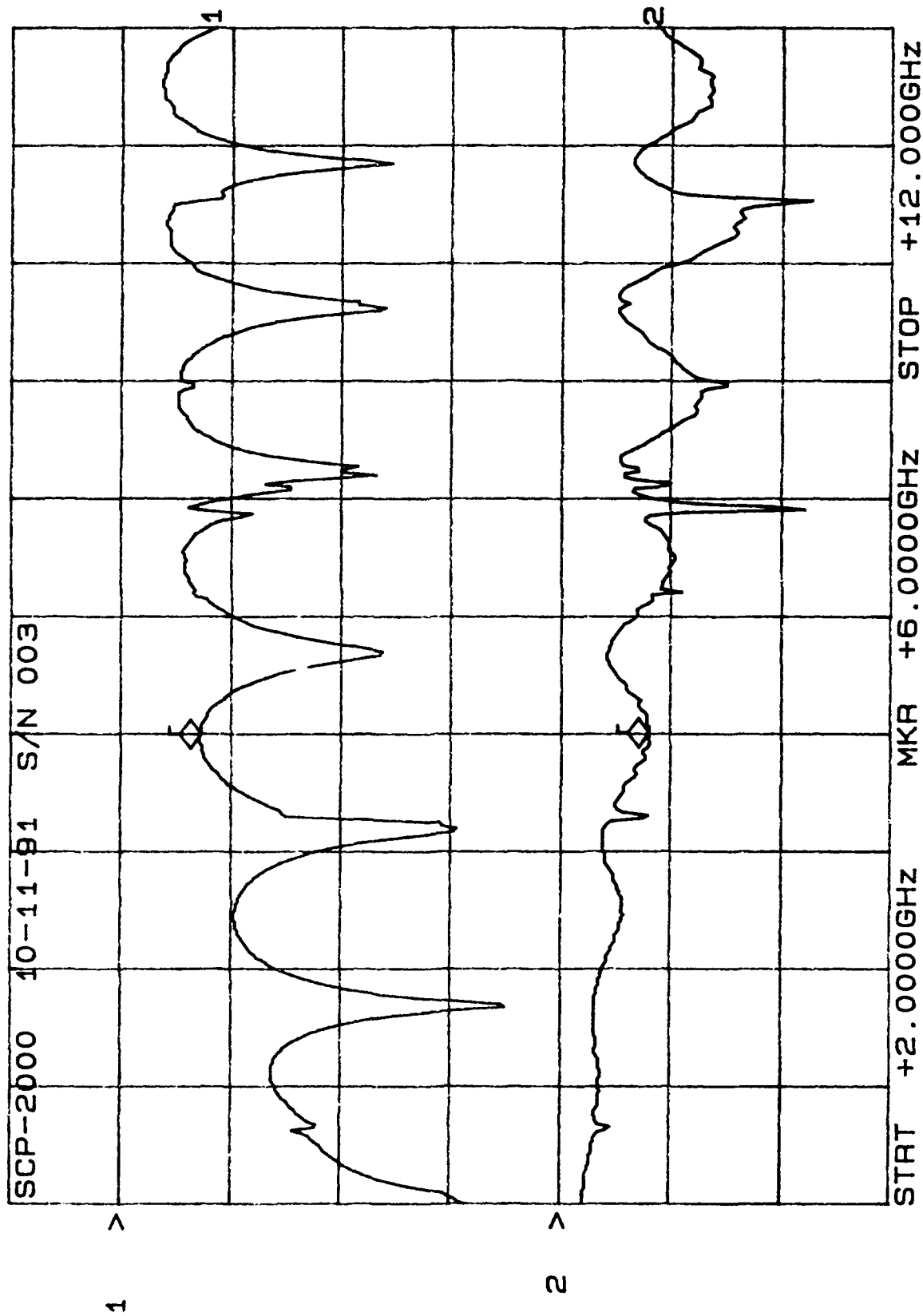
11/11/2020



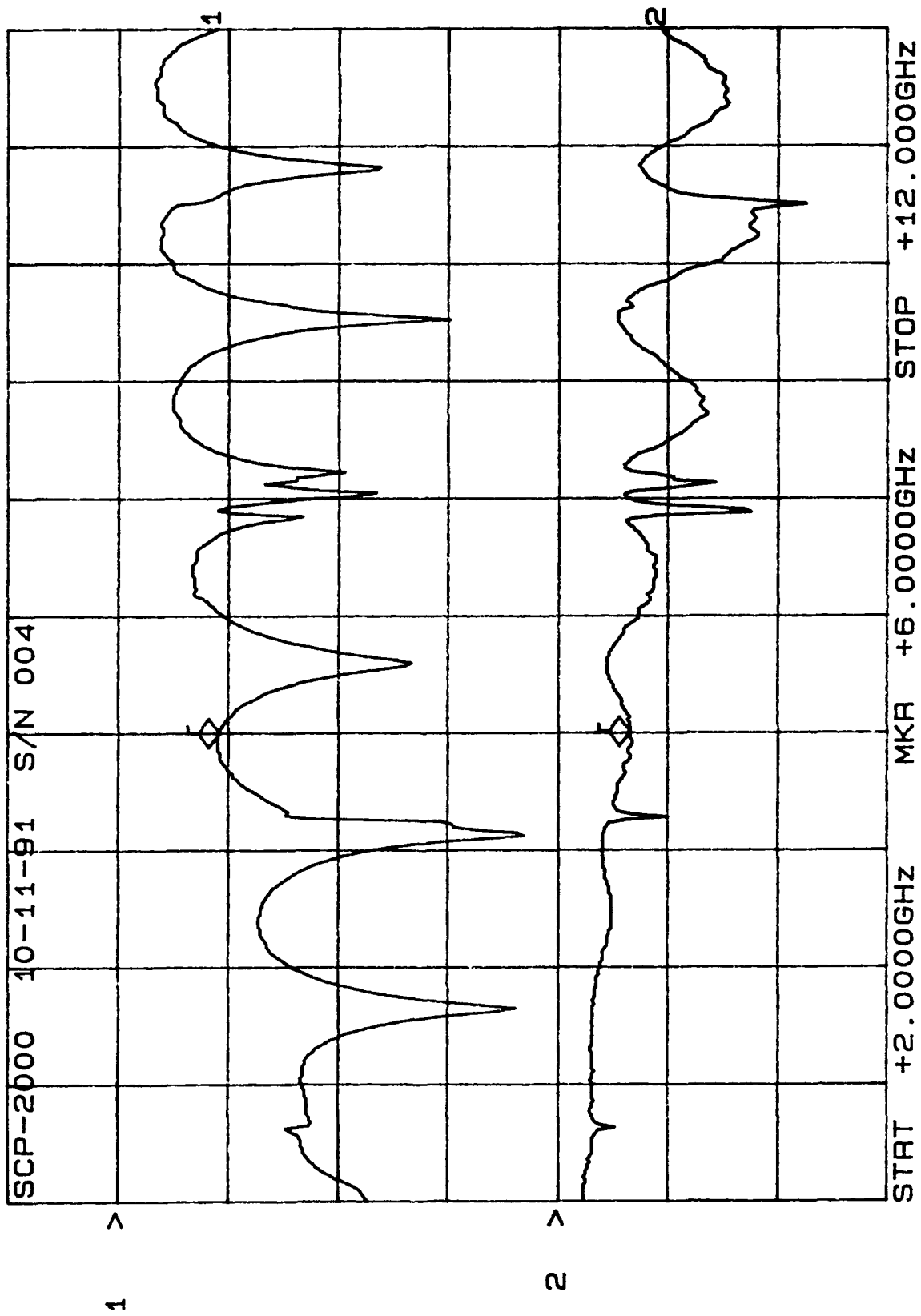
CH1: A -M REF = 7.81 dB CH2: B -M A - 1.45 dB
 10.0 dB/ REF 2.0 dB/ REF + .00 dB



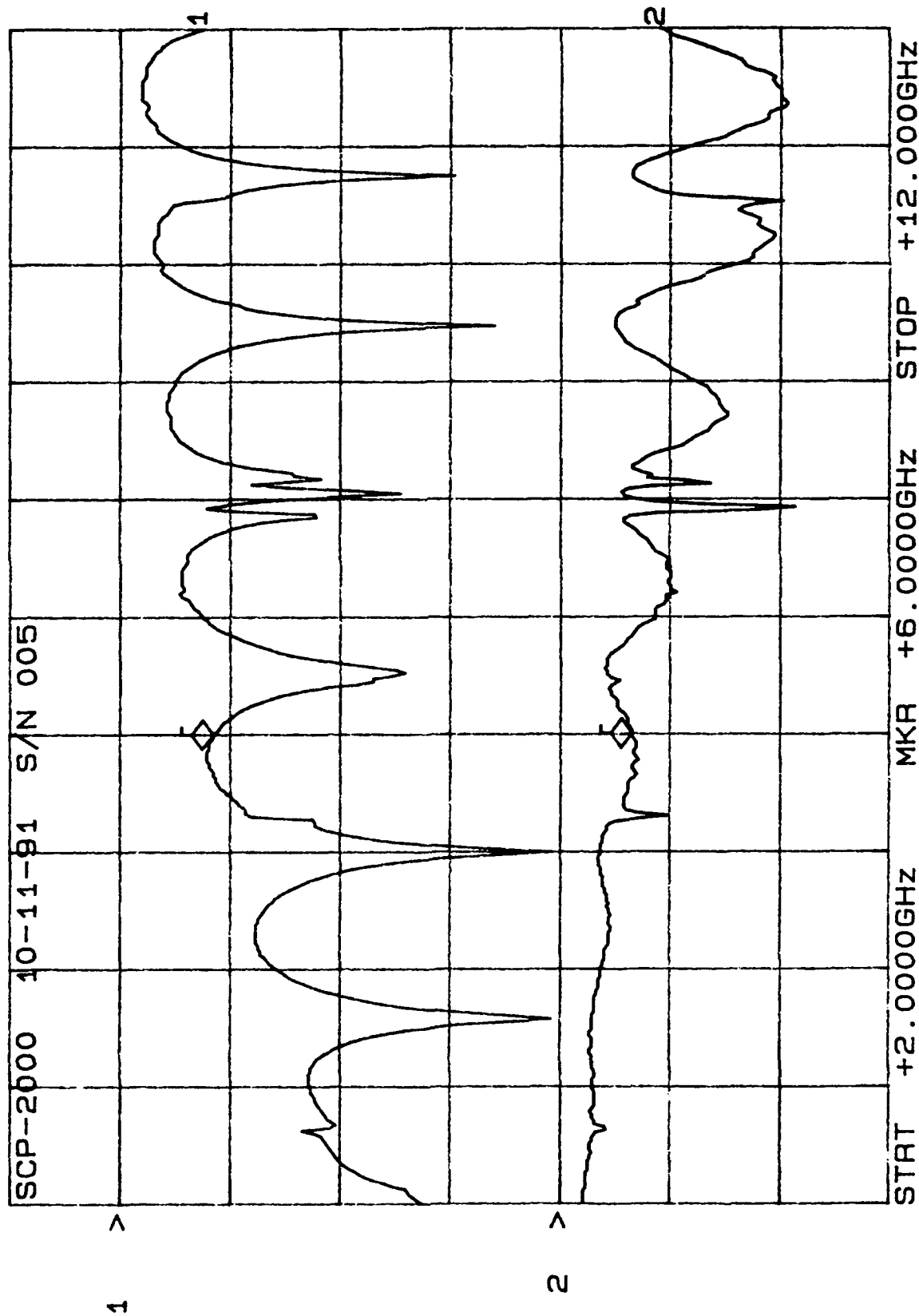
CH1: A -M REF = 7.12 dB CH2: B -M A - 1.59 dB
 10.0 dB/ REF = .00 dB 2.0 dB/ REF + .00 dB



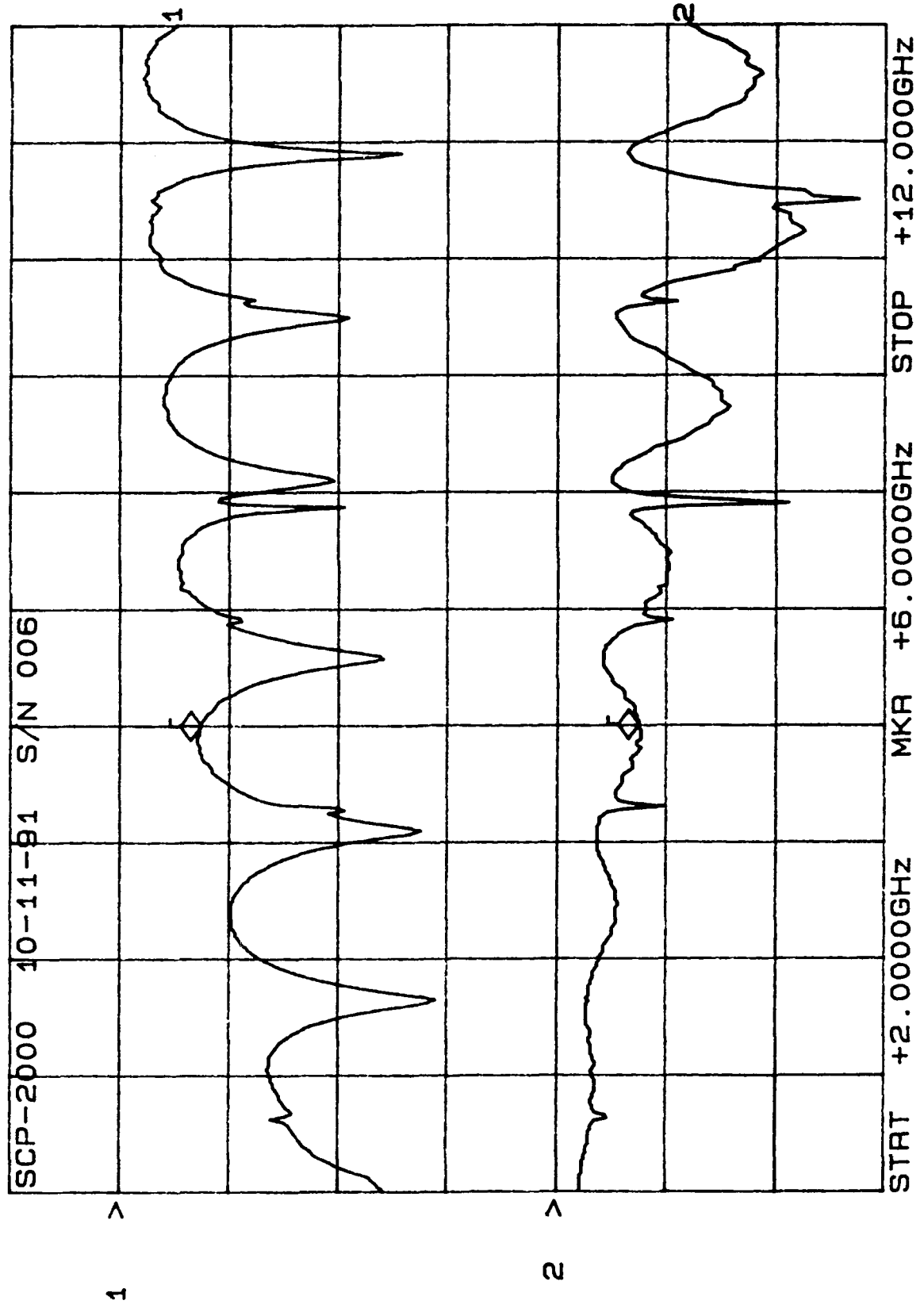
CH1: A -M REF - 9.11 dB CH2: B -M REF + 1.30 dB
 10.0 dB/ REF - .00 dB 2.0 dB/ REF + .00 dB



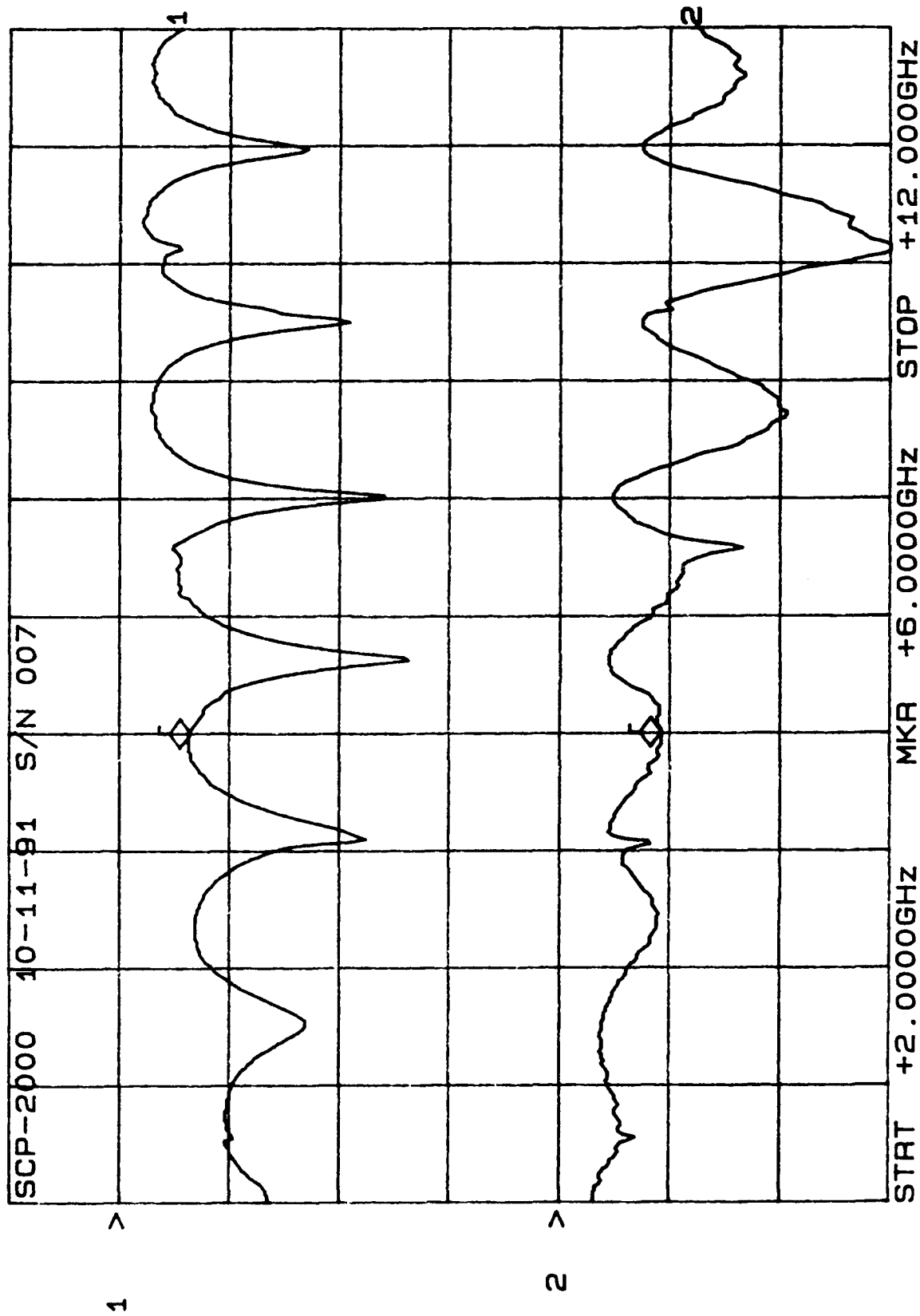
CH1: A -M REF - 8.46 dB CH2: B -M A - 1.29 dB
 10.0 dB/ REF 2.0 dB/ REF + .00 dB



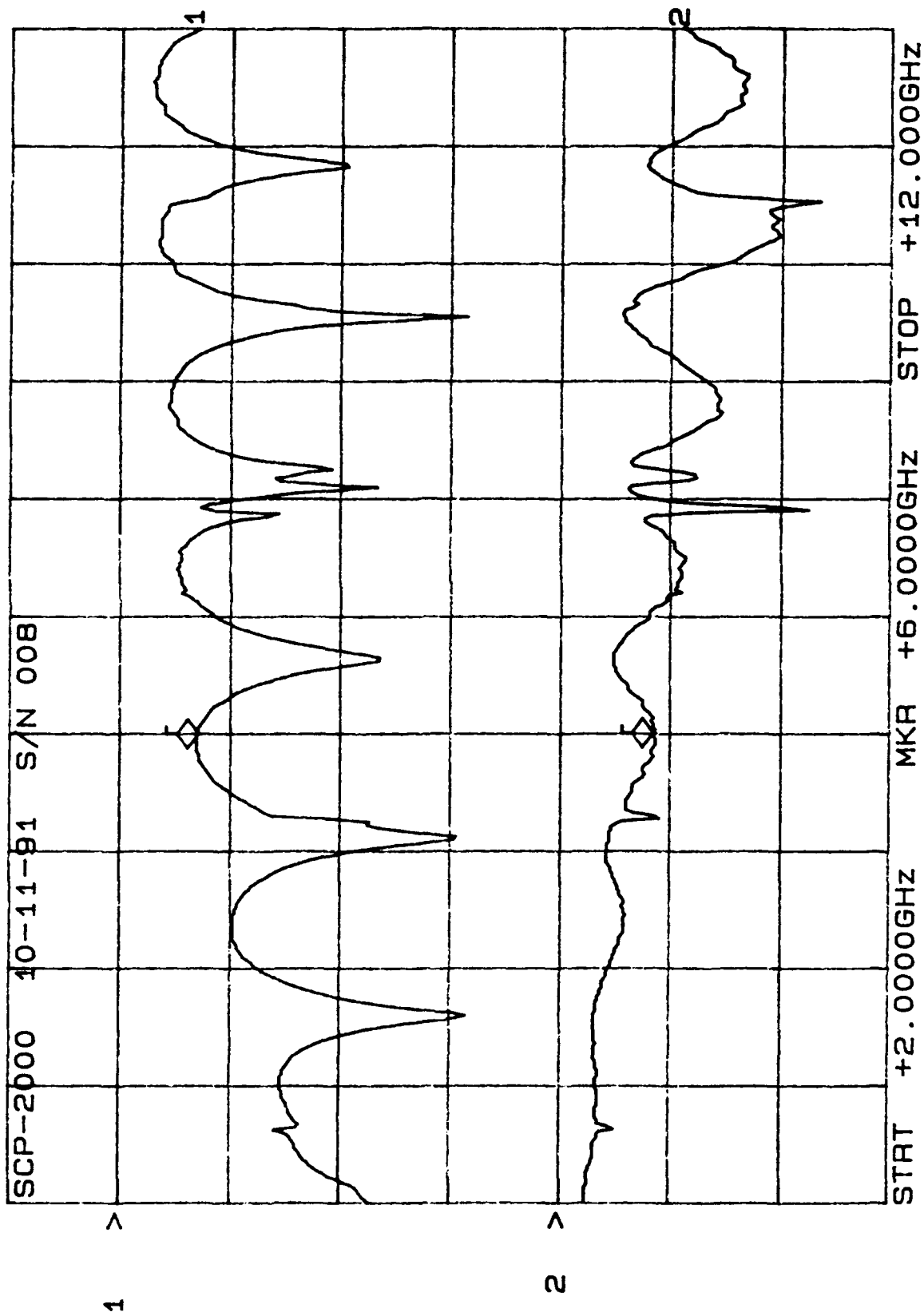
CH1: A -M - 7.36 dB CH2: B -M A - 1.49 dB
 10.0 dB/ REF - .00 dB 2.0 dB/ REF + .00 dB



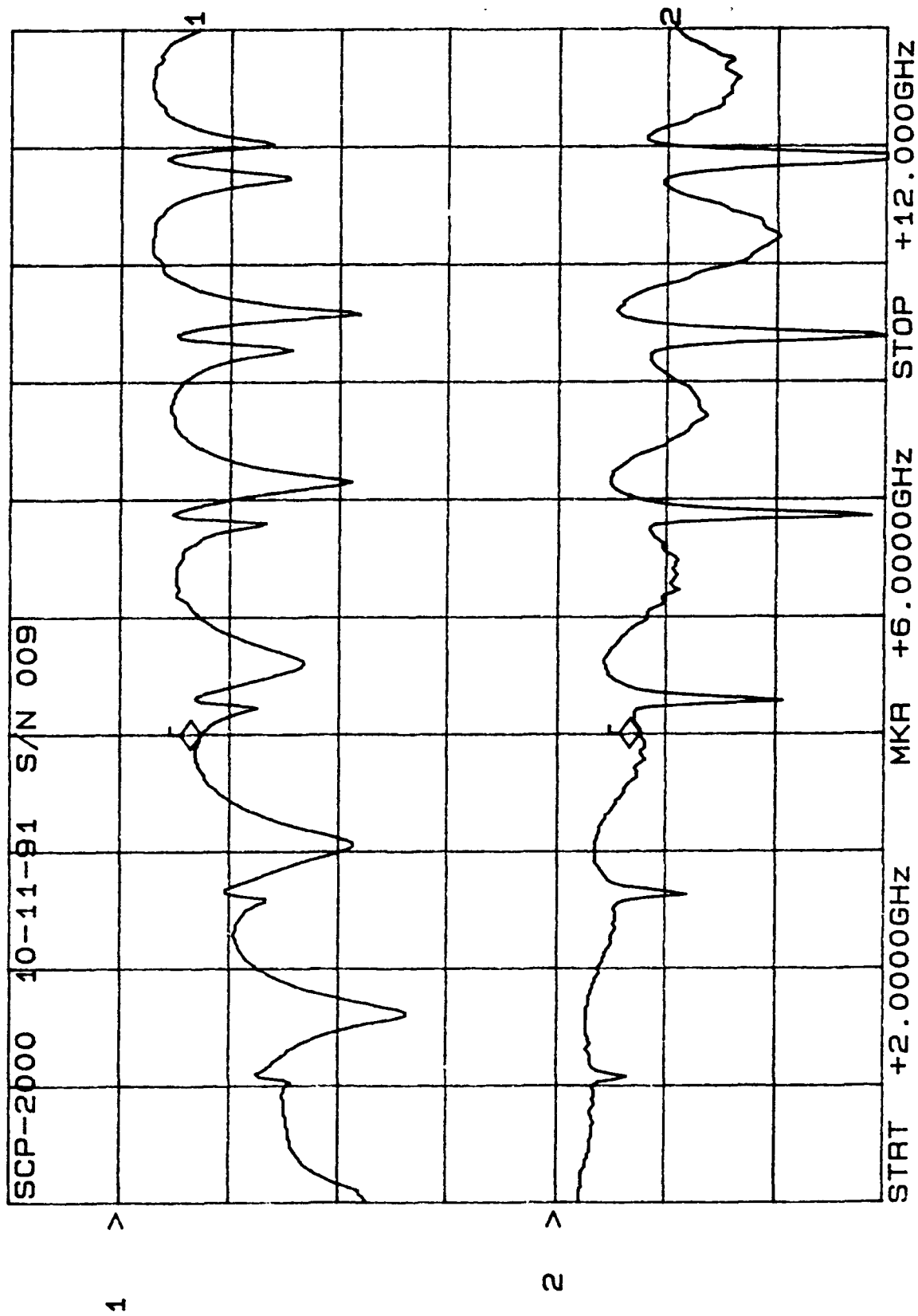
CH1: A -M REF - 6.40 dB CH2: B -M A - 1.81 dB
10.0 dB/ REF 2.0 dB/ REF + .00 dB



CH1: A -M - 6.94 dB CH2: B -M A - 1.69 dB
10.0 dB/ REF - .00 dB 2.0 dB/ REF + .00 dB

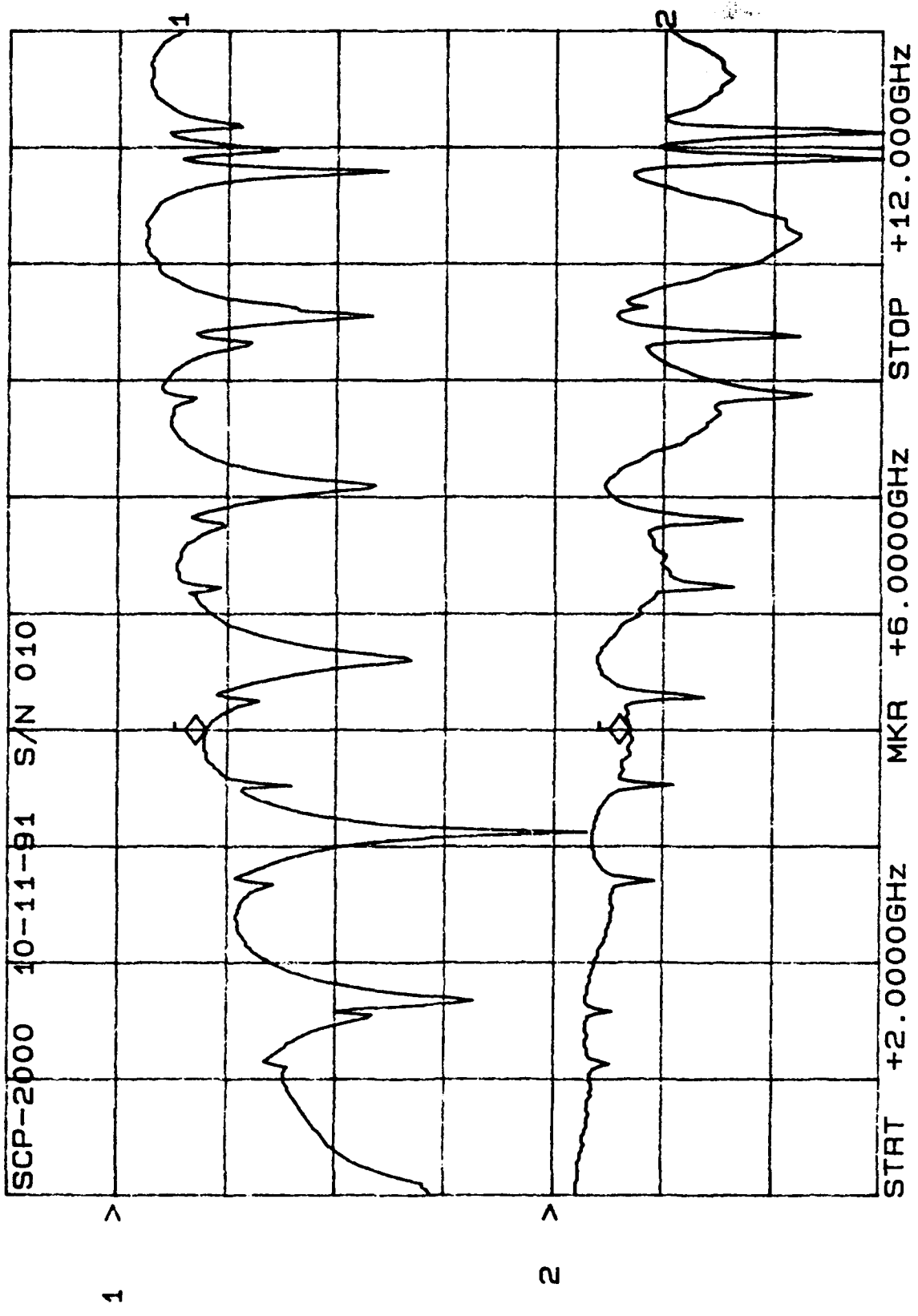


CH1: A -M REF - 7.46 dB
 10.0 dB/ REF + 1.52 dB



After 20 cycles

CH1: A -M - 8.05 dB CH2: B -M A - 1.36 dB
10.0 dB/ REF - .00 dB 2.0 dB/ REF + .00 dB



10 Cycles



After 10 cycles

CERTIFIED TEST
DATA

DEPT # 3020 DIV LOC # 2016

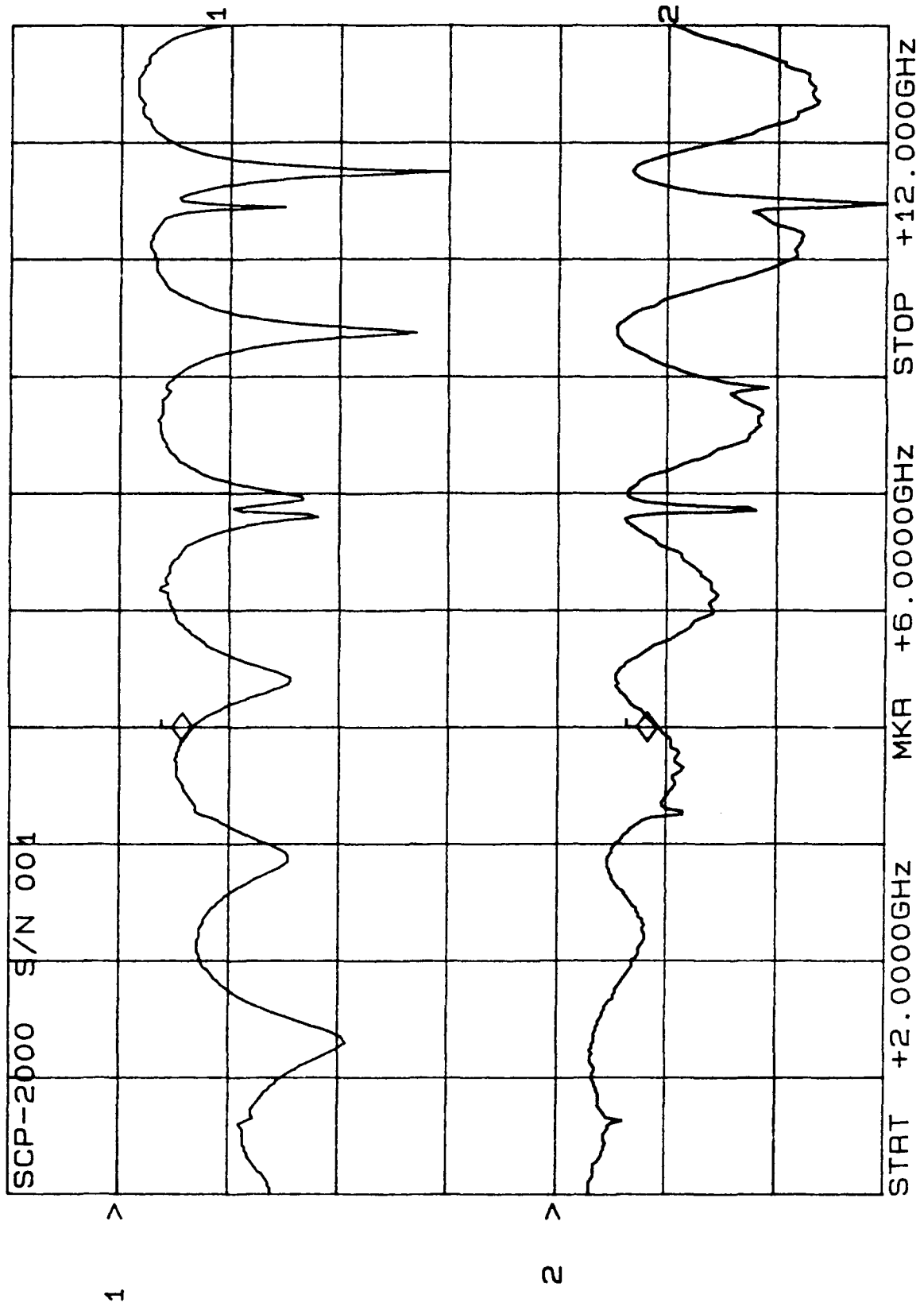


START DATE 10-9-91	CUSTOMER STEVE CHAN EXT # 4361	QUALITY ACCT
COMPL DATE 10-9-91	TYPE OF TEST AVANTEK FINE LEAK TEST J1-32	W/ESS CHARGE # TEST COND. S2016205 A
DEVICE TYPE SEP-2000	TEST REQUIREMENTS MIL STD-883C METHOD 1014.8	BOMB PRESSURE AND DURATION 30 PSI @ 2 hrs
QTY START 10	QTY COMPL 8	SENSITIVITY N/A CC/SEC
S/N LOT No. DIC # 9137	LEAK RATE (CC/SEC)	PASS/FAIL
		DWELL TIME
SN# 001	2 X 10 ⁻⁹	5 min
002	1 X 10 ⁻⁸	
003	5 X 10 ⁻⁹	
004	1 X 10 ⁻⁹	
005	5 X 10 ⁻⁹	
006	5 X 10 ⁻⁹	
007	2 X 10 ⁻⁹	
008	1 X 10 ⁻⁹	
009		
010	2 X 10 ⁻⁶	leak on pin with Red
	2 X 10 ⁻⁶	leak on pin with Red

ARROW
ARROW

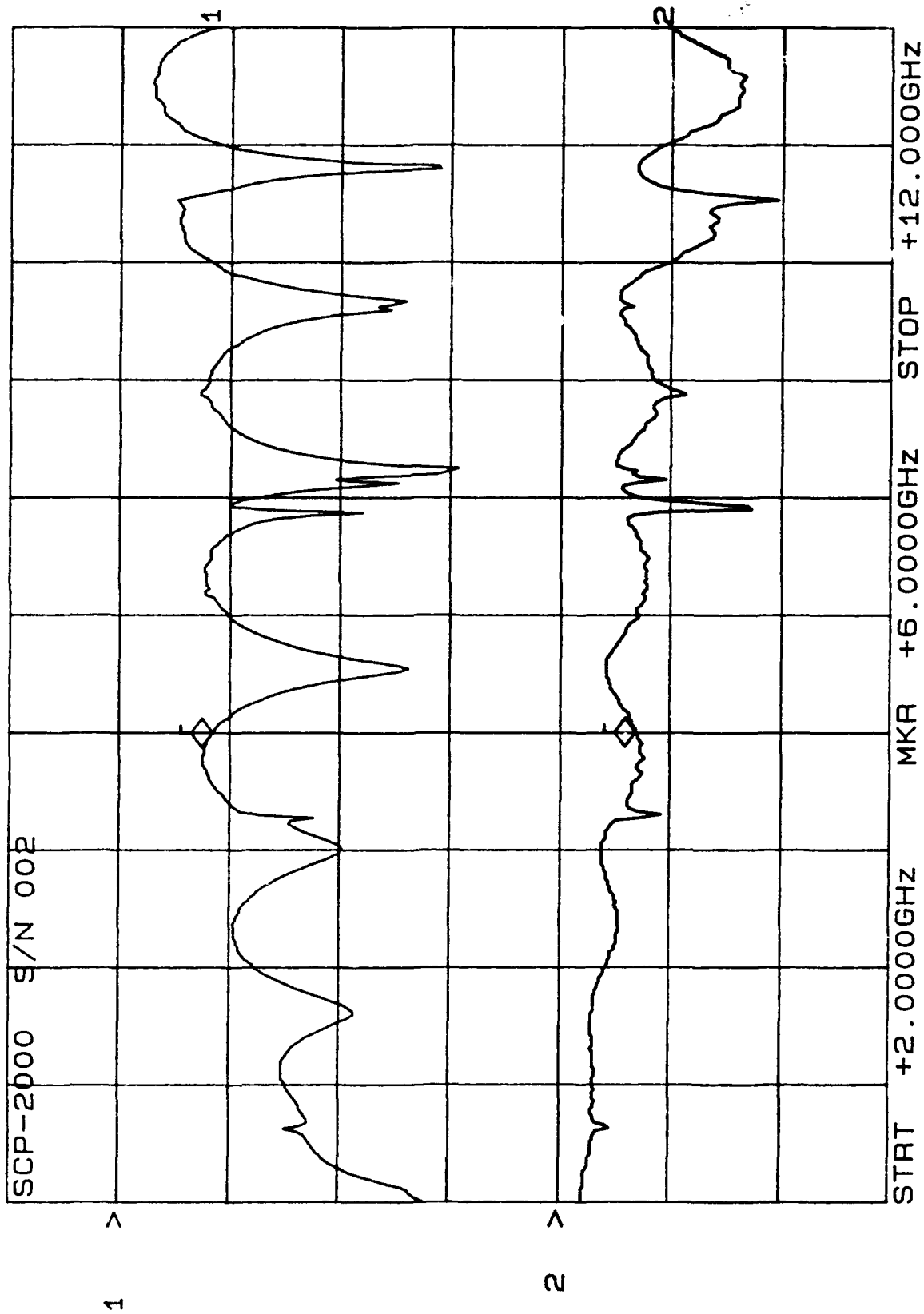
After 70 cycles

CH1: A -M REF - 10.0 dB/ REF - 6.62 dB - 1.81 dB
CH2: B -M REF + 2.0 dB/ REF + .00 dB

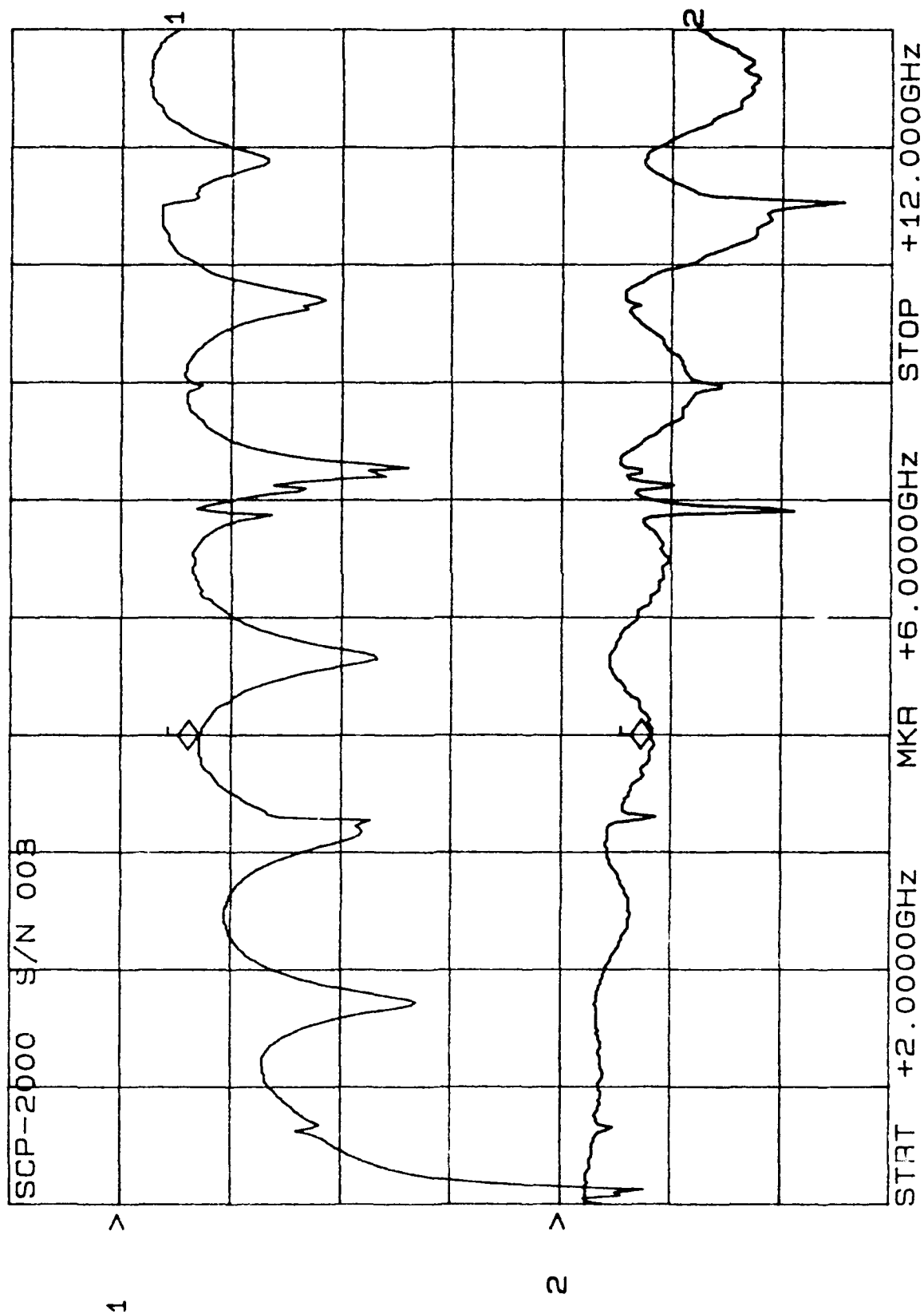


10/1-79/

CH1: A -M REF - 8.30 dB 10.0 dB/ REF - 1.38 dB
CH2: B -M REF + 2.0 dB/ REF + .00 dB

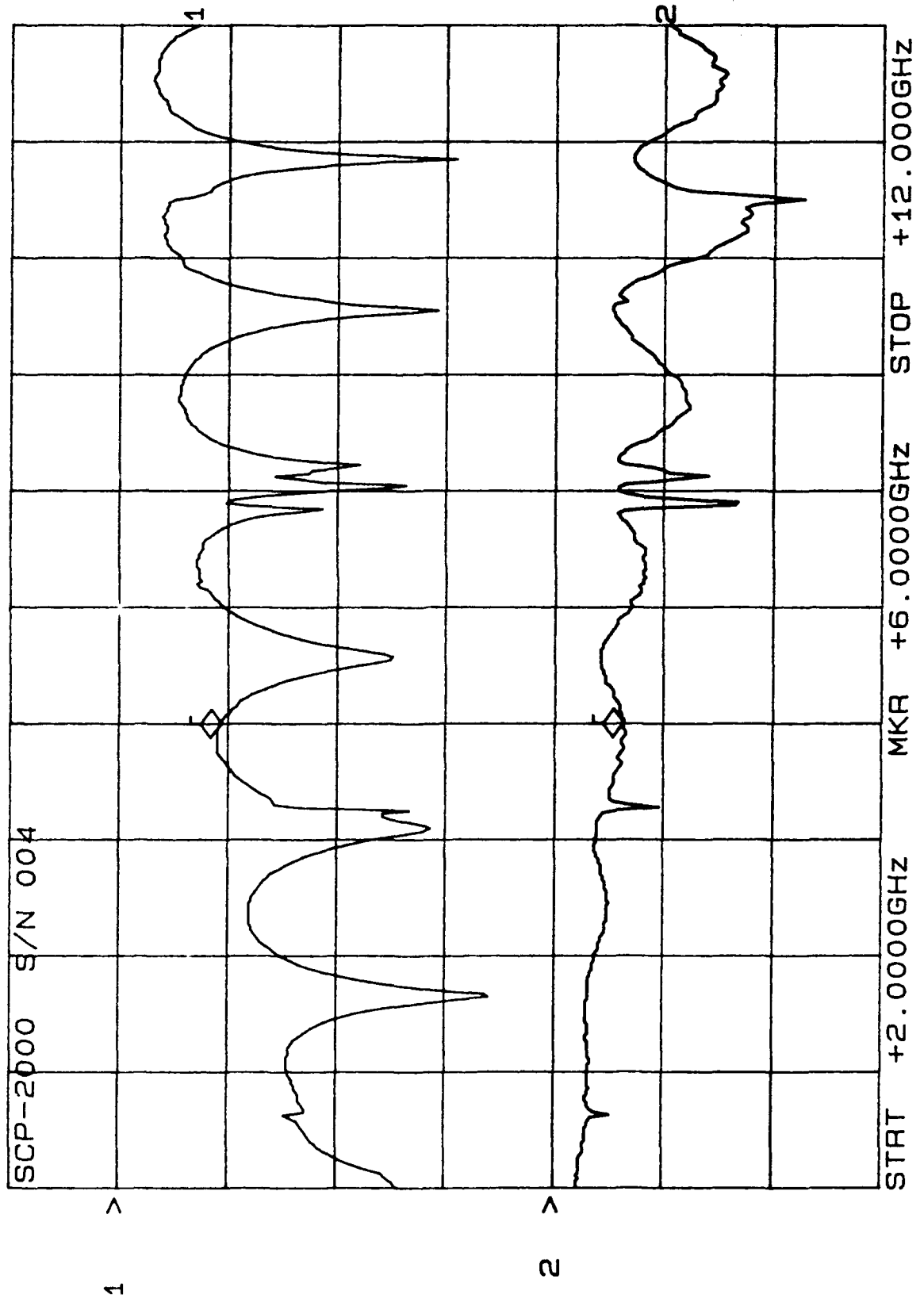


CH1: A -M REF - 7.08 dB CH2: B -M A - 1.63 dB
 10.0 dB/ REF - .00 dB 2.0 dB/ REF + .00 dB

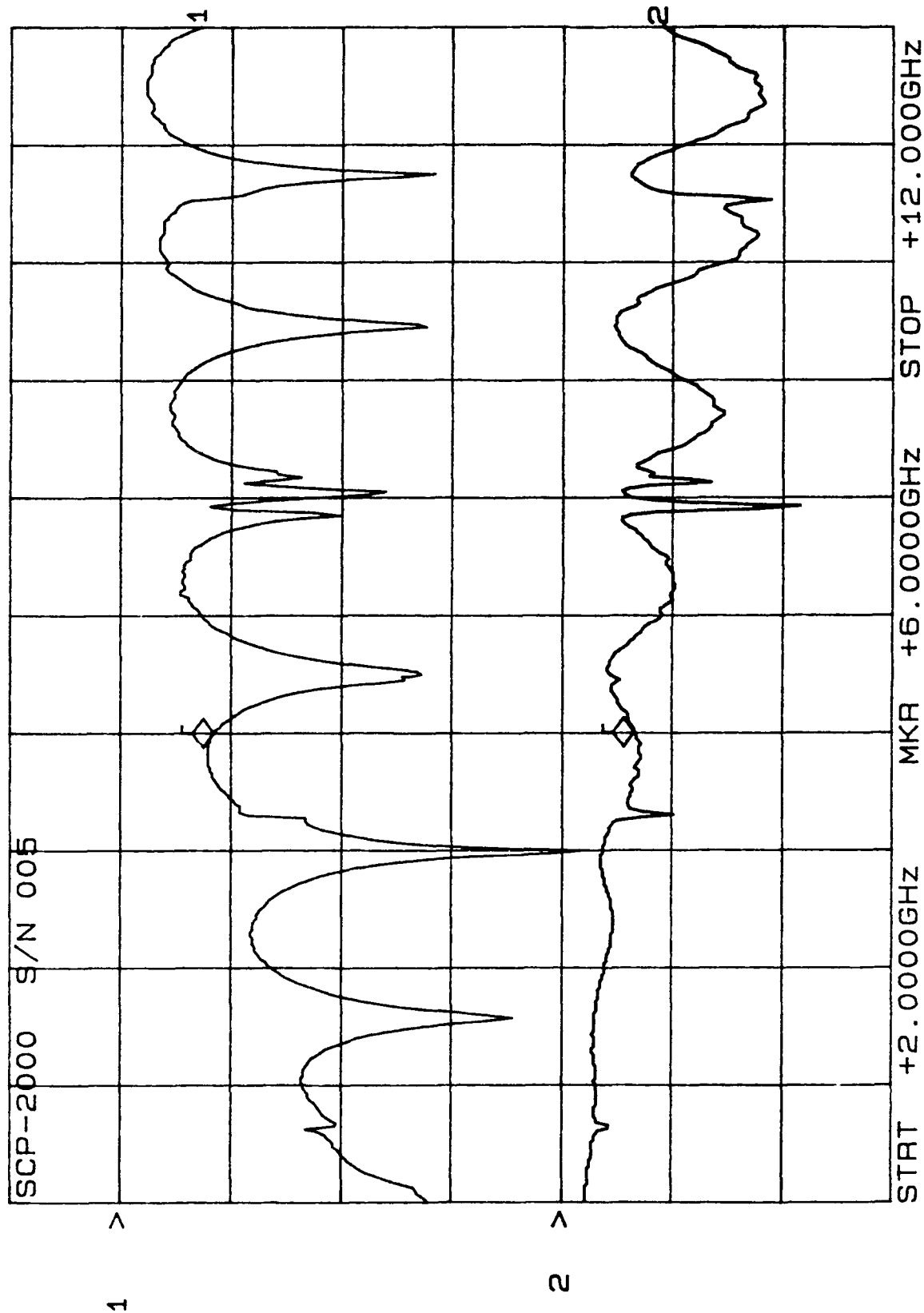


10/21/91

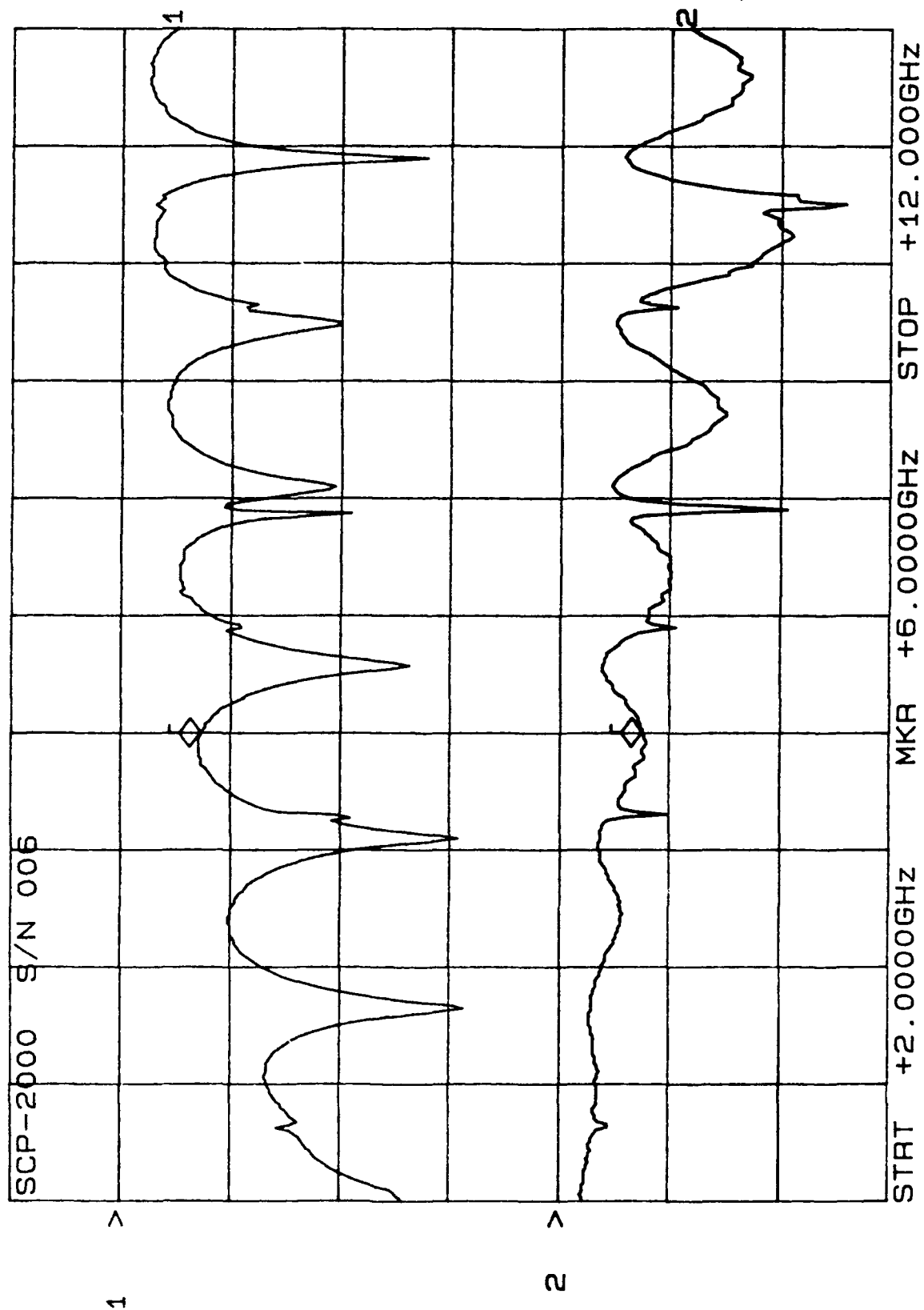
CH1: A -M - 9.24 dB CH2: B -M A - 1.23 dB
10.0 dB/ REF - .00 dB 2.0 dB/ REF + .00 dB



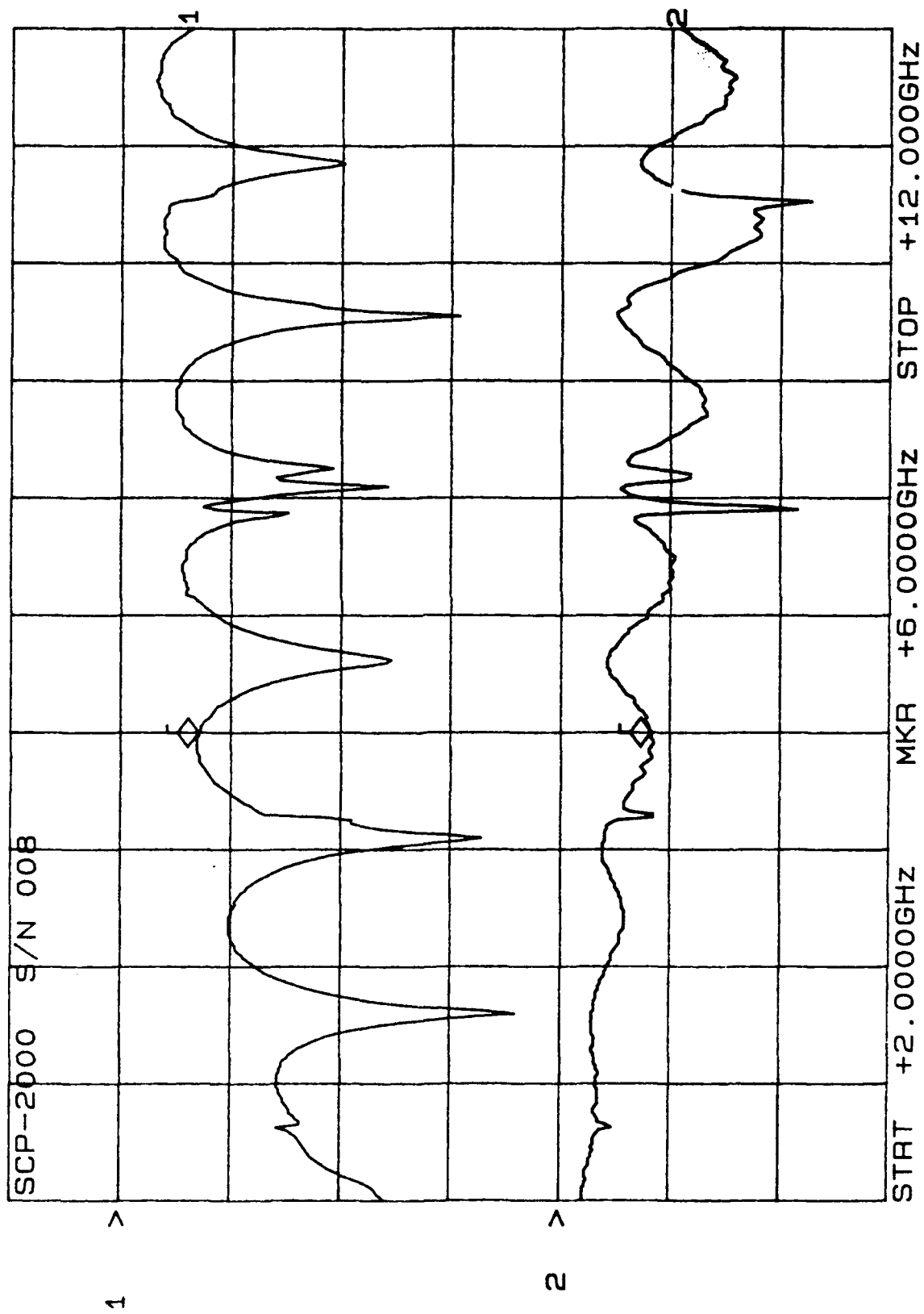
CH1: A -M - 8.42 dB CH2: B -M A - 1.29 dB
 10.0 dB/ REF - .00 dB 2.0 dB/ REF + .00 dB



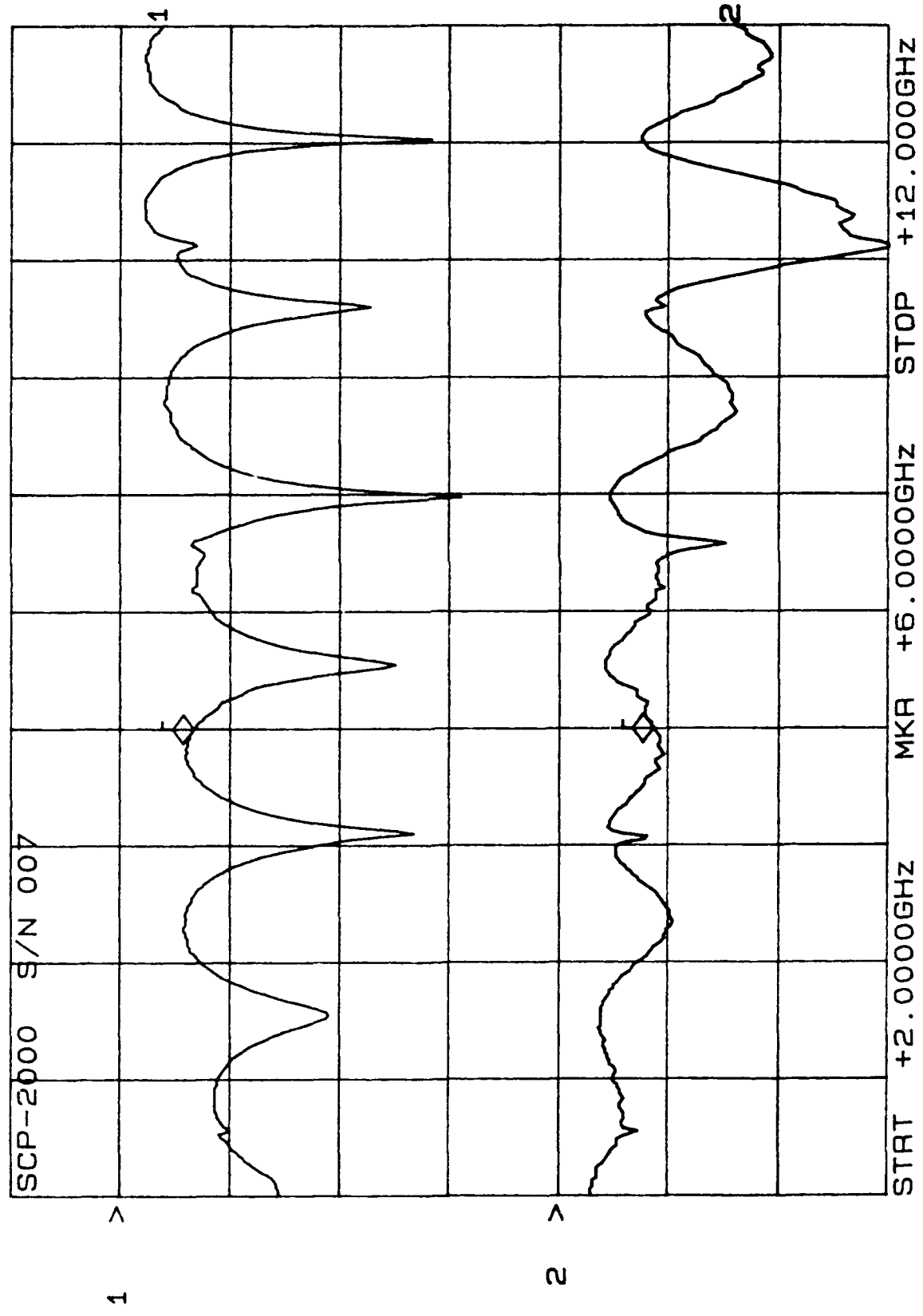
CH1: A -M REF - 7.24 dB CH2: B -M A - 1.49 dB
10.0 dB/ REF 2.0 dB/ REF



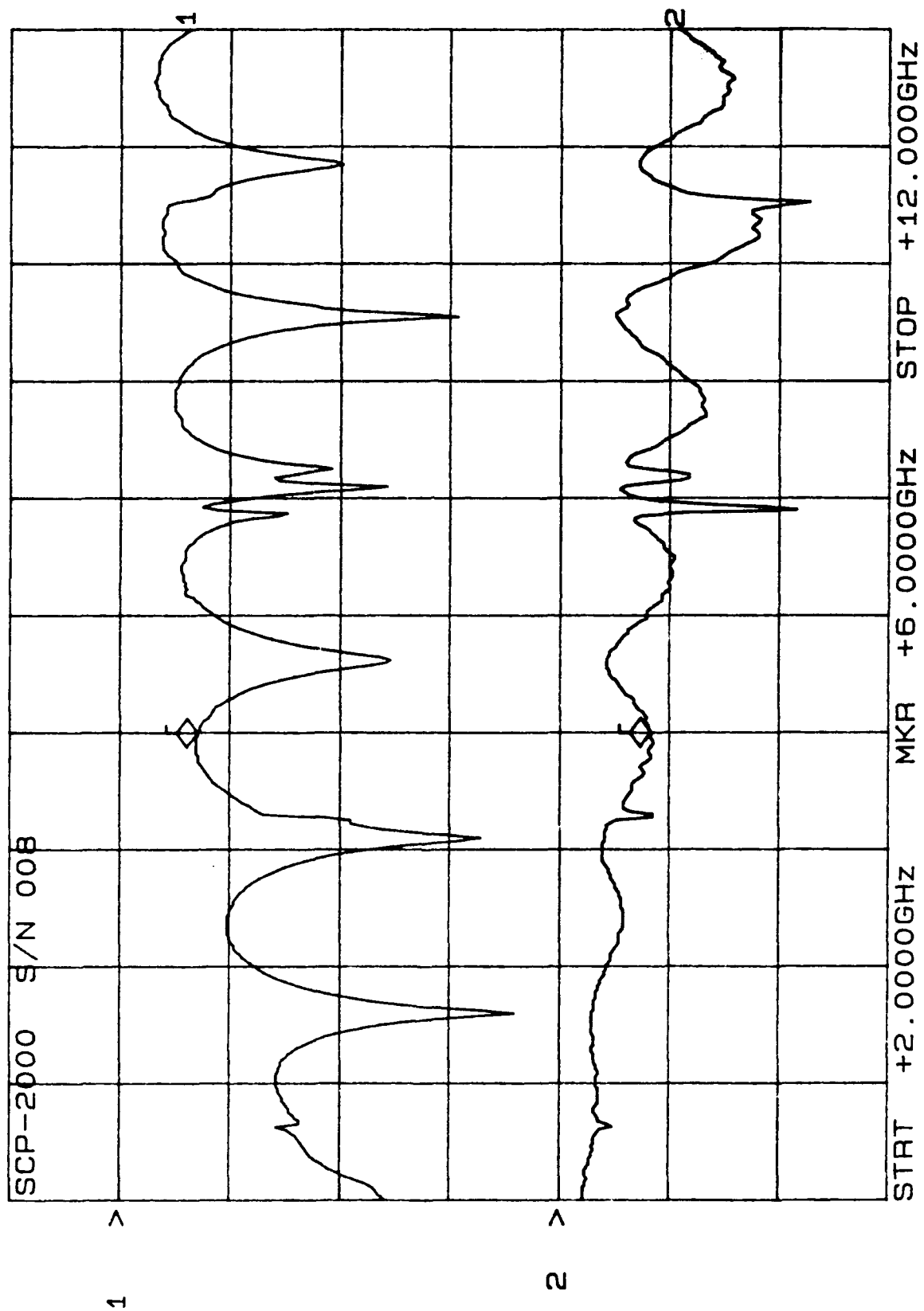
CH1: A -M REF - 7.06 dB CH2: B -M A - 1.62 dB
 10.0 dB/ REF .00 dB 2.0 dB/ REF + .00 dB



CH1: A -M REF - 6.66 dB CH2: B -M A - 1.71 dB
 10.0 dB/ REF - .00 dB 2.0 dB/ REF + .00 dB

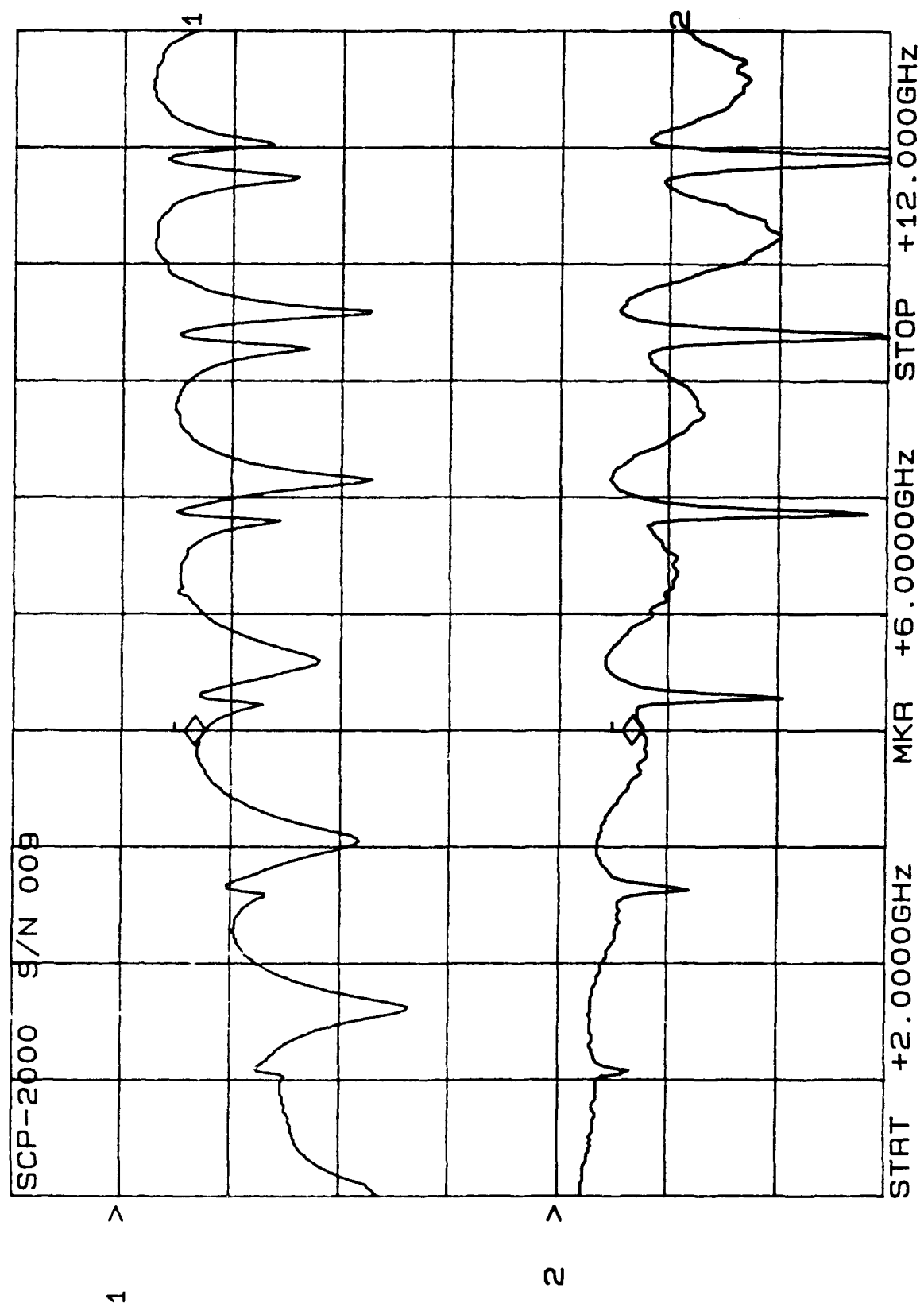


CH1: A -M REF - 7.06 dB 10.0 dB/ REF - 1.62 dB
CH2: B -M REF + 2.0 dB/ REF + .00 dB



10/9

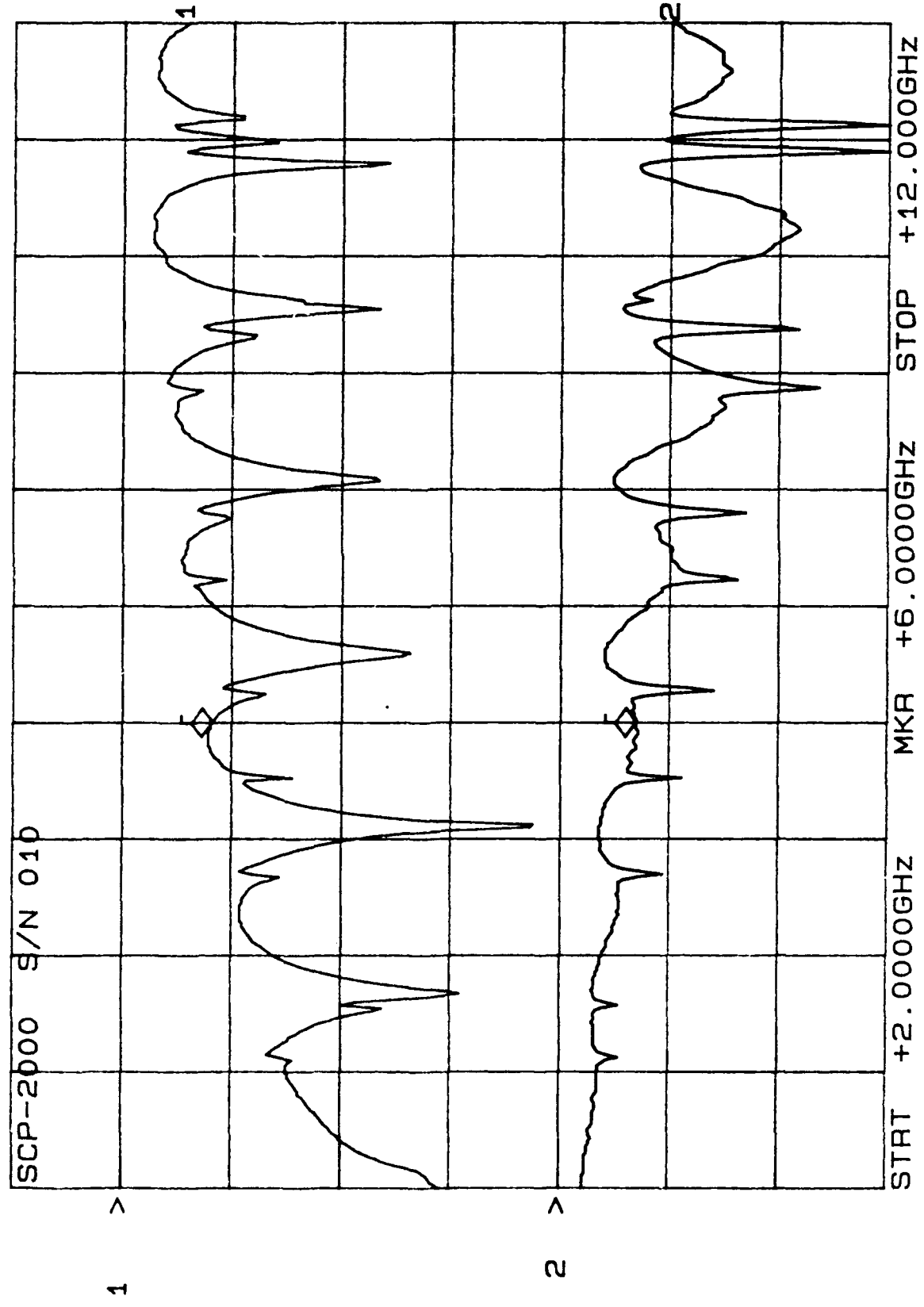
CH1: A -M REF = 7.57 dB CH2: B -M A - 1.52 dB
10.0 dB/ REF = .00 dB 2.0 dB/ REF + .00 dB



10/2/98

CH1: A -M REF - 8.16 dB
10.0 dB/ REF - .00 dB

CH2: B -M A - 1.37 dB
2.0 dB/ REF + .00 dB



5 Cycles



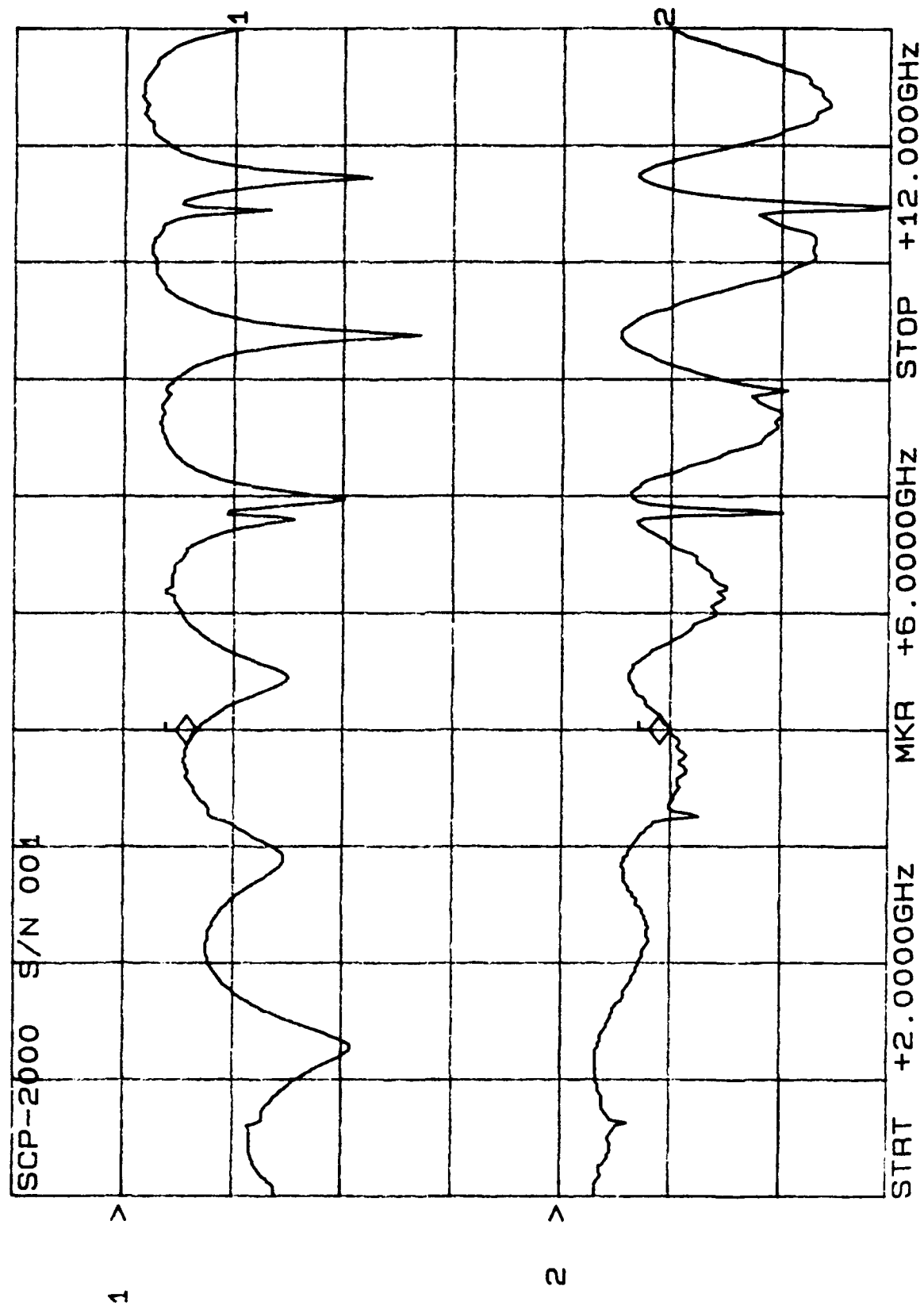
CERTIFIED TEST DATA

After 5 cycles

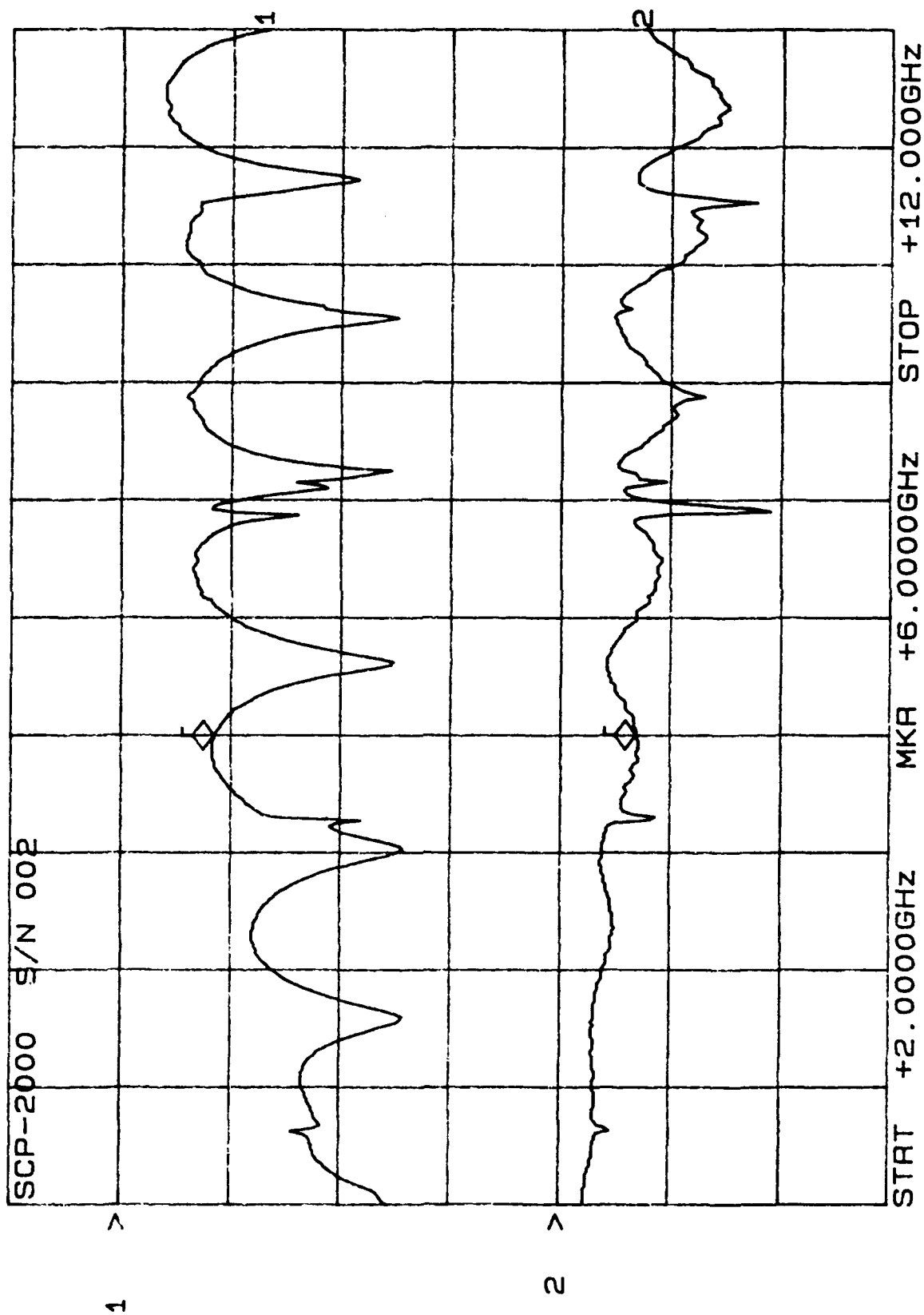
E
ACCEPT
04

START DATE 10-8-91	CUSTOMER Engineering	QUALITY ACCT
COMPL DATE 10-8-91	TYPE OF TEST AVANTEK FINE LEAK TEST J1-32	WO/CSO TEST COND. S2016205 A1
DEVICE TYPE SCP-1000/2000	TEST REQUIREMENTS MIL STD-883C METHOD 1014.8	BOMB PRESSURE AND DURATION
QTY START 10 / 10	QTY COMPL SENSITIVITY 10 / 9 5×10^{-7} CC/SEC	THIS @ 30psig
S/N LOT No.	LEAK RATE (CC/SEC)	PASS/FAIL
001 SCP-2000	1×10^{-9}	PASS
002	1×10^{-9}	
003	1×10^{-8}	
004	3×10^{-9}	
005	1×10^{-9}	
006	1×10^{-9}	
007	1×10^{-9}	
008	2×10^{-9}	
009	1×10^{-9}	
010	1×10^{-6}	FAIL
		DN 92877
001 SCP-1000	2×10^{-9}	PASS
002	5×10^{-9}	
003	2×10^{-9}	
004	2×10^{-9}	
005	5×10^{-9}	
006	3×10^{-9}	
007	2×10^{-9}	
008	1×10^{-9}	
009	4×10^{-8}	
010	1×10^{-9}	

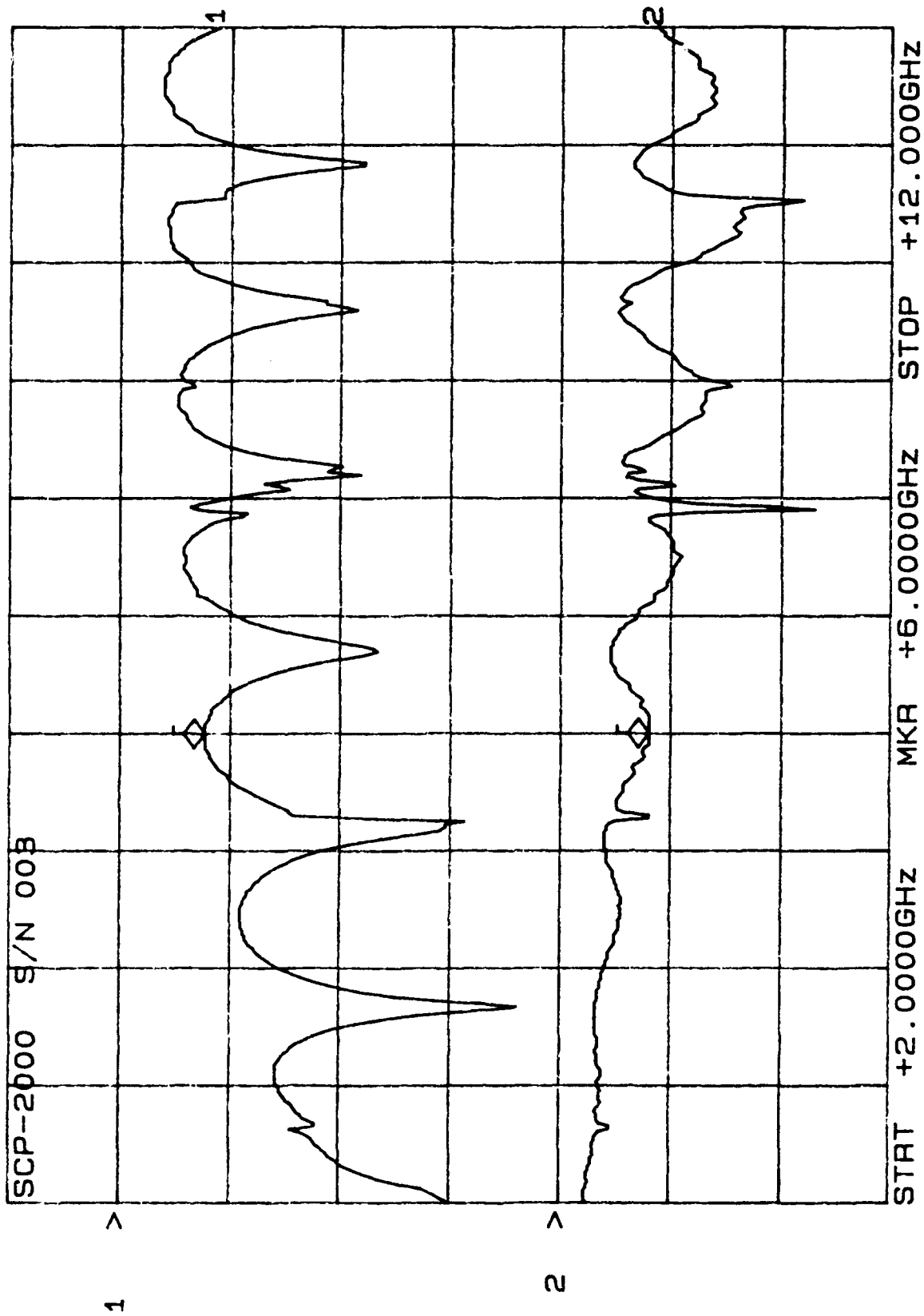
CH1: A -M REF = 6.56 dB CH2: B -M A - 1.96 dB
10.0 dB/ REF = .00 dB 2.0 dB/ REF + .00 dB



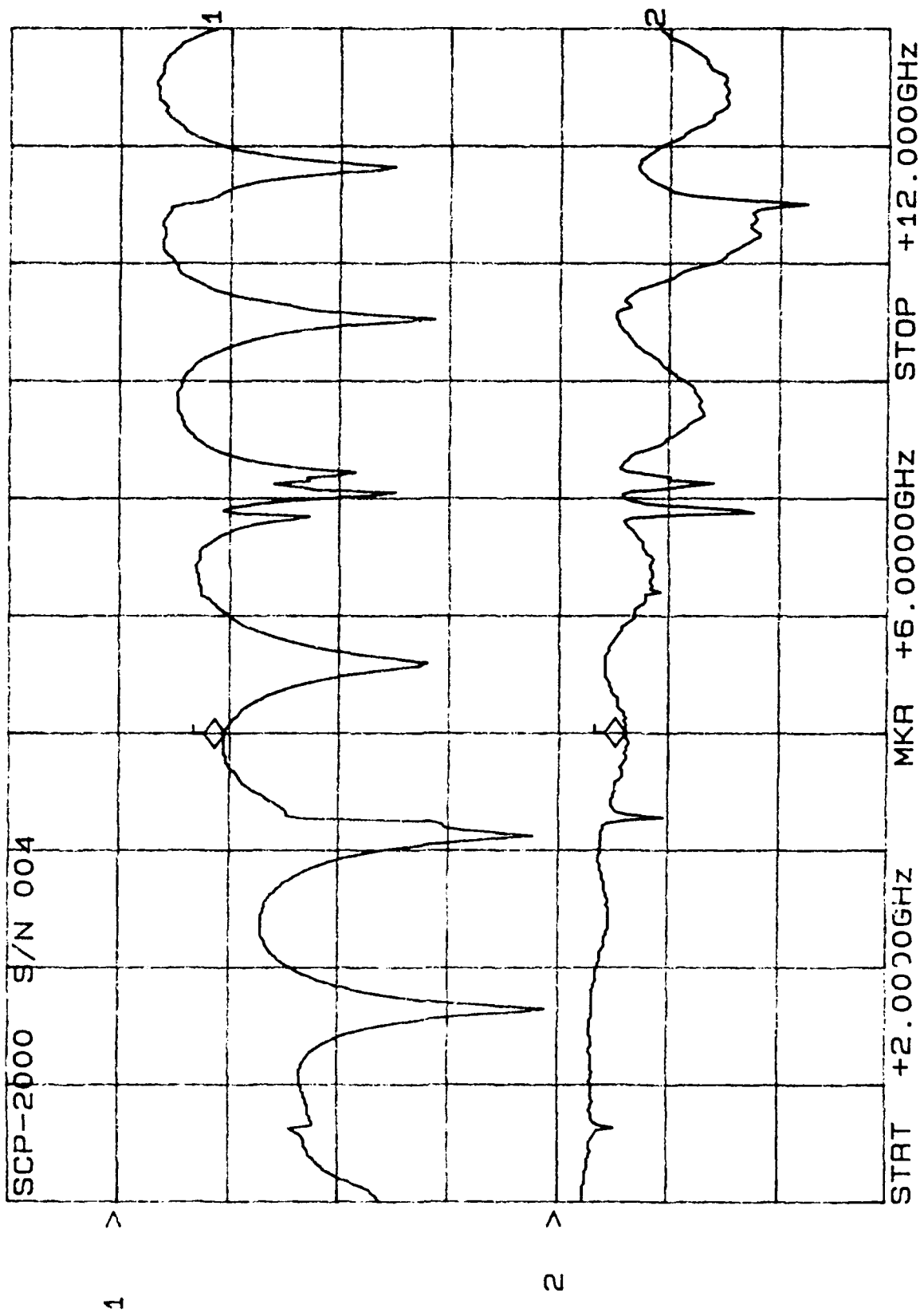
CH1: A -M REF - 8.46 dB CH2: B -M A - 1.37 dB
 10.0 dB/ REF 2.0 dB/ REF + .00 dB



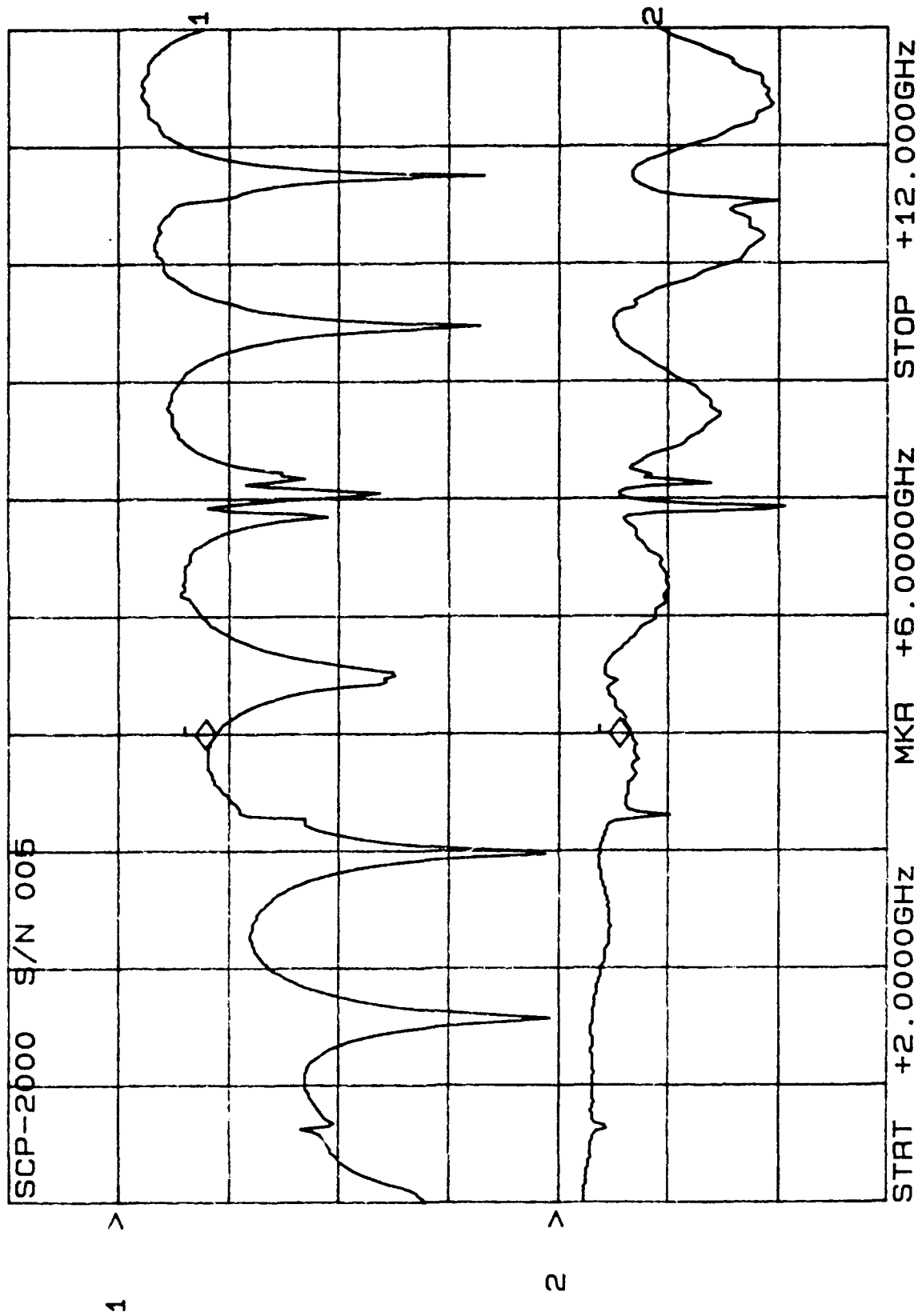
CH1: A -M REF = 7.53 dB CH2: B -M A - 1.59 dB
 10.0 dB/ REF = .00 dB 2.0 dB/ REF + .00 dB



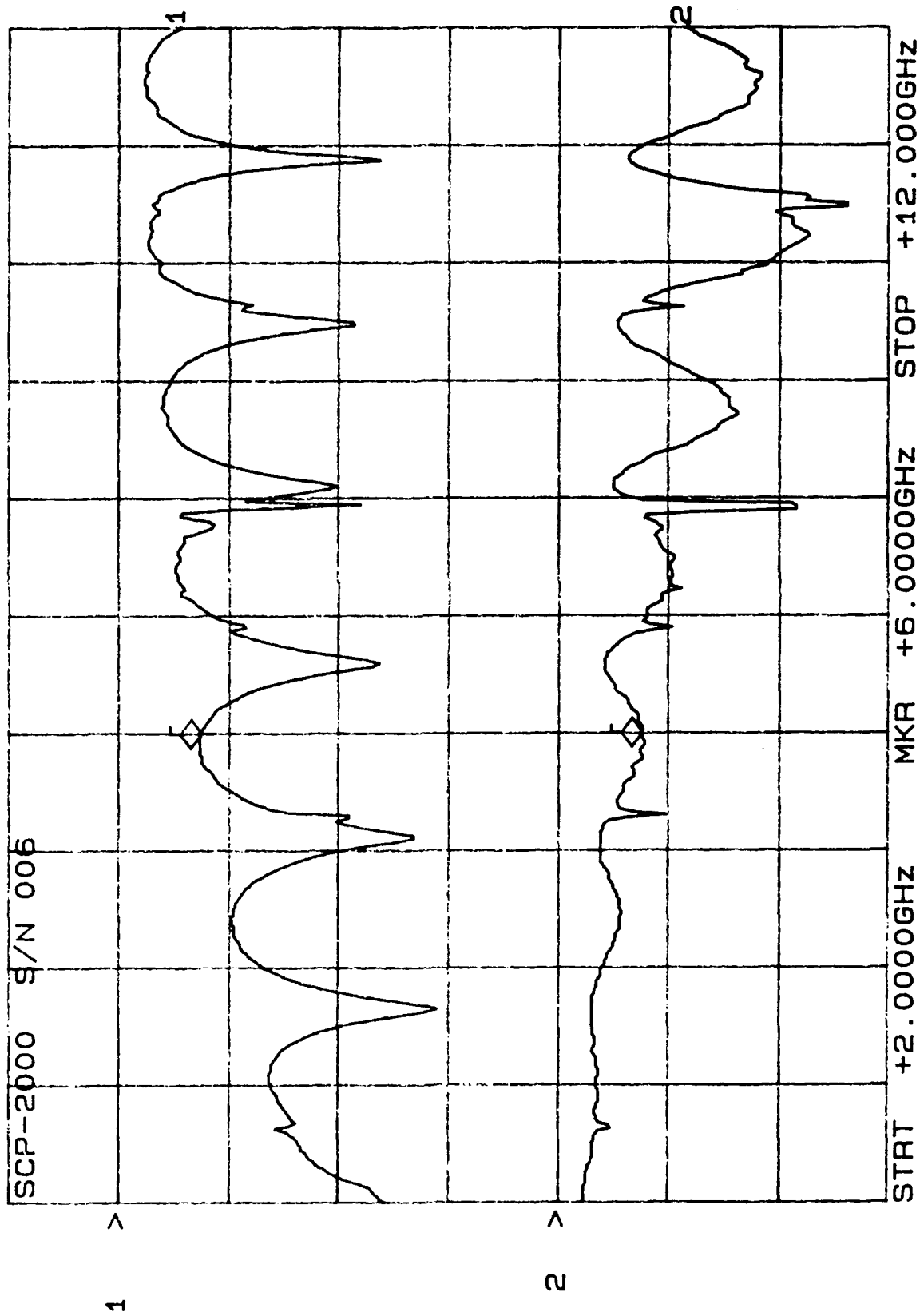
CH1: A -M REF - 9.47 dB 10.0 dB/ REF - 1.22 dB
 CH2: B -M REF + 2.0 dB/ REF + .00 dB



CH1: A -M - 8.67 dB - 1.29 dB
 10.0 dB/ REF - .00 dB 2.0 dB/ REF + .00 dB

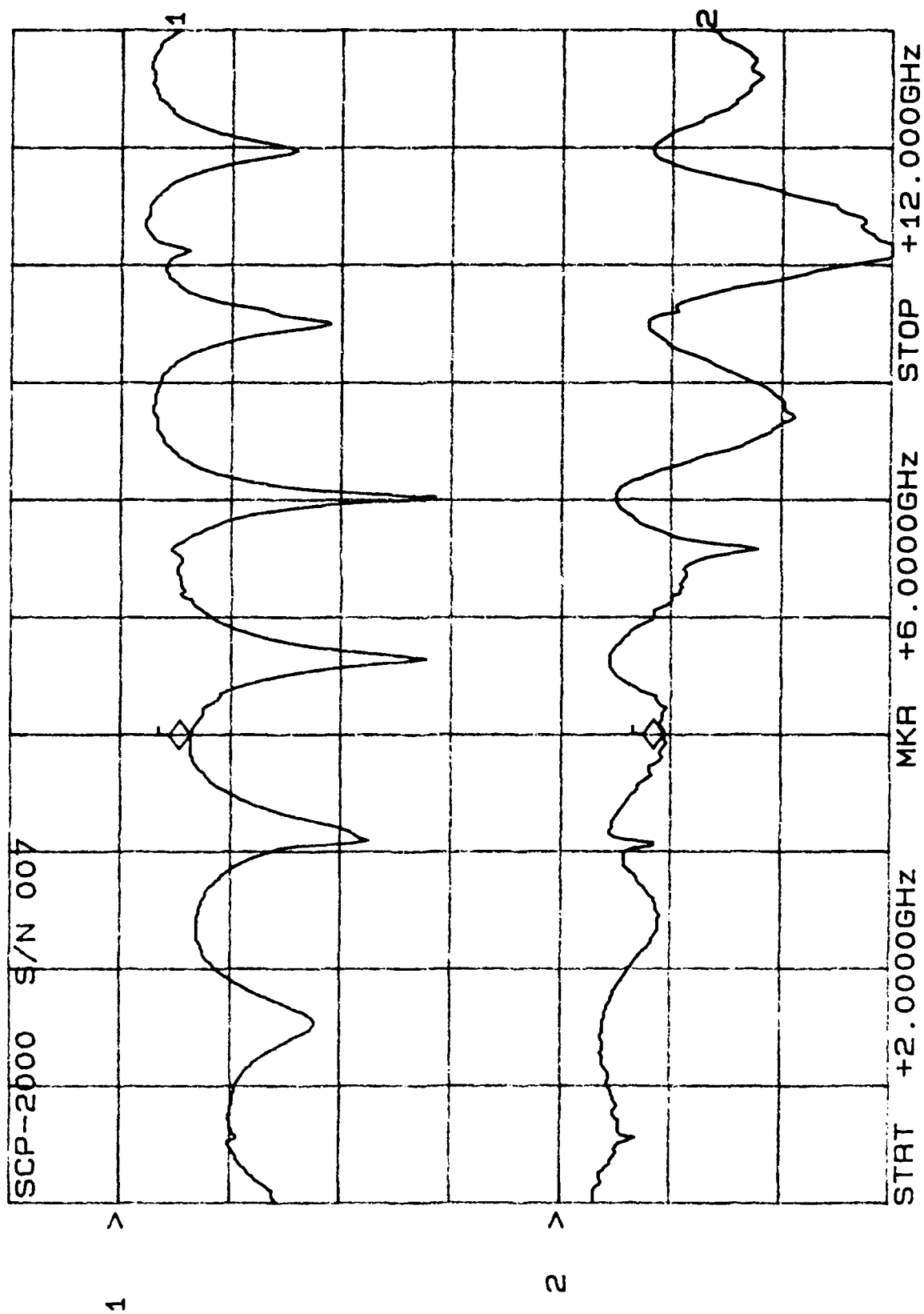


CH1: A -M - 7.35 dB CH2: B -M A - 1.52 dB
 10.0 dB/ REF - .00 dB 2.0 dB/ REF + .00 dB

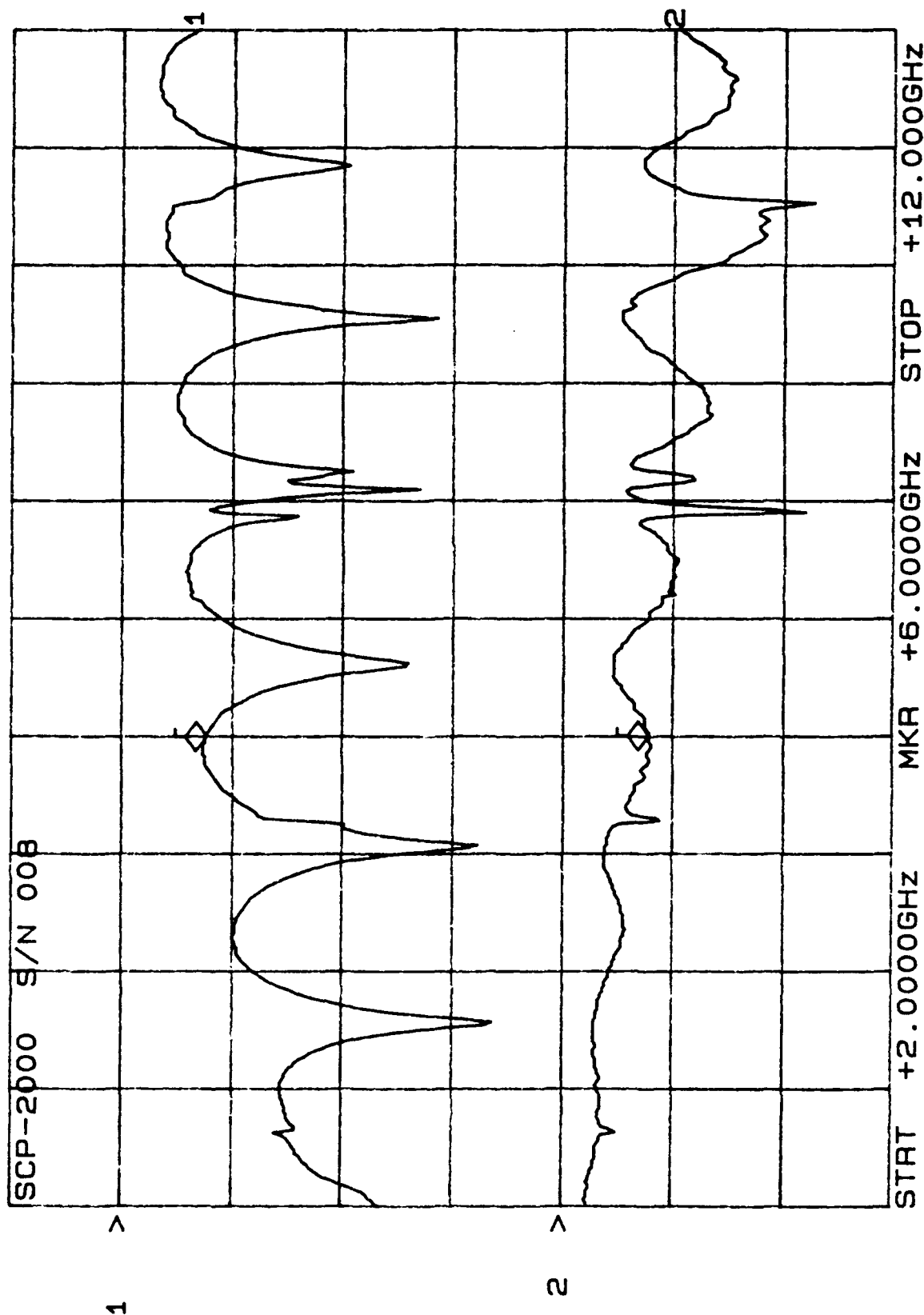


CH1: A -M REF - 6.28 dB
 10.0 dB/ REF - .00 dB

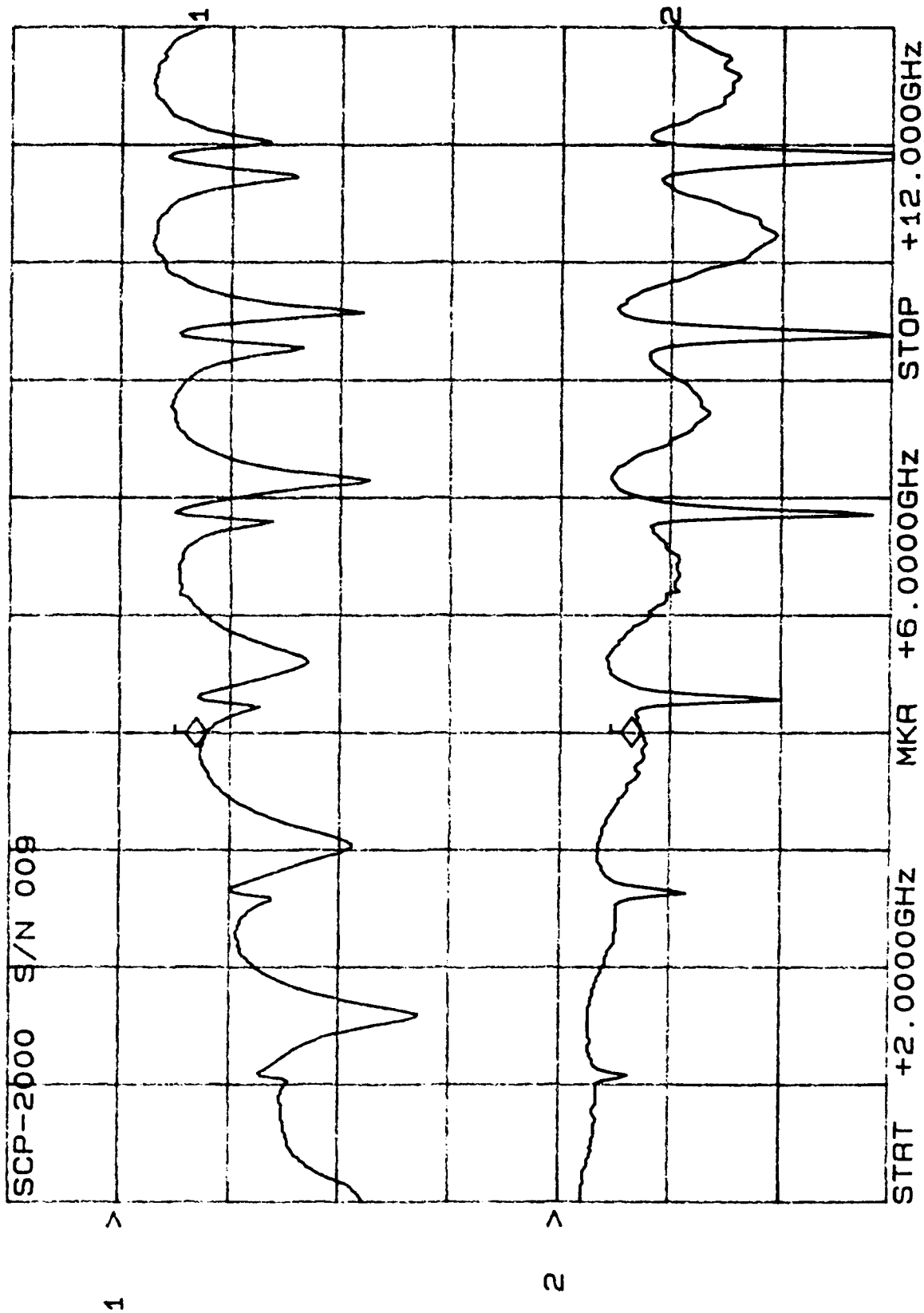
CH2: B -M A - 1.85 dB
 2.0 dB/ REF + .00 dB



CH1: A -M - 7.53 dB - 1.54 dB
10.0 dB/ REF - .00 dB + .00 dB

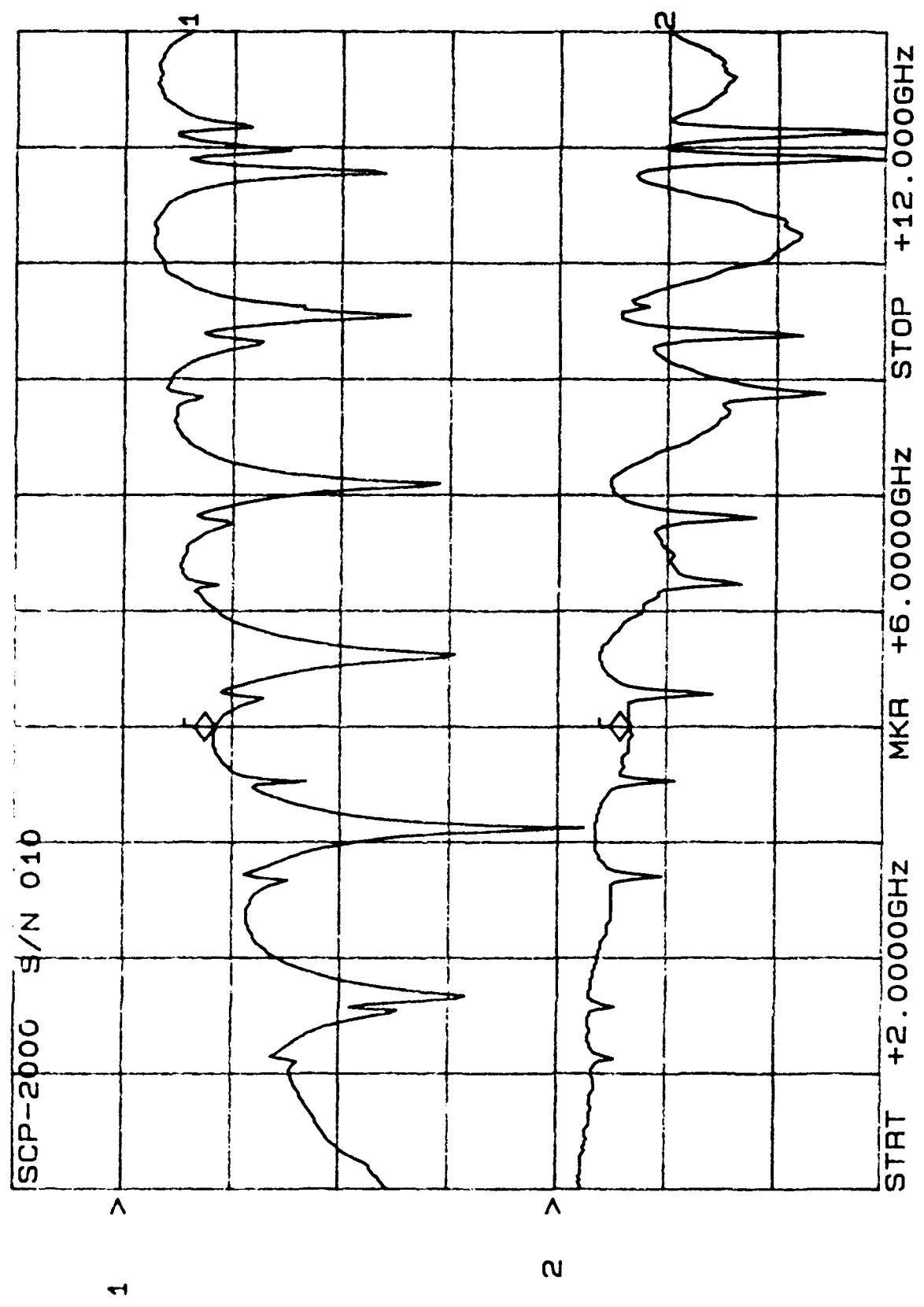


CH1: A -M - 7.86 dB CH2: B -M A - 1.47 dB
10.0 dB/ REF .00 dB 2.0 dB/ REF + .00 dB



After 5 cycles

CH1: A -M REF - 8.39 dB
10.0 dB/ REF - 1.32 dB



0 Cycles

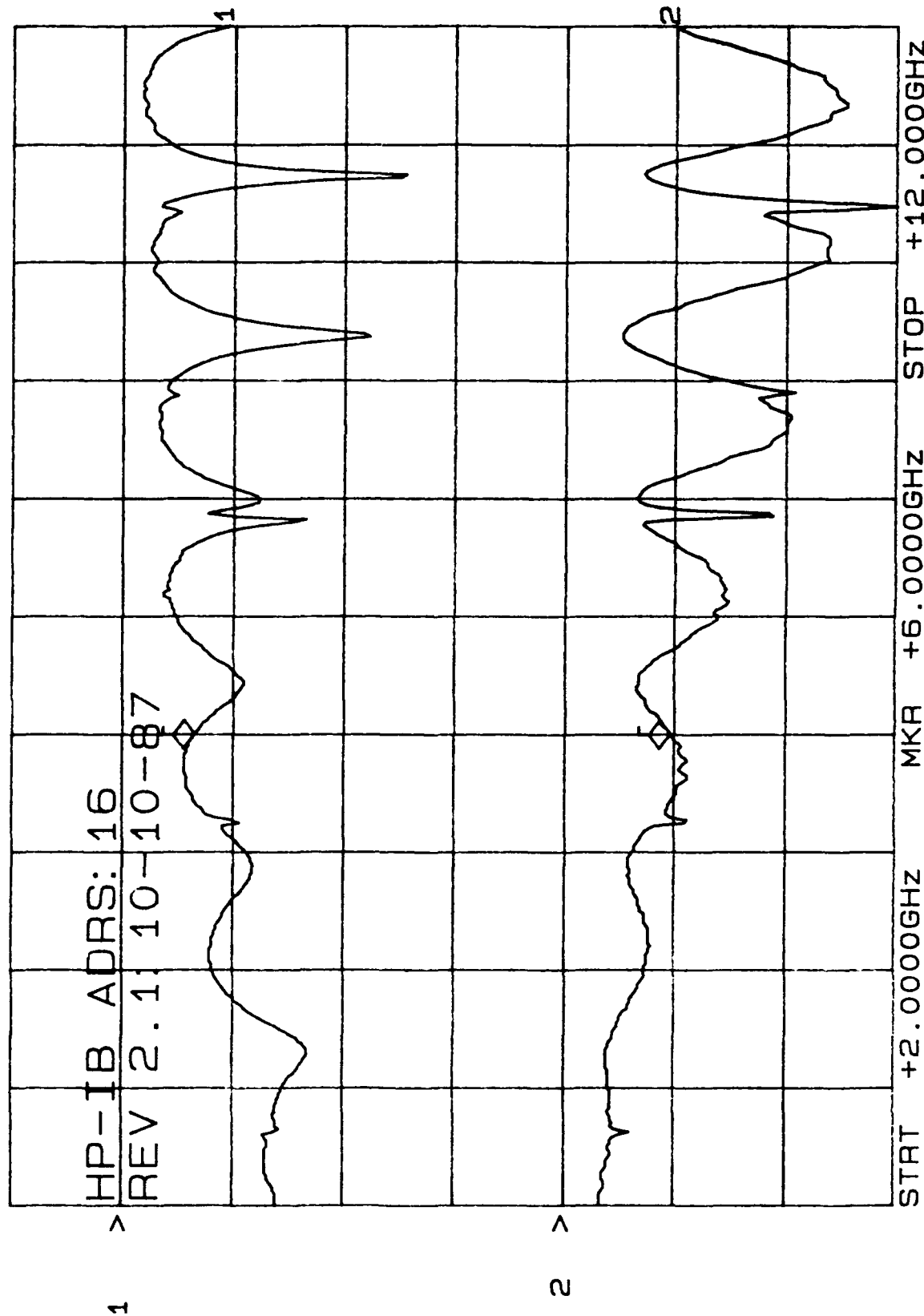
**CERTIFIED TEST
DATA**

Post weld

START DATE	CUSTOMER	QUALITY ACCTPT
9-11-91	Engineering	W0/CSO
COMPL DATE 9-11-91	TYPE OF TEST AVANTEK FINE LEAK TEST JI-32	TEST COND A1
DEVICE TYPE SLP-2000	TEST REQUIREMENTS MIL STD-883C METHOD 1014.8	BOMB PRESSURE AND DURATION Zhs @ 30psig
QTY START 10	QTY COMPL SENSITIVITY 10 2×10^{-7} CC/SEC	
S/N LOT No.	LEAK RATE (CC/SEC)	PASS/FAIL
01	$< 1 \times 10^{-8}$	PASS
02	$< 1 \times 10^{-8}$	
03	$< 5 \times 10^{-9}$	
04	$< 2 \times 10^{-9}$	
05	$< 3 \times 10^{-9}$	
06	$< 3 \times 10^{-9}$	
07	$< 5 \times 10^{-9}$	
08	$< 2 \times 10^{-9}$	
09	$< 2 \times 10^{-9}$	
10	$< 2 \times 10^{-9}$	
DWELL TIME		
10 min.		

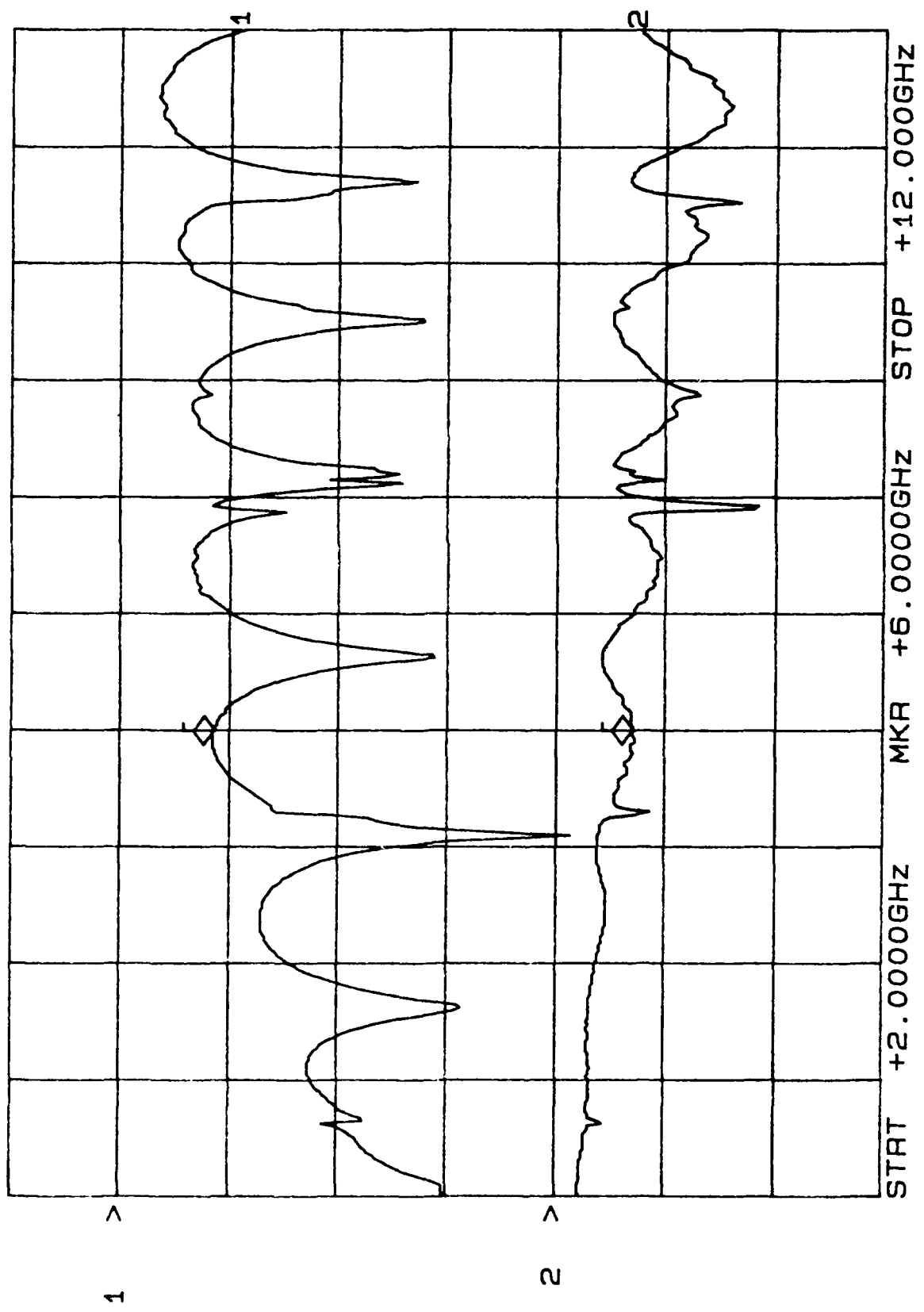


CH1: A -M REF - 6.40 dB CH2: B -M REF + 1.91 dB
10.0 dB/ REF 2.0 dB/



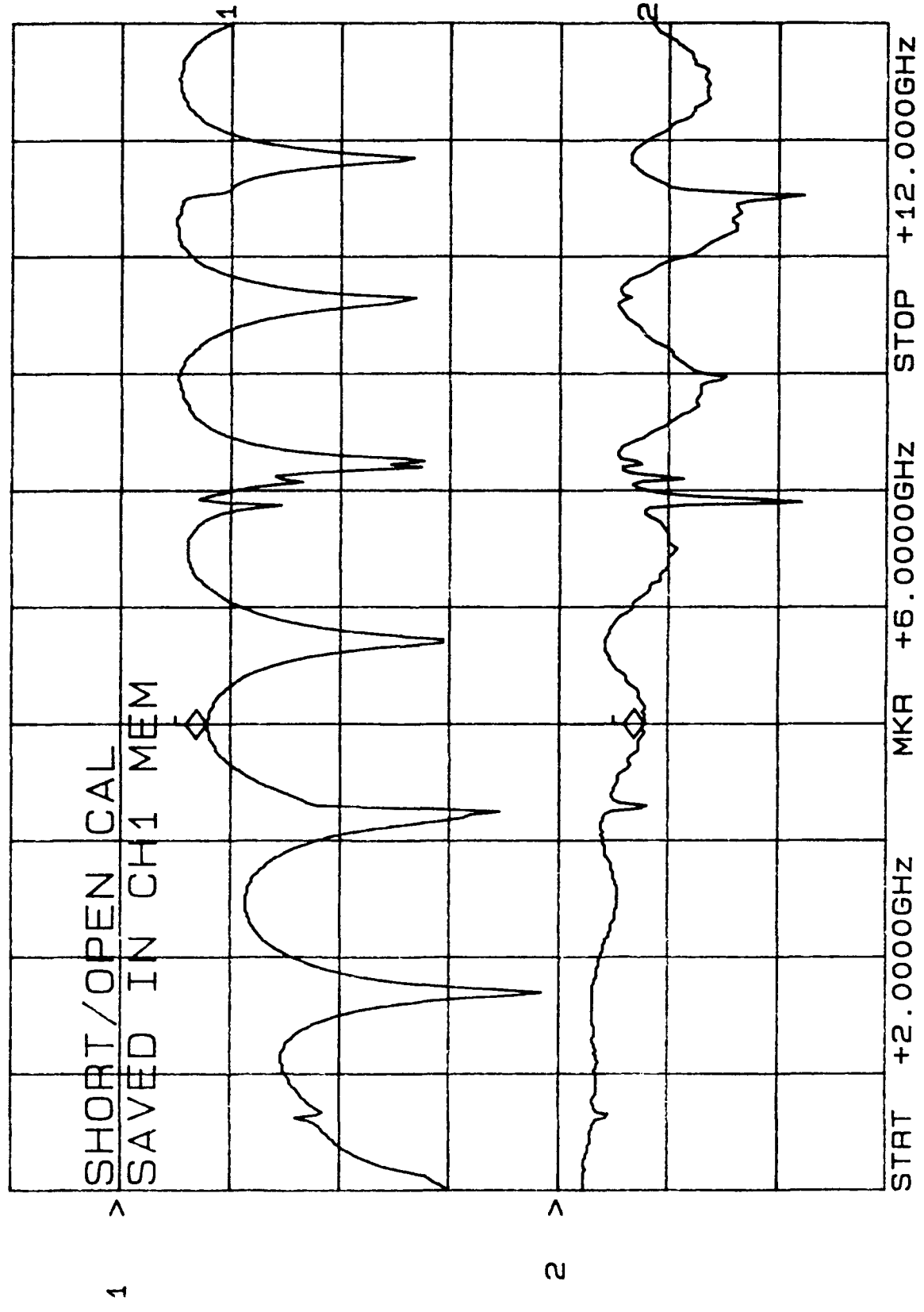
SCP-2000 Post weld 96

CH1: A -M REF - 8.51 dB
10.0 dB/ REF + 1.39 dB
CH2: B -M REF + 1.00 dB
2.0 dB/ REF

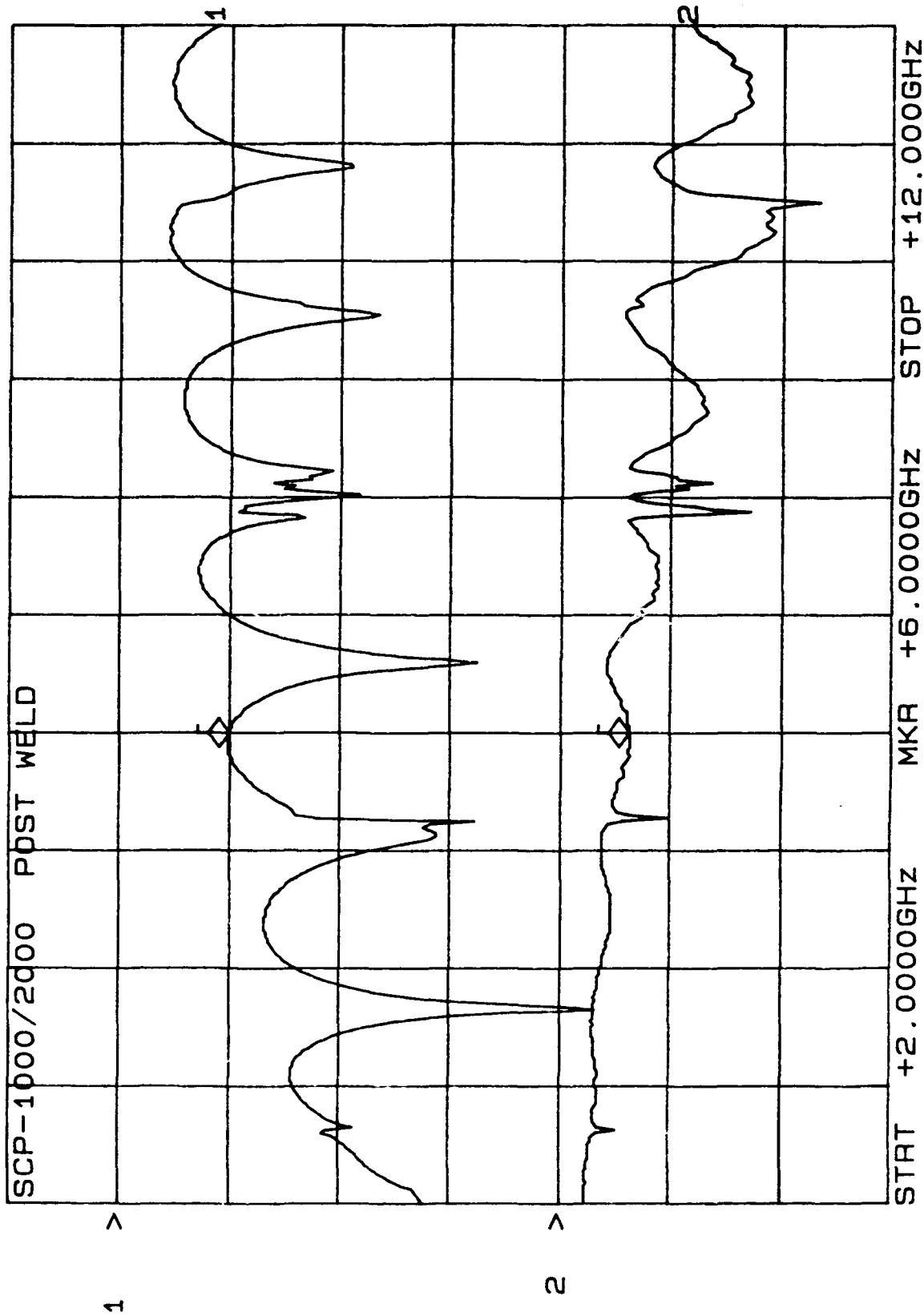


SCP-2000 Post-weld SYN 003 9/10/81

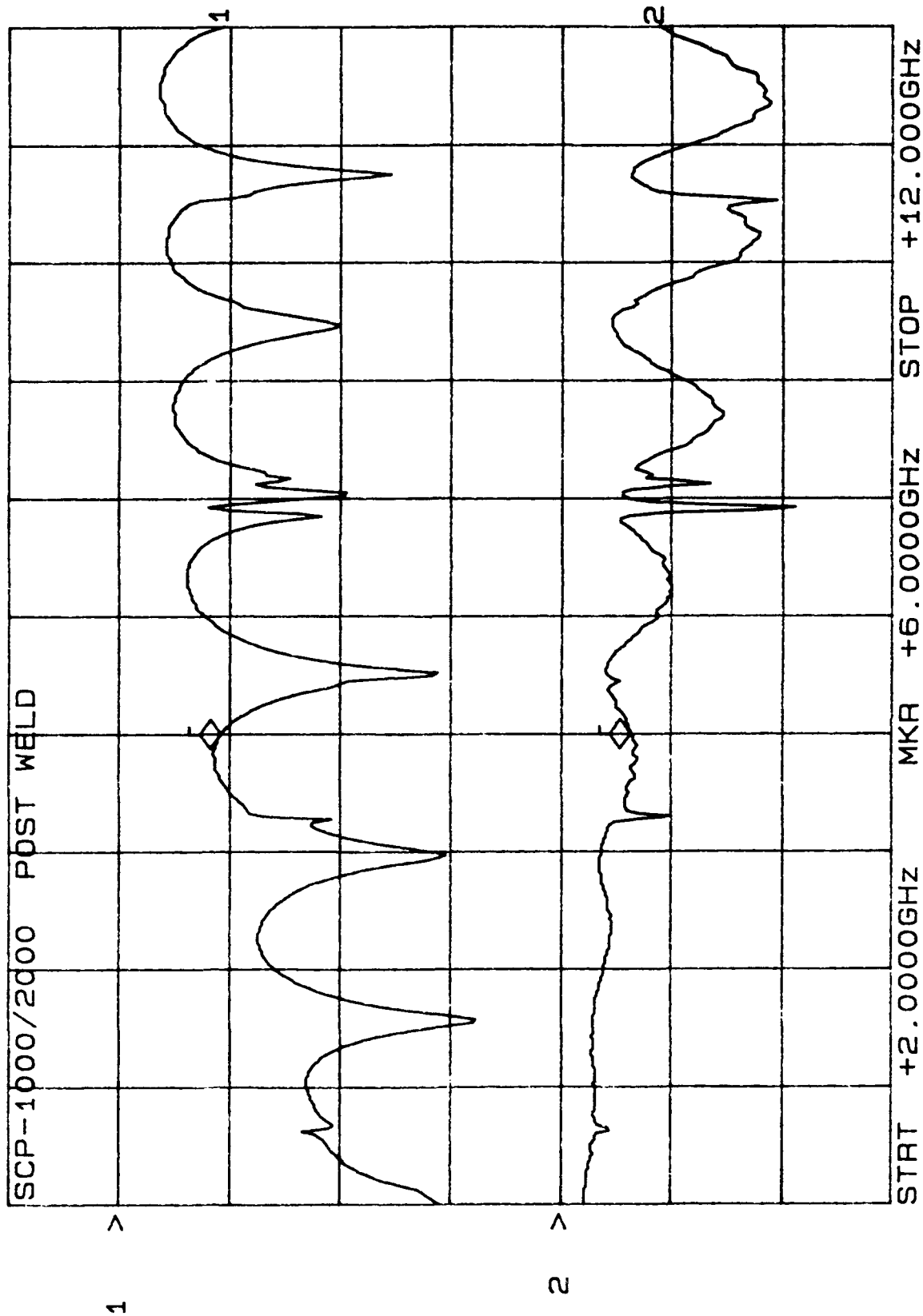
CH1: A -M - 7.84 dB CH2: B -M - 1.55 dB
10.0 dB/ REF - .00 dB 2.0 dB/ REF + .00 dB



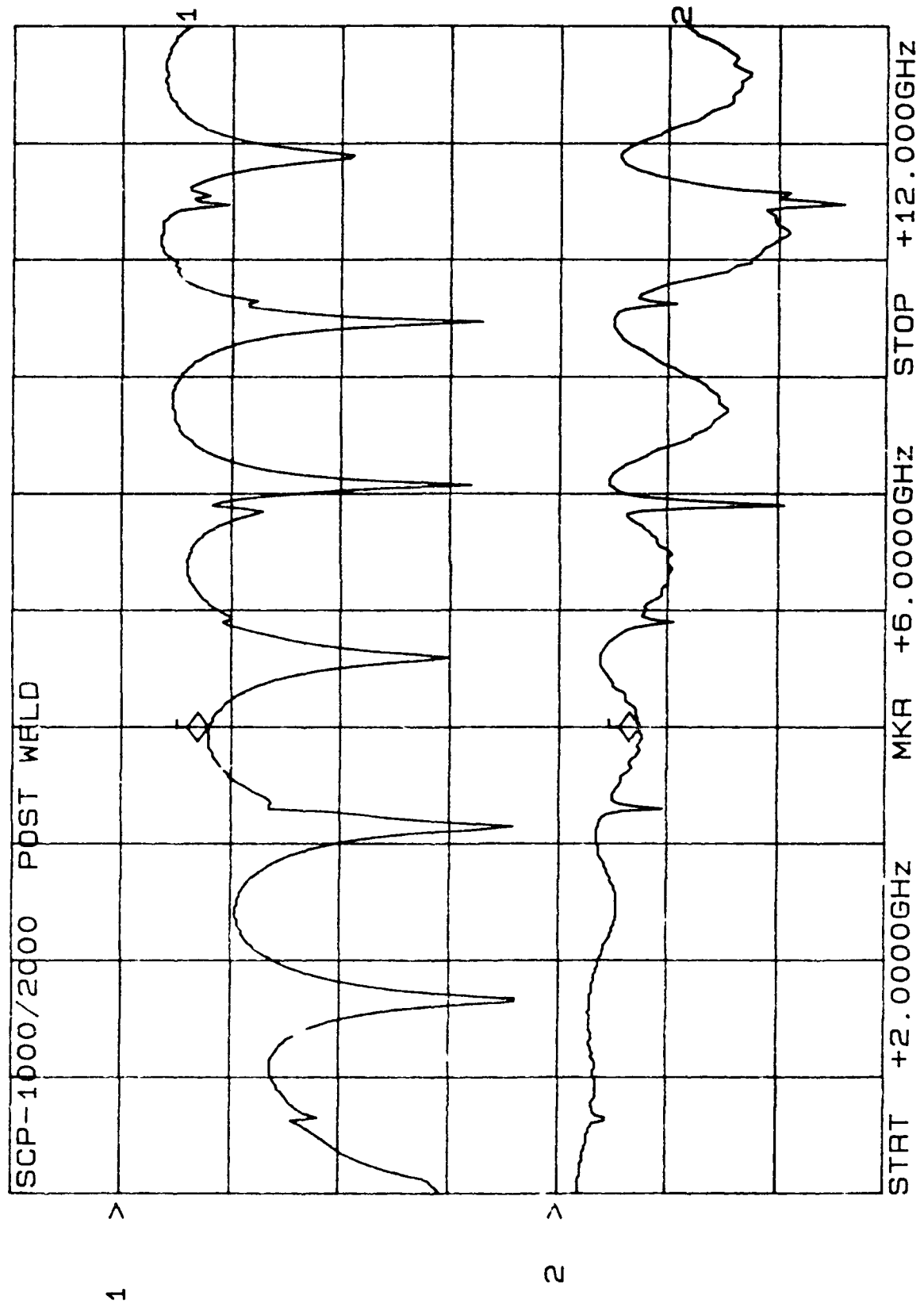
CH1: A -M - 9.81 dB - 1.24 dB
10.0 dB/ REF - .00 dB + .00 dB



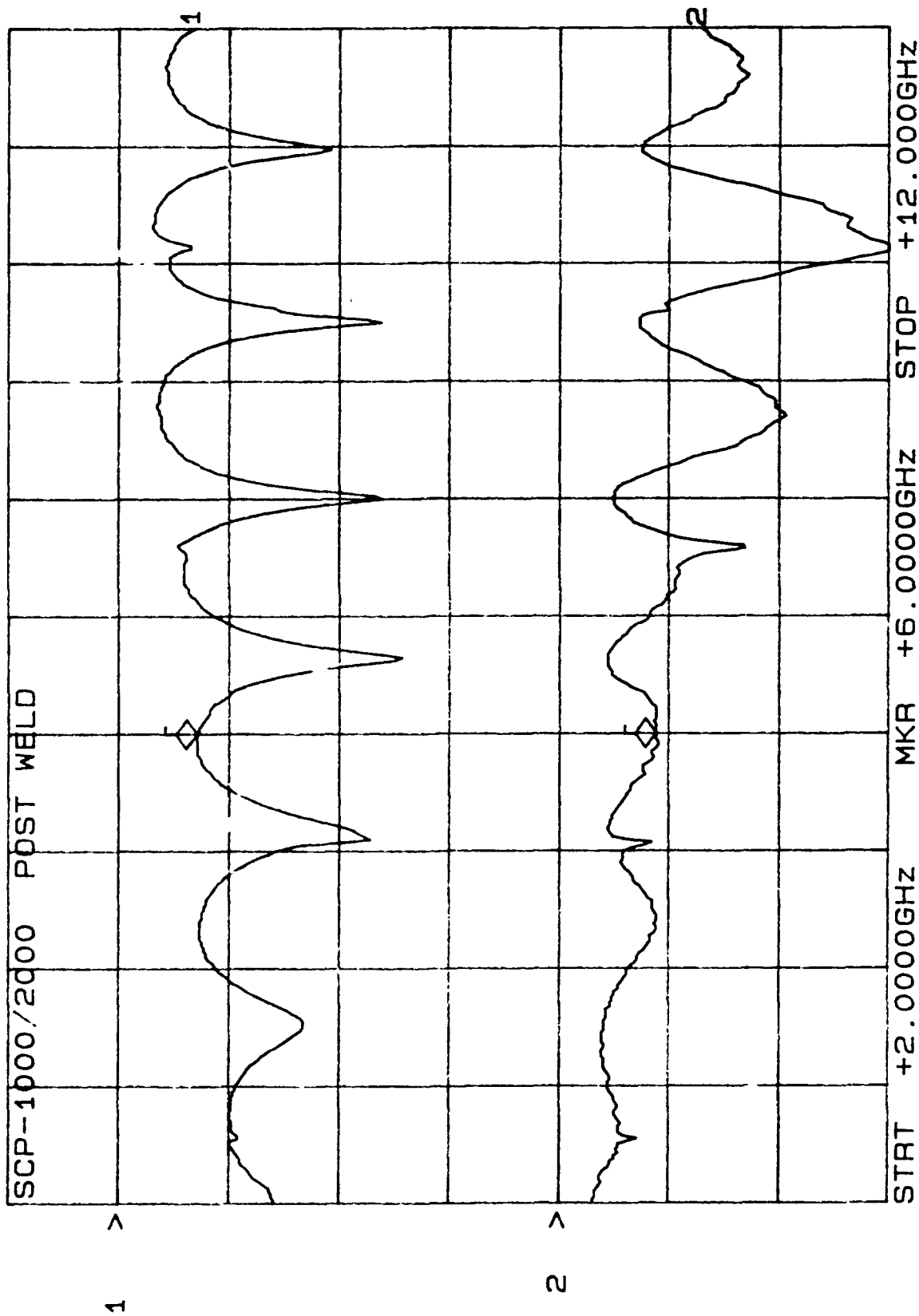
CH1: A -M - 9.17 dB CH2: B -M - 1.26 dB
10.0 dB/ REF - .00 dB 2.0 dB/ REF + .00 dB



CH1: A -M - 7.88 dB CH2: B -M - 1.48 dB
10.0 dB/ REF - .00 dB 2.0 dB/ REF + .00 dB

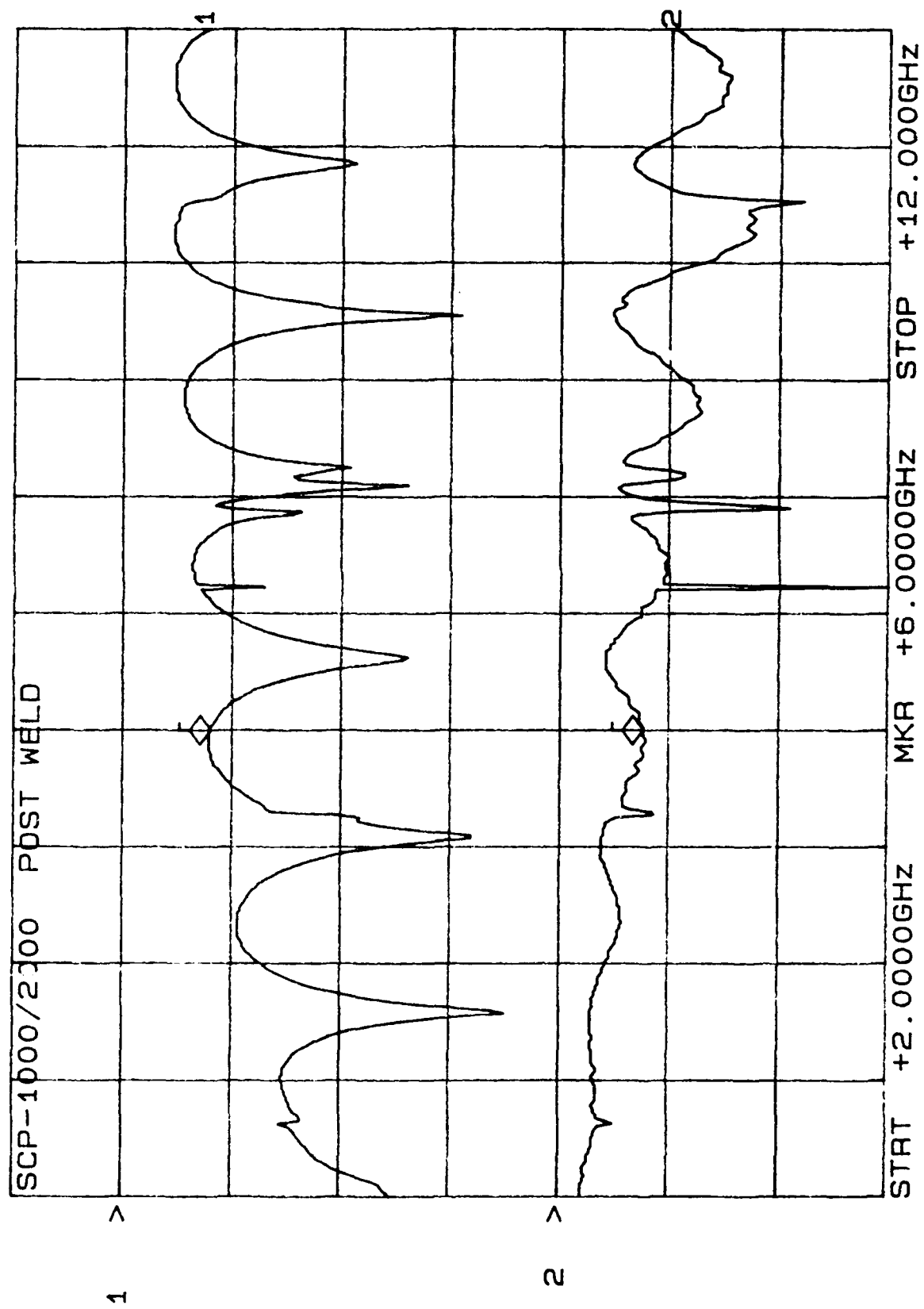


CH1: A -M - 7.06 dB CH2: B -M - 1.76 dB
10.0 dB/ REF - .00 dB 2.0 dB/ REF + .00 dB



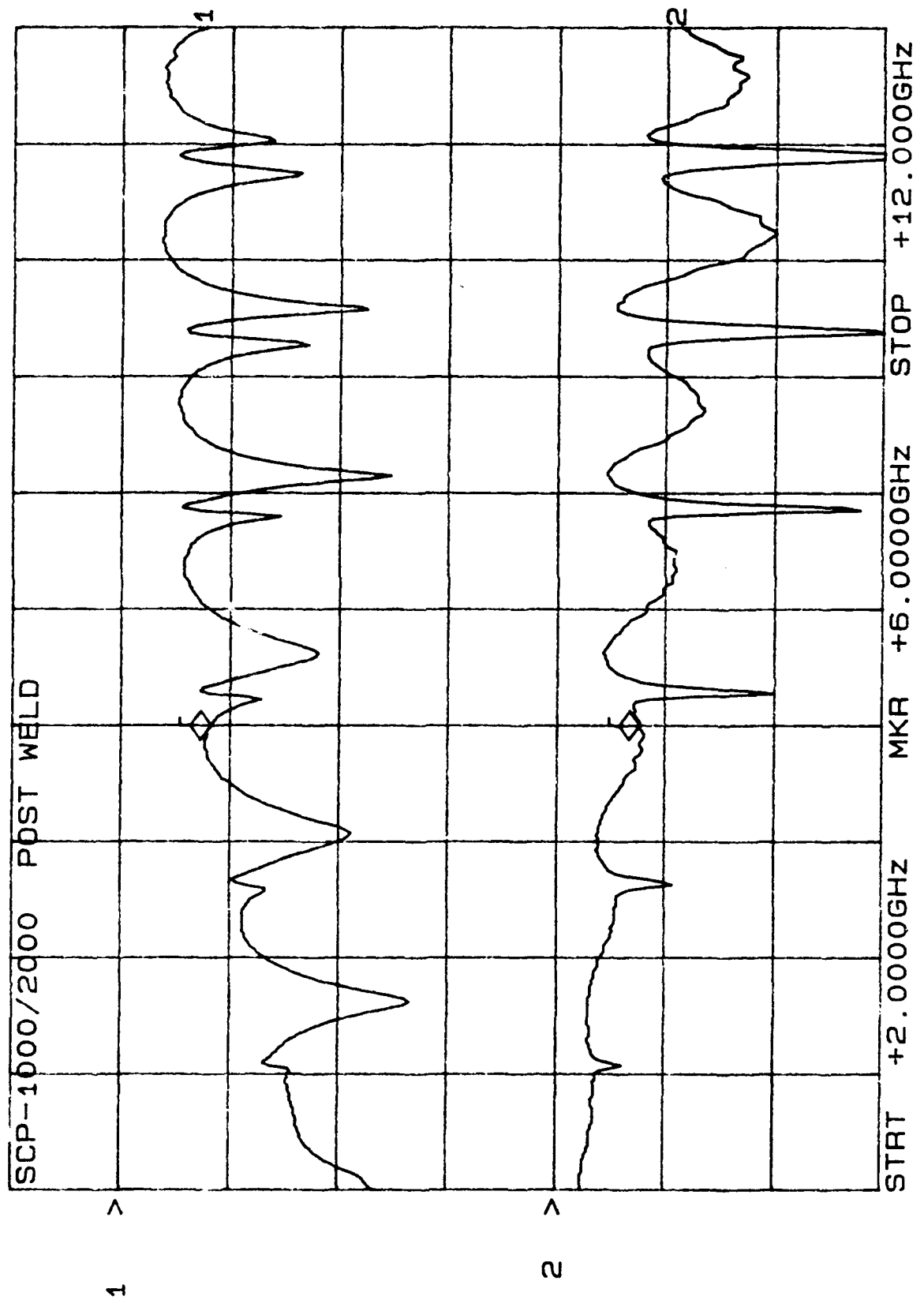
CH1: A -M - 7.95 dB
10.0 dB/ REF - .00 dB

CH2: B -M - 1.51 dB
2.0 dB/ REF + .00 dB

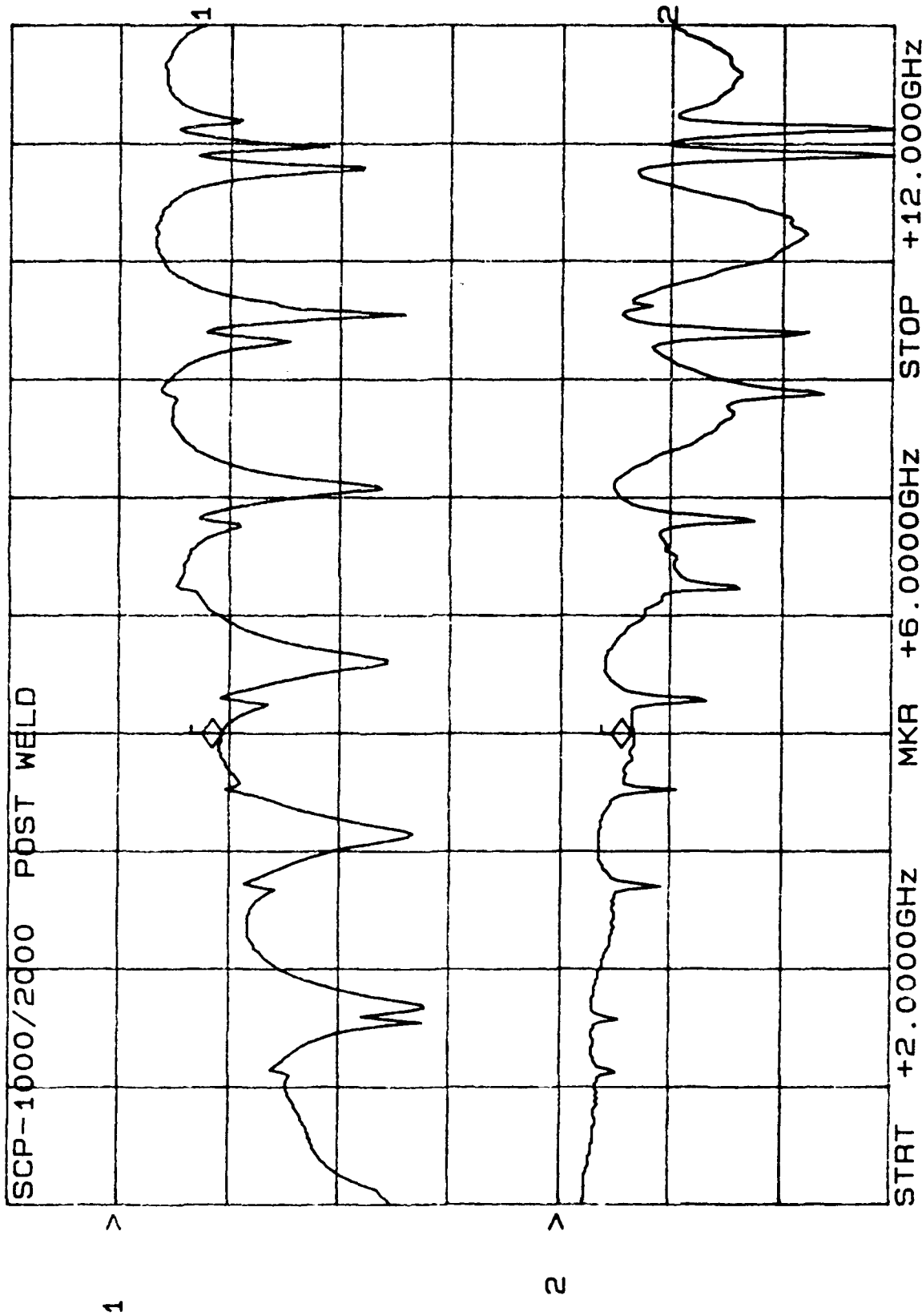


SCP-2080 S/N 007 8/11/91

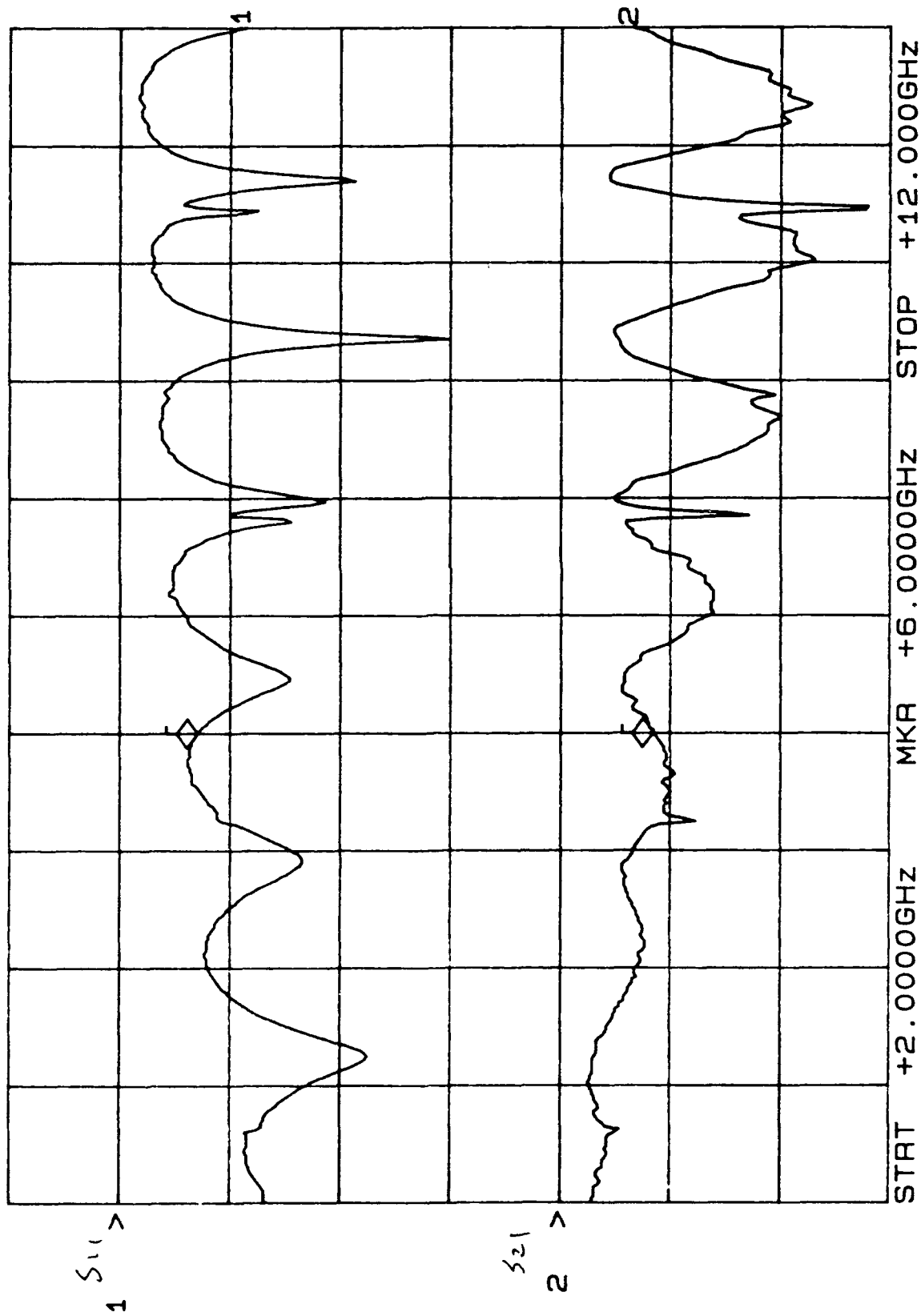
CH1: A -M REF = 8.12 dB CH2: B -M REF = 1.52 dB
10.0 dB/ REF = .00 dB 2.0 dB/ REF = .00 dB



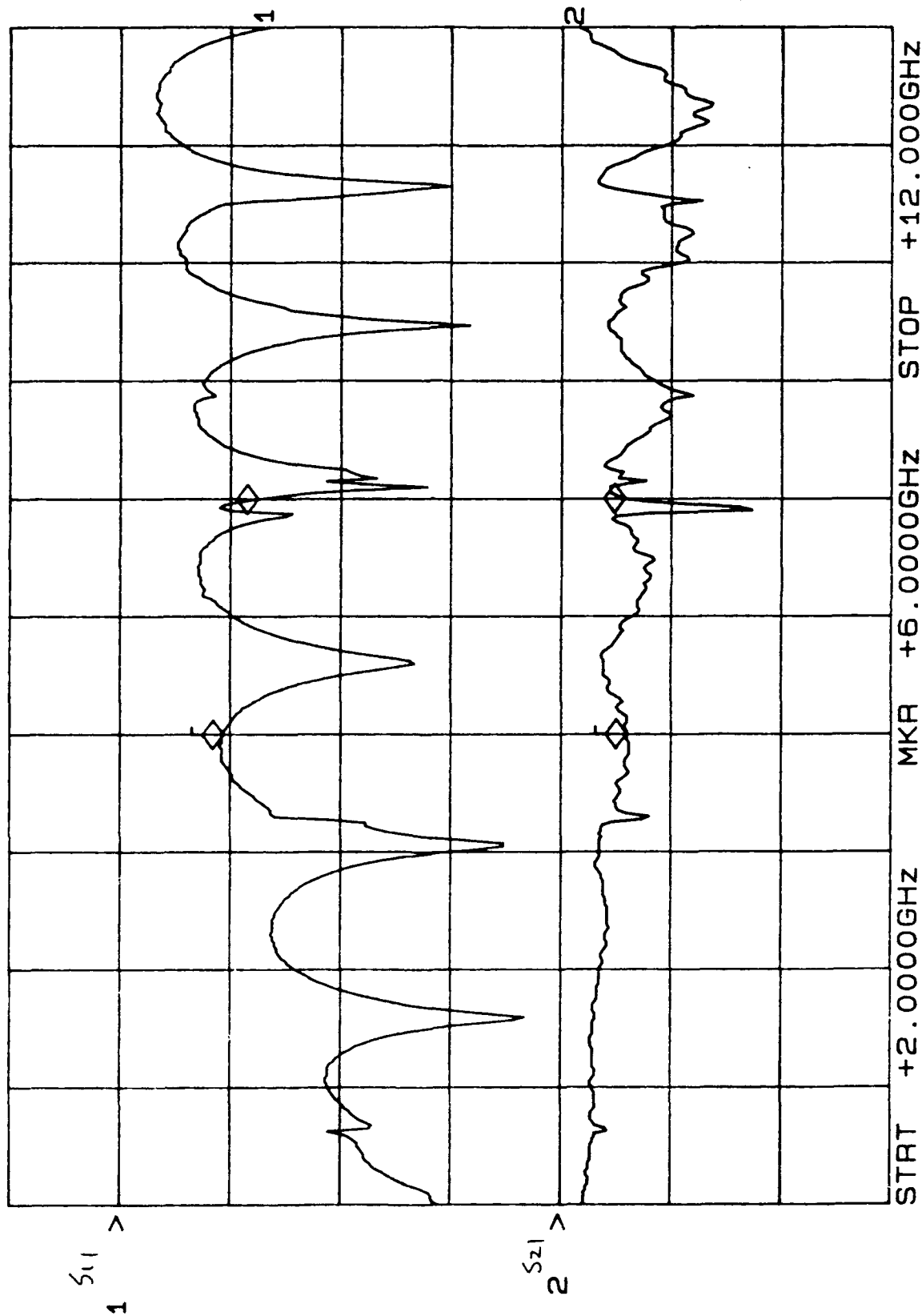
CH1: A -M - 9.25 dB CH2: B -M - 1.31 dB
10.0 dB/ REF - .00 dB 2.0 dB/ REF + .00 dB



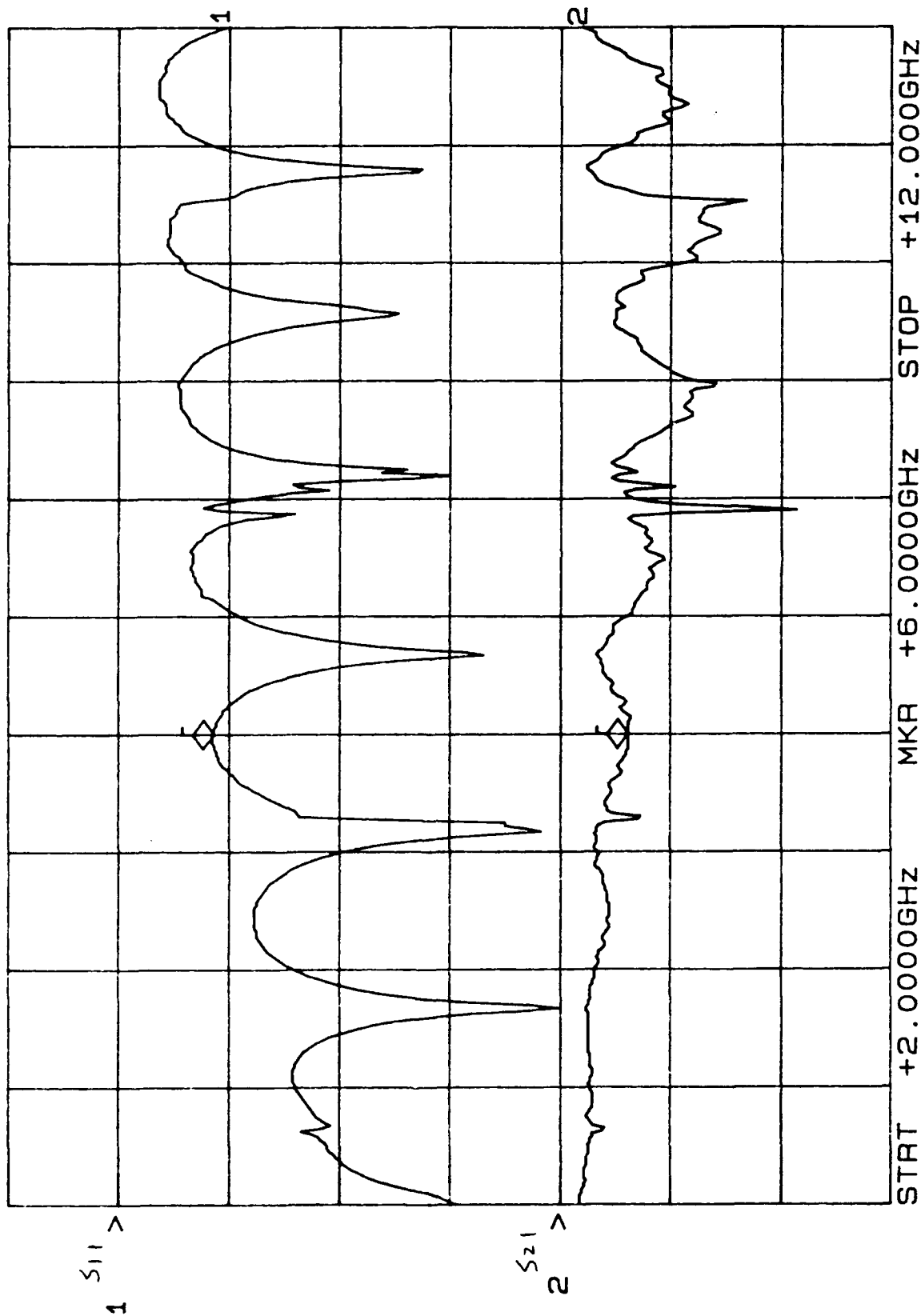
CH1: A -M REF - 7.02 dB CH2: B -M REF + 1.69 dB
 10.0 dB/ REF 2.0 dB/ REF



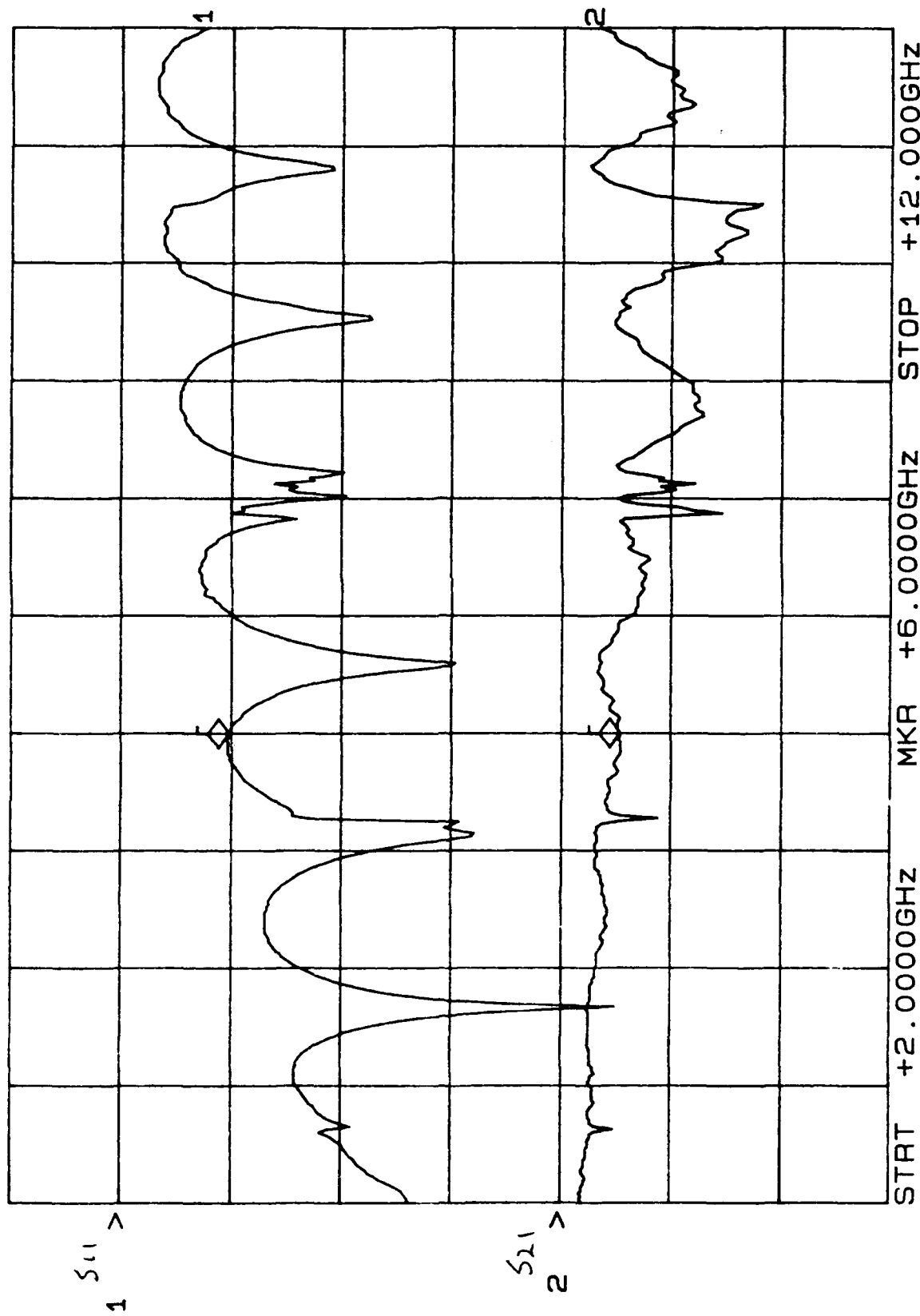
CH1: A ^{-M} REF = 9.24 dB 10.0 dB/ REF - 1.18 dB
 CH2: B ^{-M} REF + 2.0 dB/ REF + .00 dB



CH1: A -M = 8.47 dB CH2: B -M = 1.23 dB
 10.0 dB/ REF 2.0 dB/ REF + .00 dB

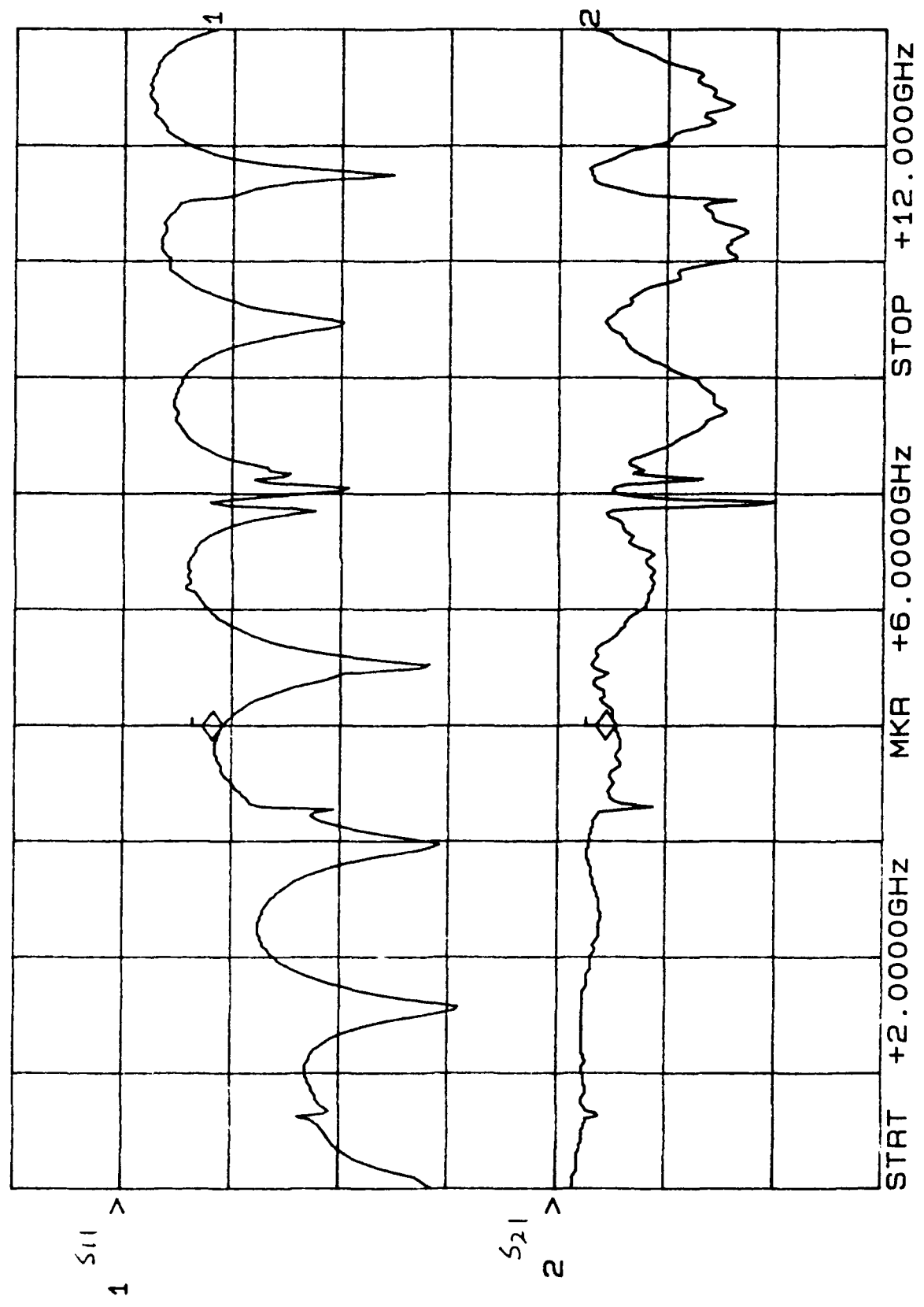


CH1: A ^{-M} REF - 9.73 dB CH2: B ^{-M} REF + 1.04 dB
 10.0 dB/ REF - .00 dB 2.0 dB/ REF + .00 dB



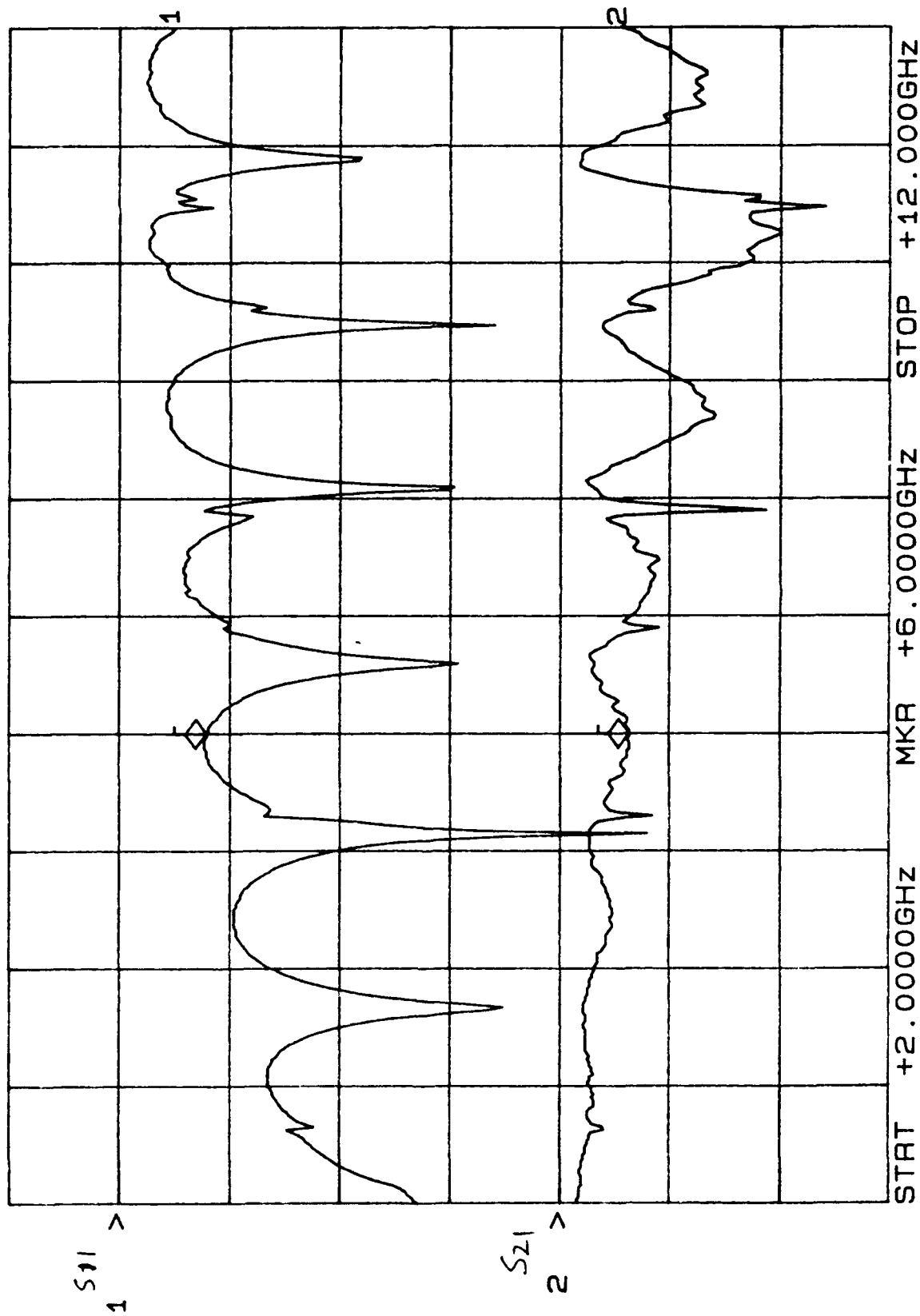
SCP-2000 Pre-weld 3/N 005- 4/779

CH1: A -M - 9.13 dB CH2: B -M - 1.05 dB
10.0 dB/ REF - .00 dB 2.0 dB/ REF + .00 dB



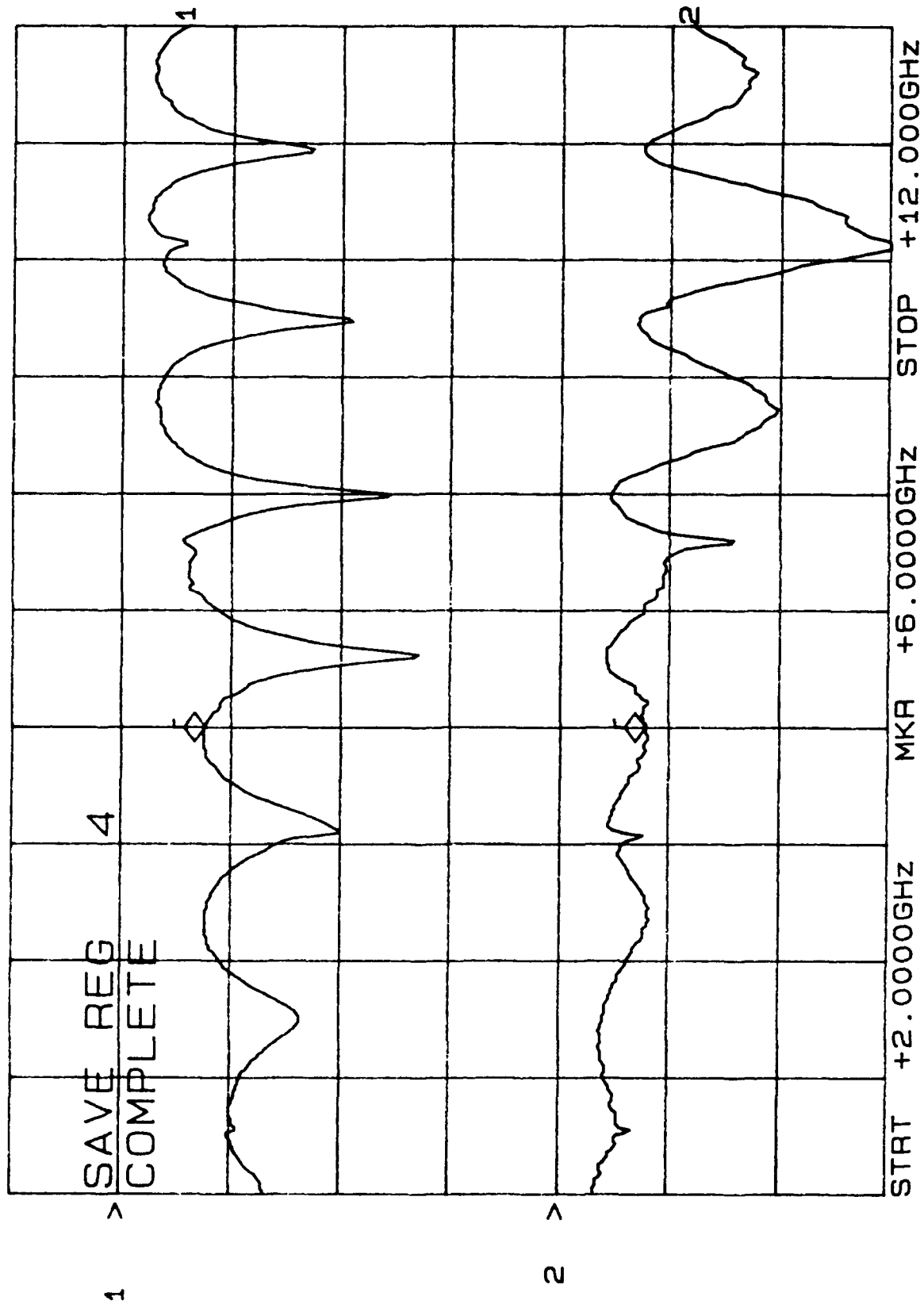
SCP-2000 Pre-weld S/N 000 1/9/11

CH1: A^{-M} REF = 7.84 dB CH2: B^{-M} REF + 1.24 dB
10.0 dB/ REF 2.0 dB/ .00 dB



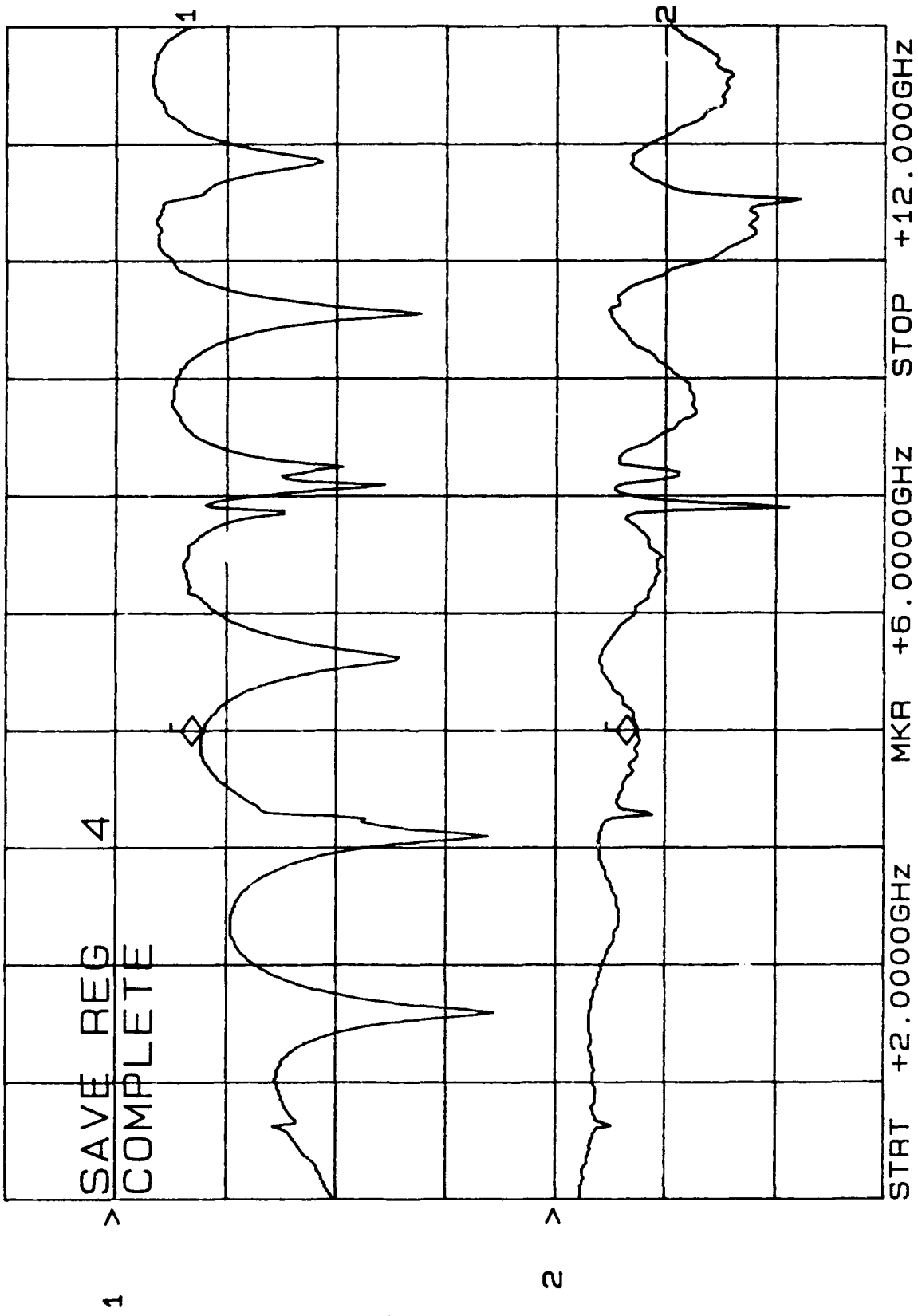
9/10/91

CH1: A -M REF = 7.53 dB CH2: B -M REF + 1.54 dB
10.0 dB/ REF = .00 dB 2.0 dB/ REF + .00 dB



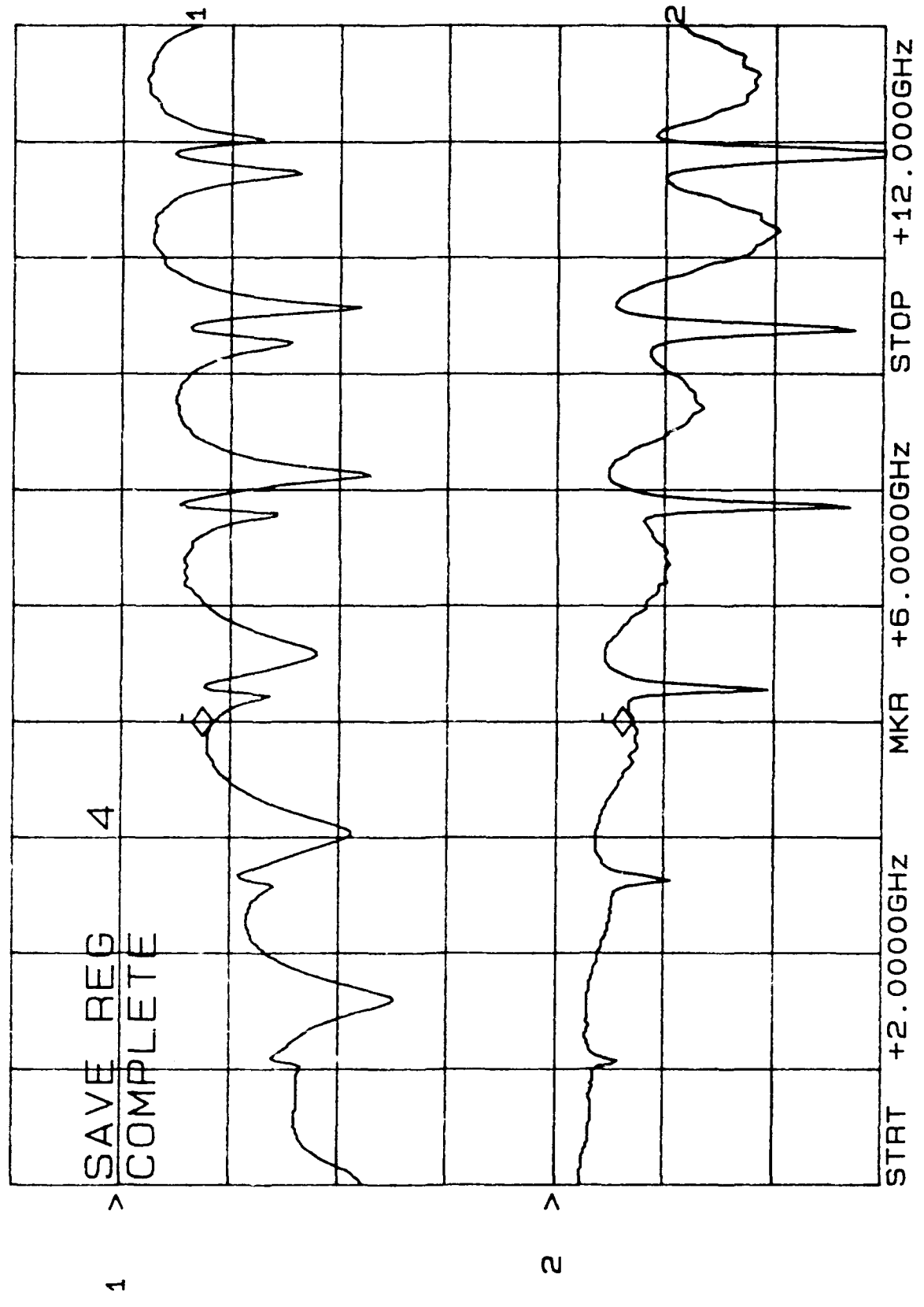
SCP-2000 Pre-weld 3/N 808 4/10/91

CH1: A -M REF - 7.79 dB CH2: B -M A - 1.48 dB
10.0 dB/ REF 2.0 dB/ REF + .00 dB



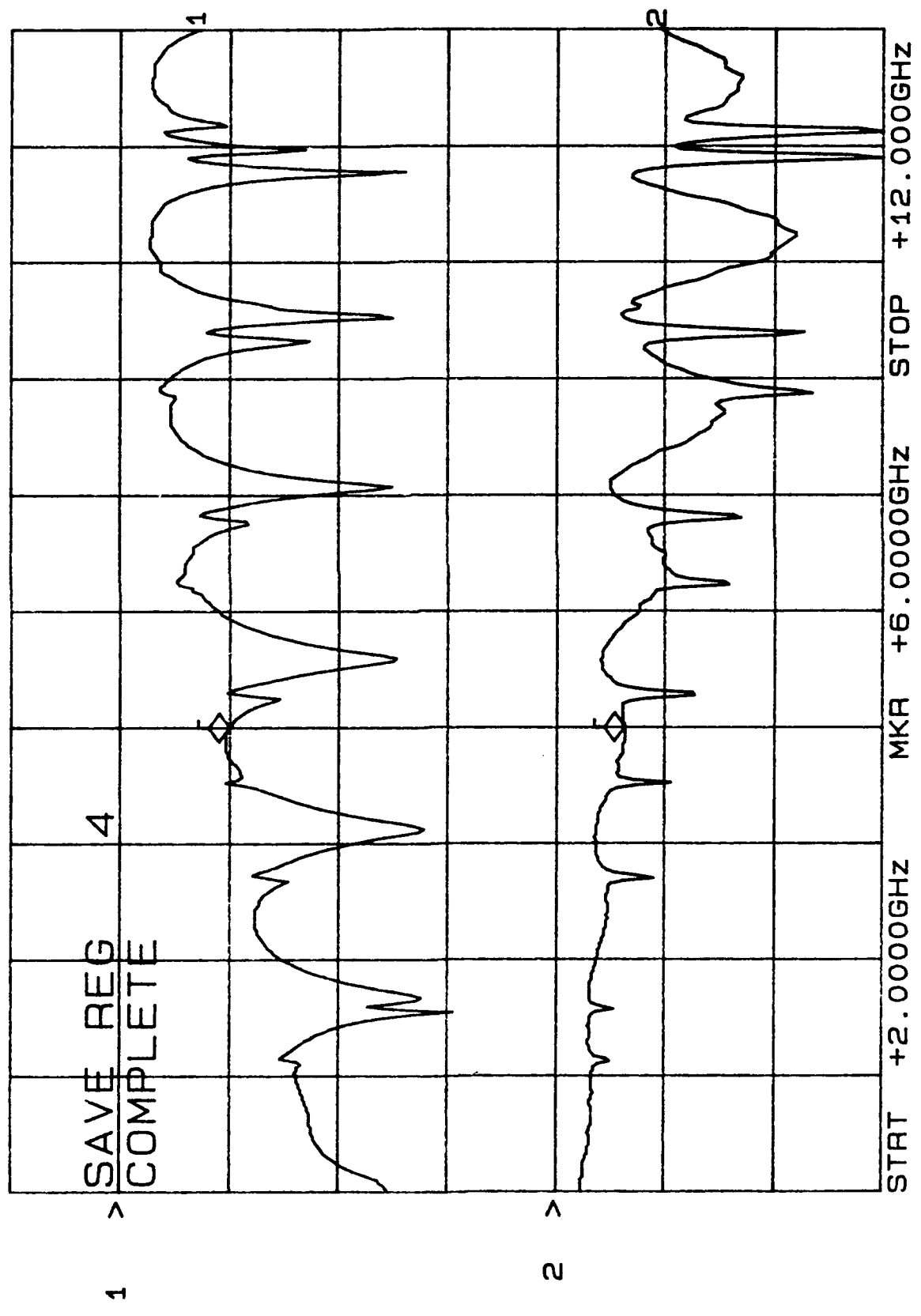
SCP-2000 7000 watt 570 800 91 491

CH1: A -M REF = 8.44 dB CH2: B -M REF = 1.40 dB
10.0 dB/ REF 2.0 dB/ REF



SCP-2000 Pre-weld 018

CH1: A -M REF - 9.83 dB
10.0 dB/ REF - 1.24 dB
CH2: B -M REF + 2.0 dB/ REF + .00 dB

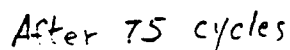




Post weld

AV-631/R-10-87

75 Cycles

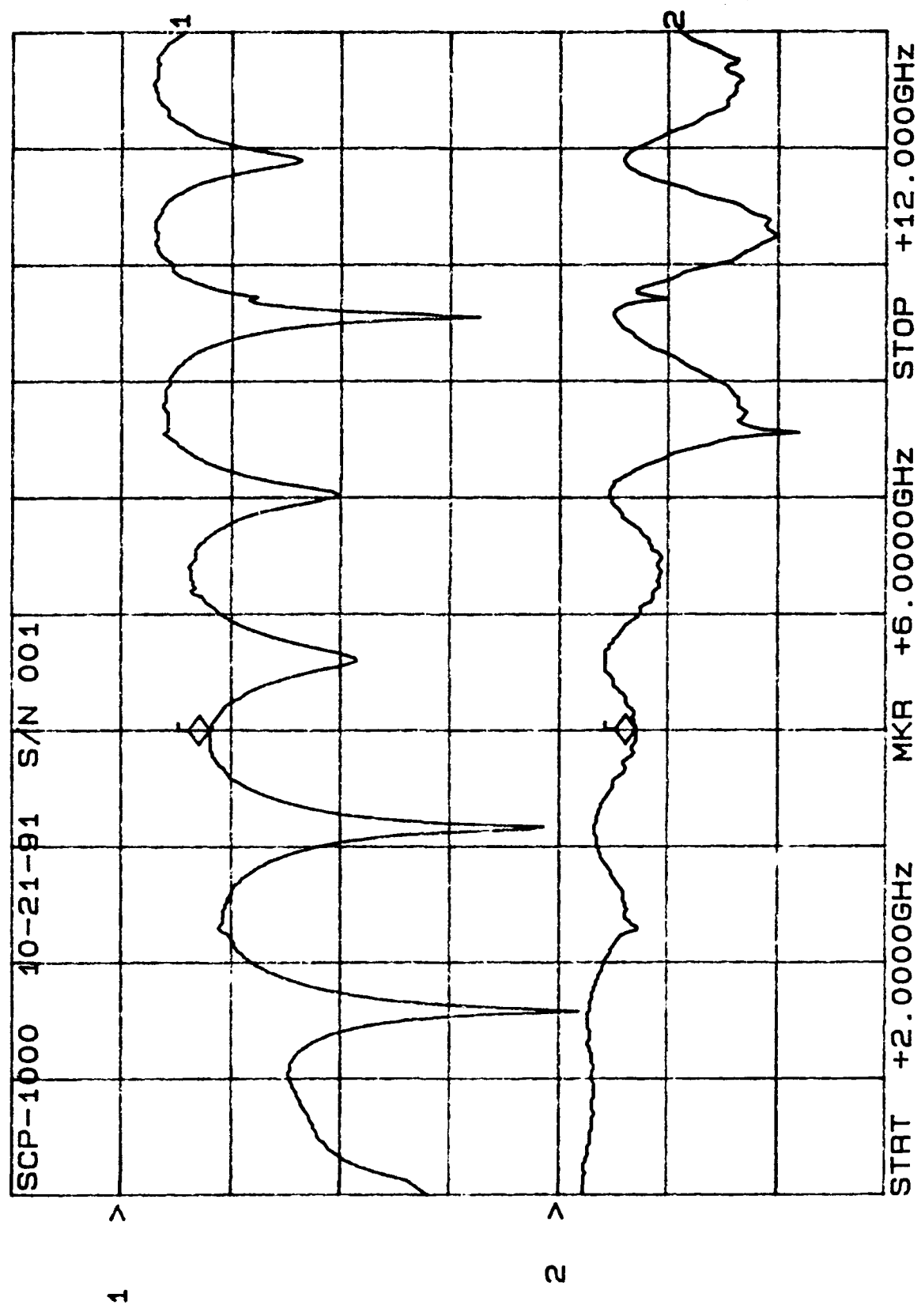


EL
ACCEPT
04

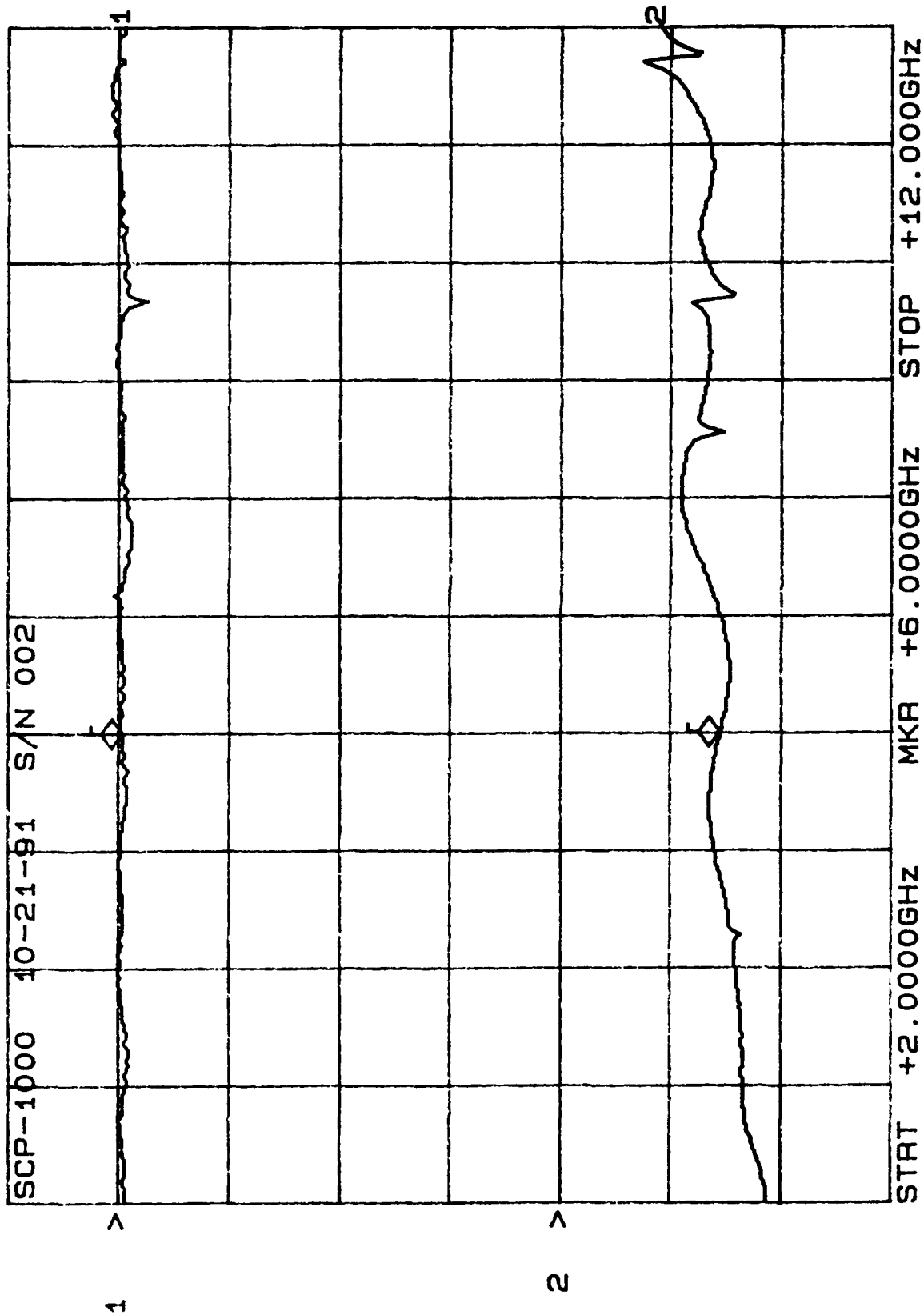
AV-631/R-10-87

Attenuator 75 cycles

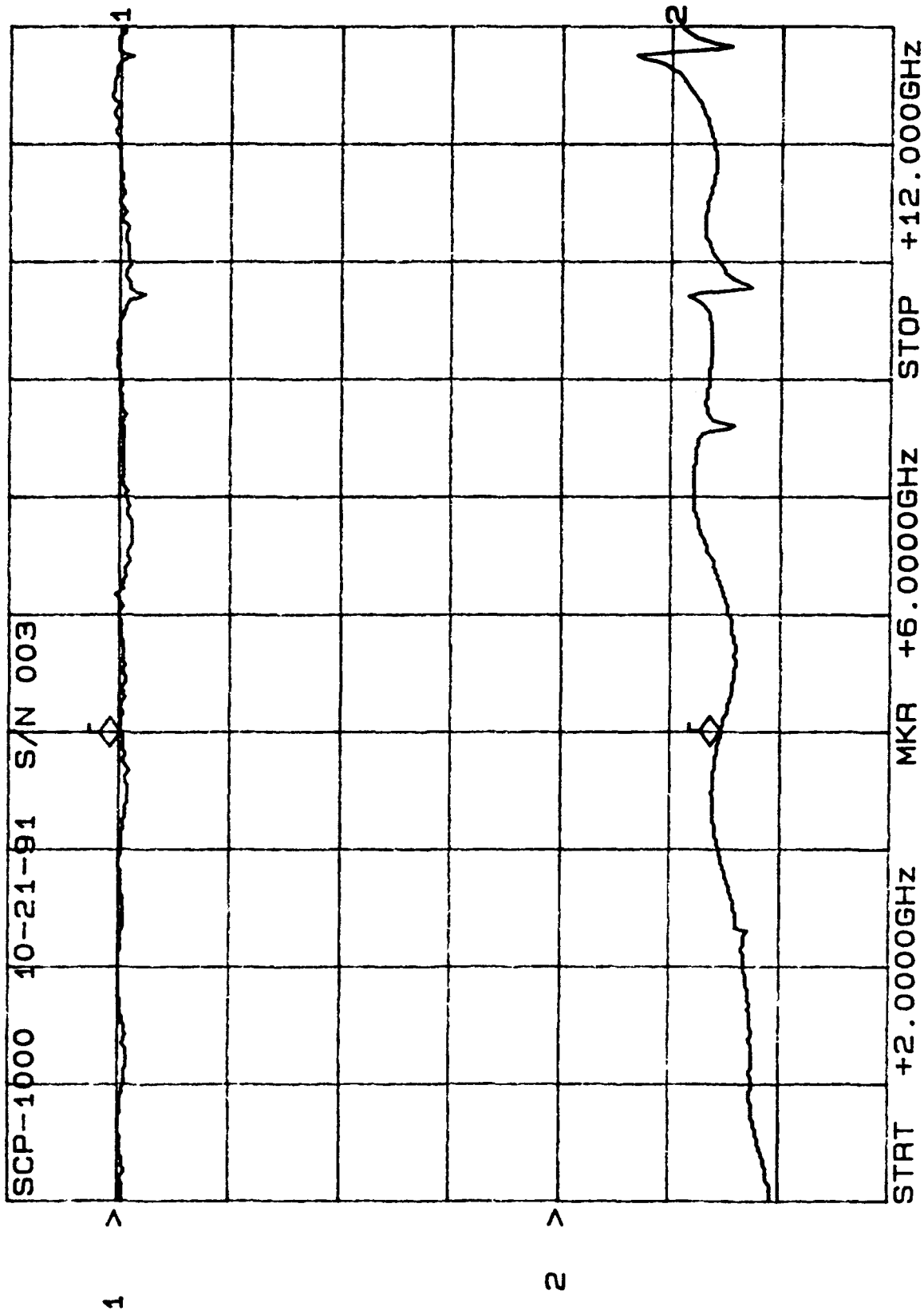
CH1: A -M 10.0 dB/ REF - 8.06 dB
CH2: B -M 2.0 dB/ REF + 1.39 dB



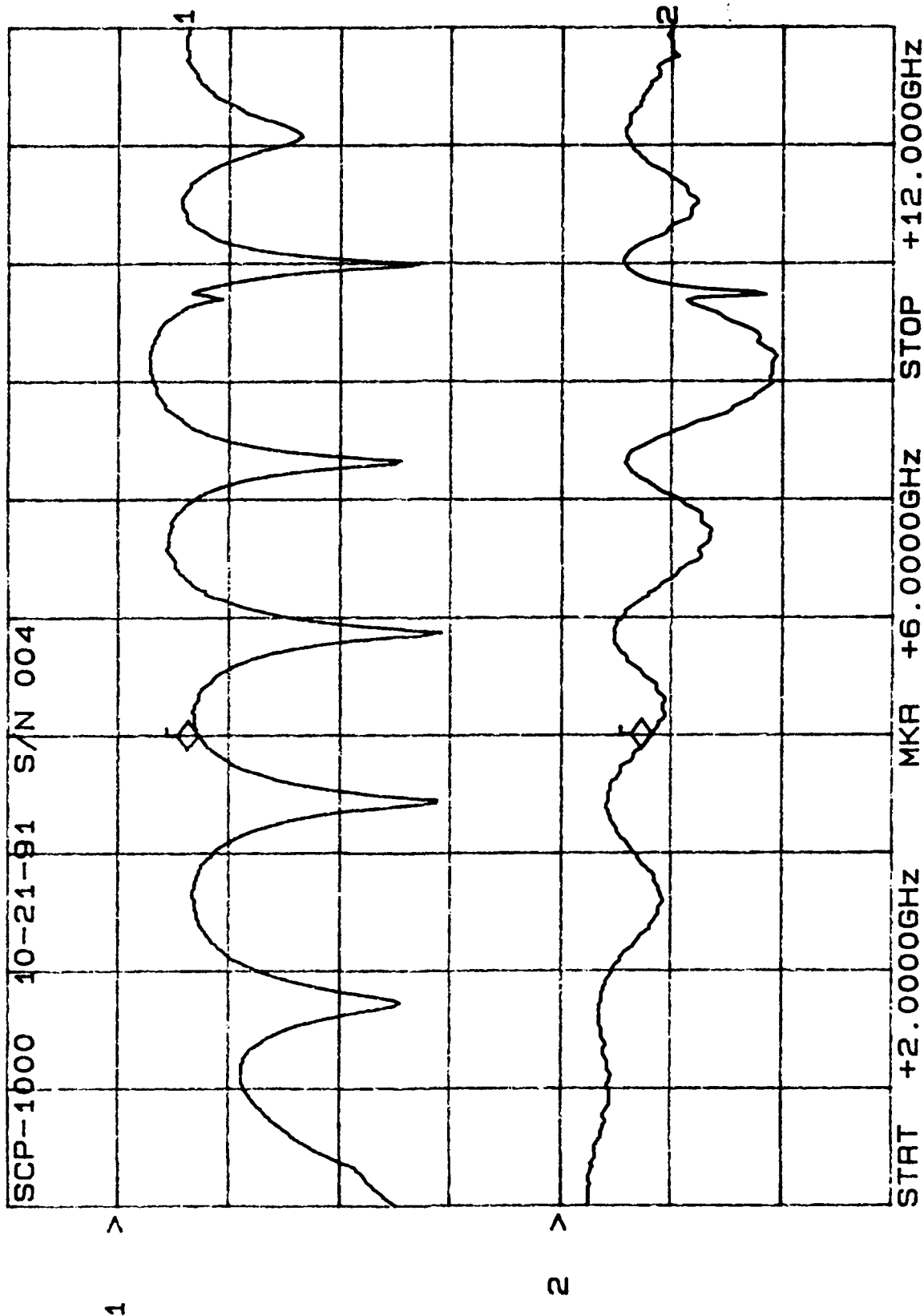
CH1: A -M REF - :20 dB CH2: B -M REF + 28.71 dB
 10.0 dB/ REF - :00 dB 20.0 dB/ REF + .00 dB



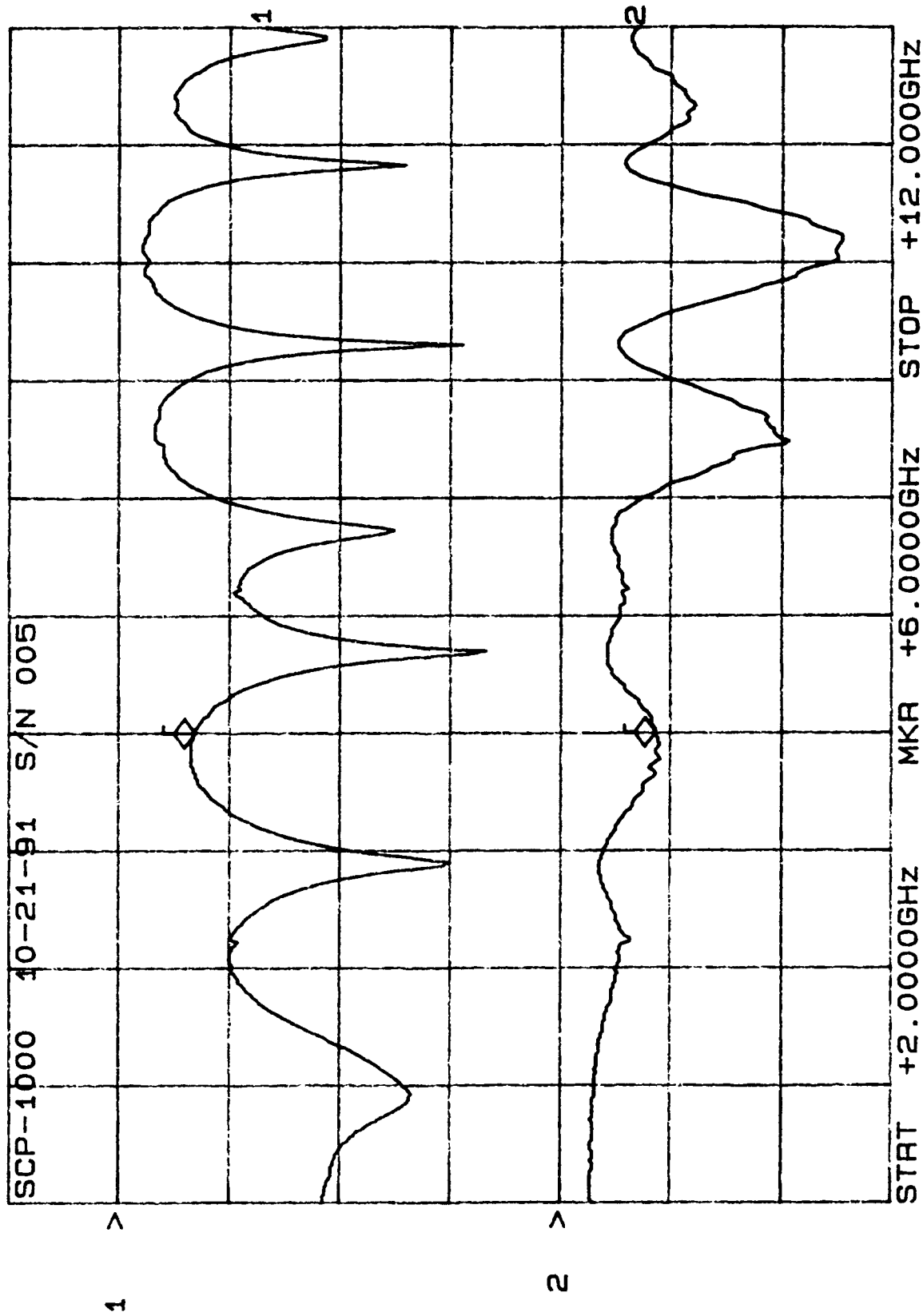
CH1: A -M REF - .19 dB CH2: B -M A - 29.06 dB
 10.0 dB/ REF 20.0 dB/ REF + .00 dB



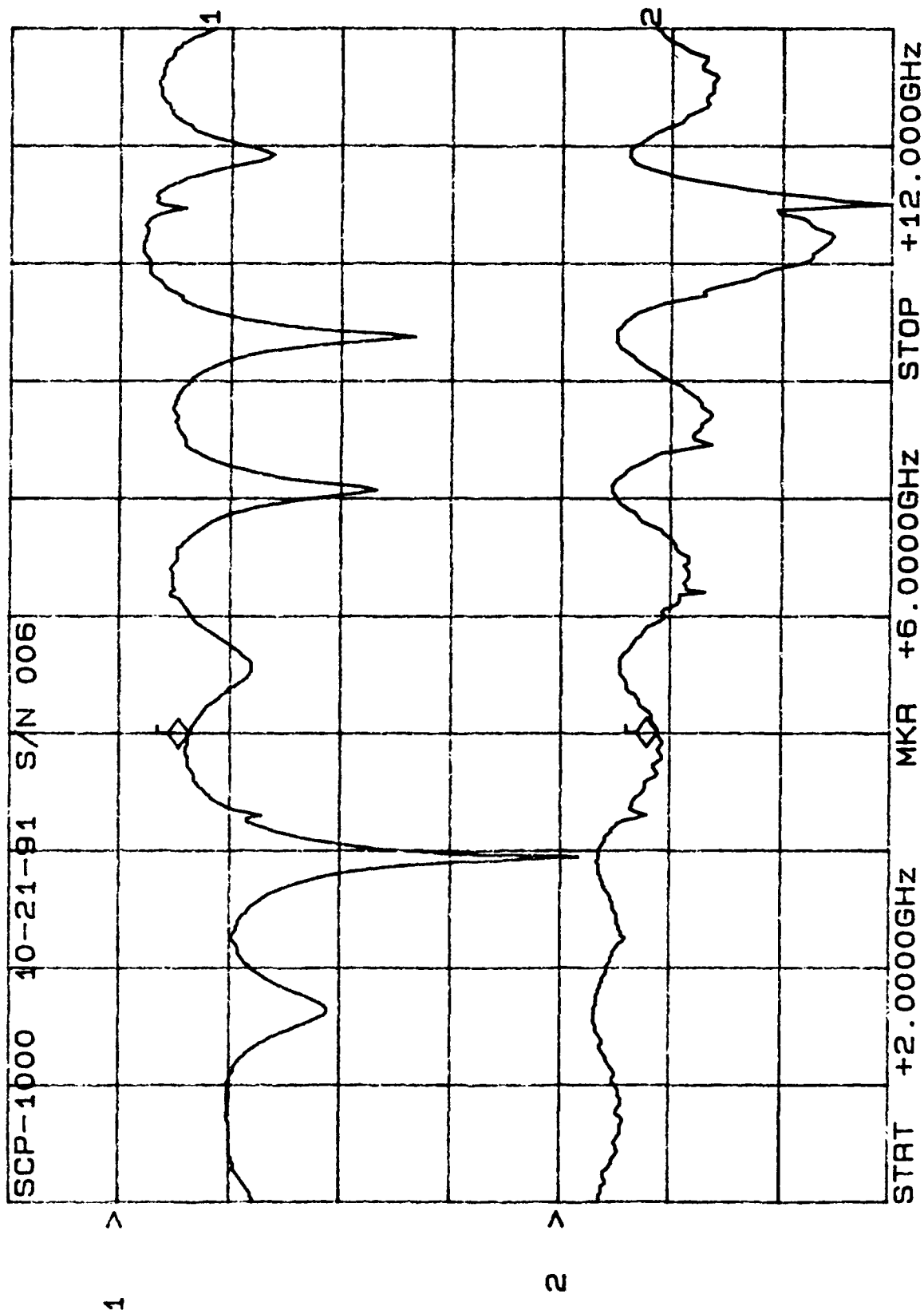
CH1: A -M - 7.25 dB CH2: B -M A - 1.64 dB
10.0 dB/ REF - .00 dB 2.0 dB/ REF + .00 dB



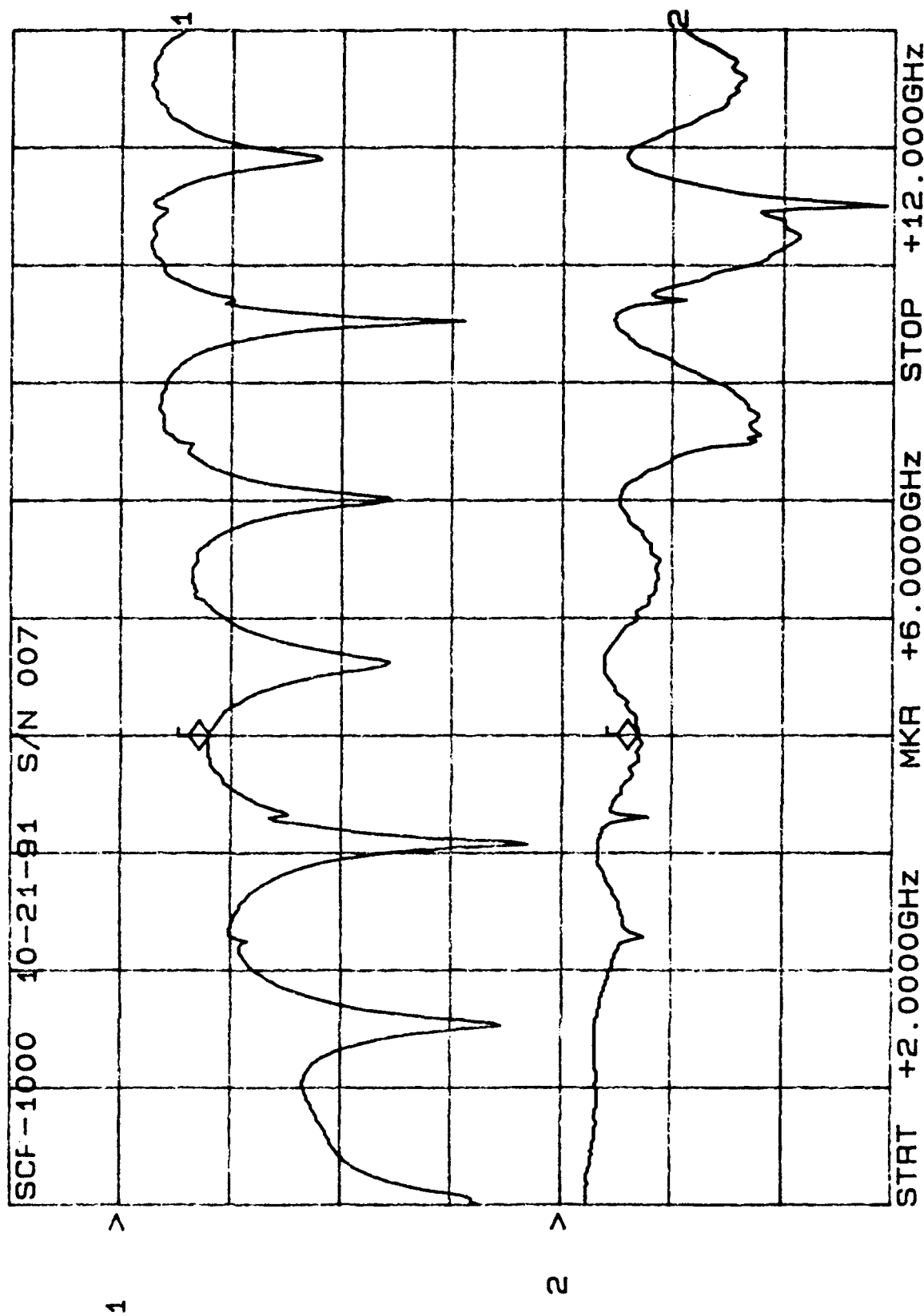
CH1: A -M REF - 10.0 dB/ REF - 6.80 dB CH2: B -M REF + 1.71 dB
 2.0 dB/ REF + .00 dB



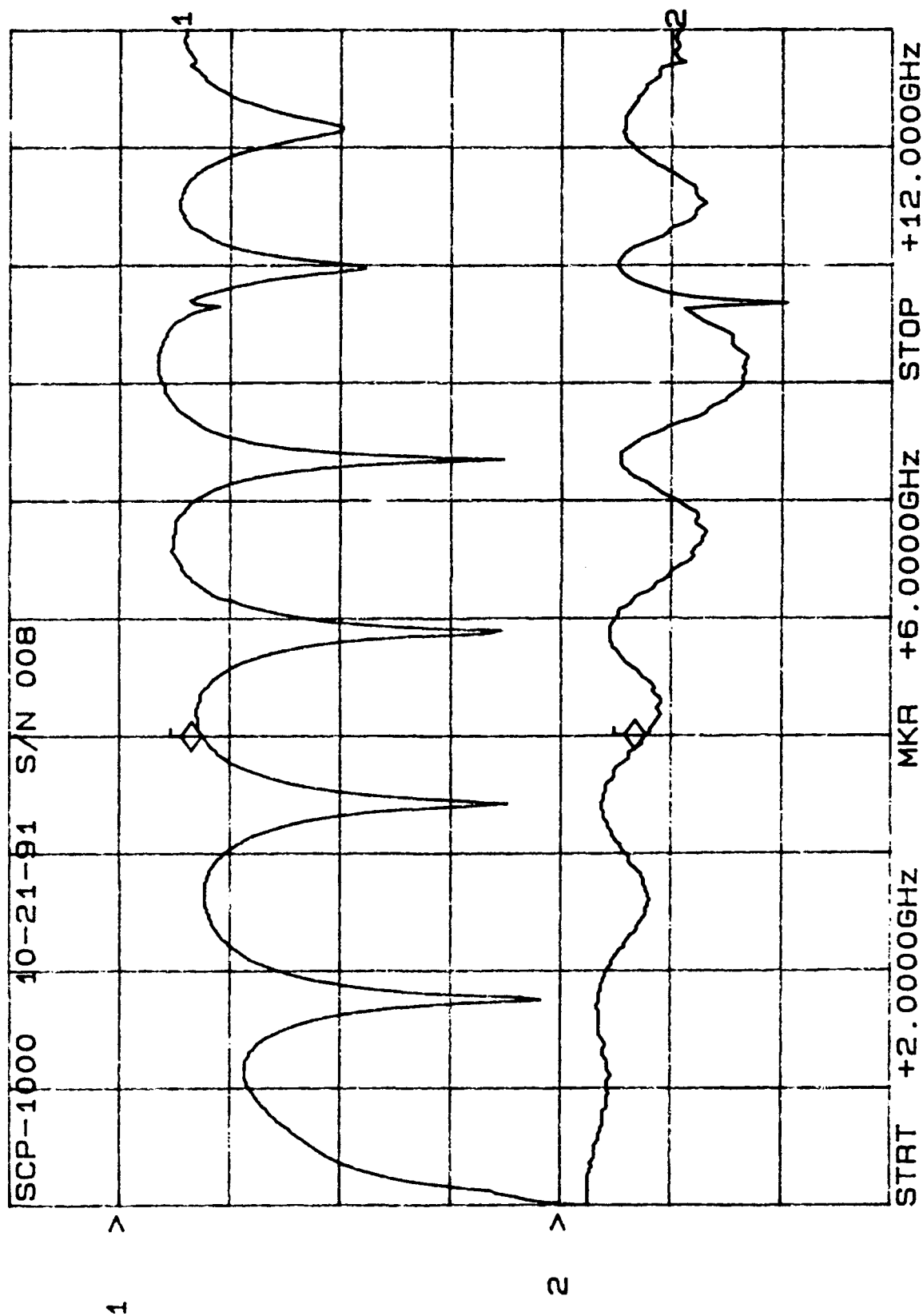
CH1: A -M REF - 6.25 dB CH2: B -M A - 1.74 dB
10.0 dB/ REF - .00 dB 2.0 dB/ REF + .00 dB



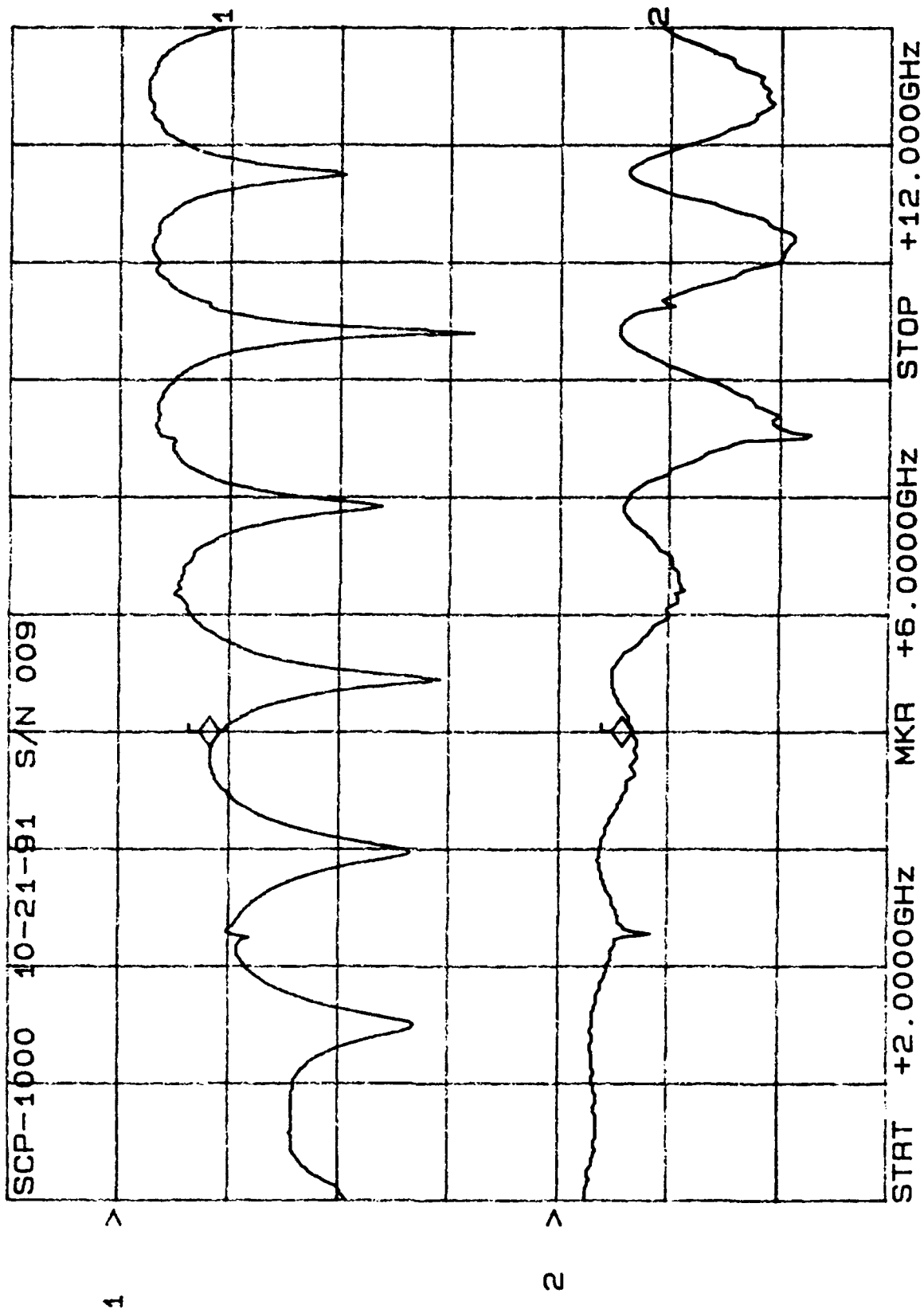
CH1: A -M REF = 7.92 dB CH2: B -M REF = 1.38 dB
 10.0 dB/ REF = .00 dB 2.0 dB/ REF = .00 dB



CH1: A -M REF = 7.37 dB CH2: B -M A - 1.52 dB
 10.0 dB/ REF = .00 dB 2.0 dB/ REF + .00 dB



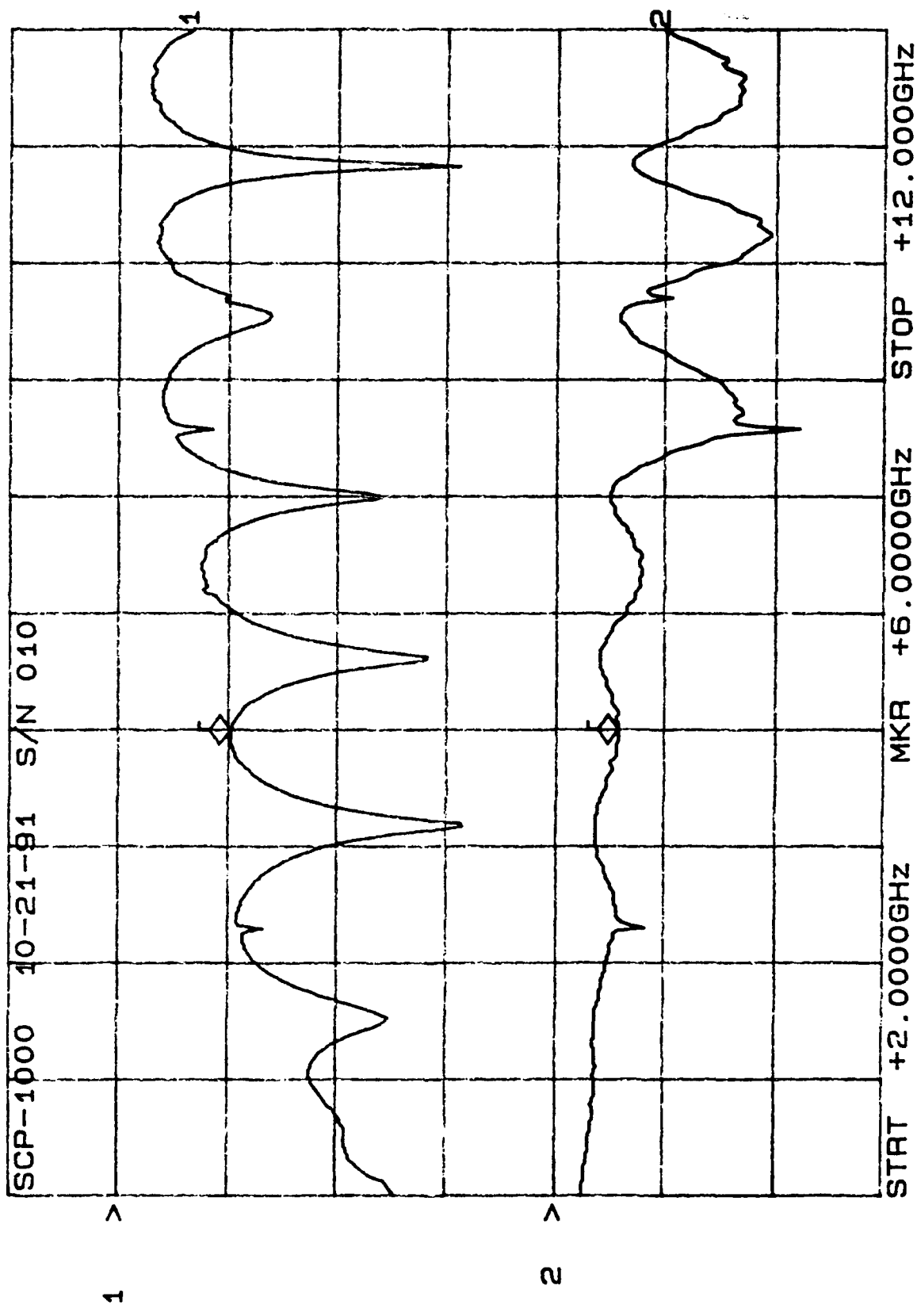
CH1: A -M - 9.23 dB CH2: B -M A - 1.32 dB
10.0 dB/ REF - .00 dB 2.0 dB/ REF + .00 dB



After 75 cycles

CH1: A -M REF - 10.19 dB
10.0 dB/ REF - .00 dB

CH2: B -M A - 1.12 dB
2.0 dB/ REF + .00 dB



50 Cycles



CERTIFIED TEST DATA

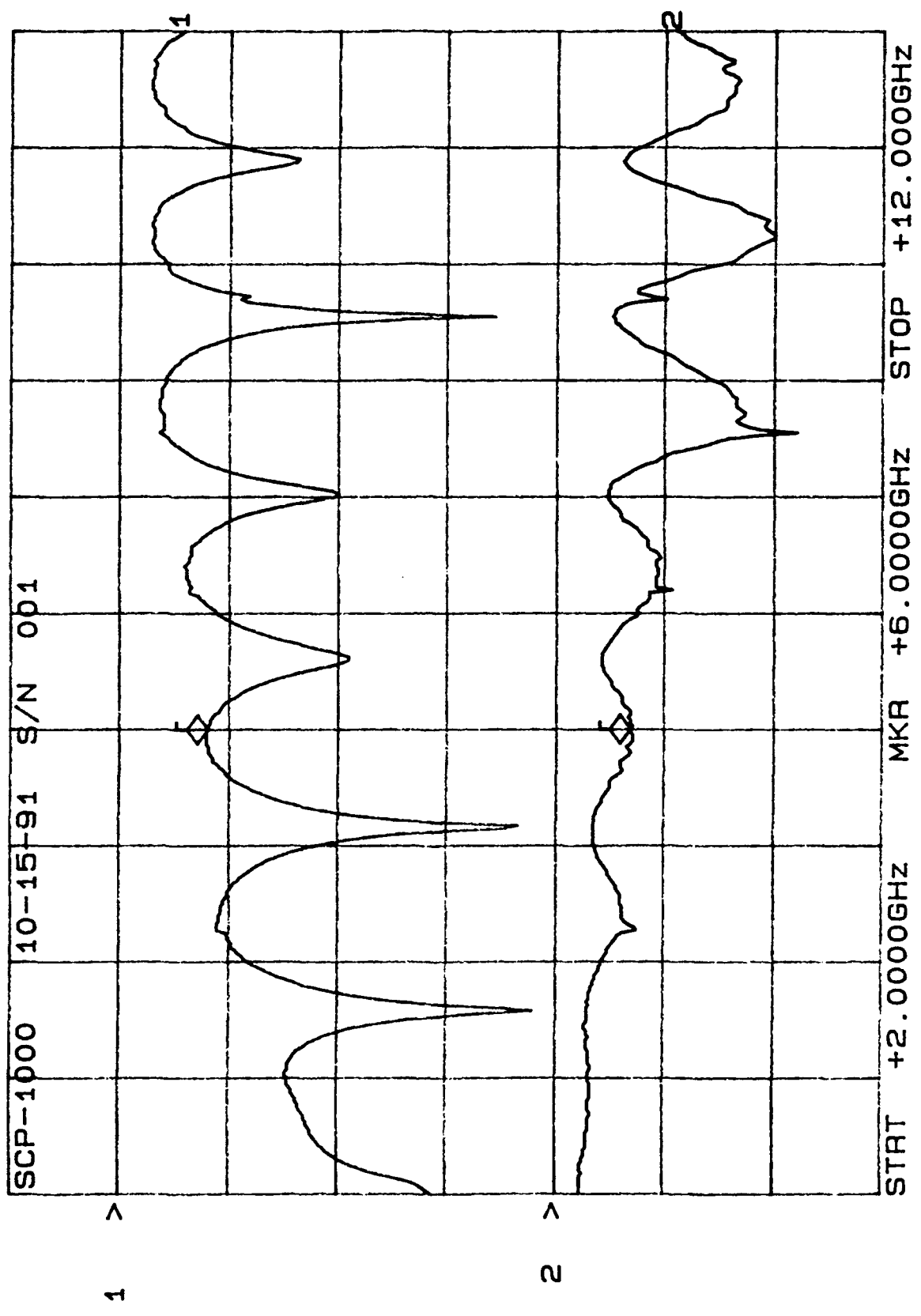
After 50 cycles

START DATE	CUSTOMER		QUALITY ACCT
10-16-91	STOCK		<div>EL ACCEPT 04</div>
COMPL DATE	TYPE OF TEST	AVANTEK	WO/CSO
10-16-91	FINE LEAK TEST	J1-32	TEST COND.
DEVICE TYPE	TEST REQUIREMENTS		BOMB PRESSURE AND DURATION
SCP-2000 SCP-1000	MIL STD-883C METHOD 1014.8		
QTY START	QTY COMPL	SENSITIVITY	
20	18	5×10^{-7} CC/SEC	2 hrs @ 30 p.s.i.
(S/N) LOT No.	LEAK RATE (CC/SEC)	PASS/FAIL	DWELL TIME
SCP-2000 001	2×10^{-9}	PASS	15 min
002			
003			
004			
005			
006			
007	10×10^{-6}	FAIL	Leak @ Feed-in on Red Arrow
008	2×10^{-9}	PASS	
009	2×10^{-7}		
010	10×10^{-6}	FAIL	Leak @ Feed-in on Red Arrow
SCP-1000 001	2×10^{-9}	PASS	
002			
003			
004			
005			
006			
007			
008			
009			
010			

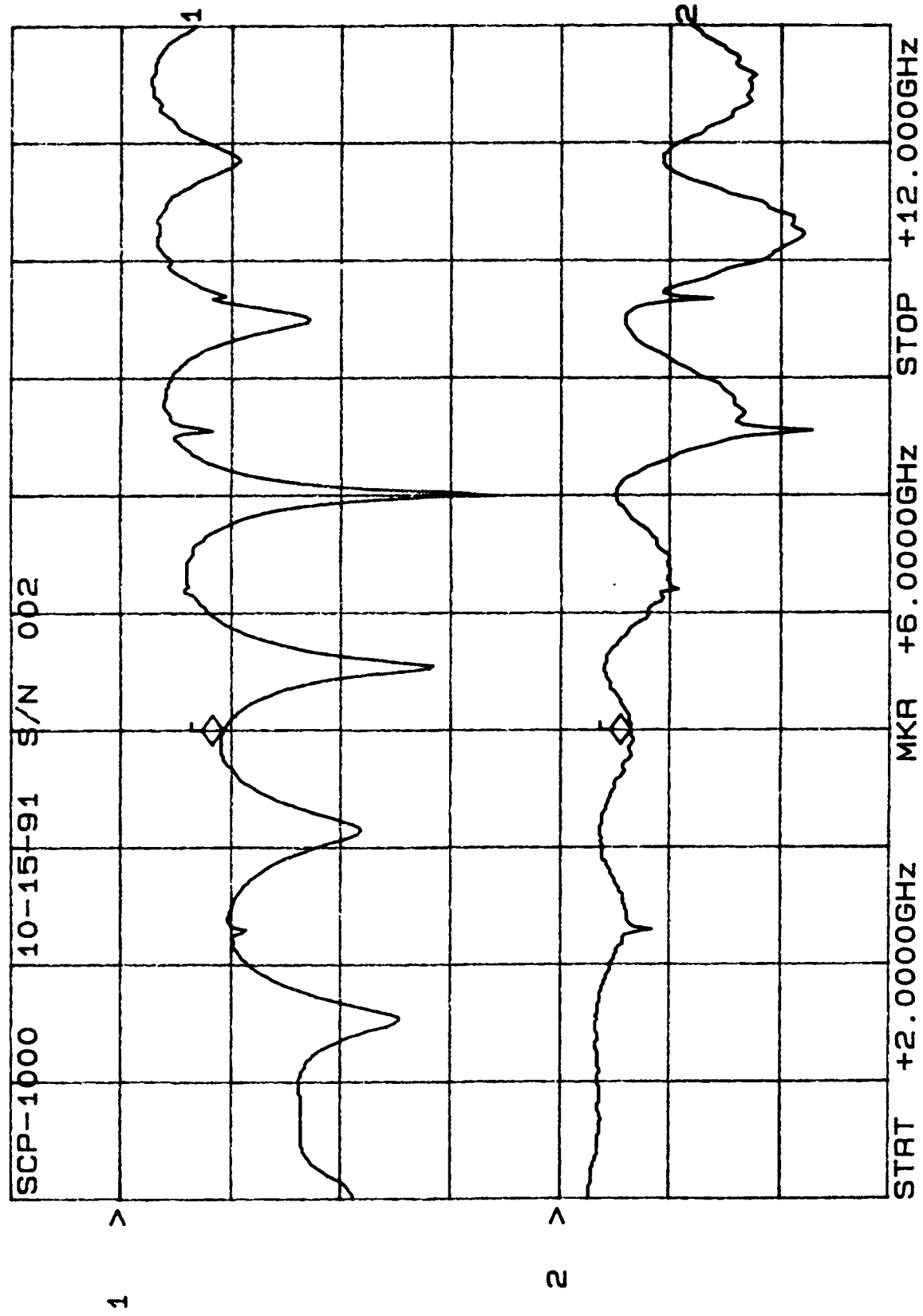
After 50 cycles

CH1: A -M REF - 7.92 dB
10.0 dB/ REF - .00 dB

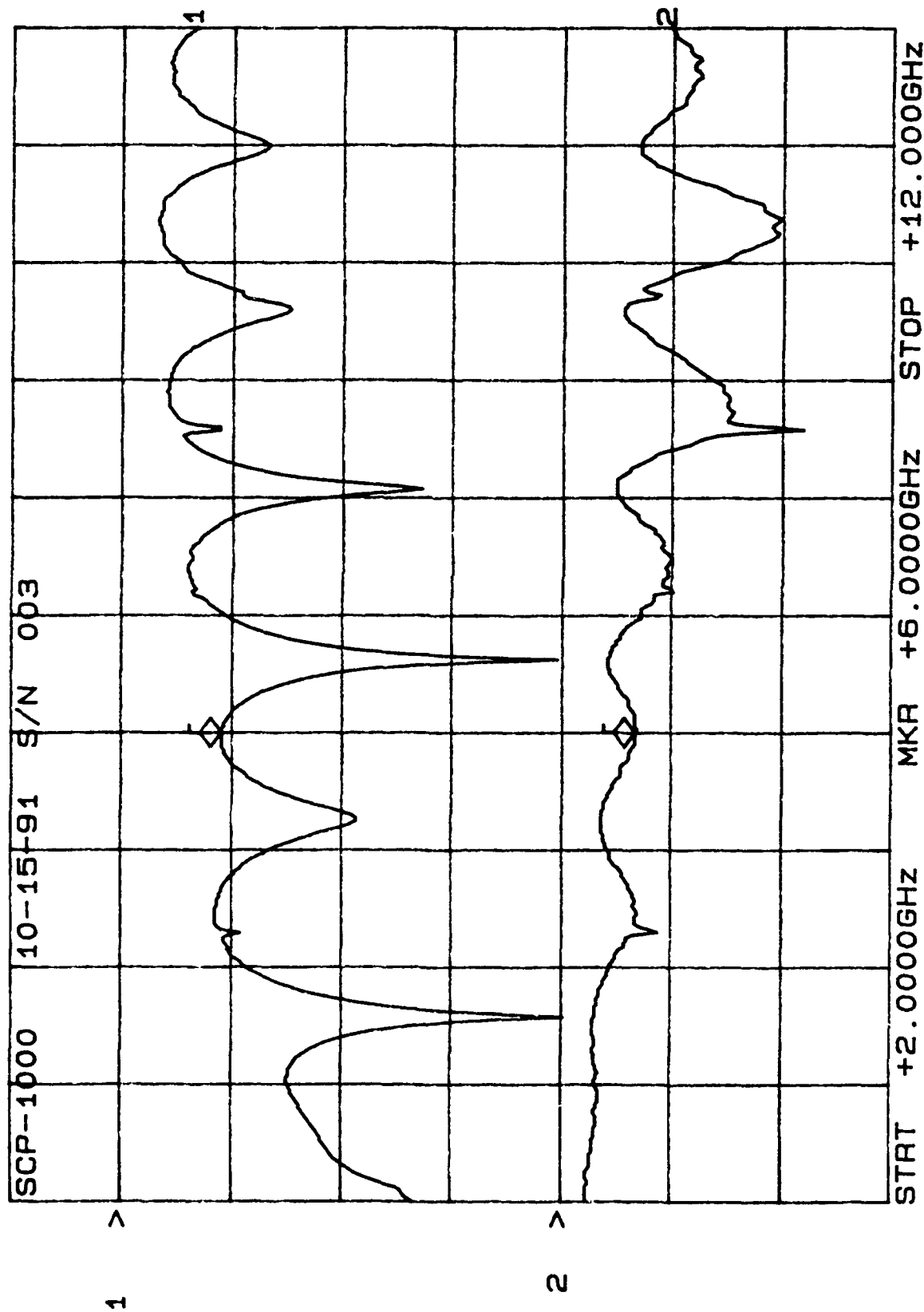
CH2: B -M A - 1.38 dB
2.0 dB/ REF + .00 dB



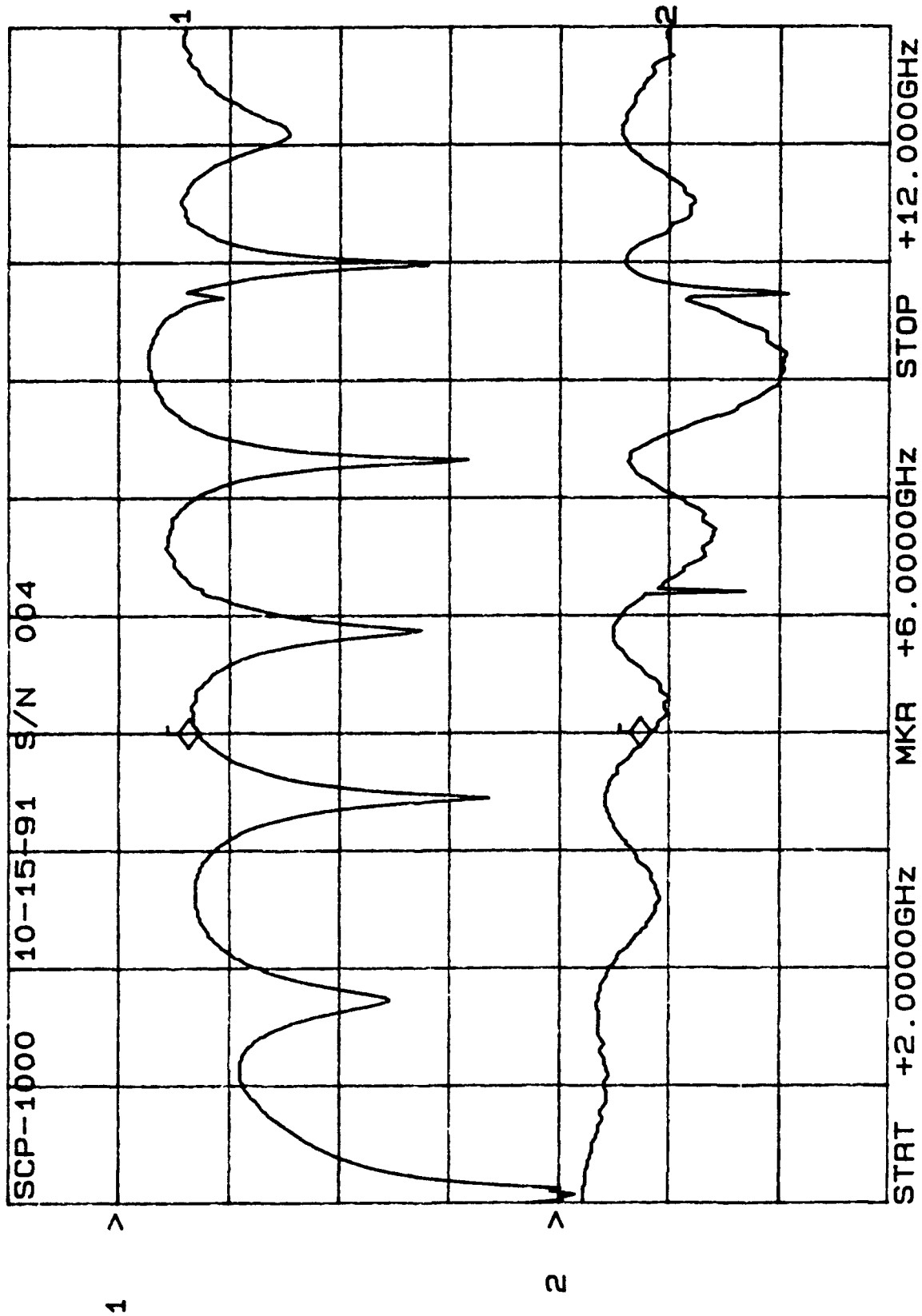
CH1: A -M REF - 9.21 dB CH2: B -M REF + 1.30 dB
 10.0 dB/ REF - .00 dB 2.0 dB/ REF + .00 dB



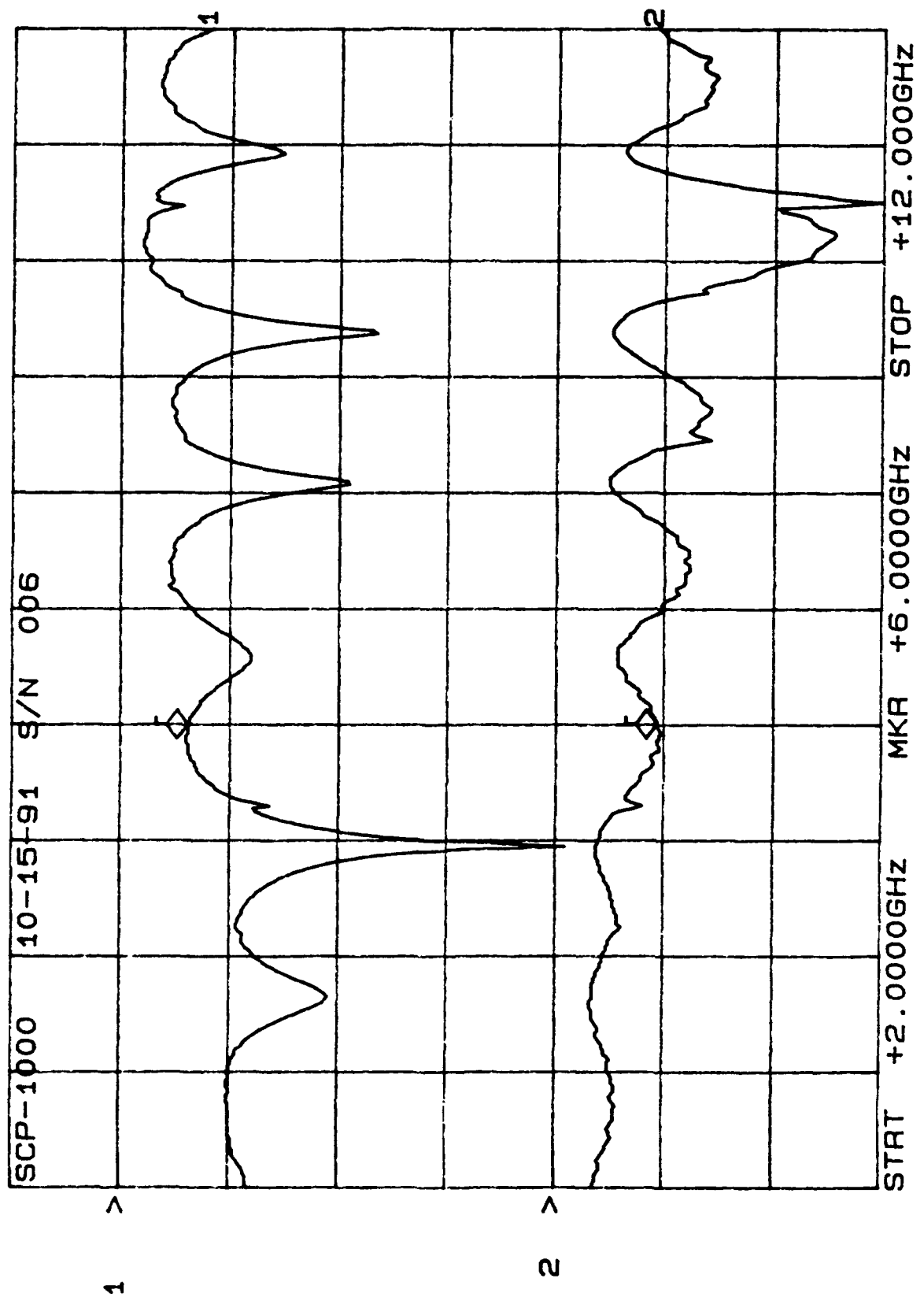
CH1: A -M REF - 8.94 dB CH2: B -M REF + 1.33 dB
 10.0 dB/ REF - .00 dB 2.0 dB/ REF + .00 dB



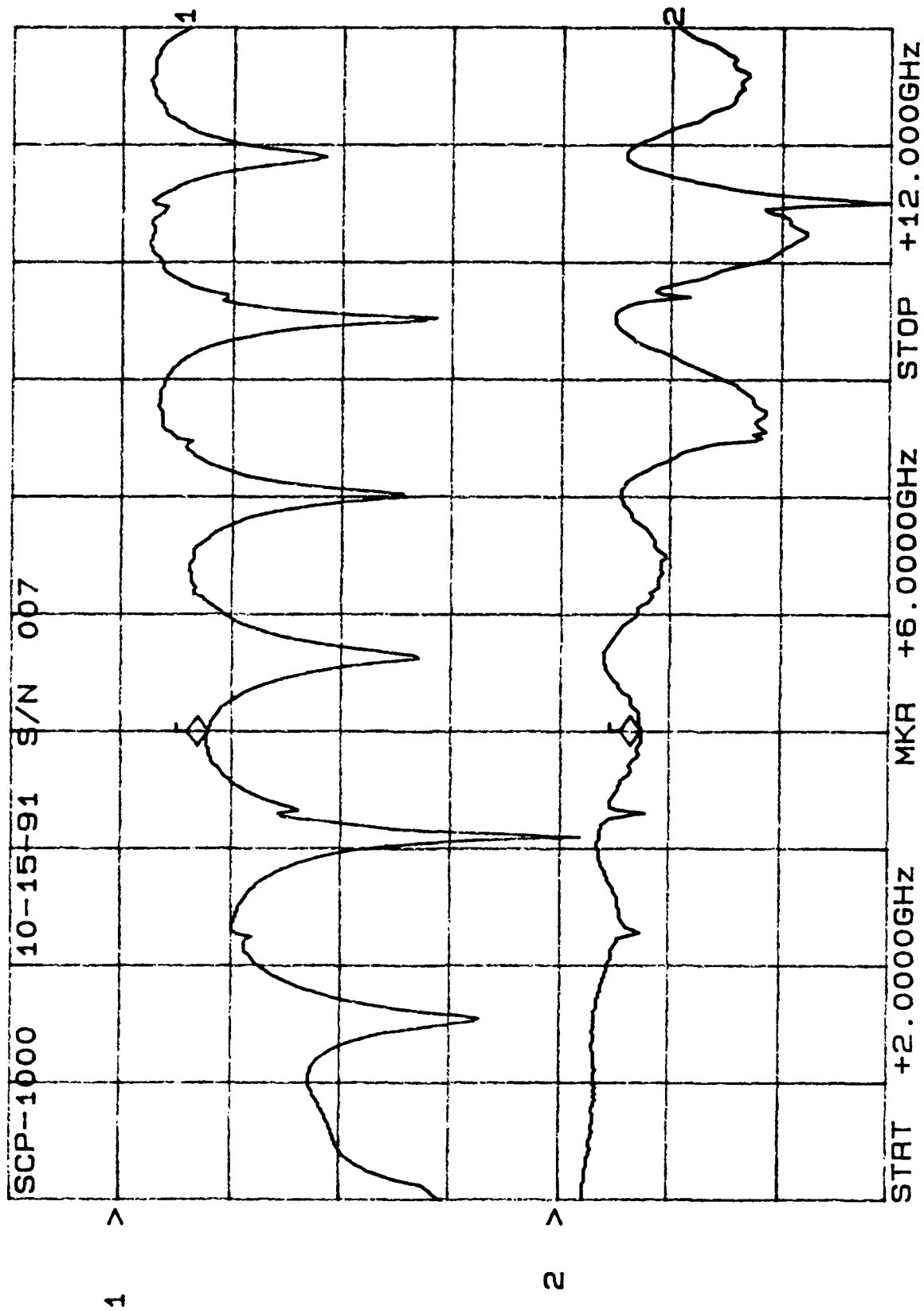
CH1: A -M = 7.13 dB CH2: B -M A - 1.68 dB
 10.0 dB/ REF - .00 dB 2.0 dB/ REF + .00 dB



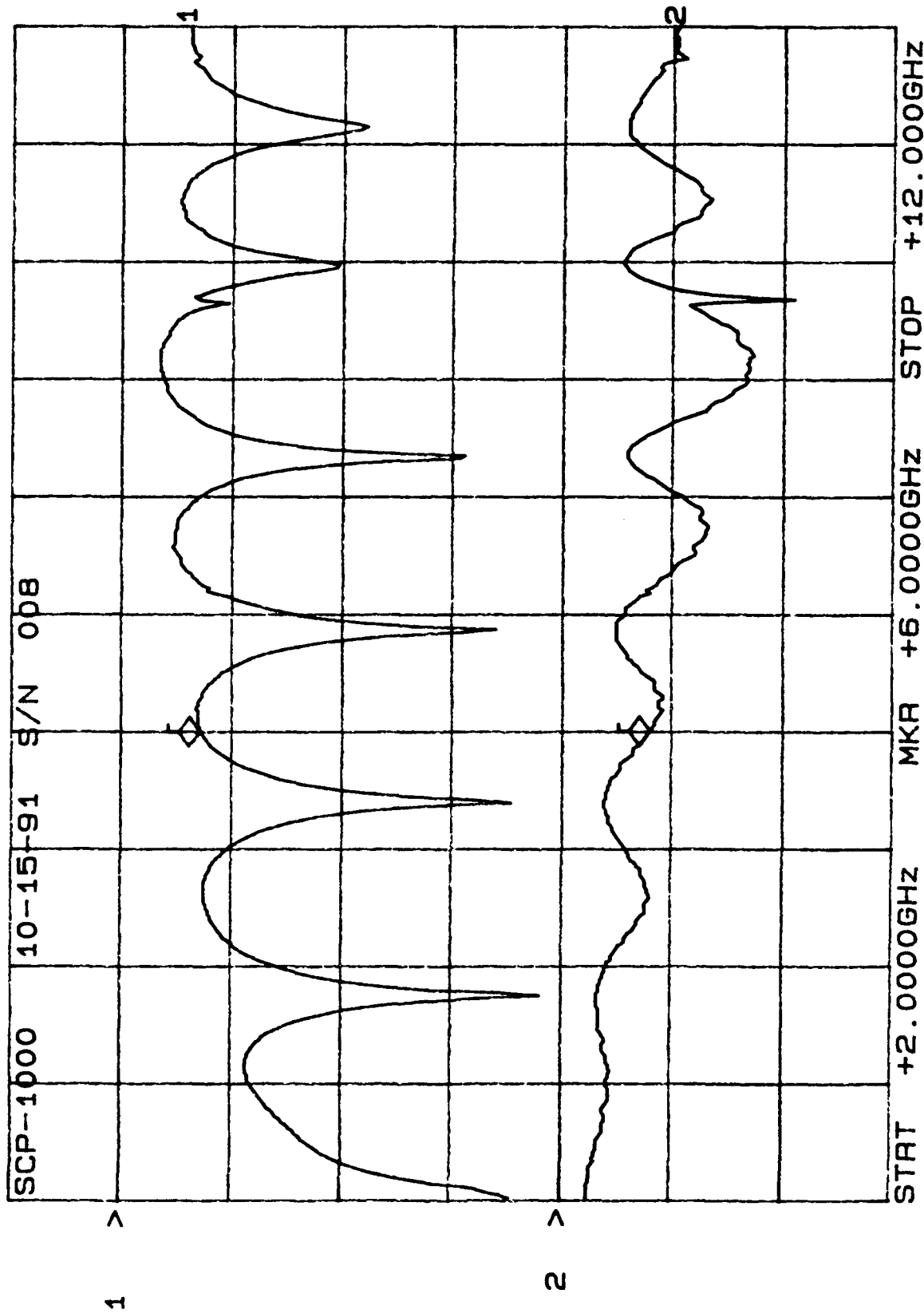
CH1: A -M REF - 6.16 dB 10.0 dB/ REF + 1.86 dB
 CH2: B -M REF + 2.0 dB/ REF + .00 dB



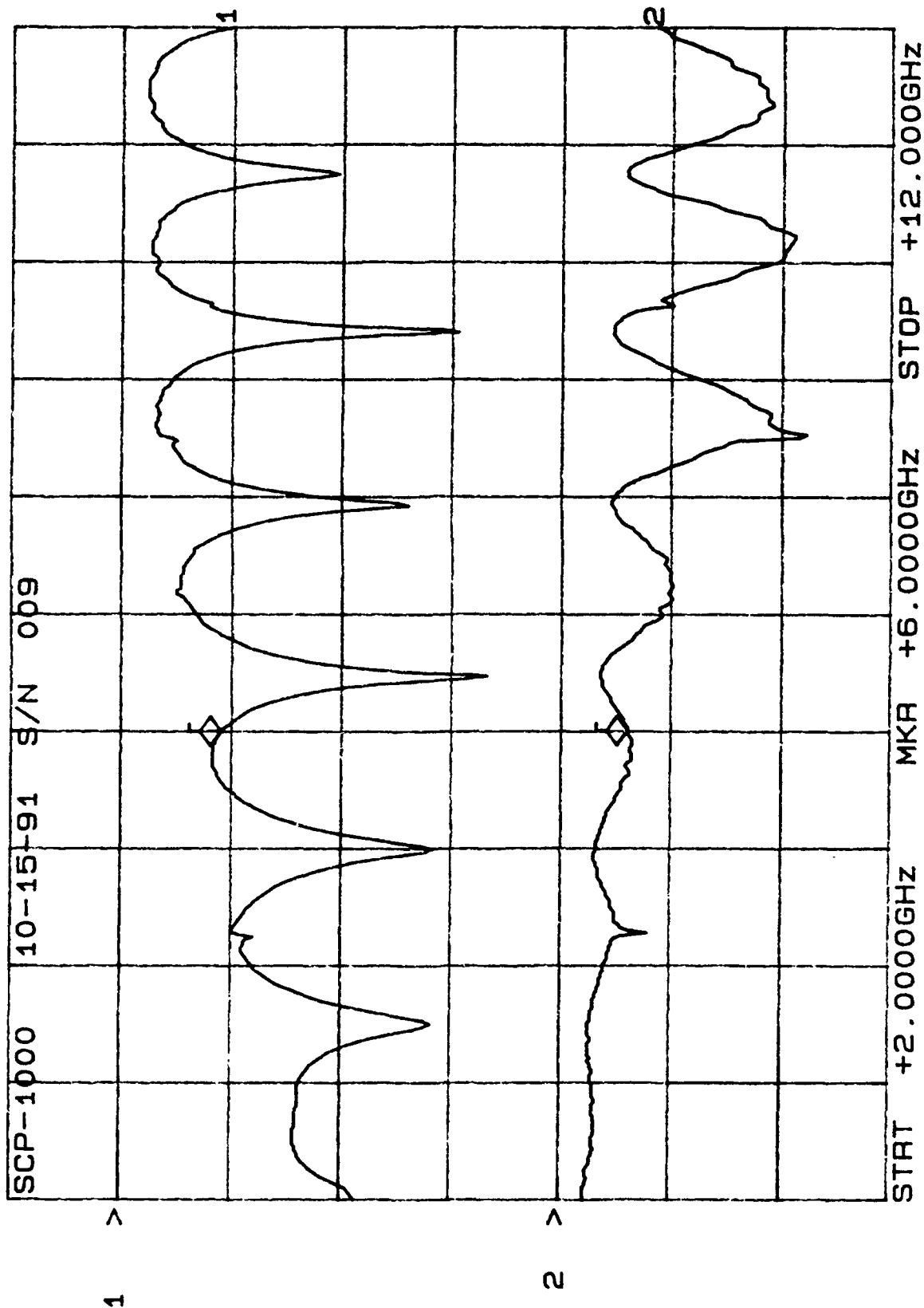
CH1: A -M REF = 7.73 dB CH2: B -M A = 1.46 dB
 10.0 dB/ REF = .00 dB 2.0 dB/ REF = .00 dB



CH1: A -M REF - 7.11 dB CH2: B -M REF + 1.59 dB
 10.0 dB/ REF - .00 dB 2.0 dB/ REF + .00 dB

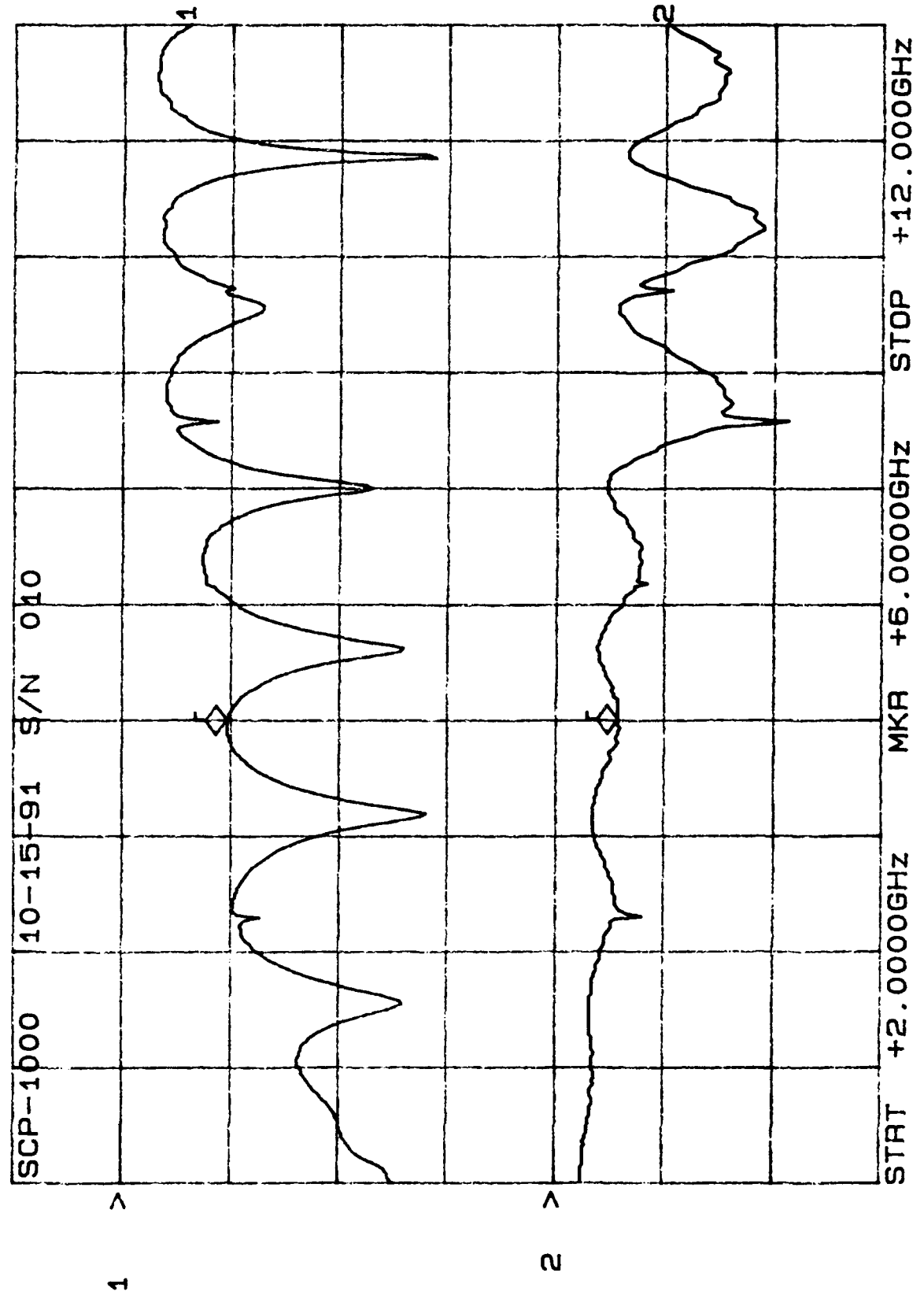


CH1: A -M REF = 8.99 dB CH2: B -M A = 1.21 dB
 10.0 dB/ REF = .00 dB 2.0 dB/ REF = .00 dB



Attenuation 50 cycles

CH1: A -M REF - 9.59 dB CH2: B -M REF + 1.15 dB
10.0 dB/ REF - .00 dB 2.0 dB/ REF + .00 dB



20 CYCLES

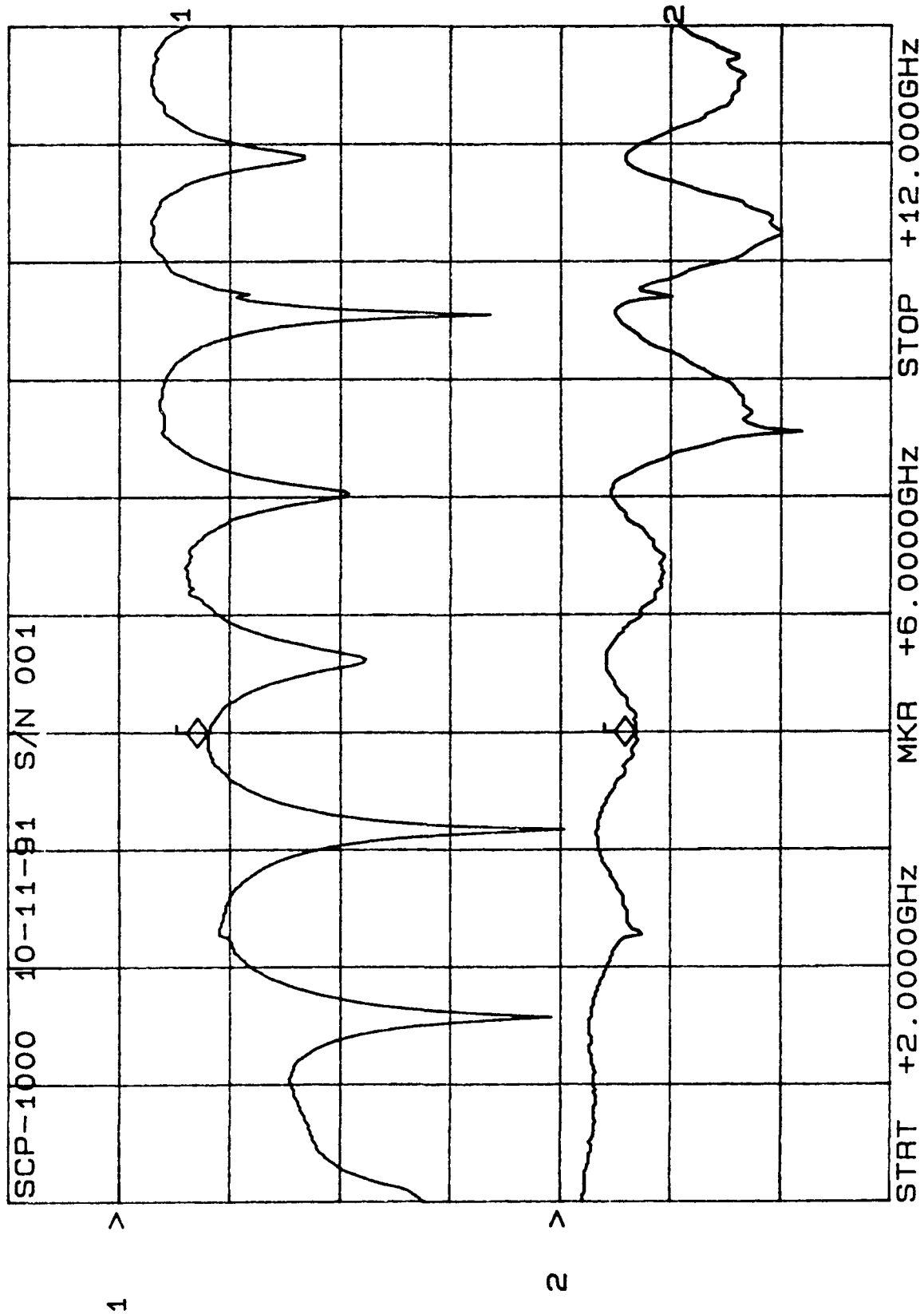


ACCEPT
02

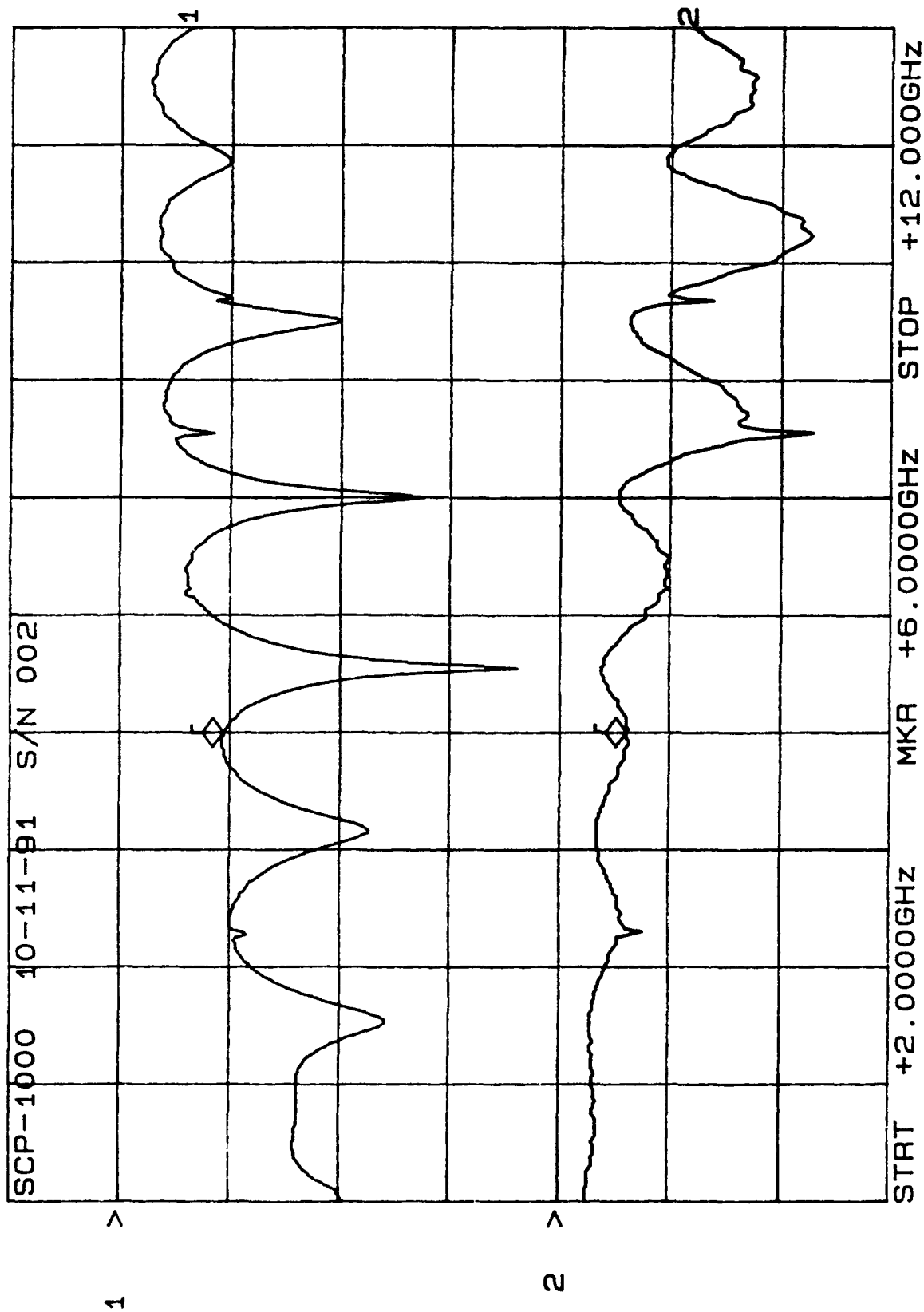
AV-631/R-10-87

After 30 cycles

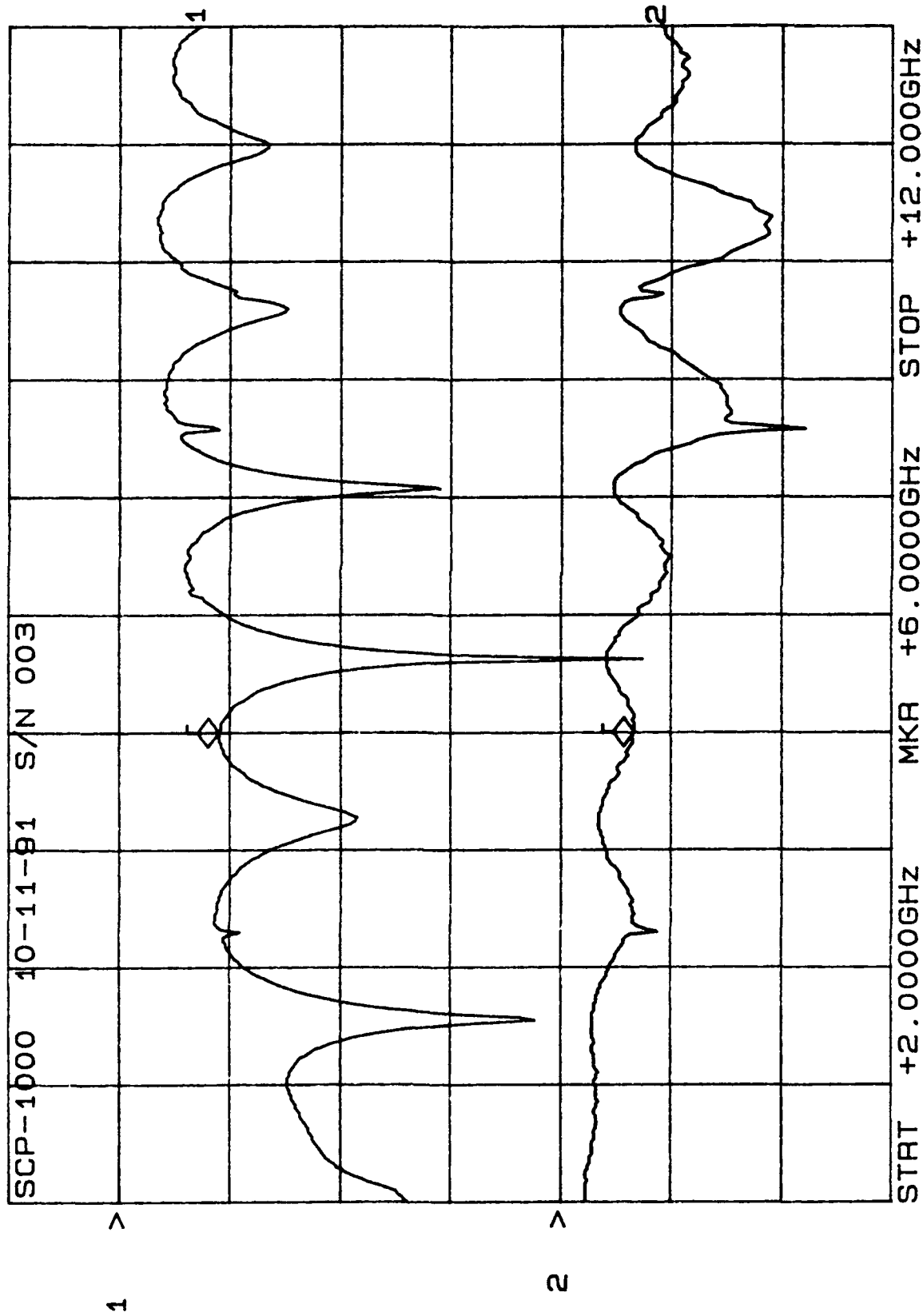
CH1: A -M 10.0 dB/ REF - 8.00 dB CH2: B -M 2.0 dB/ REF + 1.37 dB + .00 dB



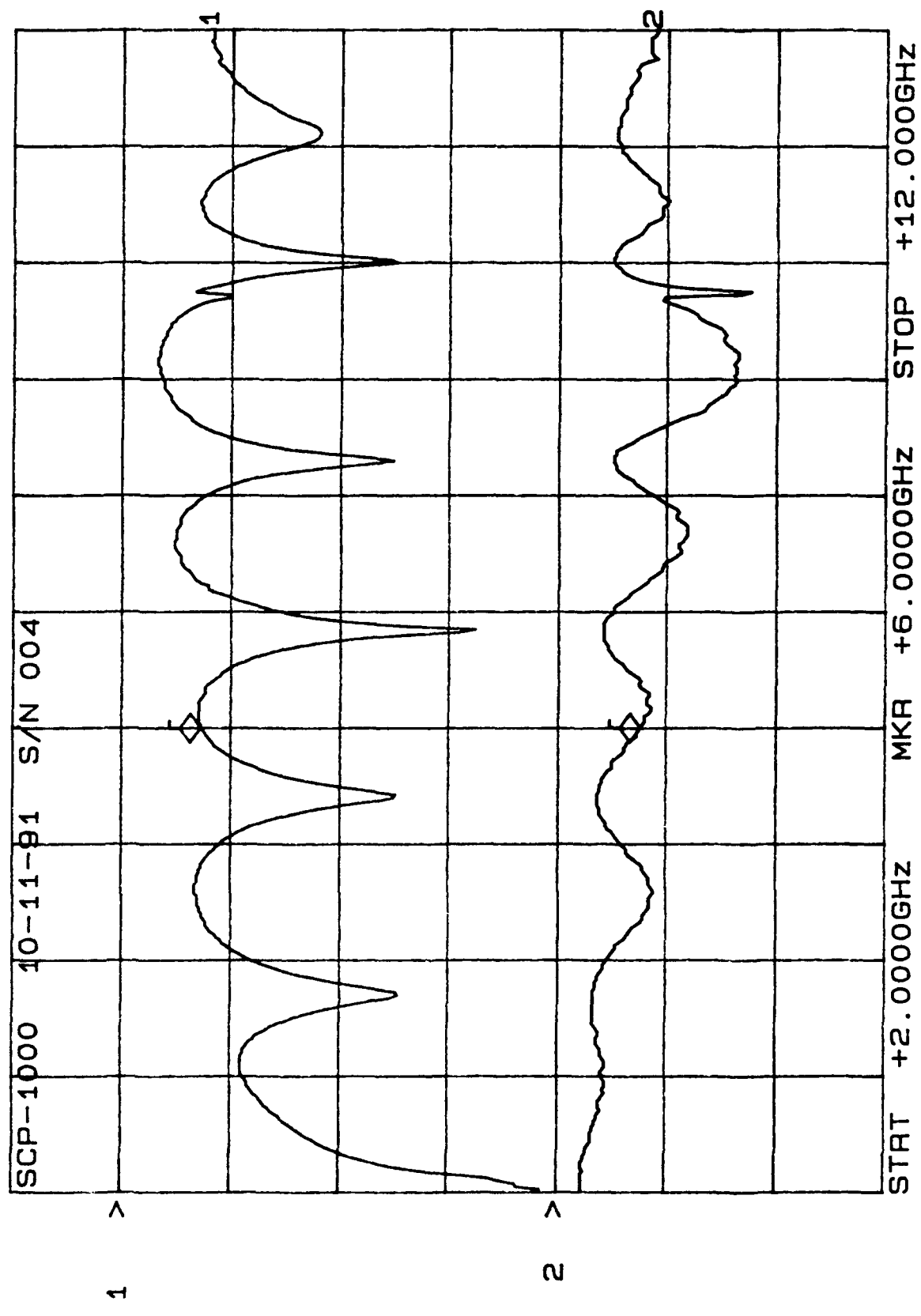
CH1: A -M REF - 9.41 dB CH2: B -M A - 1.23 dB
 10.0 dB/ REF - .00 dB 2.0 dB/ REF + .00 dB



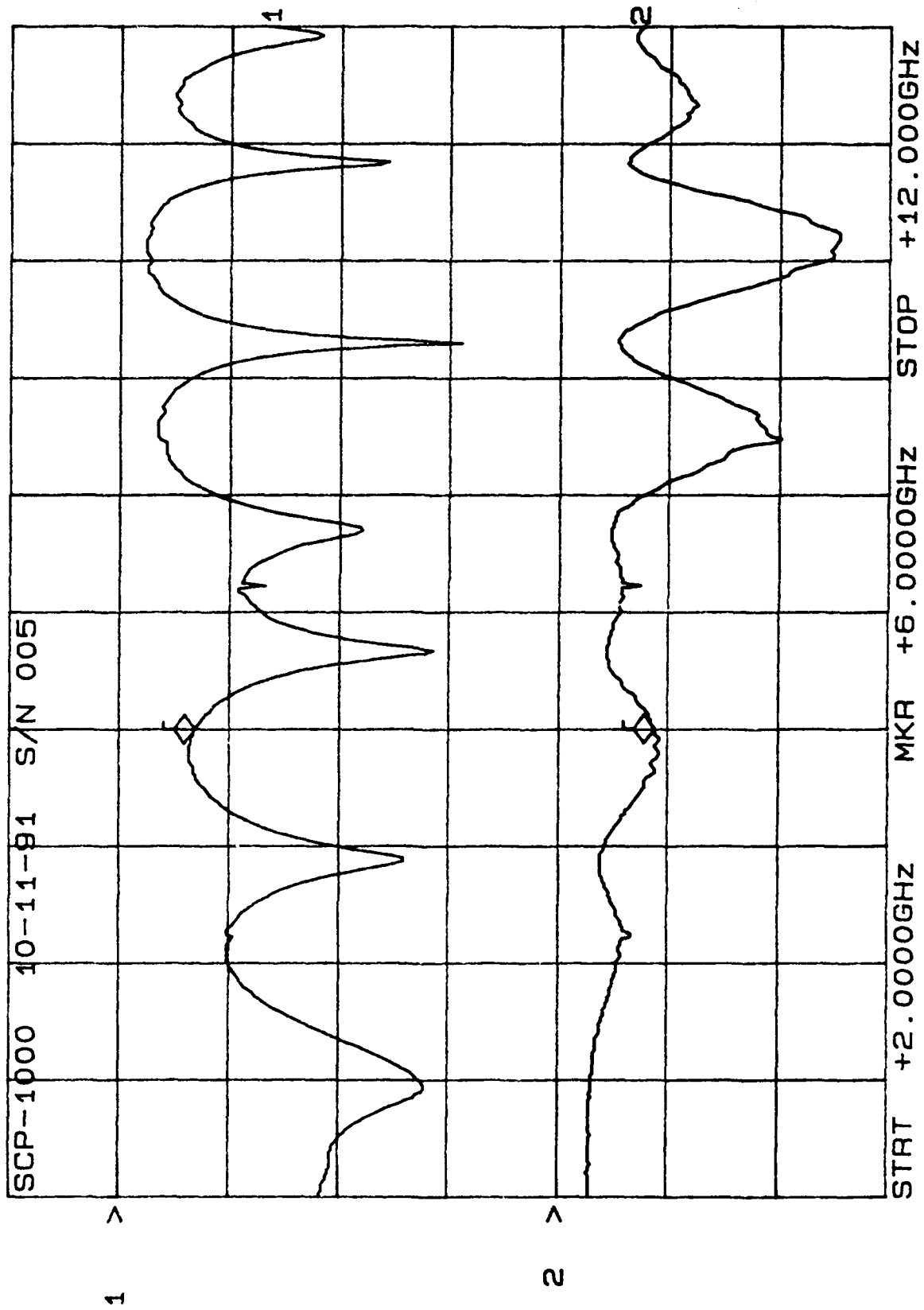
CH1: A -M REF - 10.0 dB/ REF - 9.01 dB - 1.31 dB
CH2: B -M REF + 2.0 dB/ REF + .00 dB



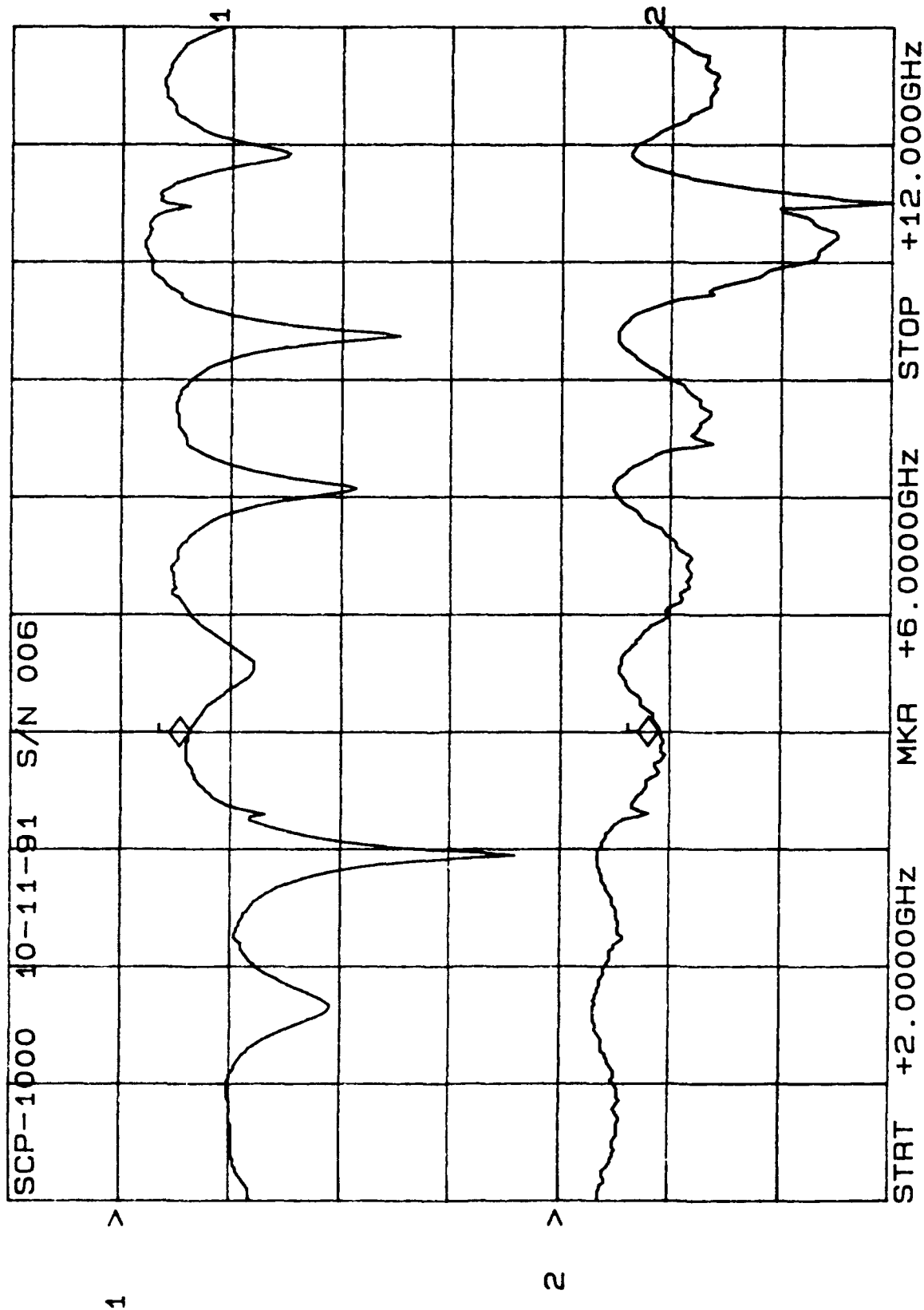
CH1: A -M REF = 7.25 dB CH2: B -M REF = 1.51 dB
 10.0 dB/ REF = .00 dB 2.0 dB/ REF = .00 dB



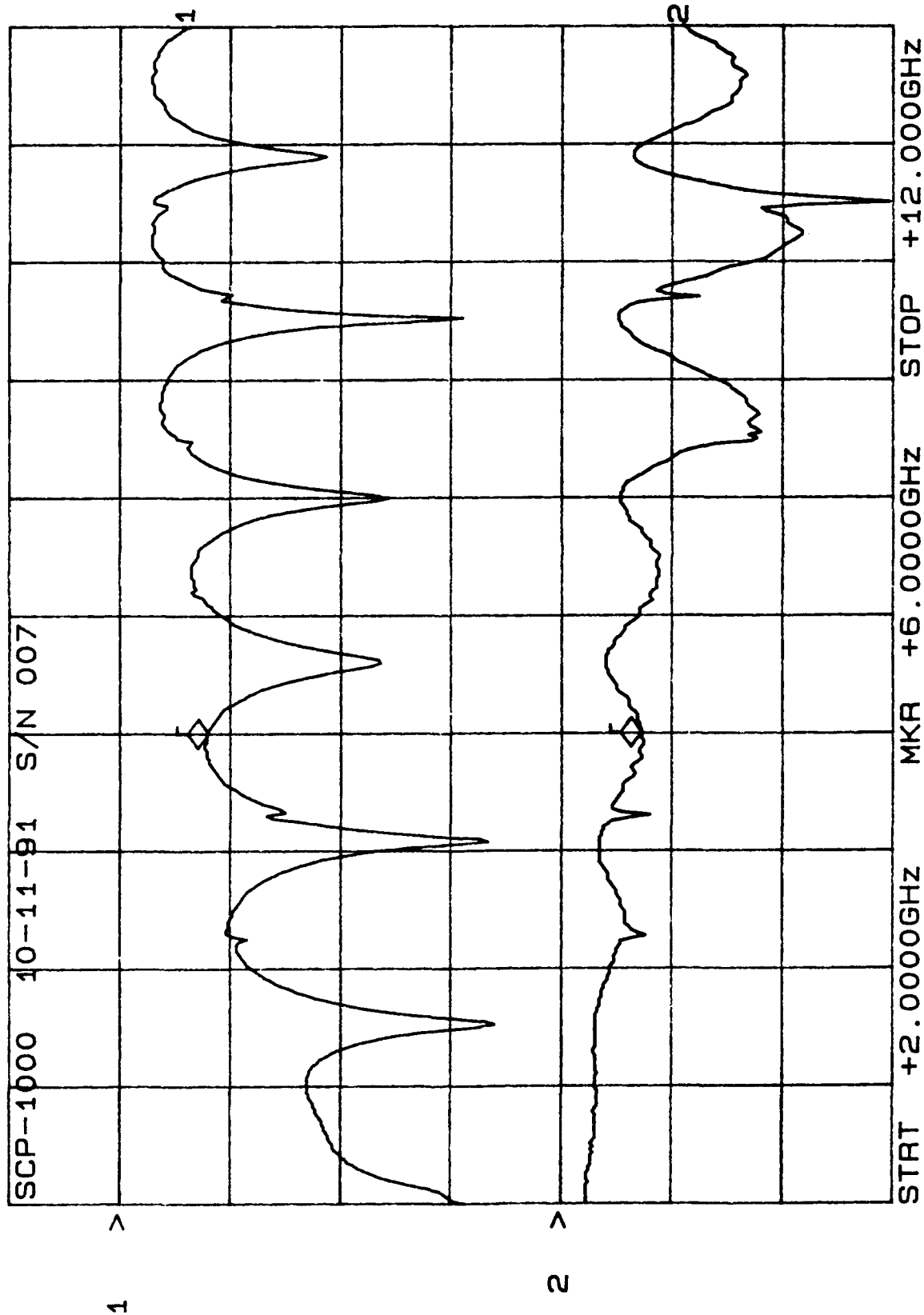
CH1: A -M REF - 6.85 dB CH2: B -M A - 1.73 dB
10.0 dB/ REF - .00 dB 2.0 dB/ REF + .00 dB



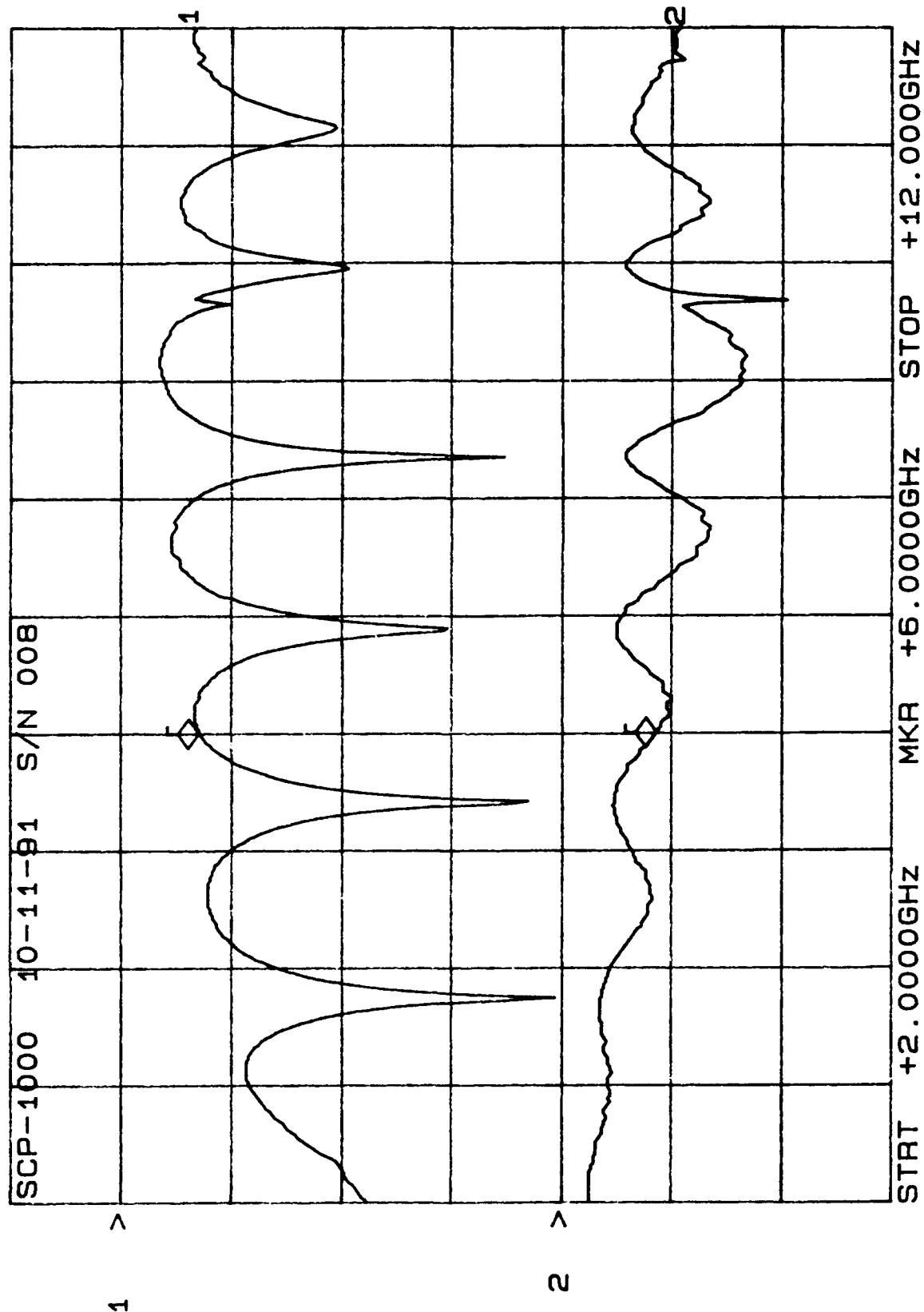
CH1: A -M REF - 6.21 dB CH2: B -M REF + 1.79 dB
 10.0 dB/ REF 2.0 dB/ REF



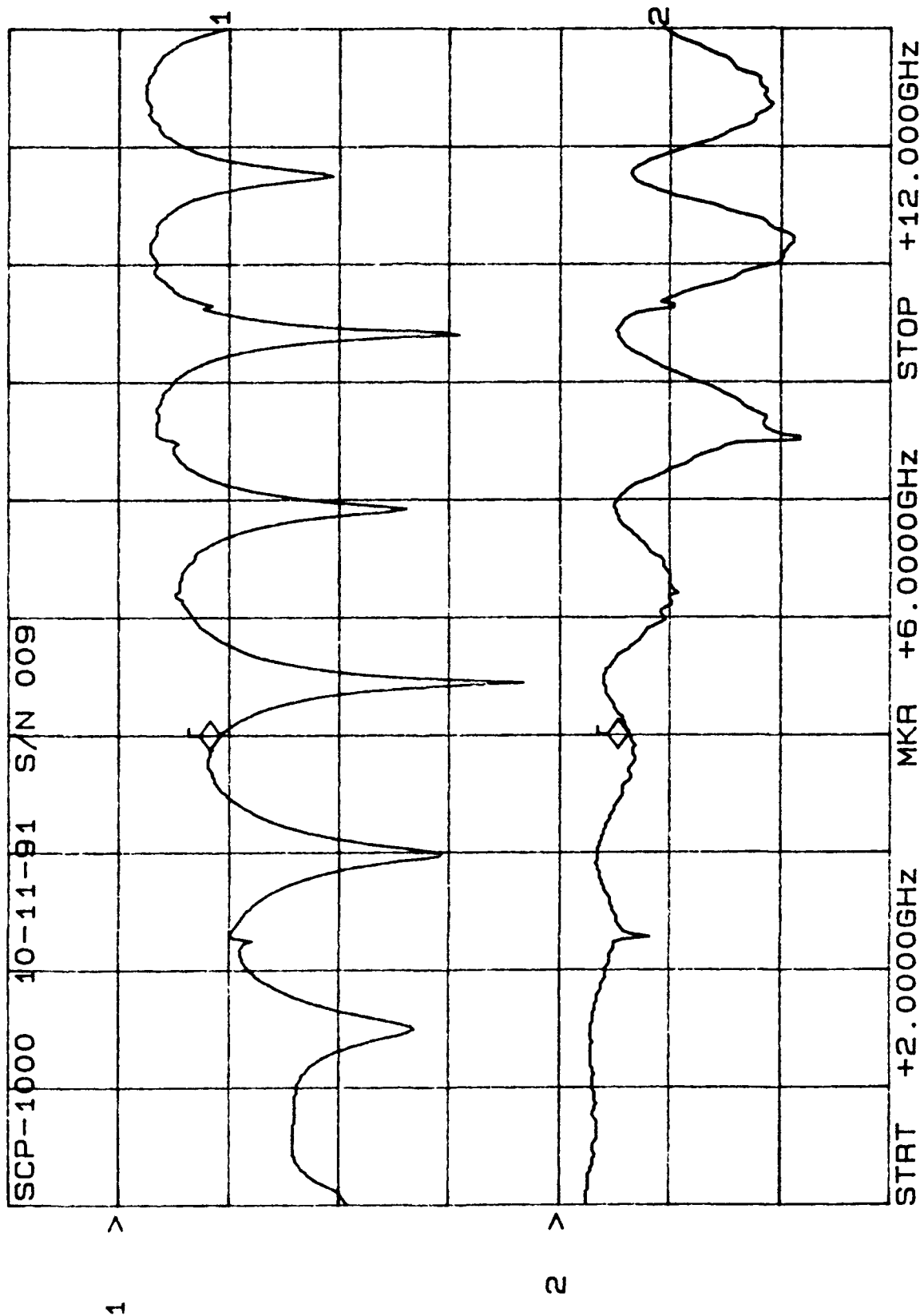
CH1: A -M - 7.91 dB CH2: B -M A - 1.44 dB
 10.0 dB/ REF - .00 dB 2.0 dB/ REF + .00 dB



CH1: A -M - 7.11 dB CH2: B -M A - 1.70 dB
10.0 dB/ REF - .00 dB 2.0 dB/ REF + .00 dB

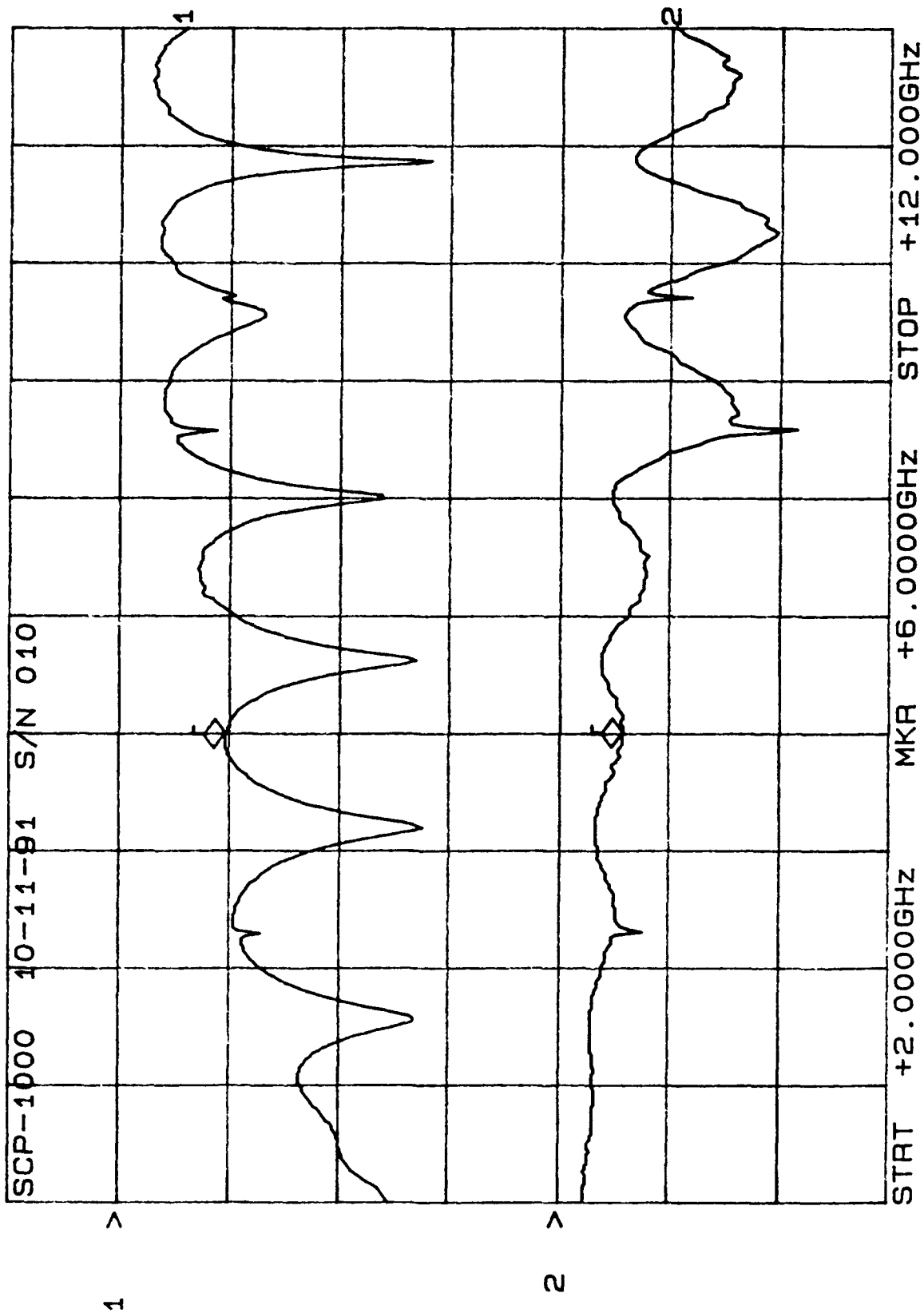


CH1: A -M - 9.14 dB CH2: B -M A - 1.26 dB
10.0 dB/ REF - .00 dB 2.0 dB/ REF + .00 dB



After 20 cycles

CH1: A -M - 9.56 dB CH2: B -M A - 1.12 dB
10.0 dB/ REF - .00 dB 2.0 dB/ REF + .00 dB



10 Cycles

After 10 cycles

CERTIFIED TEST
DATA

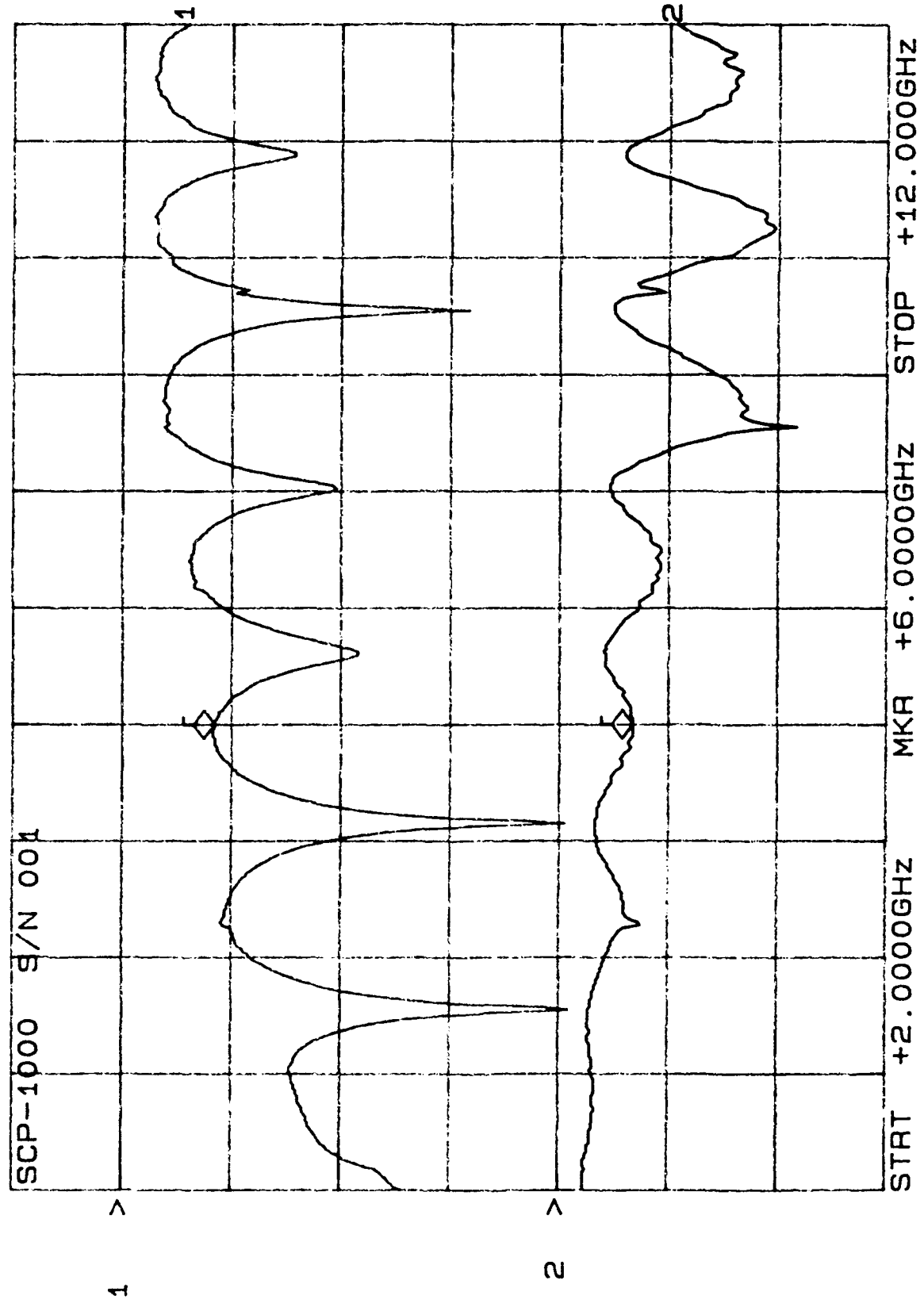
DEPT # 3020 DIV LOC # 2016



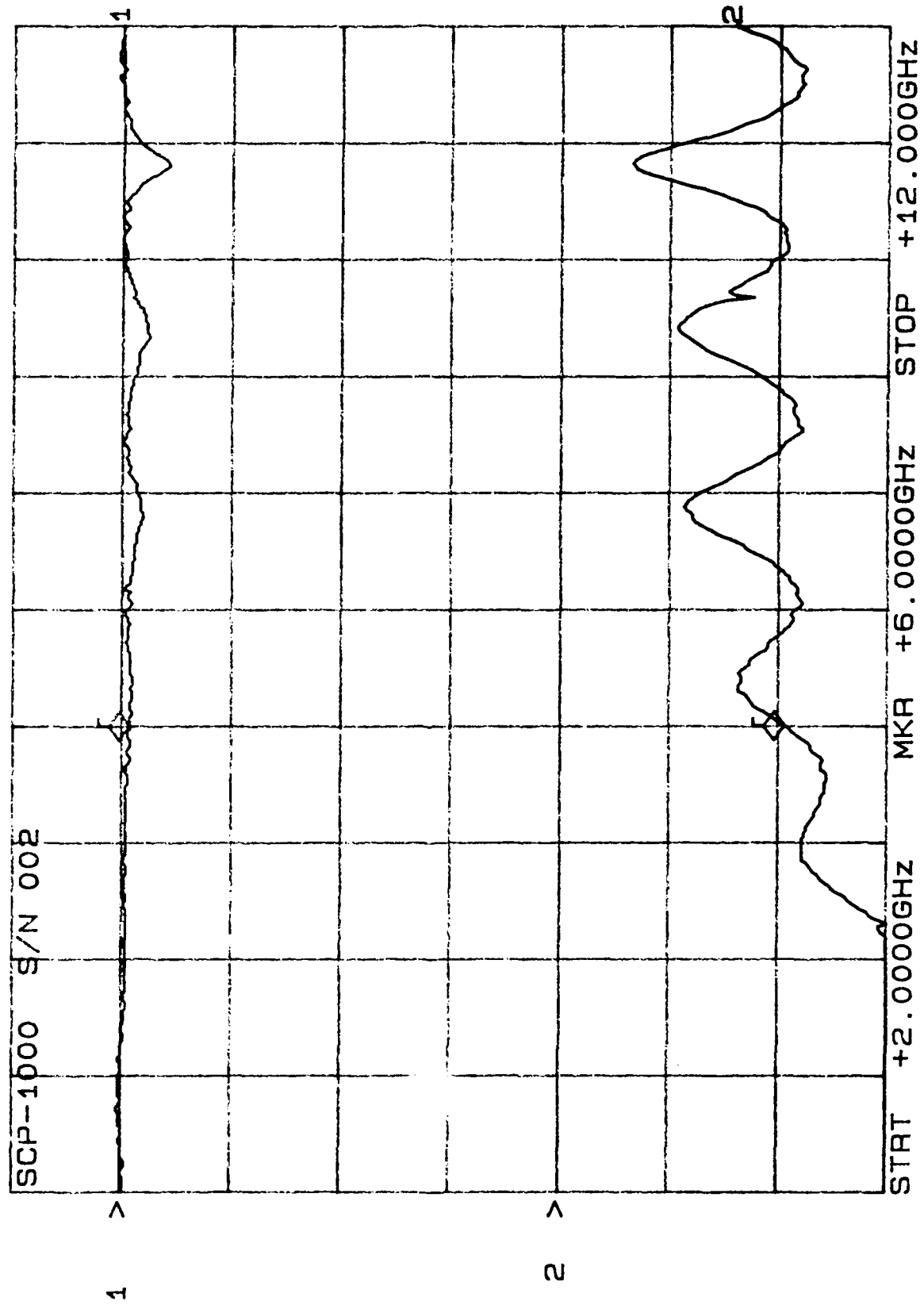
START DATE 10-9-91	CUSTOMER STEVE CHAN EXT# 4361		QUALITY ACCTPT ACCEPT 02
COMPL DATE 10-9-91	TYPE OF TEST FINE LEAK TEST	AVANTEK J1-32	TEST COND. 10-ES0 CHARGE TEST COND. 52015-205 A
DEVICE TYPE SEP-1000	TEST REQUIREMENTS MIL STD-883C METHOD 1014.8		BOMB PRESSURE AND DURATION 30 PSI @ 2 HRS
QTY START 10	QTY COMPL 10	SENSITIVITY N/A CC/SEC	
S/N LOT No.	LEAK RATE (CC/SEC)	PASS/FAIL	DWELL TIME
0/c # 9137			
S/N # 001	1 X 10 ⁻⁹		2 min
002	1 X 10 ⁻⁹		
003	1 X 10 ⁻⁹		
004	1 X 10 ⁻⁹		
005	3 X 10 ⁻⁹		
006	2 X 10 ⁻⁹		
007	1 X 10 ⁻⁹		
008	1 X 10 ⁻⁹		
009	2 X 10 ⁻⁸		
010	1 X 10 ⁻⁹		

16.7791

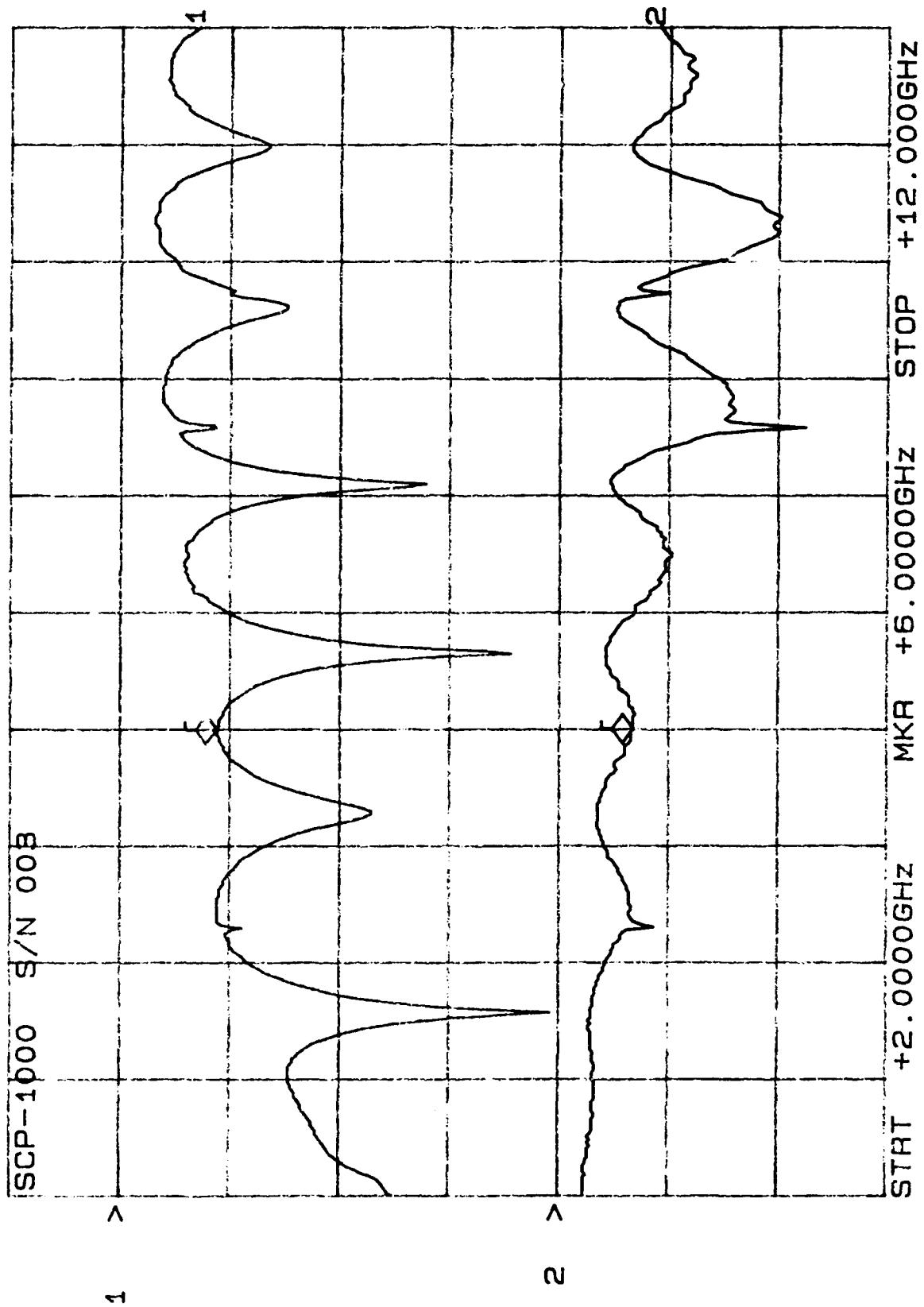
CH1: A -M REF = 8.35 dB CH2: B -M A - 1.32 dB
10.0 dB/ REF 2.0 dB/ REF + .00 dB



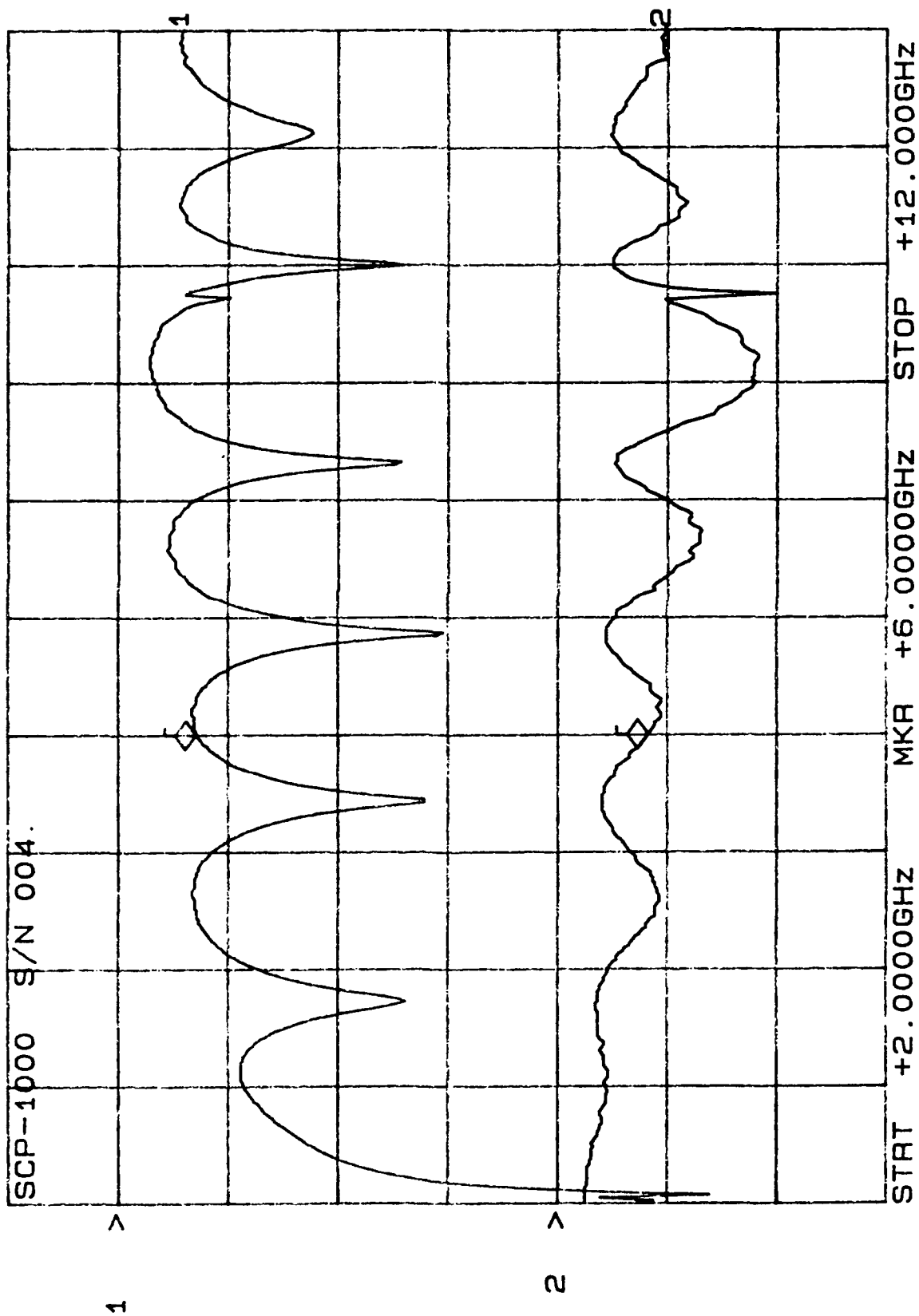
CH1: A -M REF - .67 dB CH2: B -M A - 10.22 dB
 10.0 dB/ REF - 5.0 dB/ REF + .00 dB



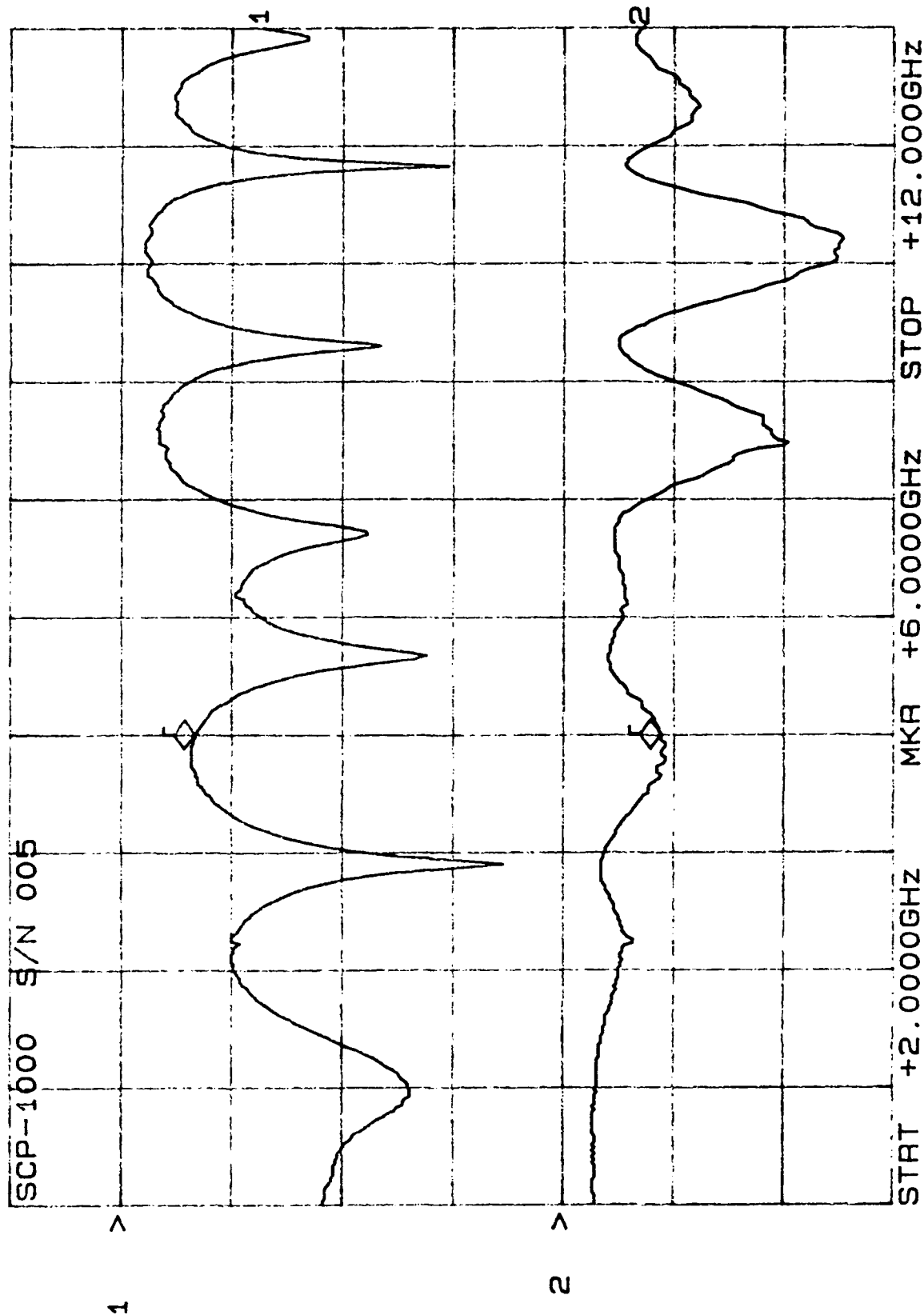
CH1: A -M REF - 8.85 dB CH2: B -M REF + 1.31 dB
 10.0 dB/ REF - .00 dB 2.0 dB/ REF + .00 dB



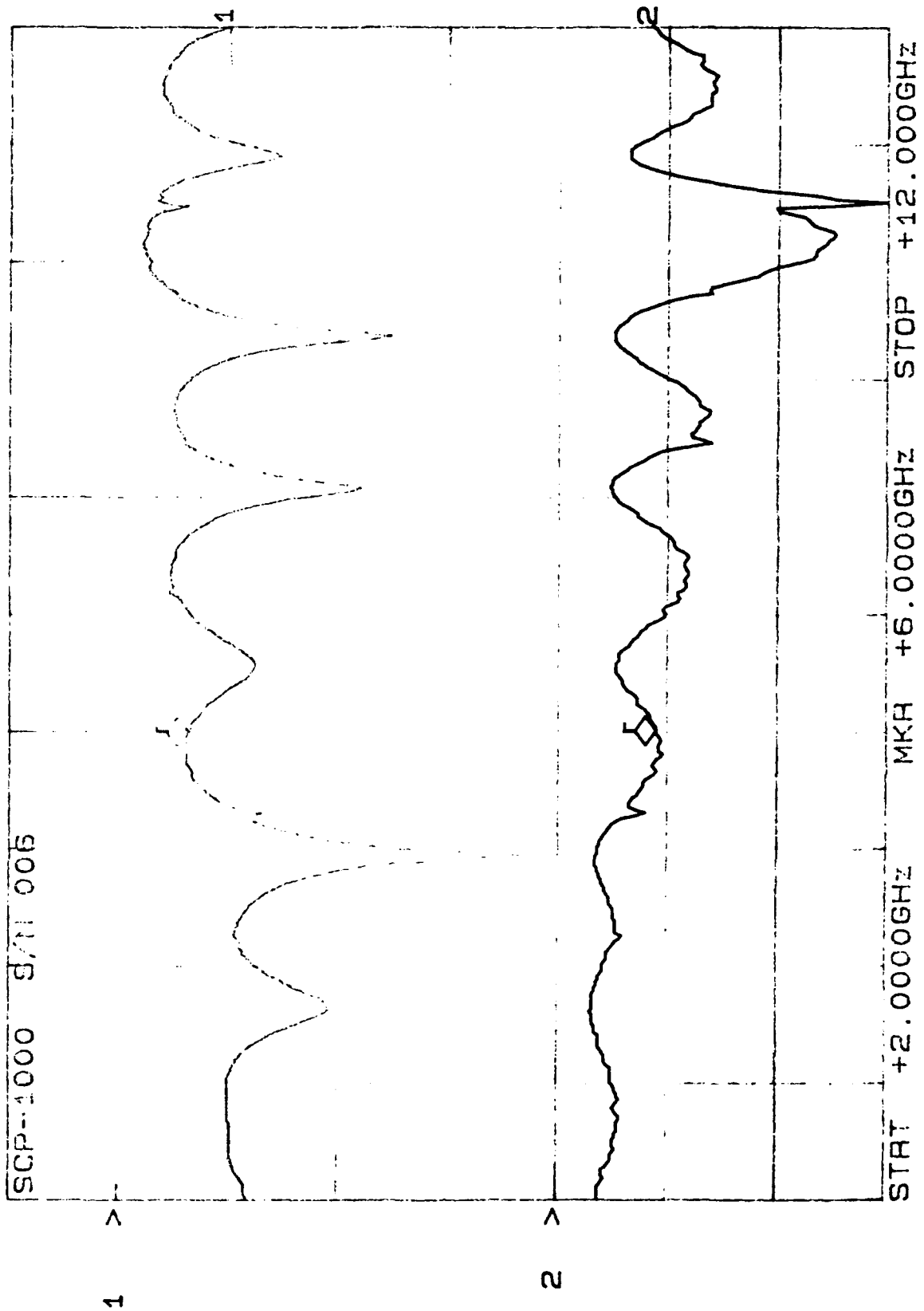
CH1: A -M REF = 7.11 dB CH2: B -M A = 1.63 dB
10.0 dB/ REF = .00 dB 2.0 dB/ REF = .00 dB



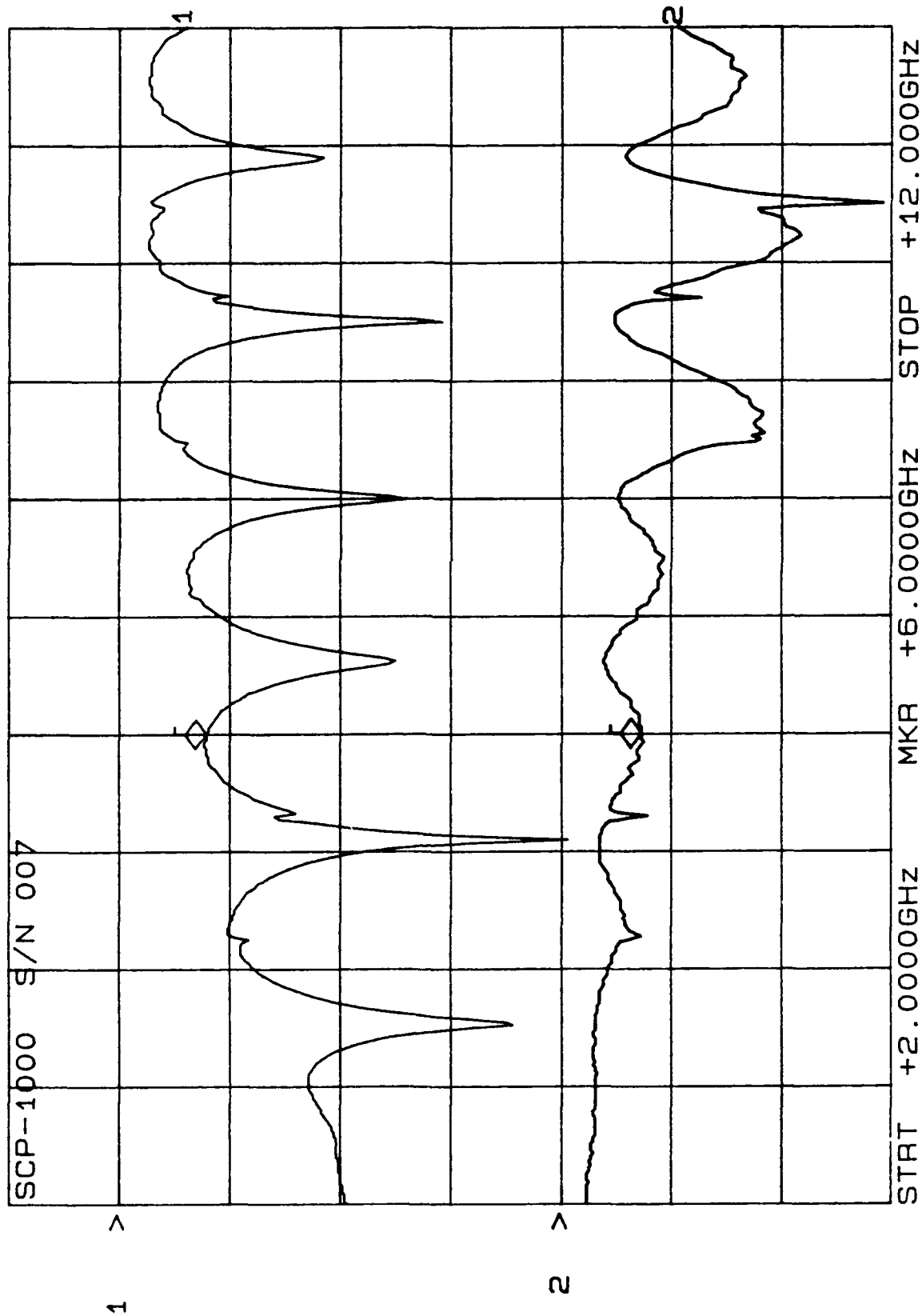
CH1: A -M REF - 6.69 dB CH2: B -M REF + 1.73 dB
10.0 dB/ REF 2.0 dB/ REF + .00 dB



CH1: A -M REF - 6.33 dB CH2: B -M A - 1.78 dB
10.0 dB/ REF 2.0 dB/ REF + .00 dB

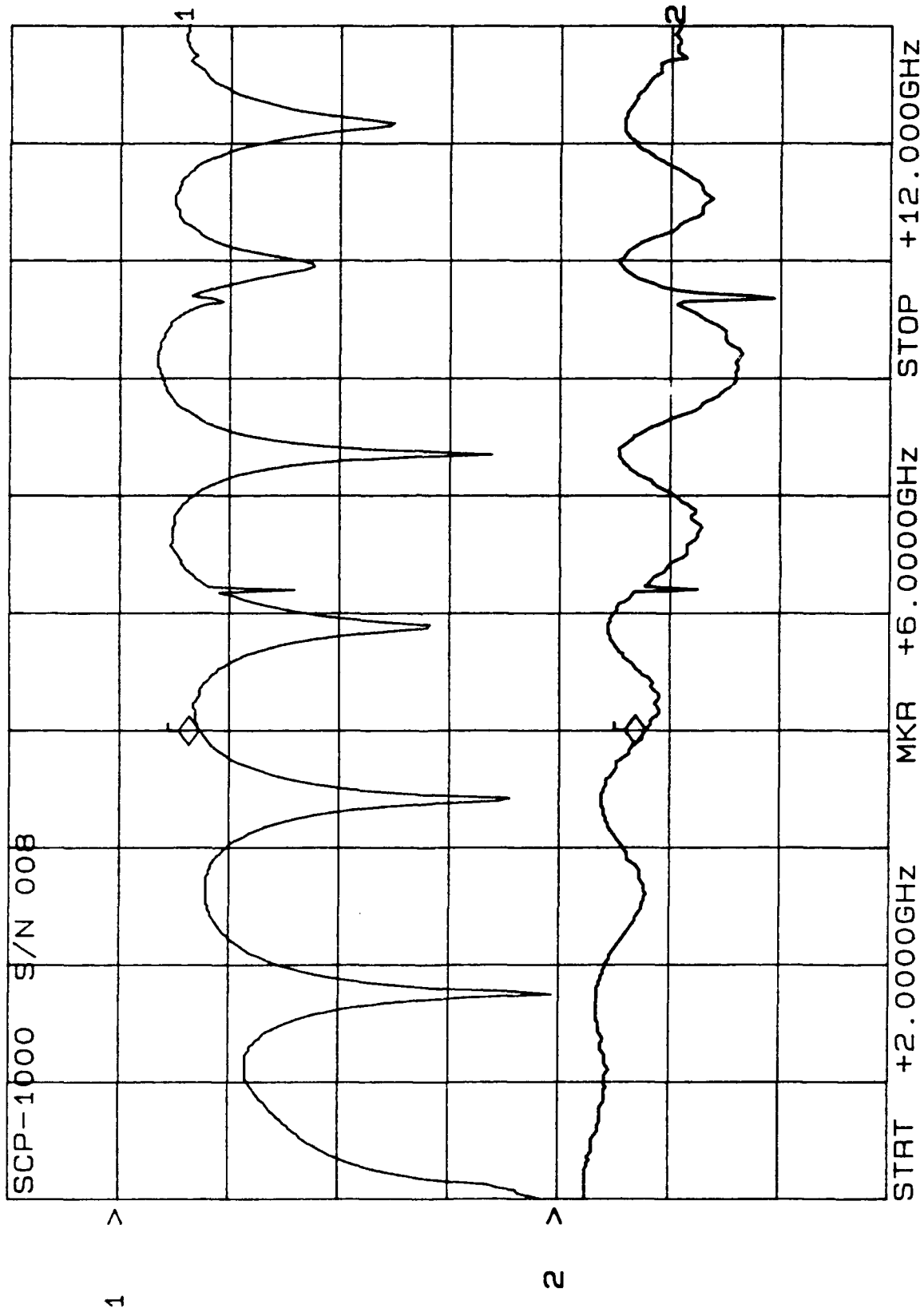


CH1: A -M - 7.83 dB CH2: B -M A - 1.45 dB
 10.0 dB/ REF - .00 dB 2.0 dB/ REF + .00 dB



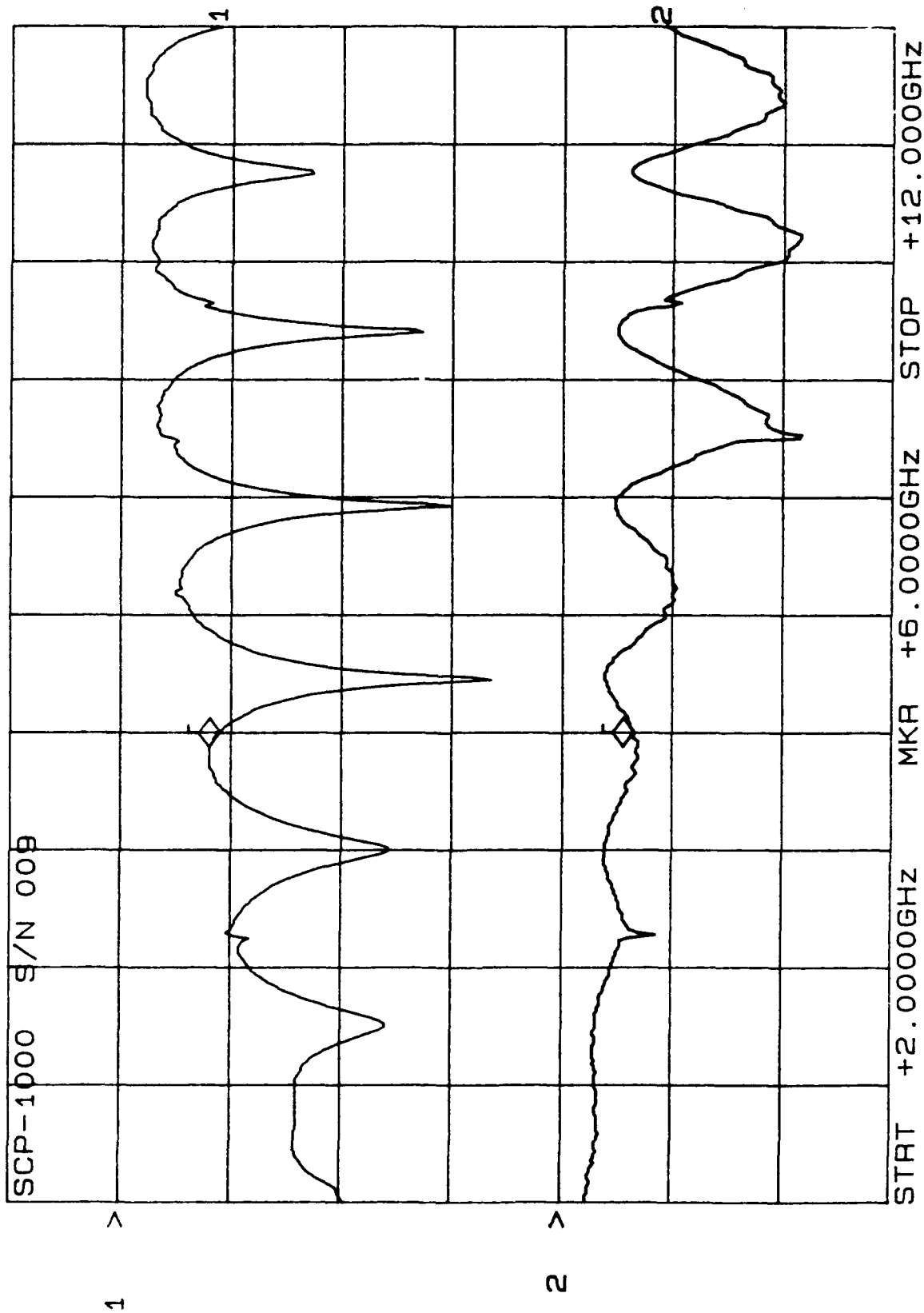
10-3/91

CH1: A -M - 7.19 dB CH2: B -M A - 1.55 dB
 10.0 dB/ REF - .00 dB 2.0 dB/ REF + .00 dB



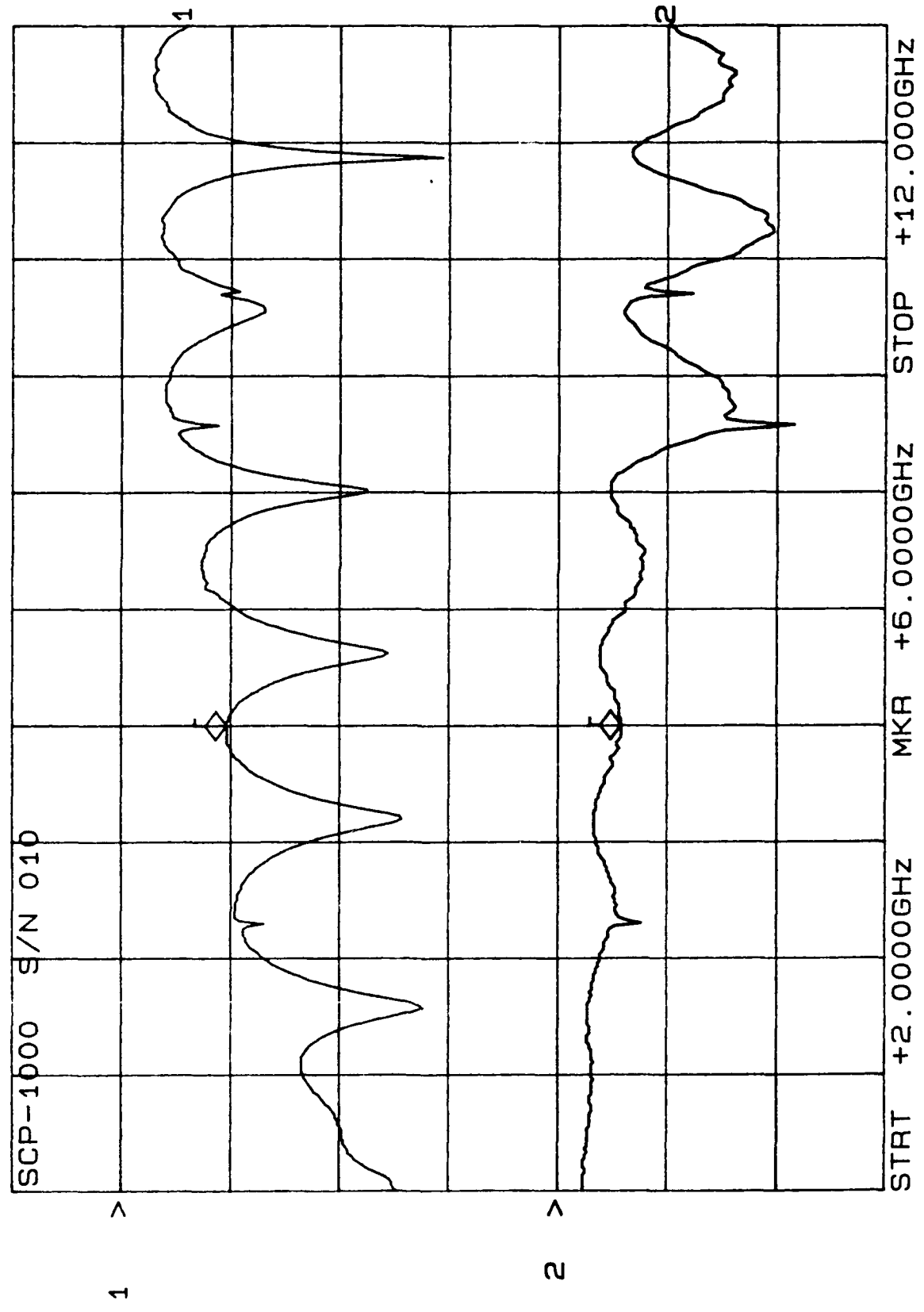
10/9/91

CH1: A -M REF = 8.86 dB
10.0 dB/ REF = 1.27 dB
CH2: B -M REF + 2.0 dB/ REF + .00 dB



After 10 cycles

CH1: A -M REF - 10.0 dB/ REF - 9.51 dB
CH2: B -M REF + 1.12 dB
2.0 dB/ REF + .00 dB



5 Cycles



CERTIFIED TEST DATA

After 5 cycles

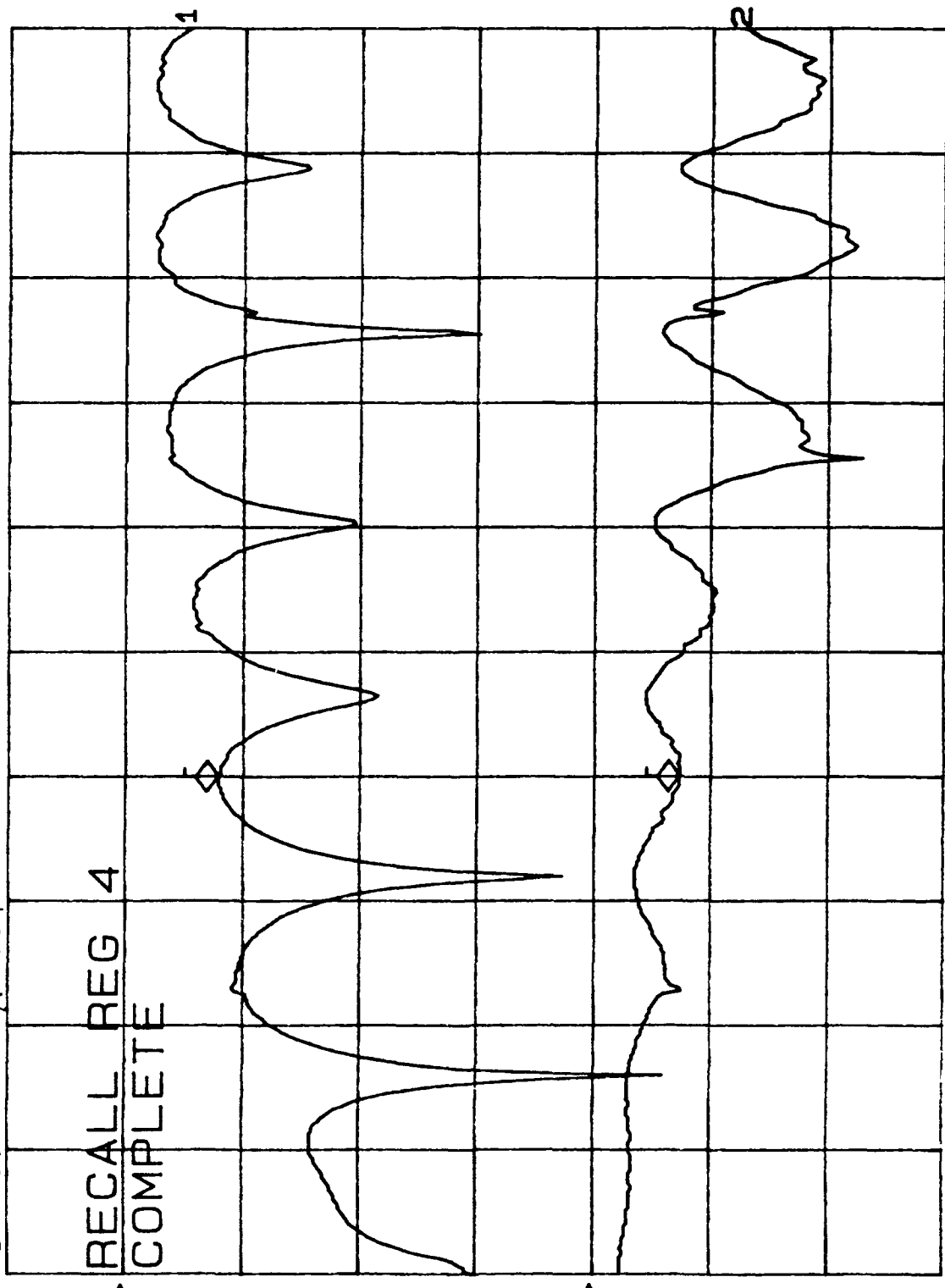


START DATE	CUSTOMER	QUALITY ACCT	TEST COND.
10-8-91	Engelberg	WD/CSO	A
COMPL DATE	TYPE OF TEST	WD/CSO	TEST COND.
10-8-91	FINE LEAK TEST	57016205	A
DEVICE TYPE	TEST REQUIREMENTS	BOMB PRESSURE AND DURATION	
SCP-1000/200	MIL STD-883C METHOD 1014.8		
QTY START	QTY COMPL	SENSITIVITY	
10/10	10/9	5x10 ⁻⁷ CC/SEC	
S/N LOT No.	LEAK RATE (CC/SEC)	PASS/FAIL	DWELL TIME
001 SCP-2000	1x10 ⁻⁹	PASS	
002	1x10 ⁻⁹		
003	1x10 ⁻⁸		
004	3x10 ⁻⁹		
005	1x10 ⁻⁹		
006	1x10 ⁻⁹		
007	1x10 ⁻⁹		
008	2x10 ⁻⁹		
009	1x10 ⁻⁹		
010	1x10 ⁻⁶	FAIL	DN 92.877
001 SCP-1000	2x10 ⁻⁹	PASS	
002	5x10 ⁻⁹		
003	2x10 ⁻⁹		
004	2x10 ⁻⁹		
005	5x10 ⁻⁹		
006	3x10 ⁻⁹		
007	2x10 ⁻⁹		
008	1x10 ⁻⁹		
009	4x10 ⁻⁸		
010	1x10 ⁻⁹		

After 3 cycles

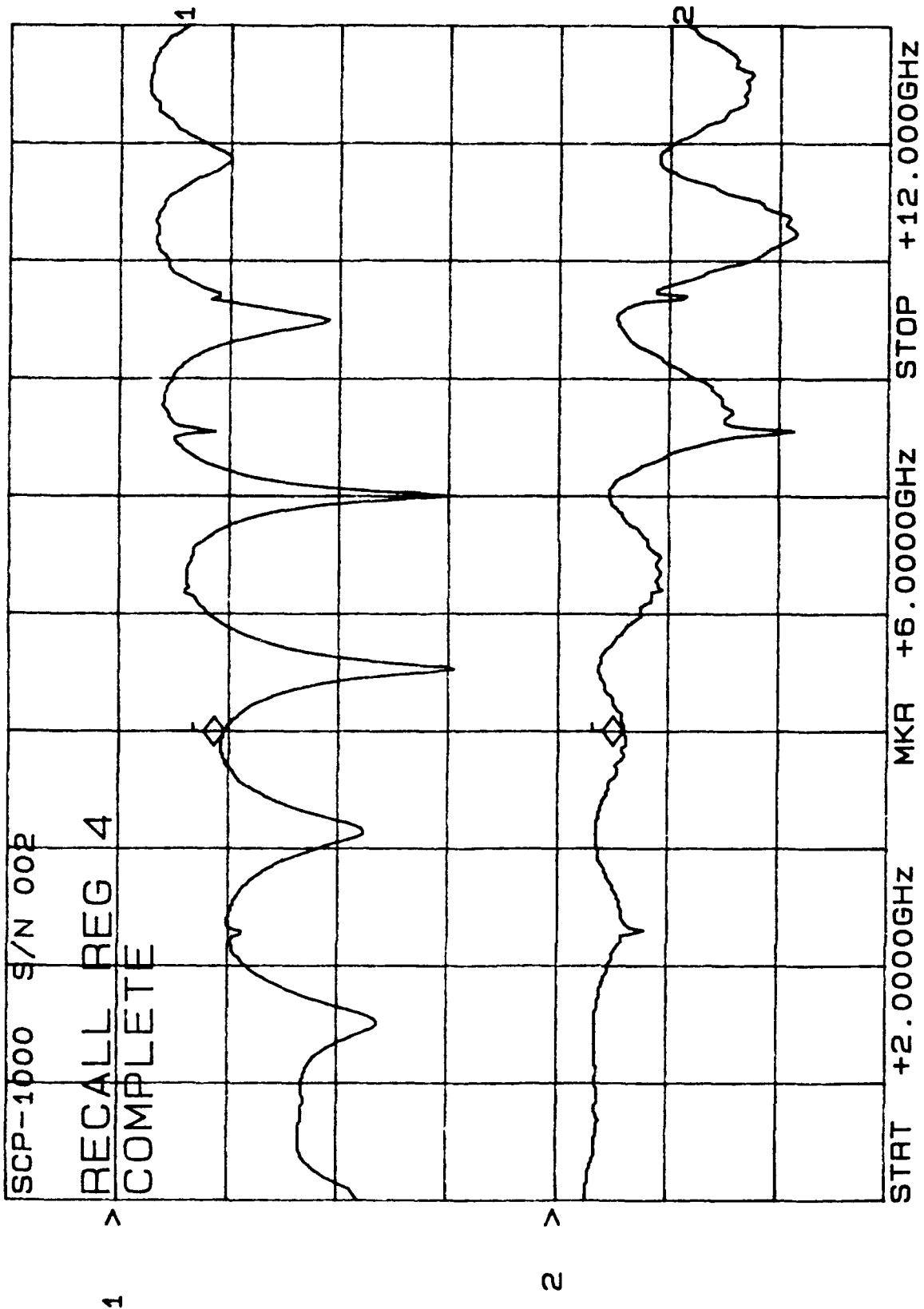
CH1: A -M REF - 7.87 dB CH2: B -M REF + 1.44 dB
10.0 dB/ REF - .00 dB 2.0 dB/ REF + .00 dB

SCP-1000 S/N 001

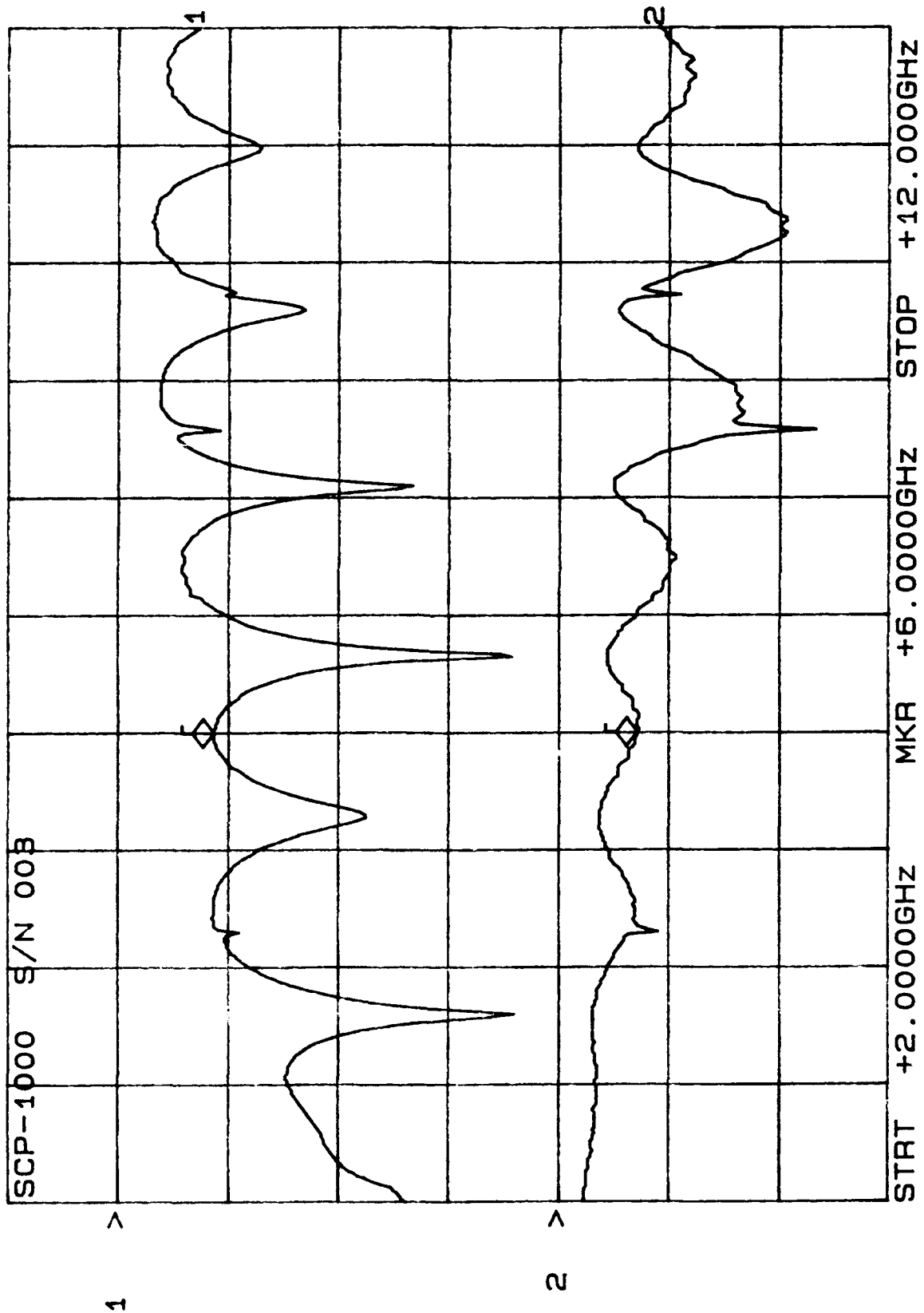


START +2.0000GHZ MKR +6.0000GHZ STOP +12.000GHZ

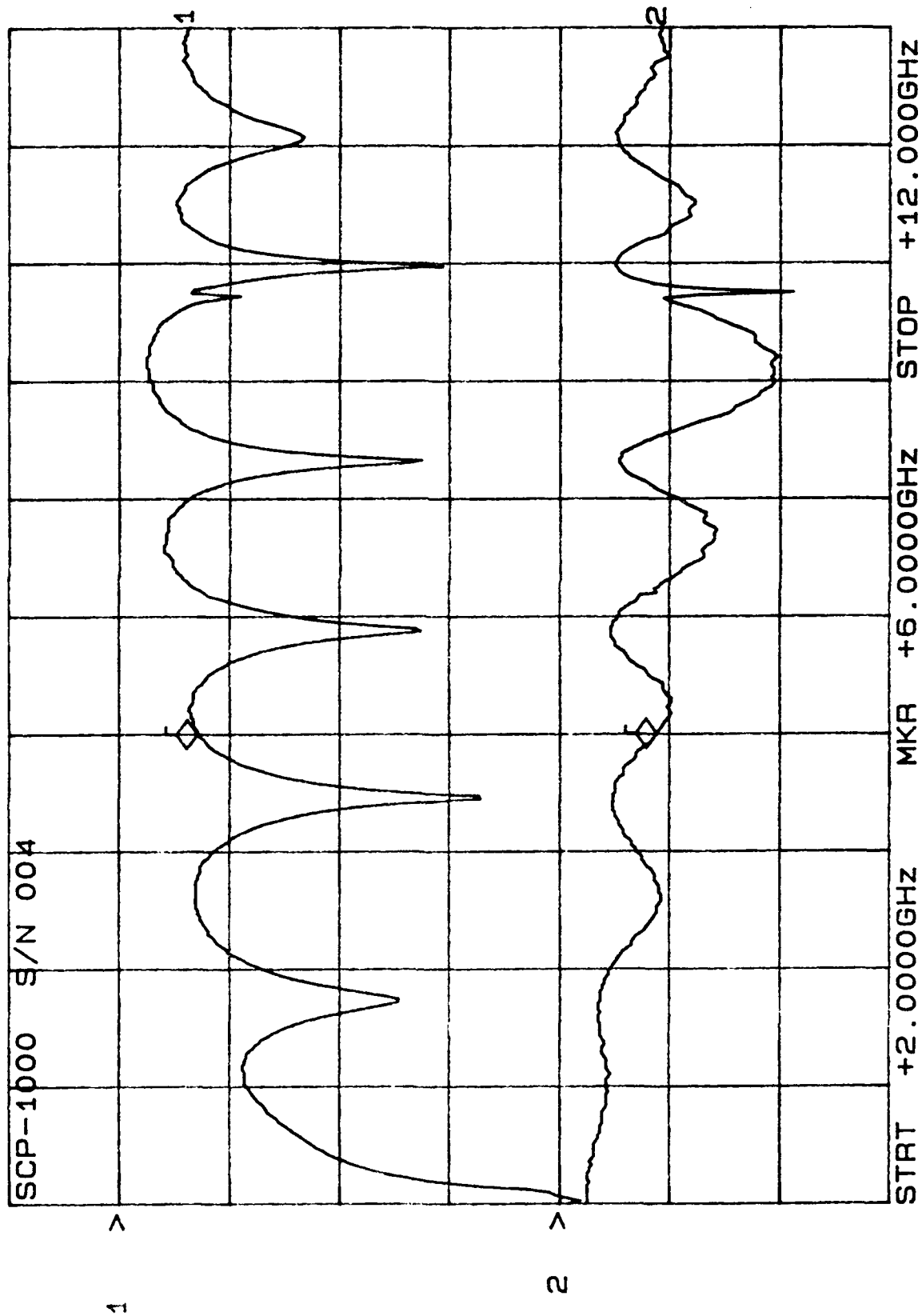
CH1: A -M - 9.47 dB CH2: B -M A - 1.18 dB
 10.0 dB/ REF - .00 dB 2.0 dB/ REF + .00 dB



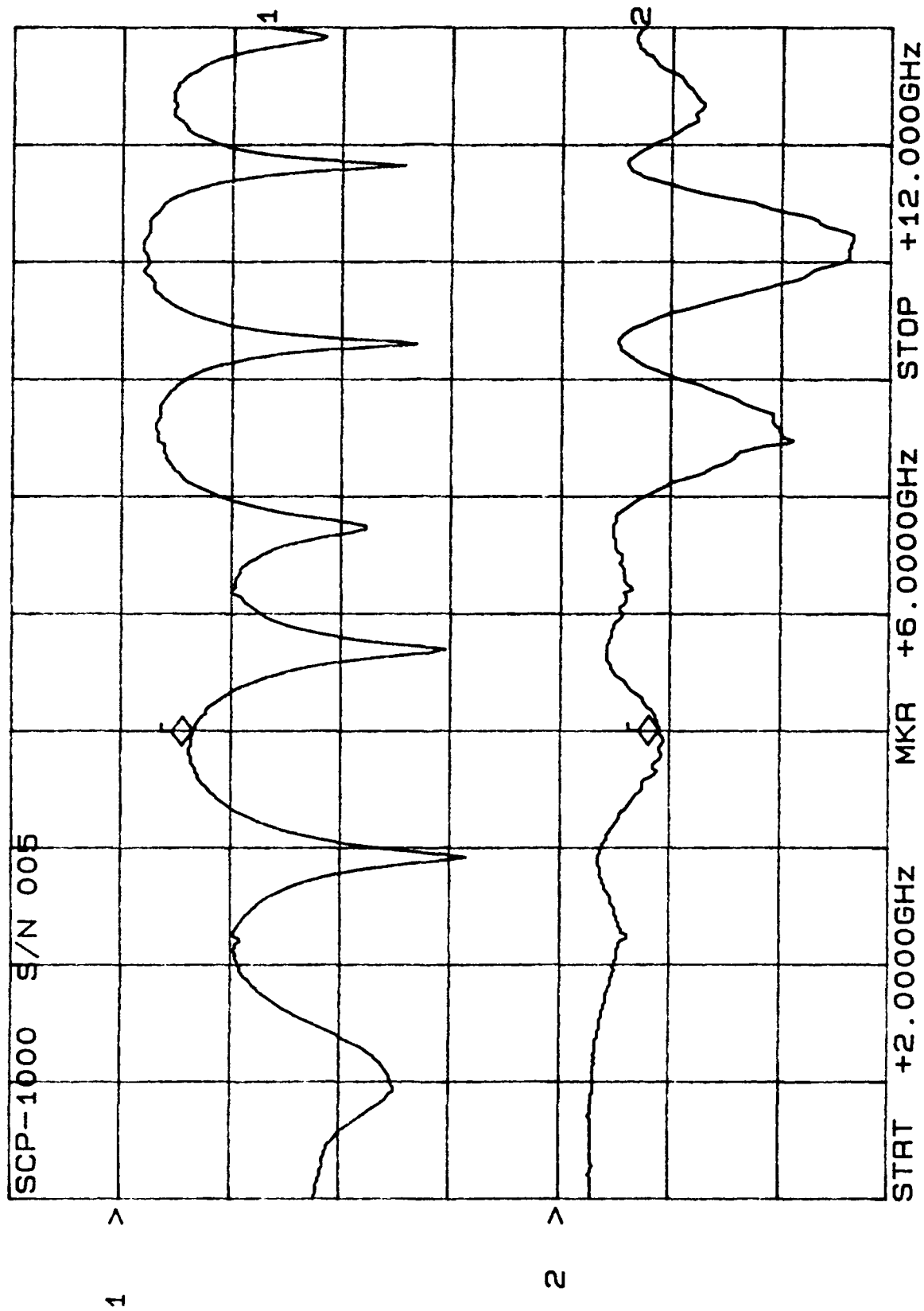
CH1: A -M - 8.60 dB CH2: B -M A - 1.40 dB
 10.0 dB/ REF - .00 dB 2.0 dB/ REF + .00 dB



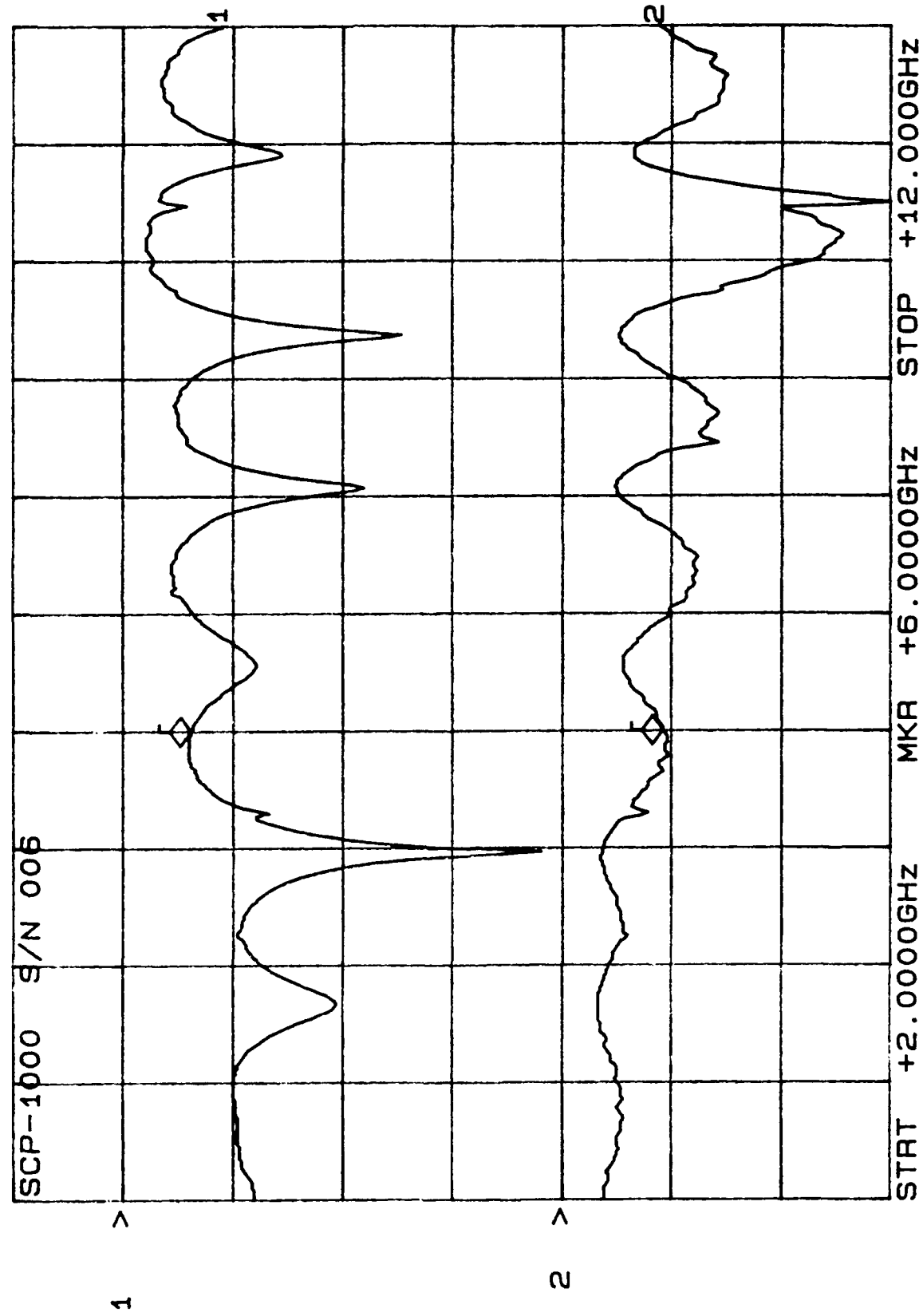
CH1: A -M REF - 7.10 dB CH2: B -M REF + 1.74 dB
 10.0 dB/ REF - .00 dB 2.0 dB/ REF + .00 dB



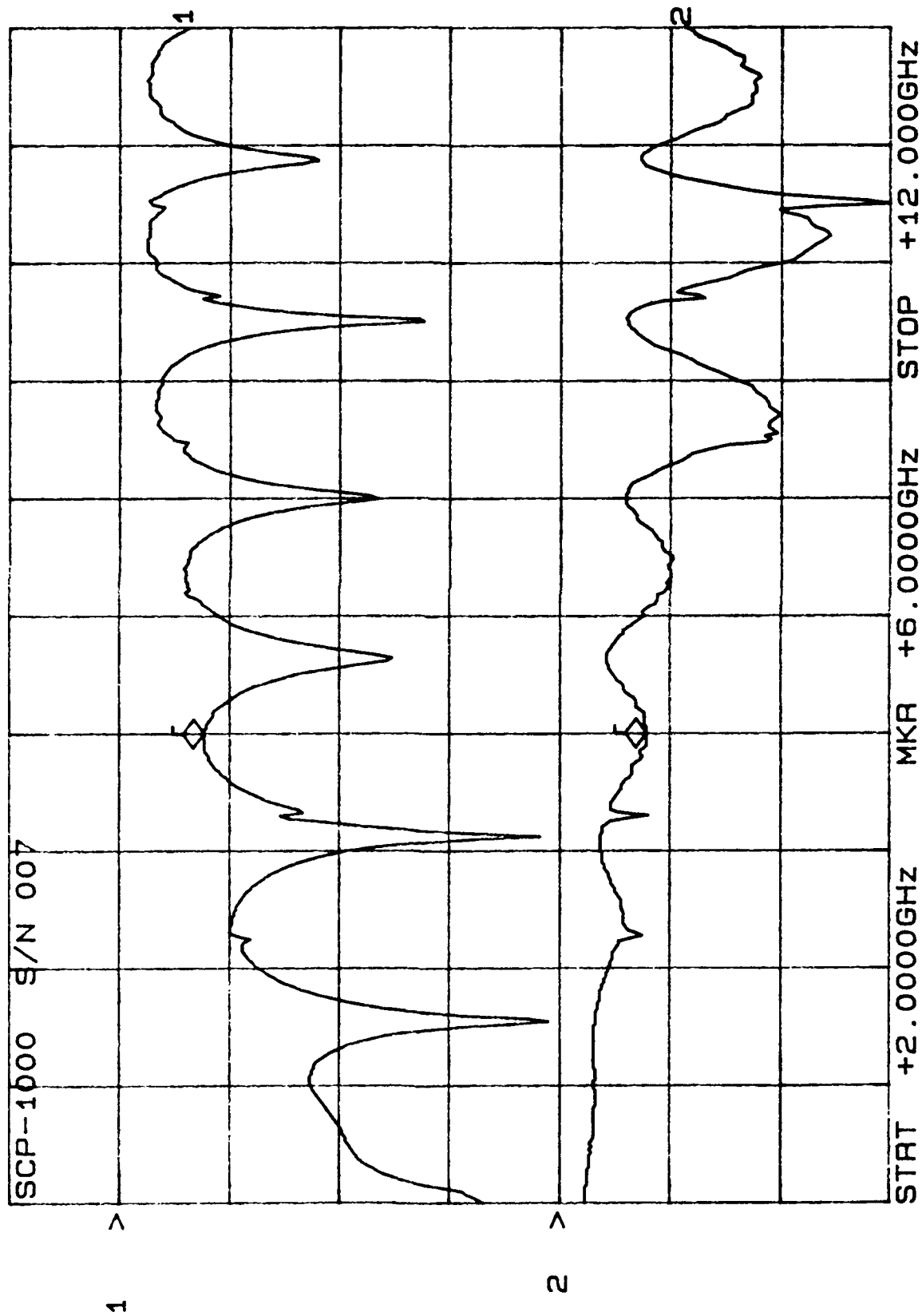
CH1: A -M REF = 6.48 dB CH2: B -M REF = 1.79 dB
 10.0 dB/ REF = .00 dB 2.0 dB/ REF = .00 dB



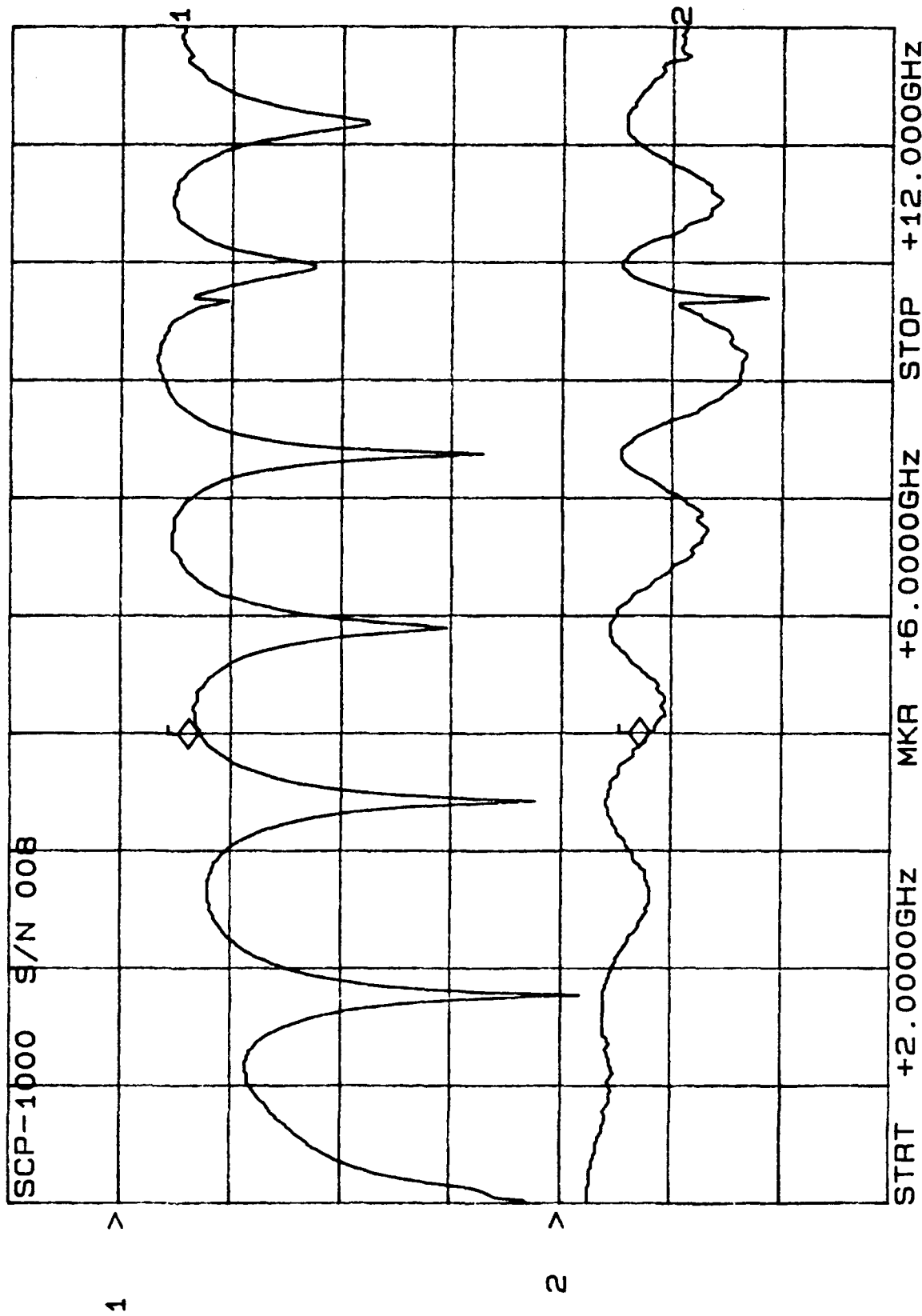
CH1: A -M REF - 6.06 dB CH2: B -M A - 1.84 dB
 10.0 dB/ REF 2.0 dB/ REF + .00 dB



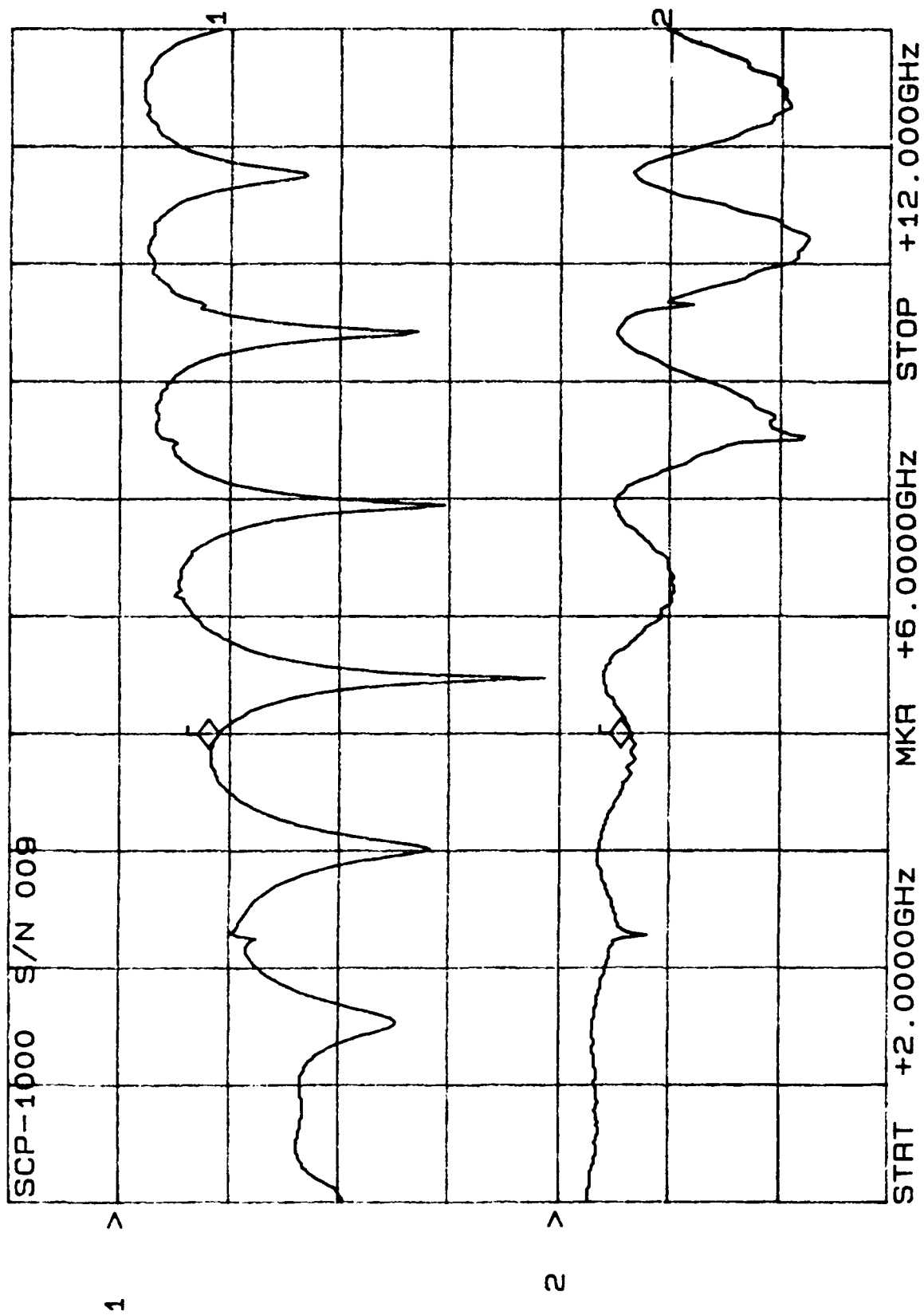
CH1: A -M REF - 7.58 dB CH2: B -M A - 1.55 dB
 10.0 dB/ REF - .00 dB 2.0 dB/ REF + .00 dB



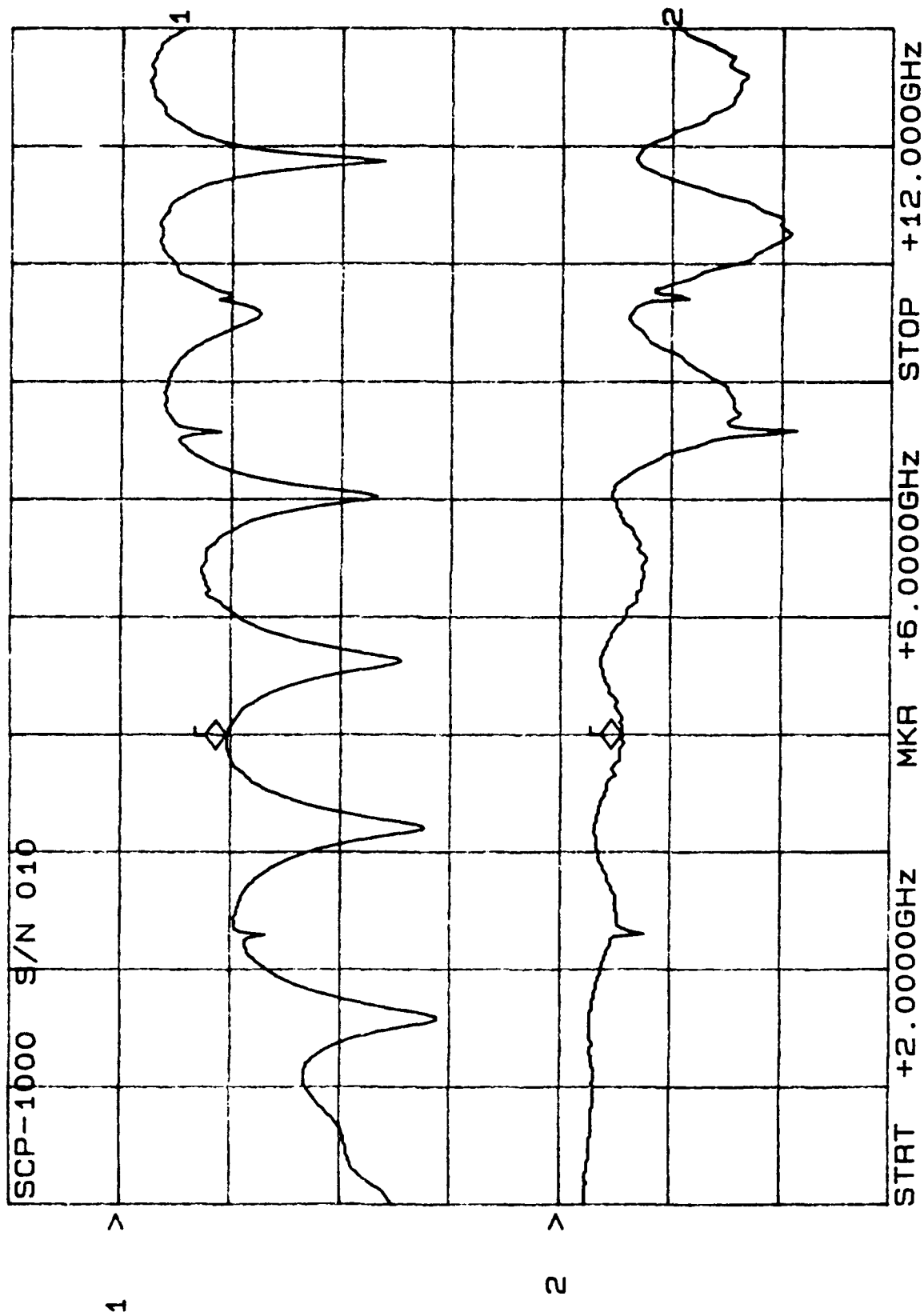
CH1: A -M REF = 7.07 dB CH2: B -M REF = 1.61 dB
 10.0 dB/ REF = .00 dB 2.0 dB/ REF = .00 dB



CH1: A -M REF - 8.94 dB CH2: B -M REF + 1.28 dB
10.0 dB/ REF - .00 dB 2.0 dB/ REF + .00 dB

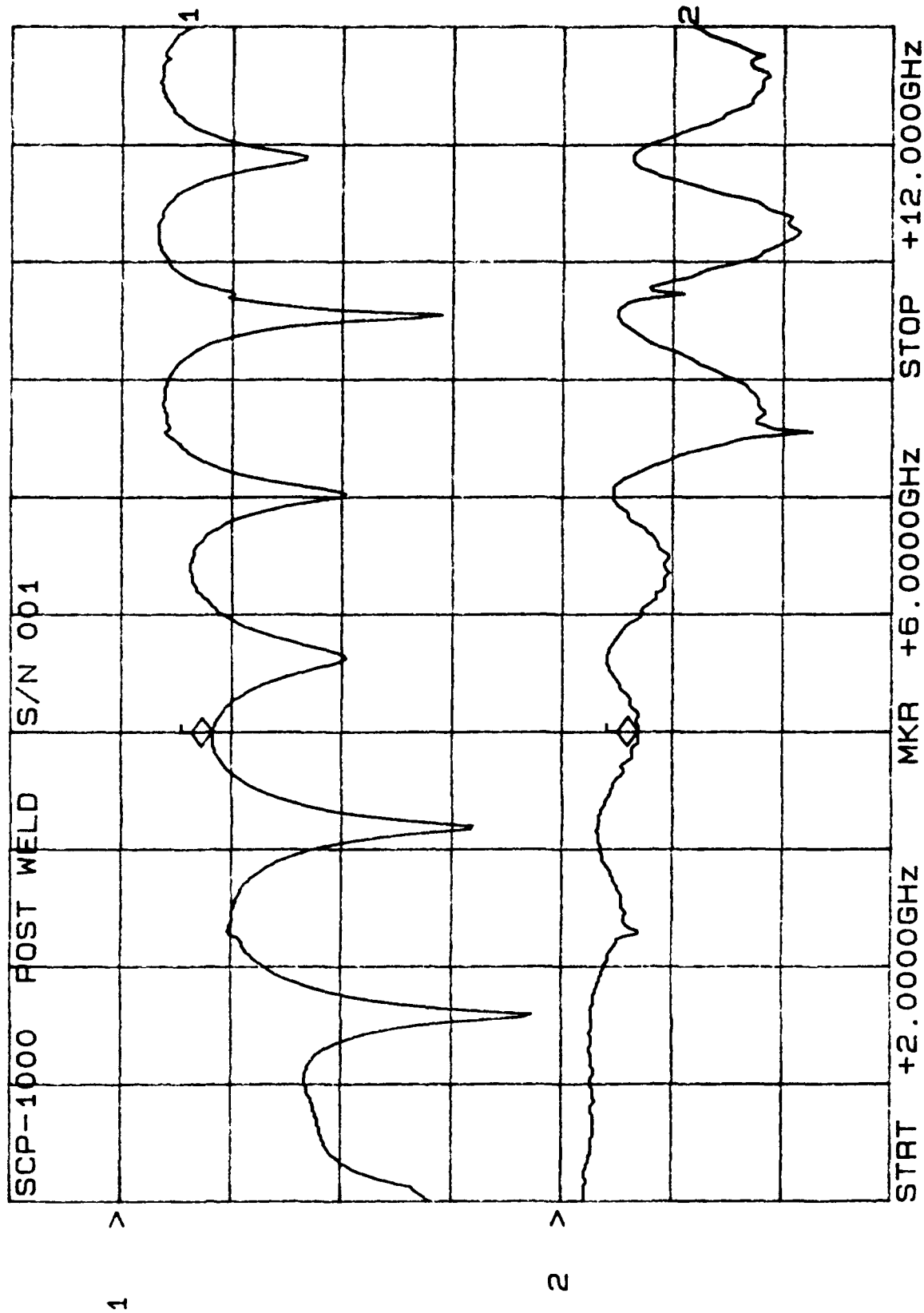


CH1: A -M - 9.55 dB CH2: B -M A - 1.10 dB
10.0 dB/ REF 2.0 dB/ REF + .00 dB

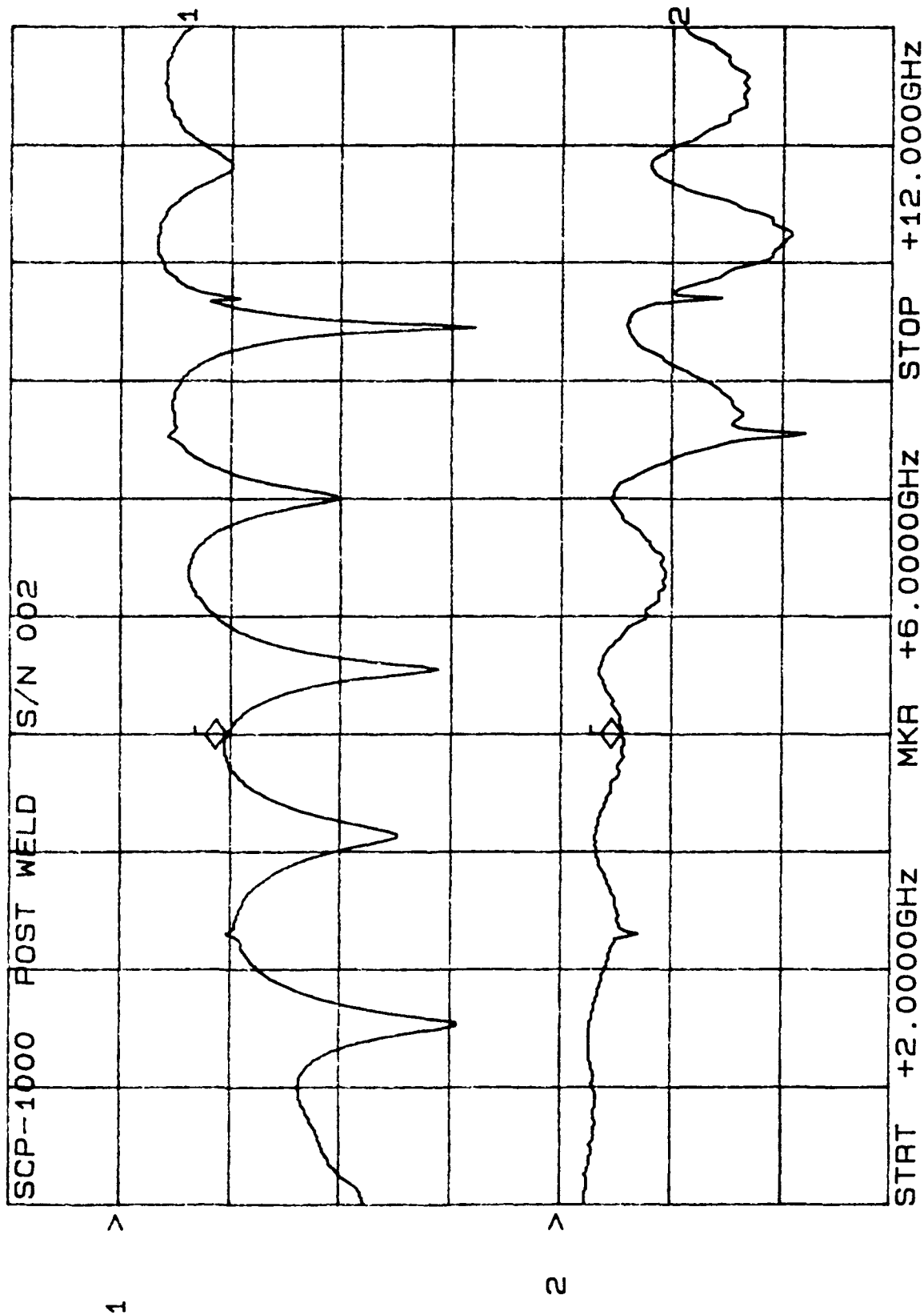


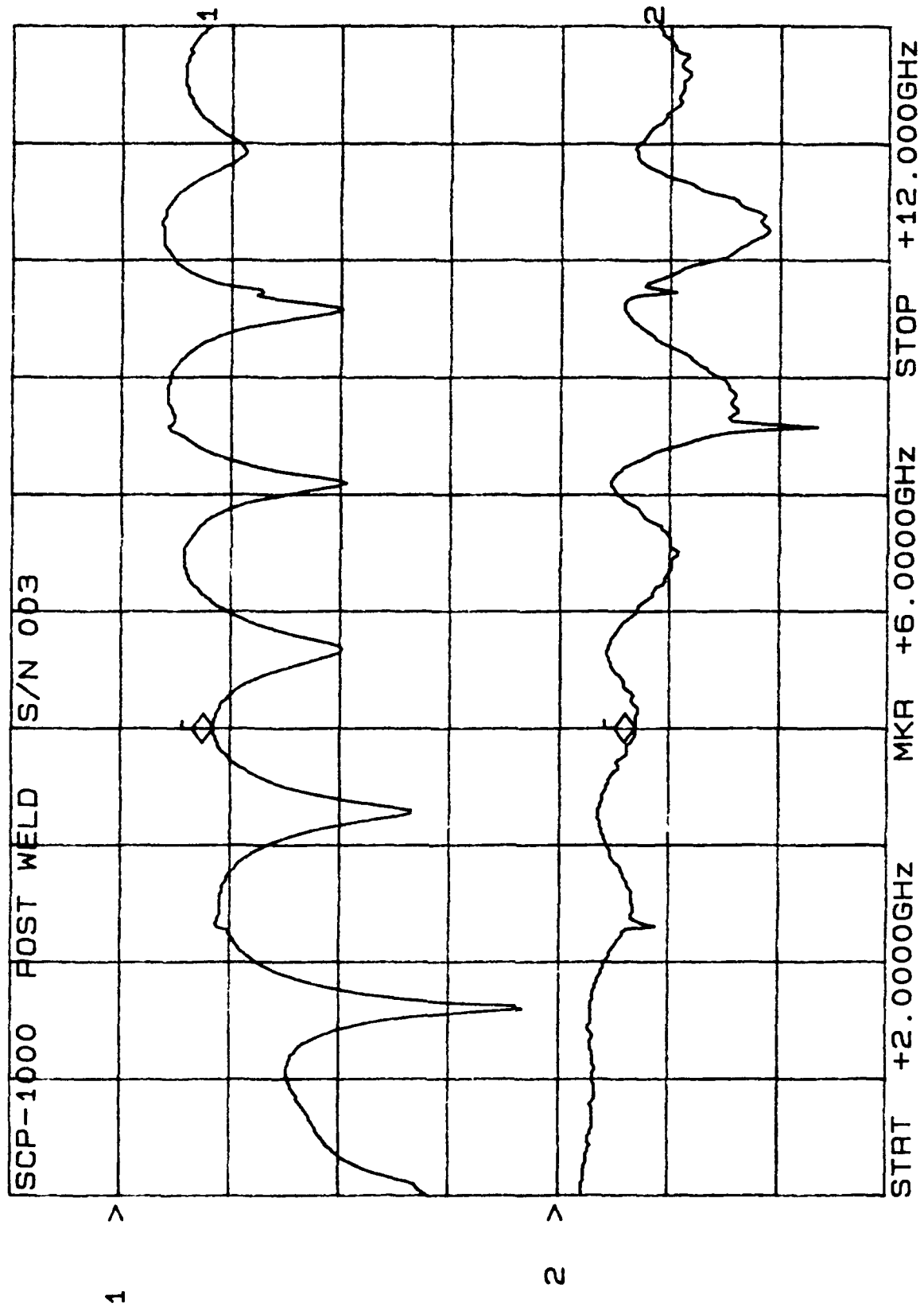
0 Cycles

CH1: A -M - 8.17 dB CH2: B -M - 1.35 dB
10.0 dB/ REF - .00 dB 2.0 dB/ REF + .00 dB



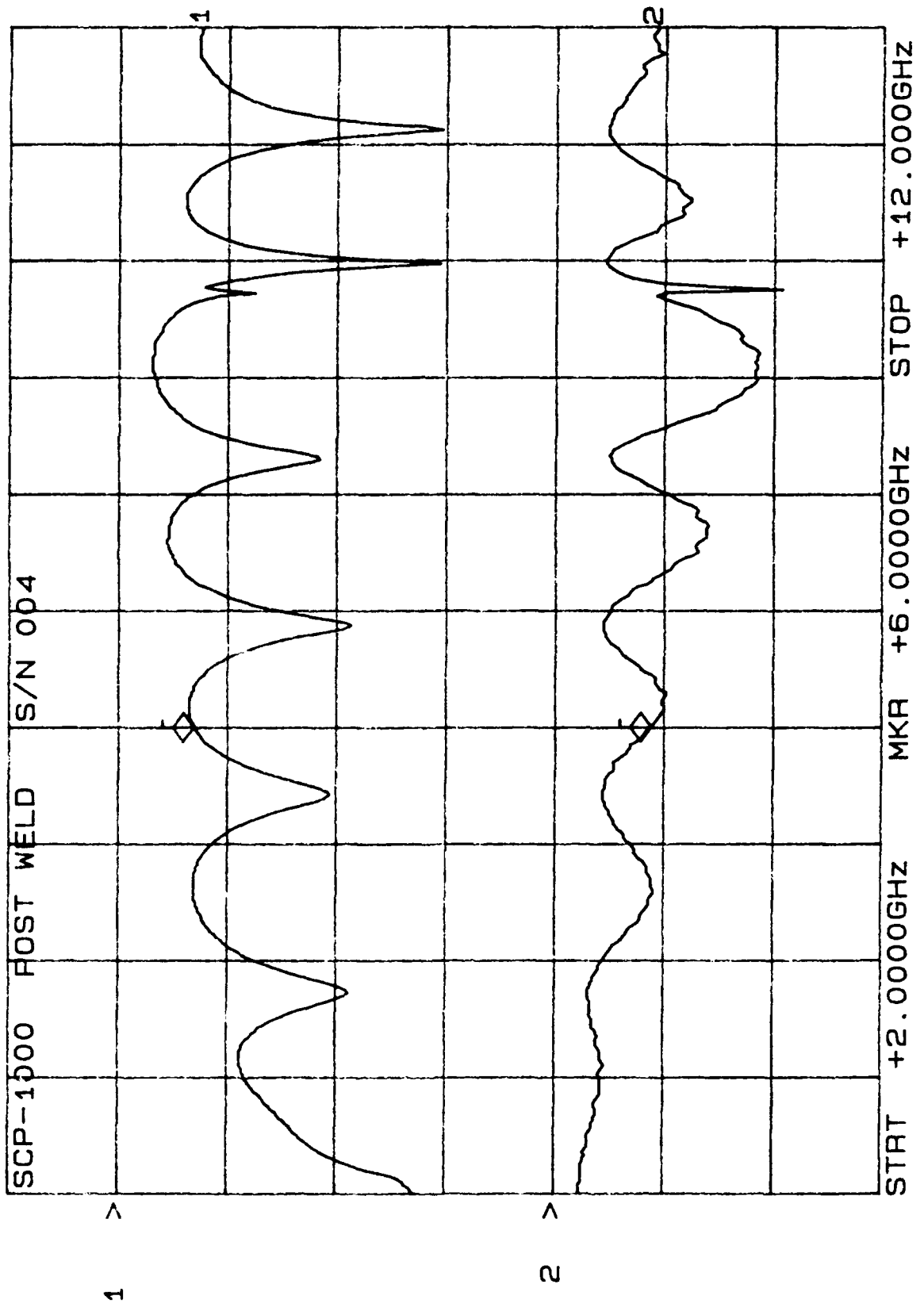
CH1: A -M REF - 9.57 dB CH2: B -M REF + 1.10 dB
10.0 dB/ REF 2.0 dB/ REF



[illegible]

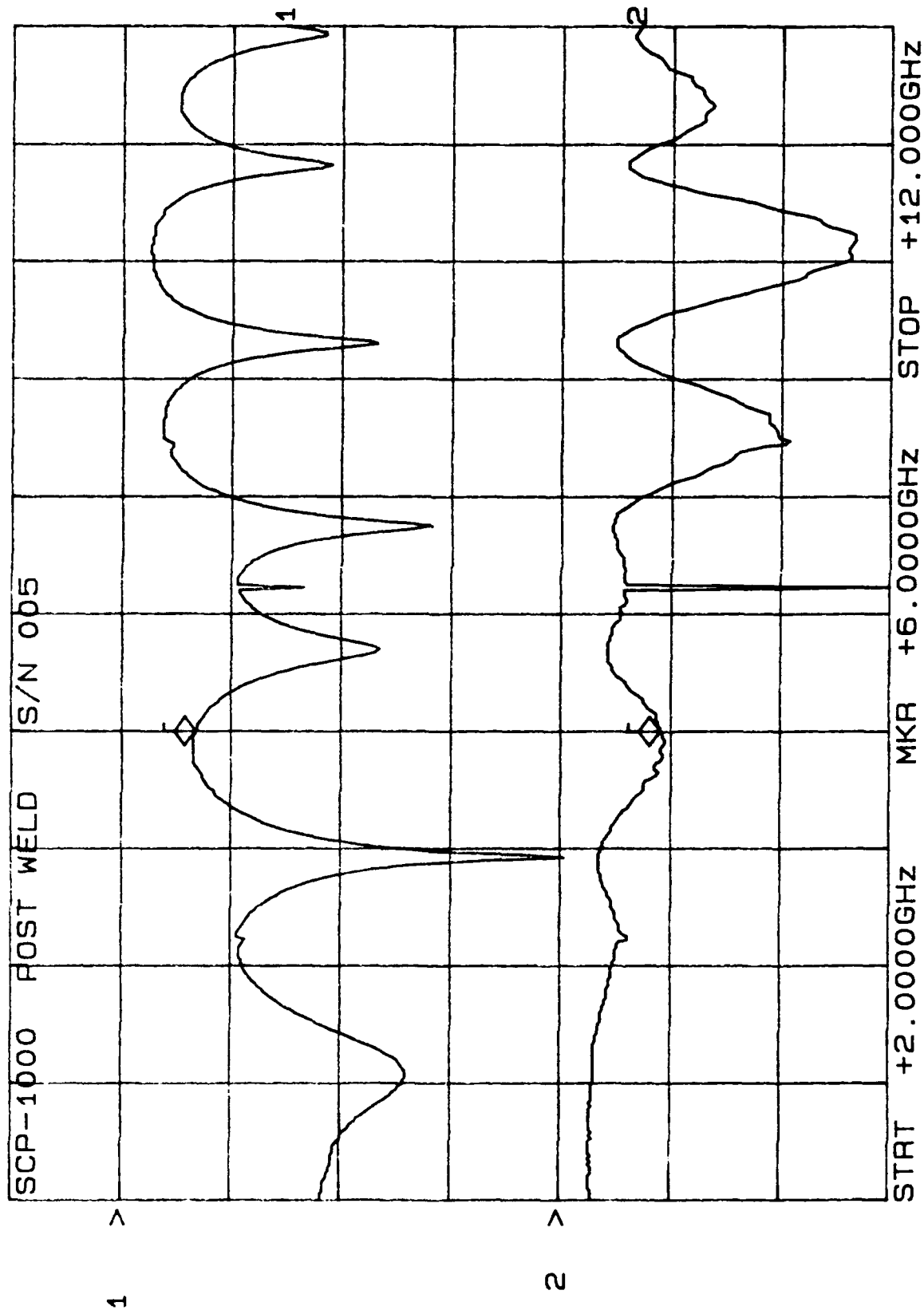
4/11/97

CH1: A -M REF - 6.85 dB CH2: B -M REF + 1.73 dB
10.0 dB/ REF .00 dB 2.0 dB/ REF + .00 dB

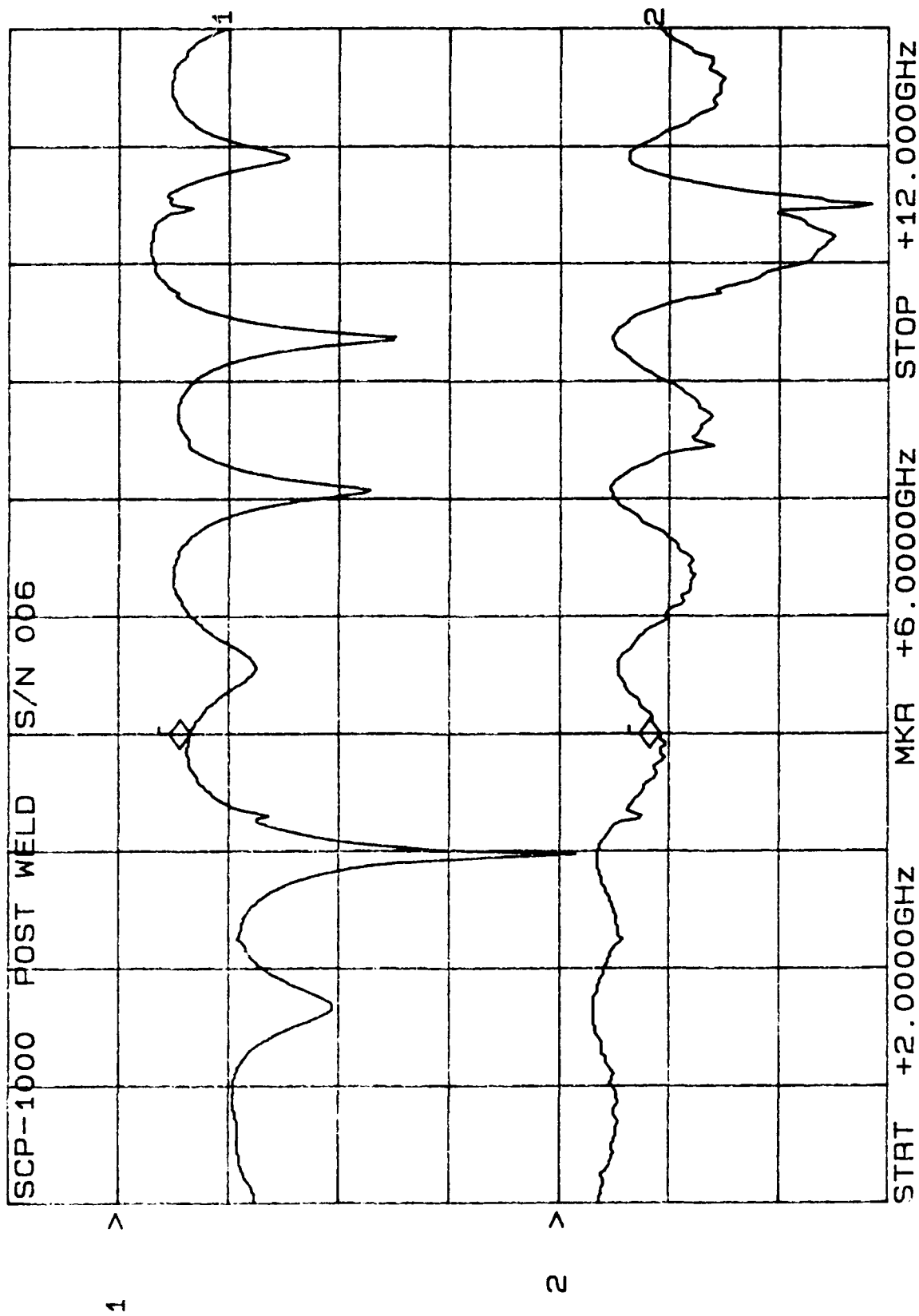


9/11/91

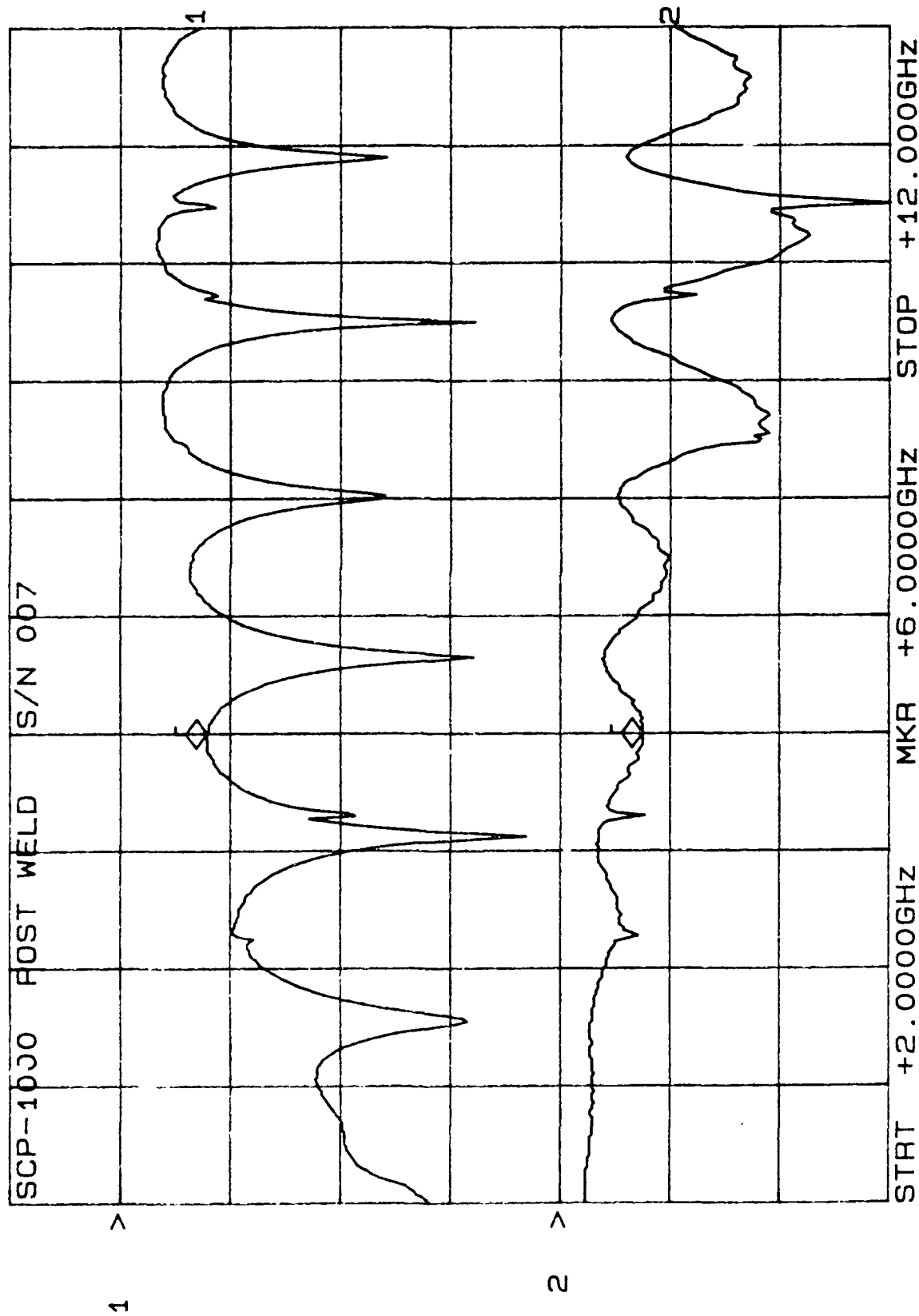
CH1: A -M REF = 6.69 dB CH2: B -M REF = 1.80 dB
10.0 dB/ REF .00 dB 2.0 dB/ REF + .00 dB



CH1: A -M - 6.41 dB CH2: B -M - 1.81 dB
10.0 dB/ REF - .00 dB 2.0 dB/ REF + .00 dB

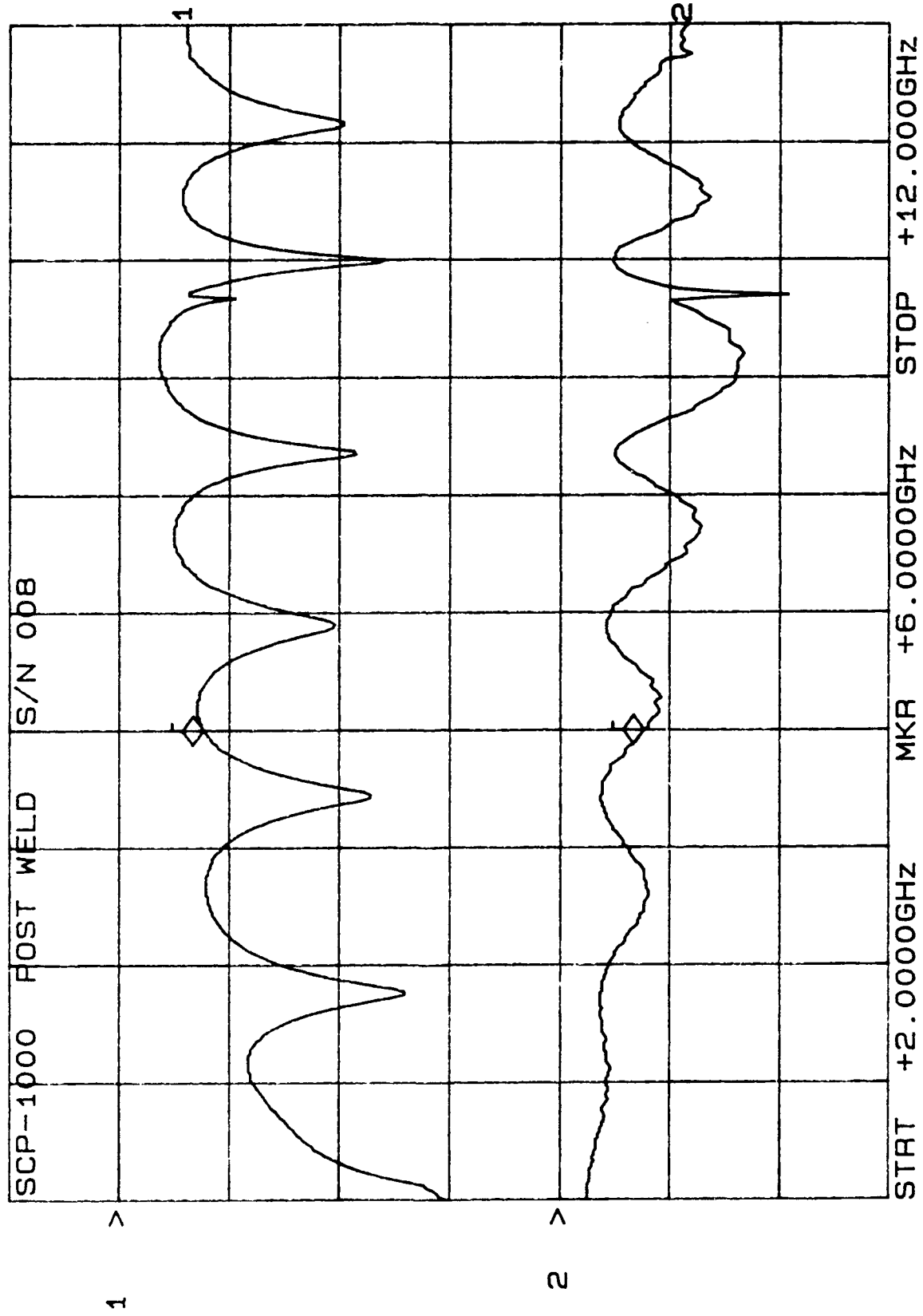


CH1: A -M - 7.83 dB CH2: B -M - 1.48 dB
 10.0 dB/ REF - .00 dB 2.0 dB/ REF + .00 dB

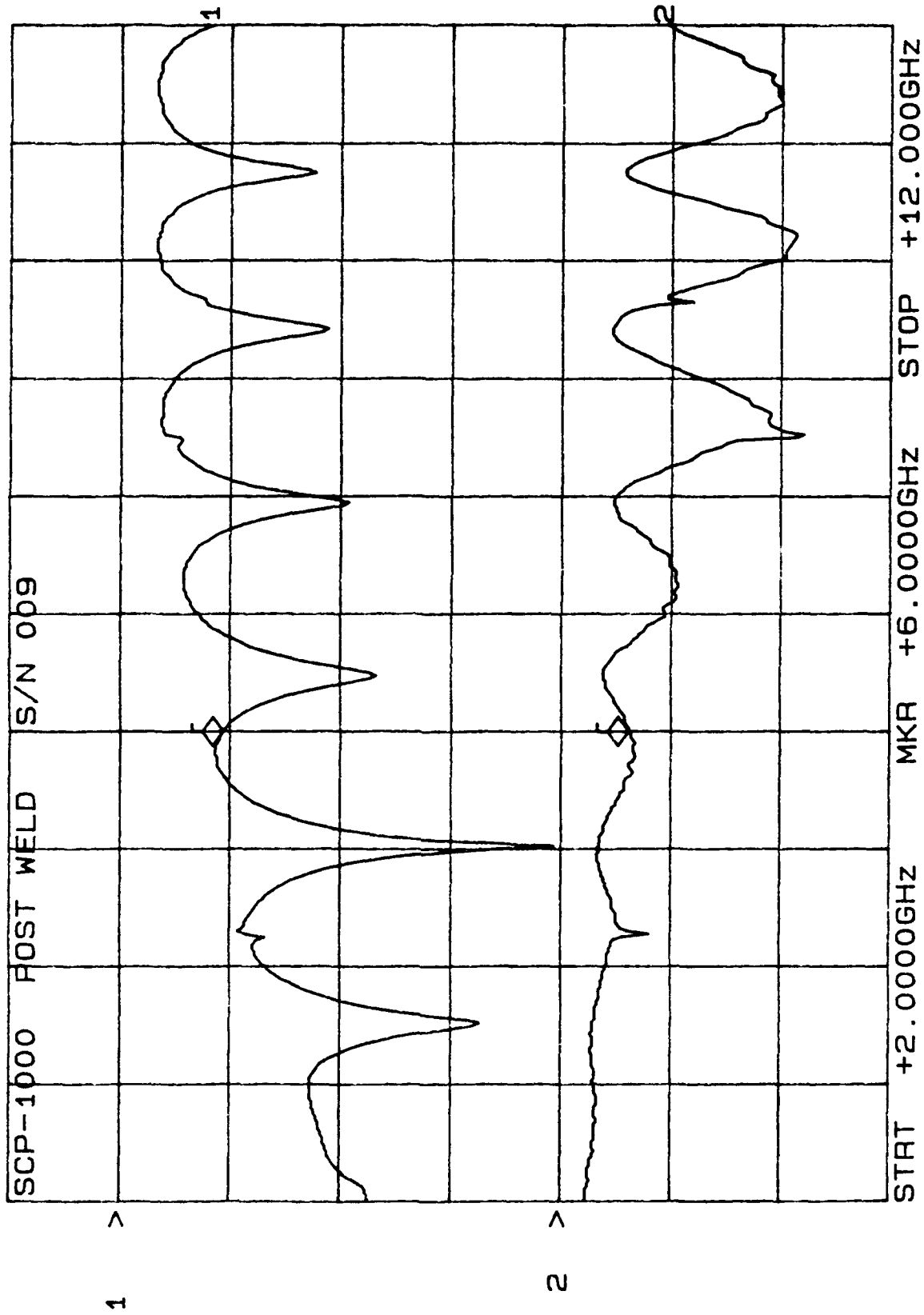


9111/91

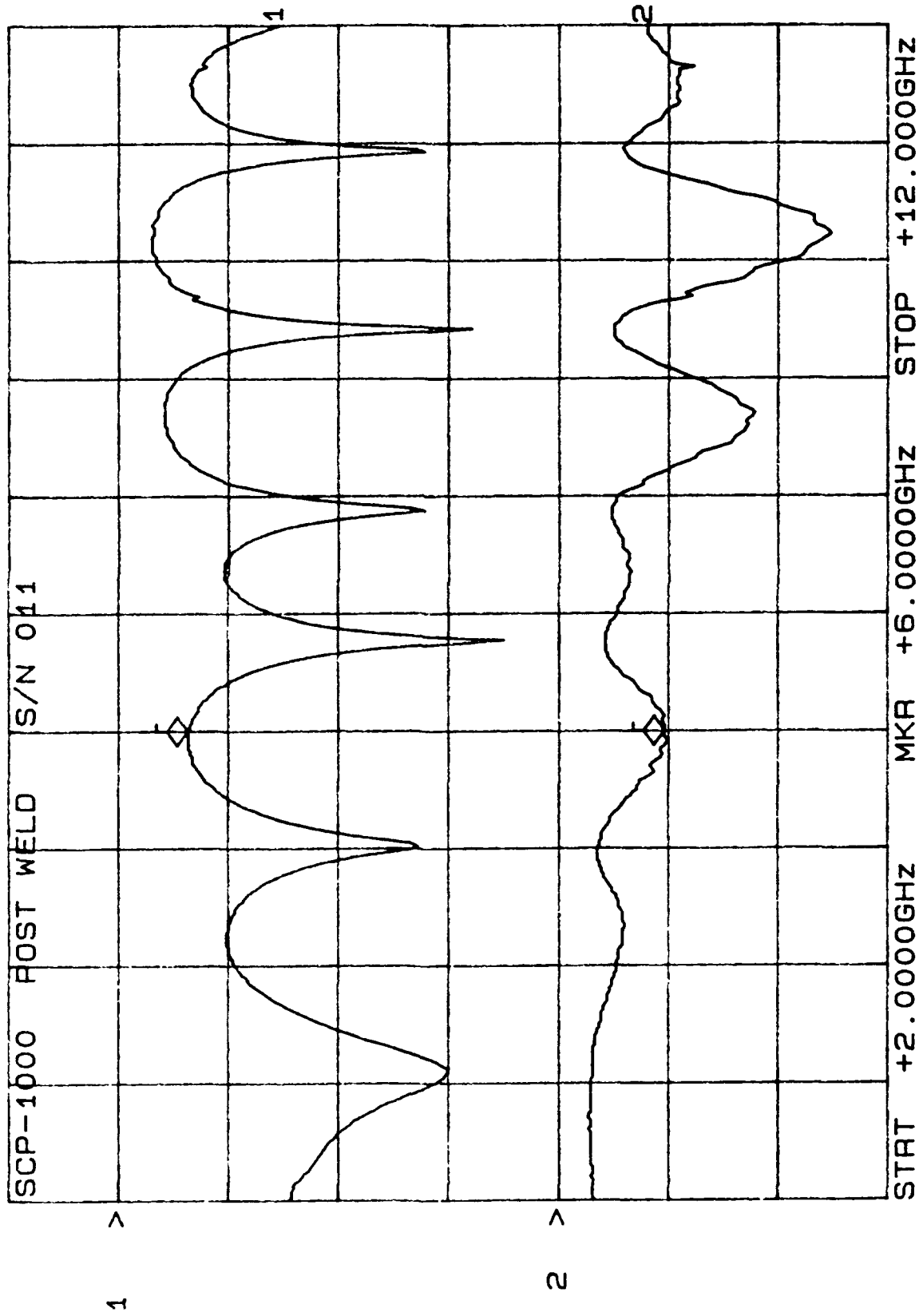
CH1: A -M - 7.57 dB CH2: B -M - 1.53 dB
10.0 dB/ REF - .00 dB 2.0 dB/ REF + .00 dB



CH1: A -M - 9.28 dB CH2: B -M - 1.22 dB
10.0 dB/ REF - .00 dB 2.0 dB/ REF + .00 dB



CH1: A -M - 6.33 dB CH2: B -M - 1.91 dB
10.0 dB/ REF - .00 dB 2.0 dB/ REF + .00 dB



AVANTEK ENVIRONMENTAL SCREENING FORM

TECHNICIAN FILLS OUT SHADED AREA

Post weld

MODEL: SCP-1000 WORK ORDER: 50016205 SUPERVISOR: DATAS

SERIAL NUMBER: 001-011 CITY: NY TECH: SCOTT

TEST REQUIREMENTS: WELD AND FINE LEAK

☐ STA-BAKE DURATION: _____ OVEN# _____ REF.#: _____ LOT#: _____
START DATE: _____ START TIME: _____ TEMP(C): _____ TECH: _____
COMPL DATE: _____ COMPL TIME: _____ TEMP(C): _____ TECH: _____

COMMENTS: _____

☐ TEMP-SHOCK LO. TEMP: _____ SOAK TIME: _____ TRANS TIME: _____ LOT#: _____
TEMP-CYCLE HI TEMP: _____ SOAK TIME: _____ CYCLES: _____
START DATE: _____ START TIME: _____ OVEN# _____ TECH: _____
COMPL DATE: _____ COMPL TIME: _____ REF.#: _____ TECH: _____

COMMENTS: _____

☐ ACCELERATION/ DATE _____ TEMP _____ RADIS _____ ACCEPT _____ LOT#: _____
CENTRIFUGE TIME _____ AXIS _____ RPM _____ REJECT _____ TECH: _____
COMMENTS: _____ REF.#: _____

☐ VIBRATION START DATE: _____ COMPL DATE: _____ LOT#: _____
COMMENTS: _____ REF.#: _____

☒ LEAK-TEST FINE _____ OTHER: _____ LOT#: _____
PS 507071 PS _____ PS _____
START DATE: 9-10-91 START TIME: 1930 TECH: 6240 ACCEPT 11
COMPL DATE: 9-11-91 COMPL TIME: 1030 TECH: 6787 REJECT 0 3×10^{-8}
COMMENTS: 001-011 - 3×10^{-8}



☐ LEAK-TEST GROSS LEAK _____ OTHER: _____ LOT#: _____
PS _____ PS _____ PS _____
START DATE: _____ START TIME: _____ TECH: _____ ACCEPT _____
COMPL DATE: _____ COMPL TIME: _____ TECH: _____ REJECT _____
COMMENTS: _____

☐ BURN-IN DURATION: _____ It: _____ VOLT: _____ TEMP: _____ LOT#: _____
START DATE: _____ START TIME: _____ TEMP: _____ It: _____ TECH: _____
COMPL DATE: _____ COMPL TIME: _____ TEMP: _____ It: _____ TECH: _____
OVEN#: _____ VOLT#: _____ CURRENT#: _____ REF.#: _____ It @ 25C: _____
COMMENTS: _____

☐ TEMP-CYCLE/ LO. TEMP: _____ SOAK TIME: _____ TRANS TIME: _____ LOT#: _____
POWER BURN-IN HI TEMP: _____ SOAK TIME: _____ VOLT: _____ CYCLES: _____
START DATE: _____ START TIME: _____ TEMP: _____ It: _____ TECH: _____
COMPL DATE: _____ COMPL TIME: _____ TEMP: _____ It: _____ TECH: _____
OVEN#: _____ VOLT#: _____ CURRENT#: _____ REF.#: _____

COMMENTS: _____

REV																					
SHEET	44	45	46	47	48	49	50	51	52	53	54	55	56	57	58	59	60	61	62	63	64
REV																					
SHEET	23	24	25	26	27	28	29	30	31	32	33	34	35	36	37	38	39	40	41	42	43
REV	-																				
SHEET	2	3	4	5	6	7	8	9	10	11	12	13	14	15	16	17	18	19	20	21	22

UNLESS OTHERWISE SPECIFIED			APPROVALS		SIGNATURE AND DATE		 AVANTEK	
DIMENSIONS ARE IN INCHES			DRAWN		L. VELASQUEZ 12/90			
TOLERANCES			CHECKED				MECHANICAL OPERATION SHEET CASE ASSEMBLY SCP-1000/2000	
FRACTIONS DECIMALS ANGLES			APPROVED		m. Daly 12-26-90			
ALL SURFACES ✓ EXCEPT AS NOTED			MFG ENG		Phil S. Holt 12/26/90			
MATERIAL			QA		P. Palacios 12-26-90			
NOTE: DEBURN AND BREAK ALL SHARP EDGES EXCEPT AS NOTED					SIZE		CODE IDENT NO.	
DO NOT SCALE THIS DRAWING					A		24539	
			SCALE		WEIGHT		SHEET 1 OF 2	
							REV	

MECHANICAL OPERATION SHEET

PART #: 320-558128-001 REV W.O.# 52016205

PART NAME: CASE ASSY scp-1000

START / /

FINISH / /

STEP	OPERATION DESCRIPTION	REF DOC	REV	OPER	DATE	QTY IN	QTY OUT
------	-----------------------	---------	-----	------	------	--------	---------

1.	VERIFY BIN-UP	320-558128		9164	5/3/91	15	15
2.	SOLDER RF F/T (2 PLACES)	AP-0286C5 AD-557963		2592	5/13/91	15	15
3.	VAPOR DEGREASE PARTS	PS-023886		2592	5/13/91	15	15
4.	FINE LEAK CHECK	PS-029238		2592	5/13/91	15	15
5.	VAPOR DEGREASE CASE	PS-023886		2592	5/13/91	15	15
6.	100% MFG INSPECT	AWS-014355-800 AD-557963		2592	5/3/91	15	15
7.	INSTALL RF/DC CONTACT (2 PLACES)	340-028489-001 AD-557963		9164	5/4/91	15	15
8.	EPOXY THRU LINE INTO CASE	AD-557963 PS-505313		N/A			
9.	INSTALL RF FILTER AND SMA CONNECTORS	AD-557963		9164	5/10/91	15	15
10.	GAP WELD CONTACT RIBBON TO THRU LINE	PS-501206 AD-557963		9164	9/6/91	15	15
11.	CLEAN CASE	PS-023886		9164	9/6/91	15	15
12.	100% MFG INSPECT	AWS-014355-800 AD-557963		9164	9/9/91	15	15
	Weld			6240	9/10/91	11	11
13.	100% QA INSPECT	AD-557963 JI-0235					



S-ZE

CODE IDENT NO

A

24539

MOS-558/28

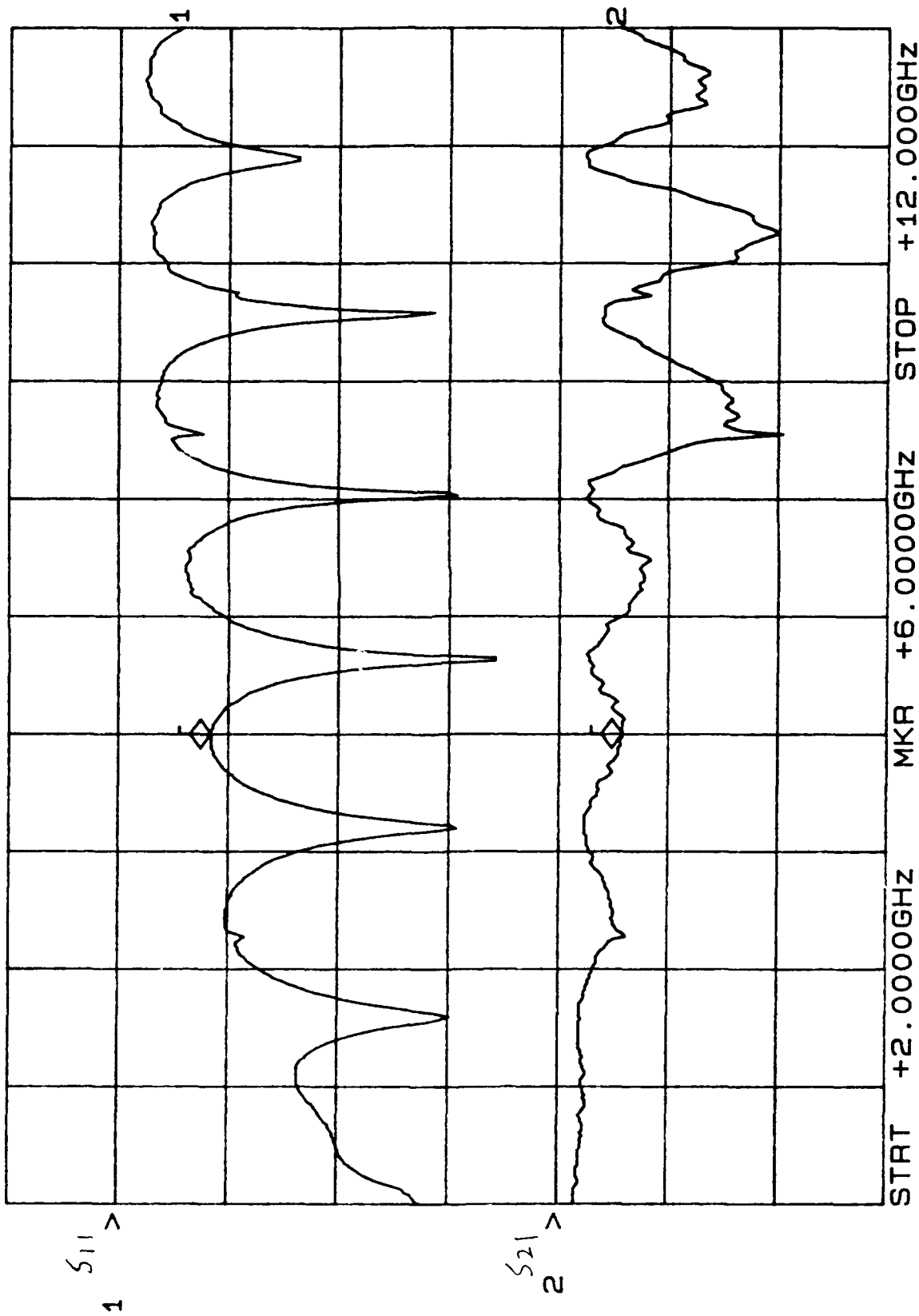
SCALE

WEIGHT

SHEET 2 OF 2

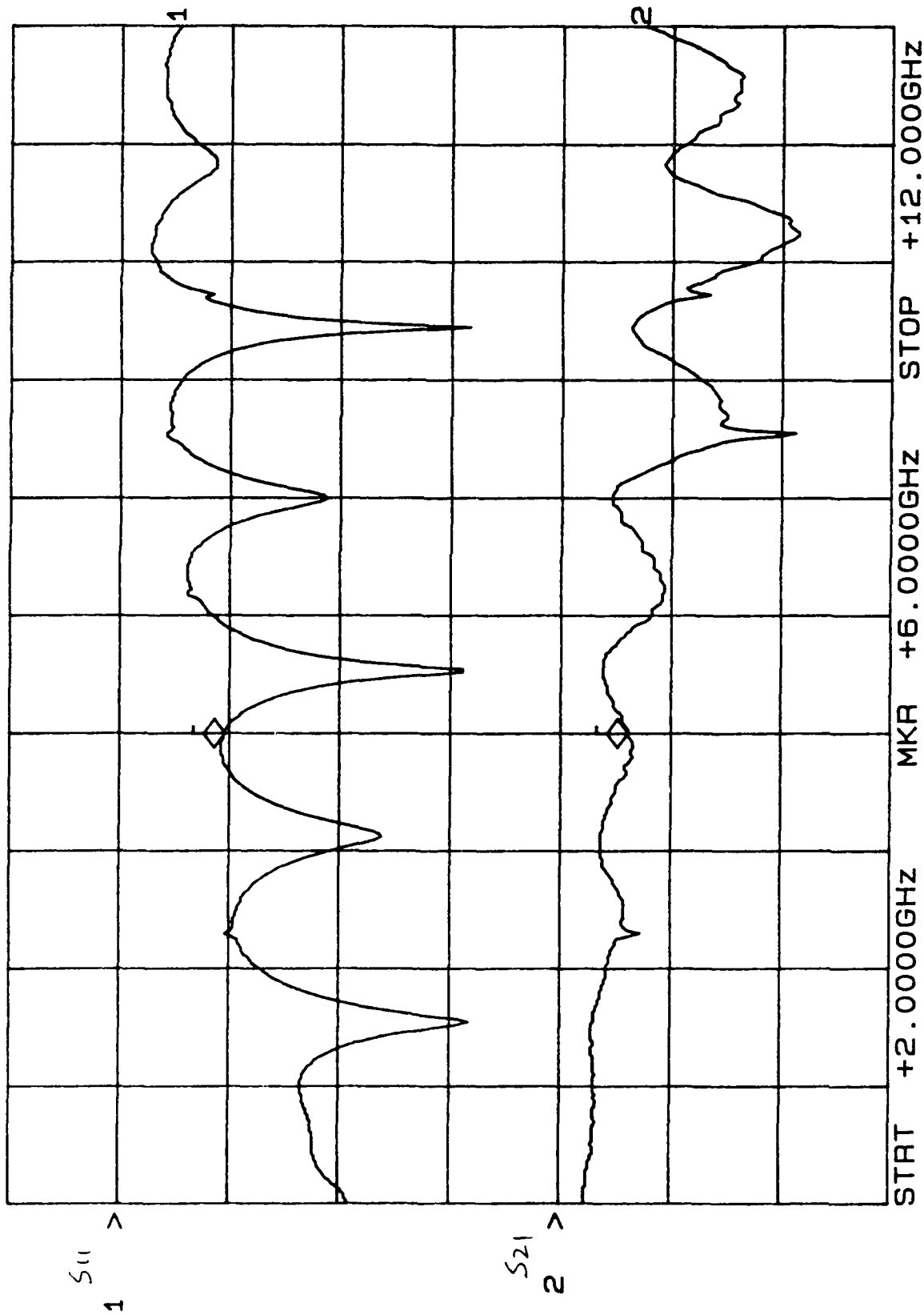
REV

CH1: A -M REF = 8.37 dB CH2: B -M REF = 1.13 dB
 10.0 dB/ REF 2.0 dB/ REF



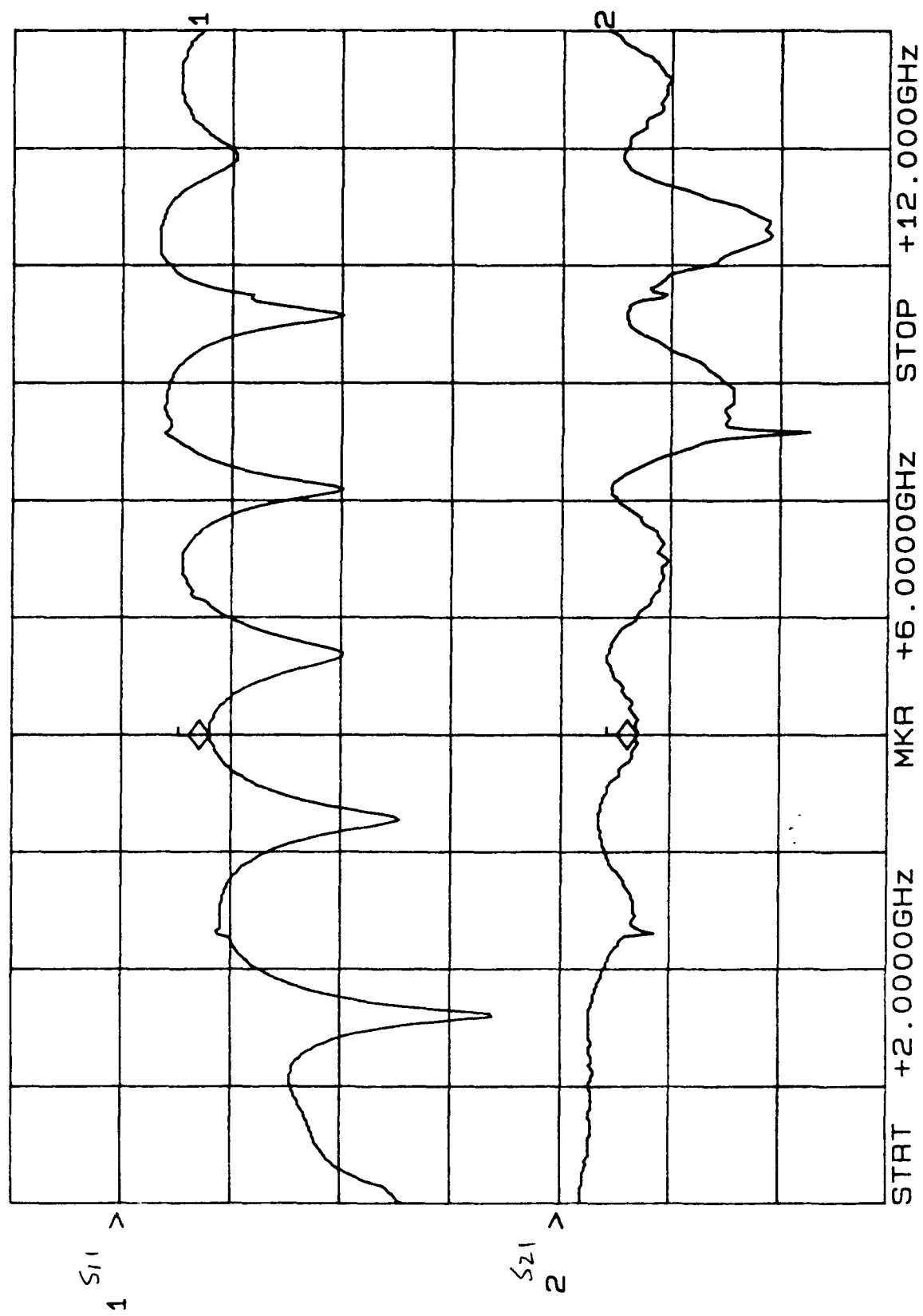
SCP-1000 Pre-weld

CH1: A -M - 9.45 dB CH2: B -M - 1.21 dB
10.0 dB/ REF - .00 dB 2.0 dB/ REF + .00 dB

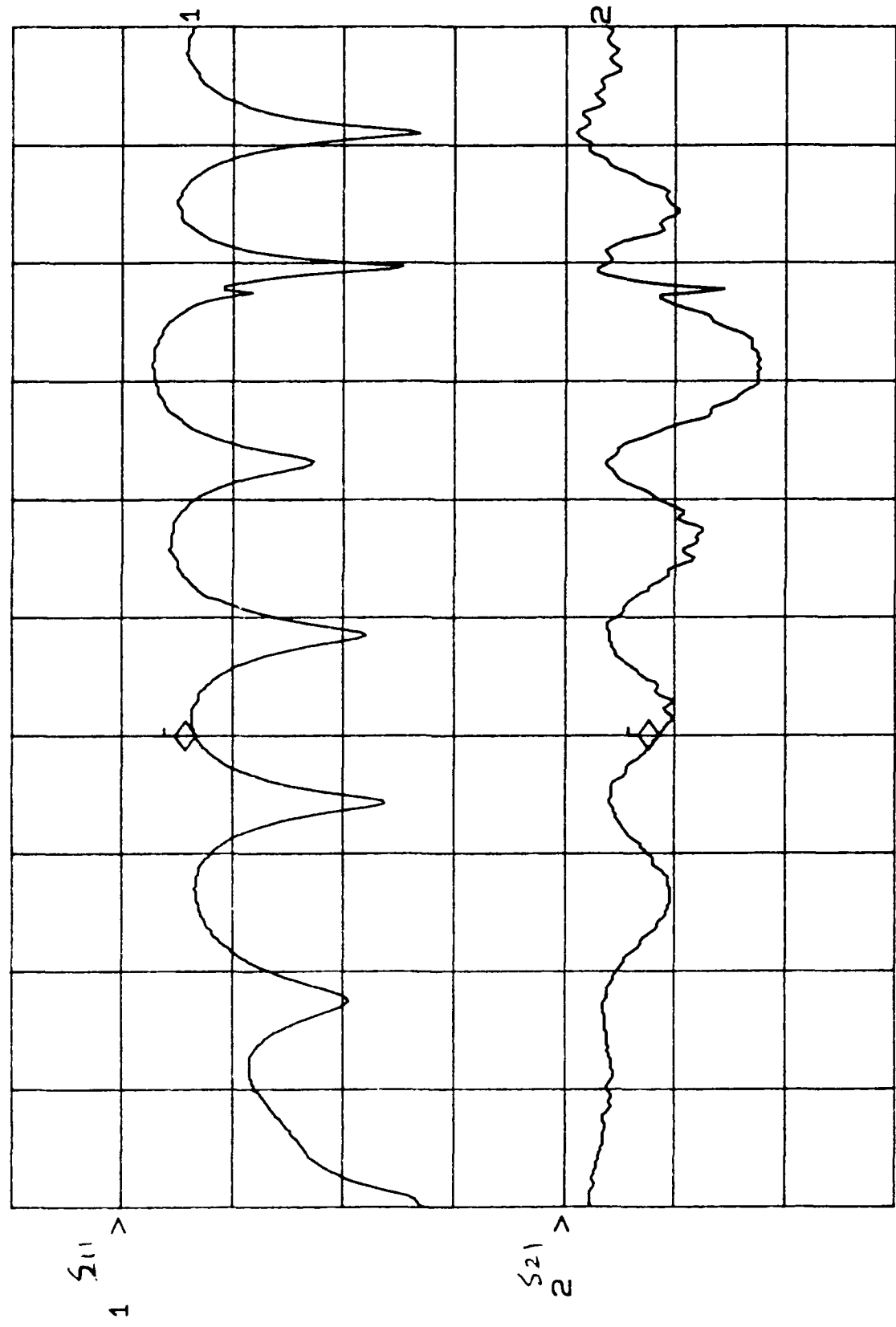


SCP=1000 1/N 9651

CH1: A -M REF = 7.99 dB CH2: B -M REF = 1.39 dB
10.0 dB/ REF 2.0 dB/ REF



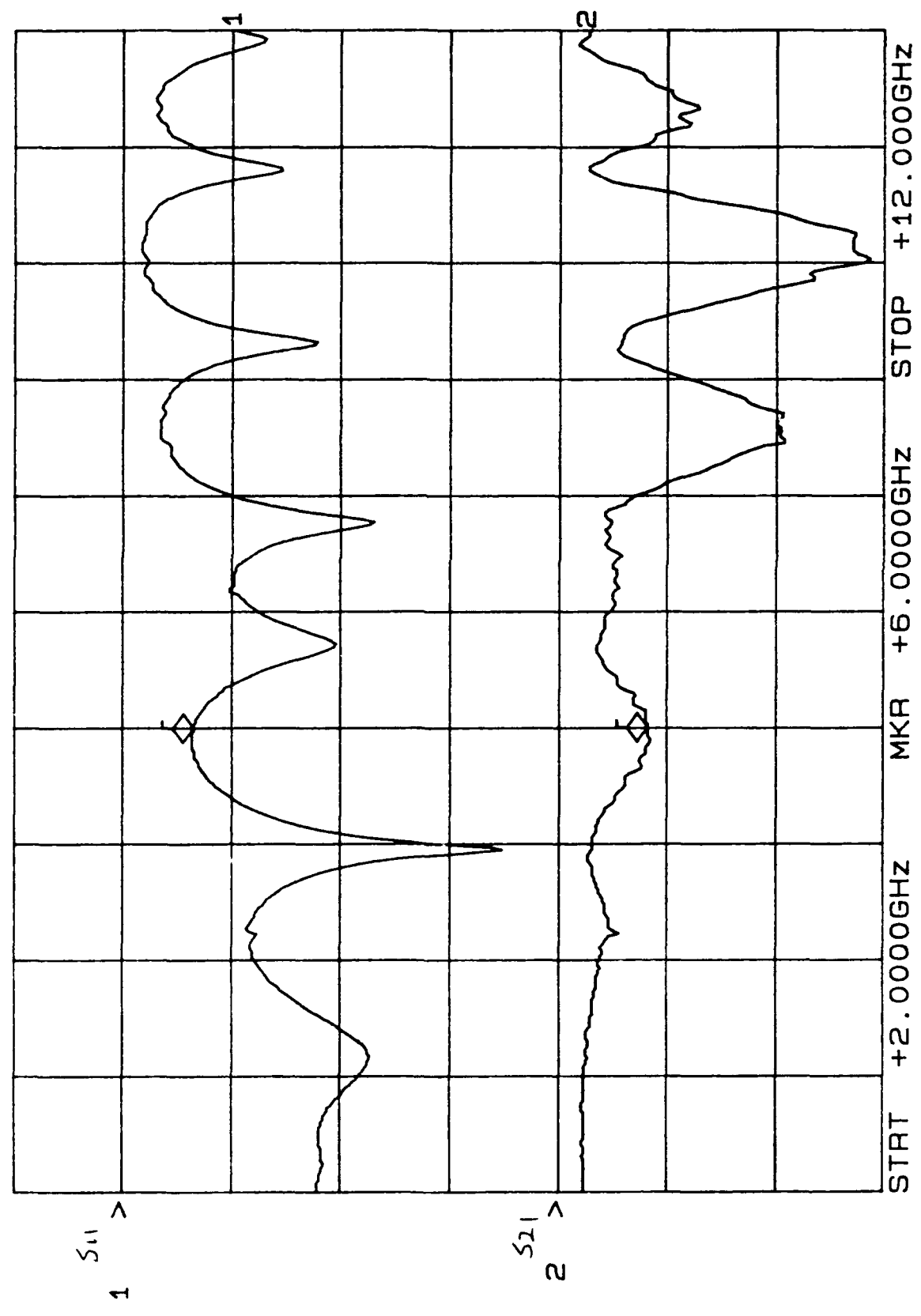
CH1: A -M REF - 6.57 dB CH2: B -M REF + 1.72 dB
 10.0 dB/ REF - .00 dB 2.0 dB/ REF + .00 dB



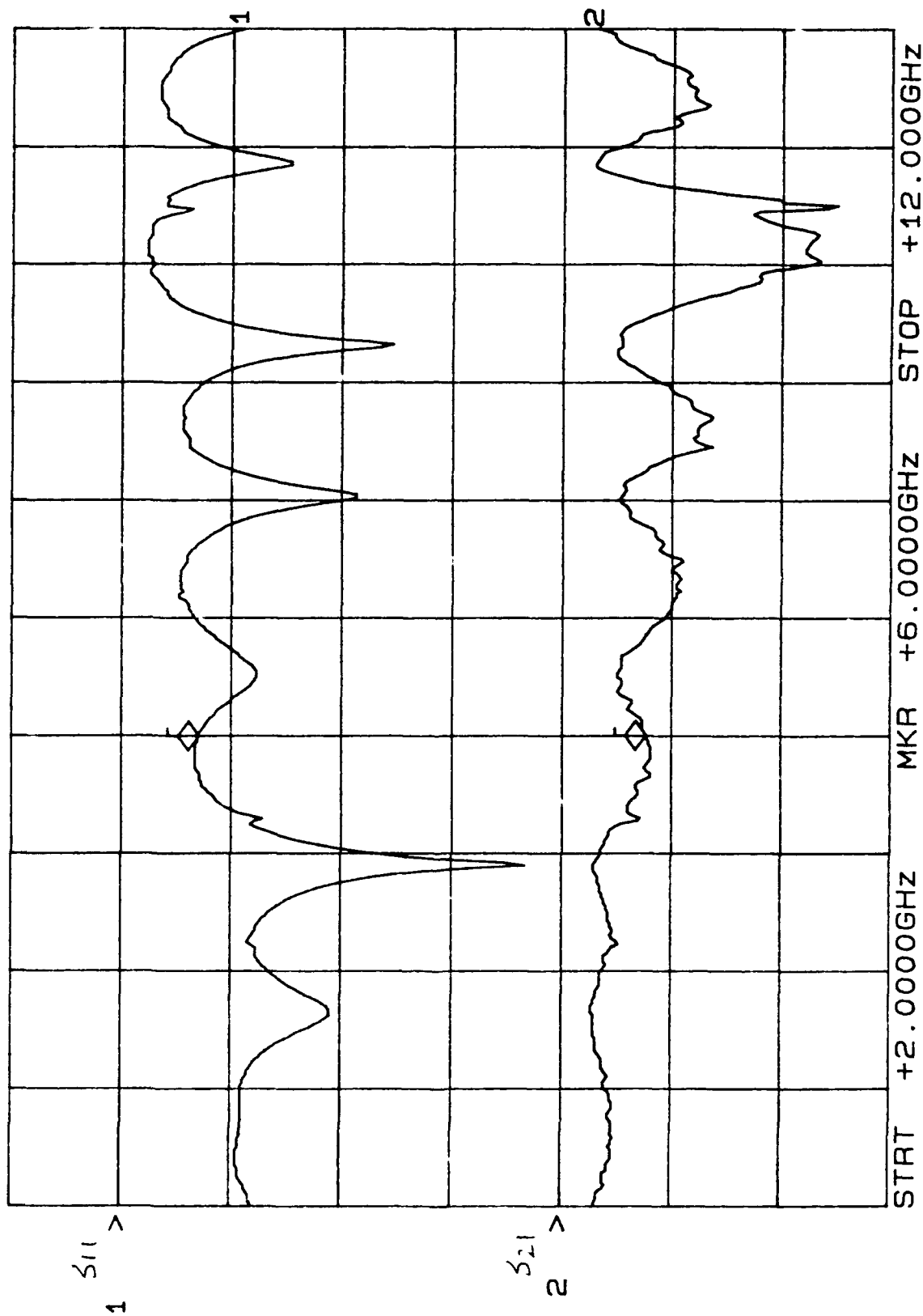
STRT +2.0000GHz MKR +6.0000GHz STOP +12.0000GHz

916, 27

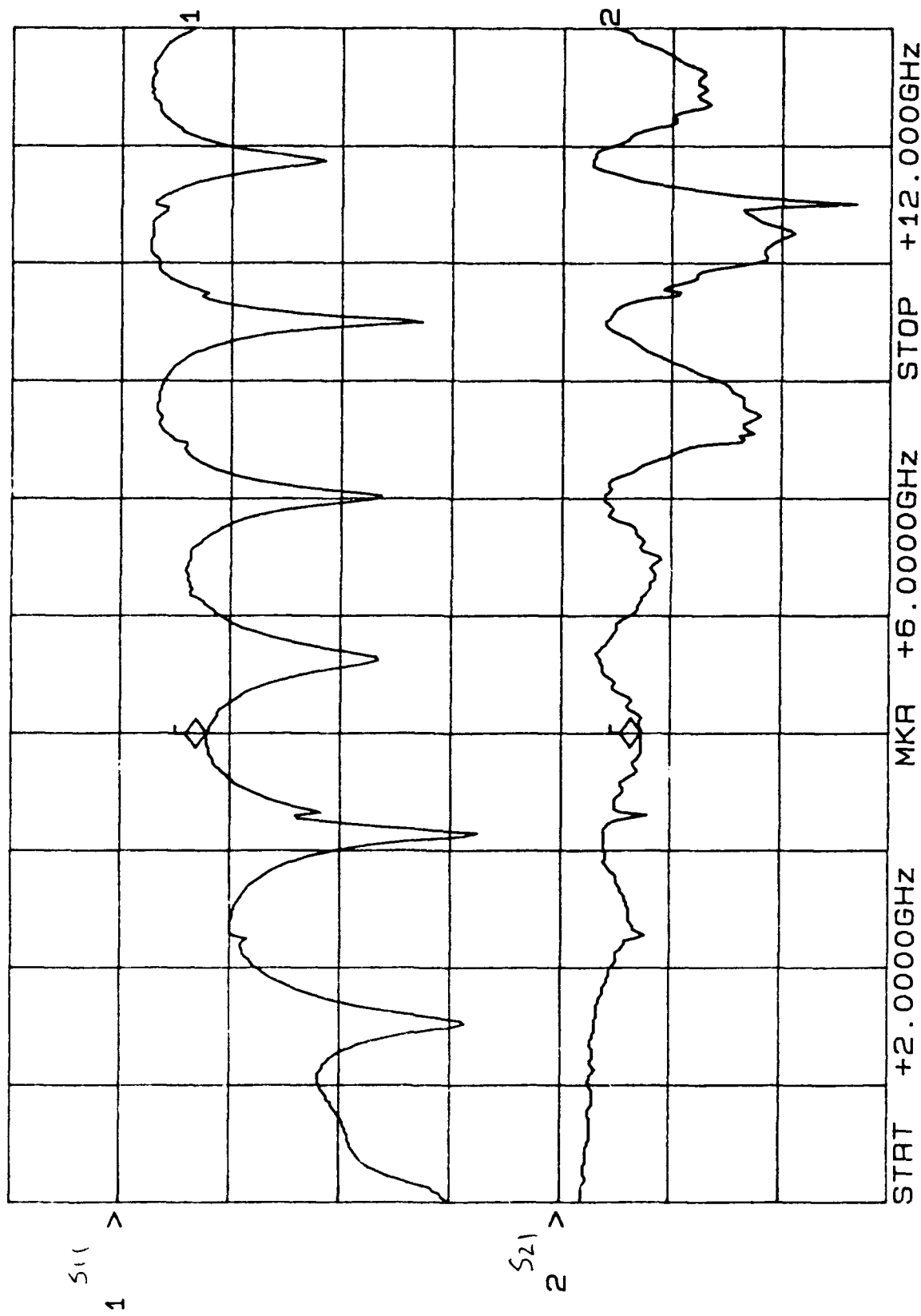
CH1: A -M REF - 6.45 dB CH2: B -M REF + 1.64 dB
10.0 dB/ REF 2.0 dB/ REF



CH1: A ^{-M} REF = 6.97 dB CH2: B ^{--M} REF = 1.51 dB
 10.0 dB/ REF = .00 dB 2.0 dB/ REF = .00 dB

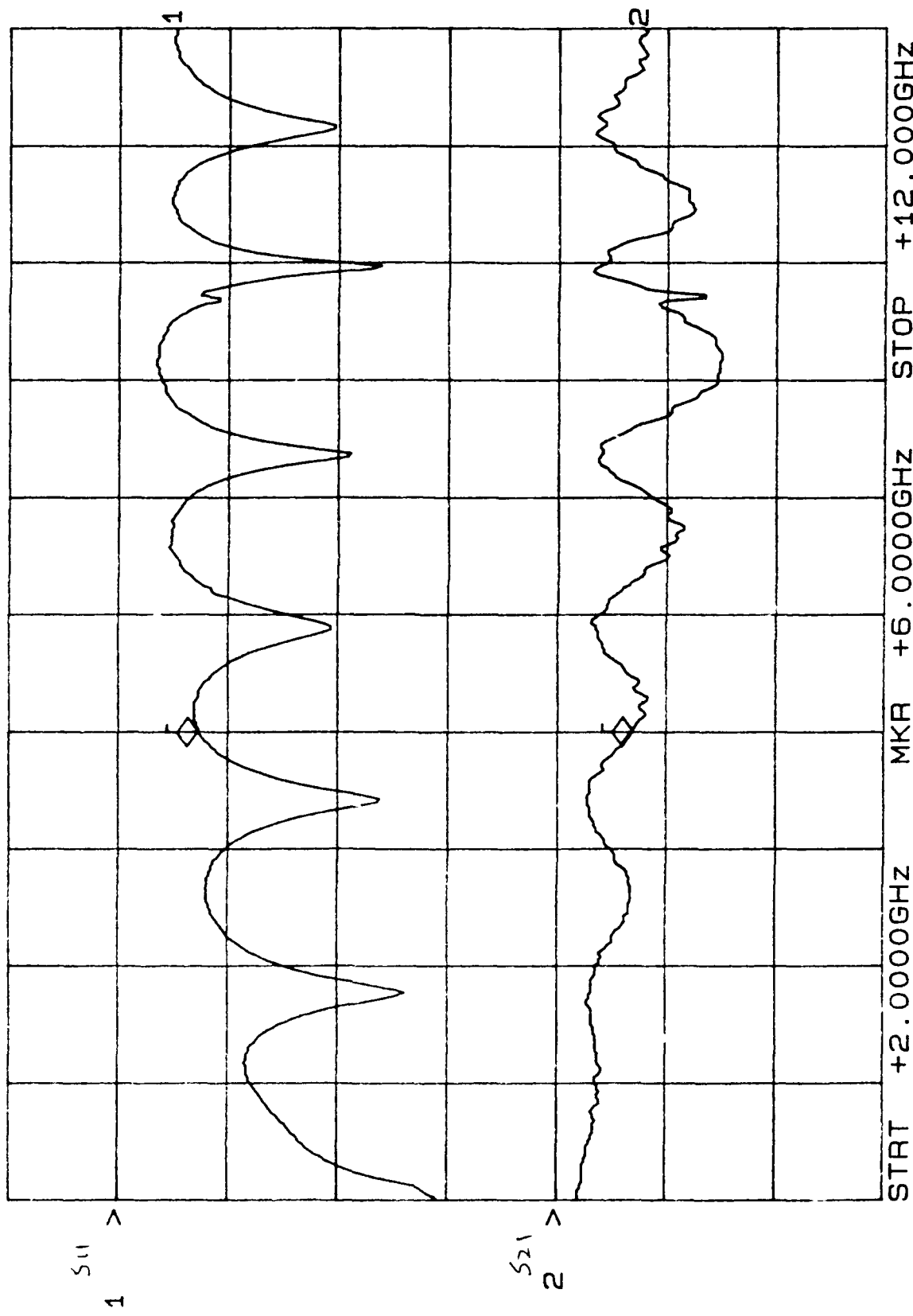


CH1: A -M - 7.88 dB CH2: B -M - 1.45 dB
 10.0 dB/ REF - .00 dB 2.0 dB/ REF + .00 dB



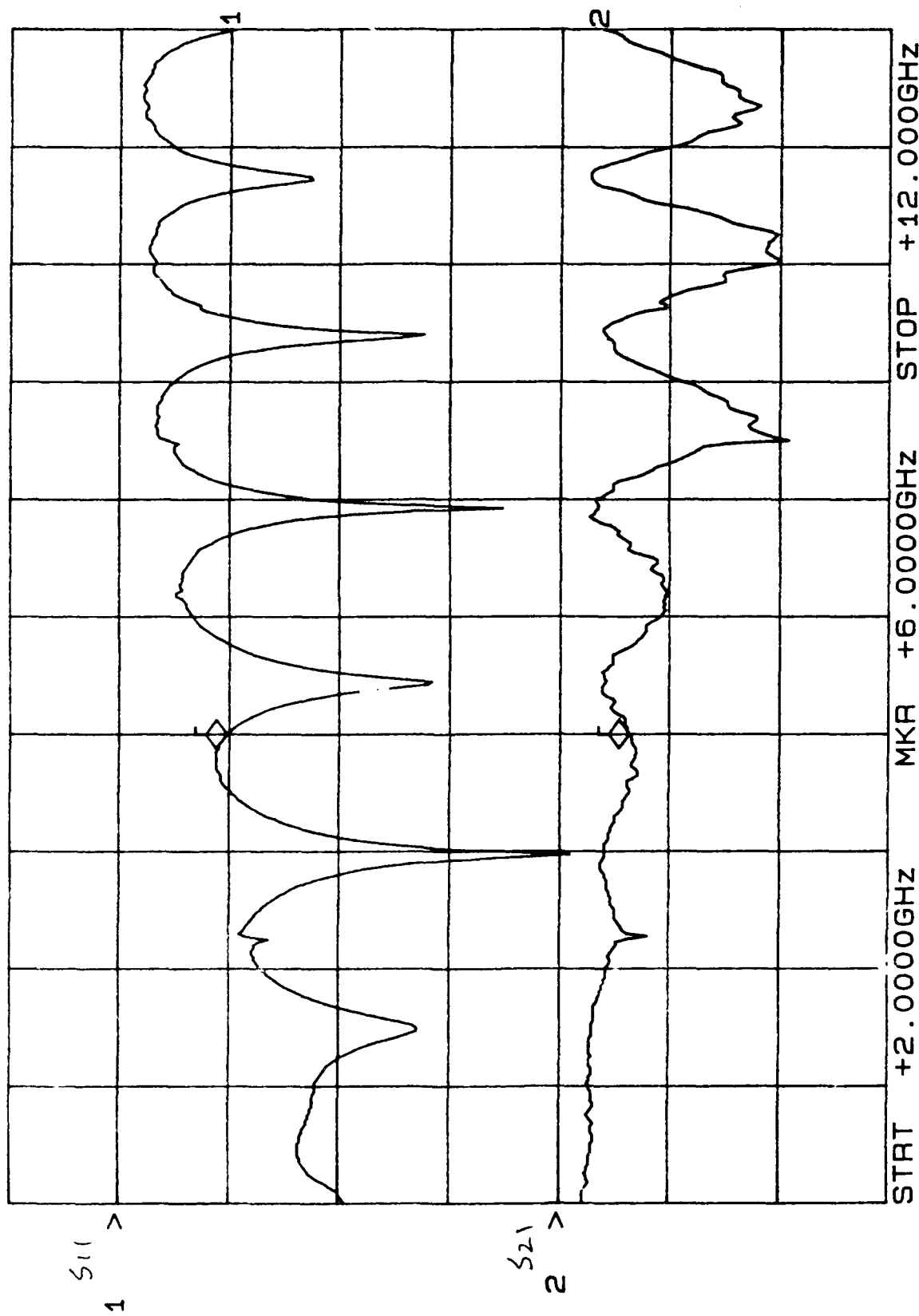
SCP-1000 Pre-weld 5/N 008

CH1: A -M 10.0 dB/ REF - 7.30 dB - 1.34 dB
 CH2: B -M 2.0 dB/ REF + .00 dB

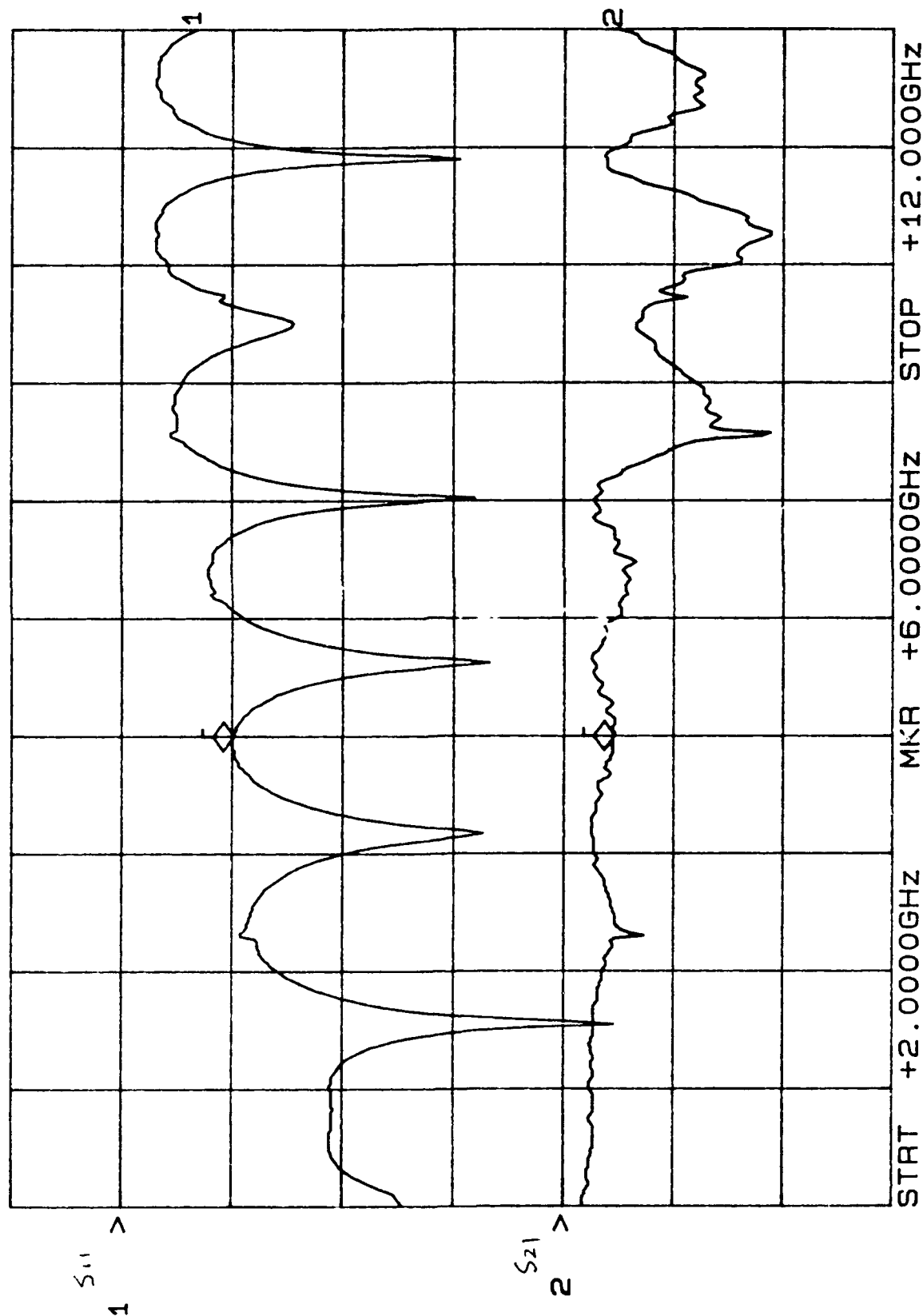


SCP-1000 Pre-weld

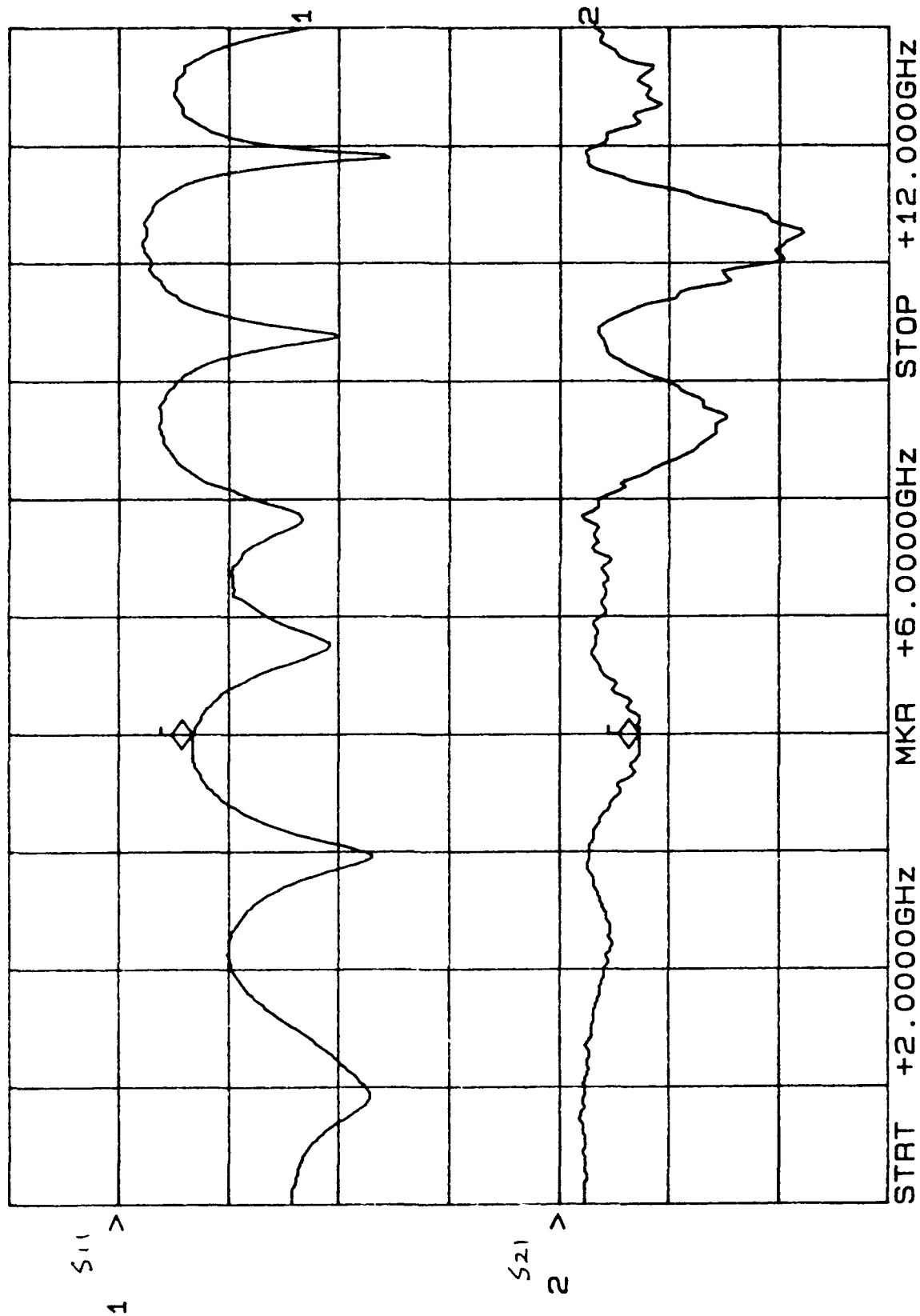
CH1: A -M - 9.76 dB CH2: B -M - 1.26 dB
10.0 dB/ REF - .00 dB 2.0 dB/ REF + .00 dB



CH1: A -M REF - 10.02 dB CH2: B -M REF + .89 dB
 10.0 dB/ REF - .00 dB 2.0 dB/ REF + .00 dB



CH1: A -M REF = 6.72 dB CH2: B -M REF = 1.45 dB
 10.0 dB/ REF 2.0 dB/ REF



APPENDIX 2

SPC-2000

AND


SPC-1000

DOCUMENTATION

SPC-2000

APPLICATION		REVISIONS				
NEXT ASSEMBLY	USED ON	LTR	CC	DESCRIPTION	DATE	APPROVED
320-557963	KU-BAND DSO	--	00	INITIAL RELEASE	12-26-90	<i>m. D. Del</i>

REV																					
SHEET	44	45	46	47	48	49	50	51	52	53	54	55	56	57	58	59	60	61	62	63	64
REV																					
SHEET	23	24	25	26	27	28	29	30	31	32	33	34	35	36	37	38	39	40	41	42	43
REV	-																				
SHEET	2	3	4	5	6	7	8	9	10	11	12	13	14	15	16	17	18	19	20	21	22

UNLESS OTHERWISE SPECIFIED		APPROVALS		SIGNATURE AND DATE		 AVANTEK	
DIMENSIONS ARE IN INCHES		DRAWN		L. VELASQUEZ 12/90			
TOLERANCES		CHECKED		<i>m. D. Del</i> 12-26-90		MECHANICAL OPERATION SHEET CASE ASSEMBLY SCP-1000/2000	
FRACTIONS	DECIMALS	APPROVED					
ALL SURFACES ✓ EXCEPT AS NOTED		MFG ENG		<i>Phil Delacruz</i> 12-26-90		SIZE A CODE IDENT NO. 24539 MOS-558/28	
MATERIAL		QA		<i>Phil Delacruz</i> 12-26-90			
NOTE: DEBurr AND BREAK ALL SHARP EDGES EXCEPT AS NOTED		RELEASED DEC 28 1990		SCALE		WEIGHT	
DO NOT SCALE THIS DRAWING				SHEET 1 OF 2		REV	

MECHANICAL OPERATION SHEET

PART #: 320-558373-001		REV		W.O.# 52016205			
PART NAME: CASE ASSY SCP-2000							
START 6/17/91				FINISH 1 1			
STEP	OPERATION DESCRIPTION	REF DOC	REV	OPER	DATE	QTY IN	QTY OUT

1.	VERIFY BIN-UP	320-55		9164	6/17/91	10	10
2.	SOLDER RF F/T (2 PLACES)	AP-0286C5 AD-557963		2592	6/25/91	10	10
3.	VAPOR DEGREASE PARTS	PS-023886		2592	6/25/91	10	10
4.	FINE LEAK CHECK	PS-029238		2592	6/26/91	10	10
5.	VAPOR DEGREASE CASE	PS-023886		2592	6/26/91	10	10
6.	100% MFG INSPECT	AWS-014355-800 AD-557963		1765	6/26/91	10	10
7.	INSTALL RF/DC CONTACT (2 PLACES)	340-028489-001 AD-557963		N/A			
8.	EPOXY THRU LINE INTO CASE SC	AD-557963 PS-505313		N/A			
9.	INSTALL RF FILTER AND SMA CONNECTORS	AD-557963		2592	6/28/91	10	10
10.	GAP WELD CONTACT RIBBON TO THRU LINE	PS-501206 AD-557963		9164	9/10/91	10	10
11.	CLEAN CASE	PS-023886		9164	9/10/91	10	10
12.	100% MFG INSPECT	AWS-014355-800 AD-557963		9164	9/10/91	10	10
	Laser Weld			1393	9/10/91	10	10
13.	100% QA INSPECT	AD-557963 JI-0235					



SIZE

CODE IDENT NO

A

24539

MOS-558128

SCALE

WEIGHT

SHEET 2 OF 2

REV

COMPONENT INFORMATION

RD REF DES	ITEM PART NUMBER	C DESCRIPTION	RV QTY	UM	C EFFECTIVITY	
					FROM	TO
/	0001 380558372001	2 SK-CAS, SCP-2000	02	1	EA	2
/	0002 510029824001	5 SMA JACK CONNECT L	2	EA	2	
/	0003 526027290001	5 RF FEEDTHRU	C	2	EA	2
/	0004 513029238002	5 CONTACT PIN	A	2	EA	2
/	0005 453013328001	5 2X15X 3/16" LG. B	0	AR	2	
/	0006 370505182001	5 SUB 50 OHM THRU	-	2	EA	2
/	0007 361013796001	5 STD O&C GROUND S C	6	EA	2	
/	0008 380013798001	5 SPACER, STD OSC	B	6	EA	2
/	0009 603558199002	5 SCR, 0-80, PNH, CR, -	6	EA	2	
/	0010 606558200002	6 SCR, 2-56, PNH, CR, -	4	EA	2	
/	0011 627558223003	5 WSHR, .1720D, LKSH -	4	EA	2	
/	9999 OS-558128000	OPERATION SHEET,	0	RF	2	

SEP 19 1991

CONFIGURATION MANAGEMENT
 PREPRODUCTION CONTROL FILE
 AUTHORIZED BY: PC

DATE INTO FILE 09/19/91 REVISION 02

OK 04/04/91
09/16/91

AMPS53R007
 PROFIT CENTER: DOC
 REQUESTOR : ANN
 PARENT PART: 310538374001 DESC: SK-SCP-2000
 AVANTEK - DOCUMENTATION
 PRODUCTION BILL OF MATERIALS
 PSCM-24539
 RUN-DATE 09/12/91 PAGE 1
 REPORT-DATE 09/12/91 SHOP 03967

REV: 2 STATUS: 2 REV DATE:

COMPONENT INFORMATION

RD REF DES	ITEM PART NUMBER	C DESCRIPTION	RV QTY UM	C EFFECTIVITY	
				8 FROM	TO P
/	0001 320558373001	2 SK-ASSY,CASE,SCP 2	1 EA 2	-----	-----
/	0002 380558409001	LID, SCP-2000	1 EA 2	-----	-----
/	9999 AD-558374000	ASSEMBLY DWR,SCP	0 RF 2	-----	-----
/	9999 IN-558374000	INSTALATION DWC,	1 RF 2	-----	-----

SEP 19 1991

CONFIGURATION MANAGEMENT
 PREPRODUCTION CONTROL FILE
 AUTHORIZED BY: AC

DATE INTO FILE 091991 REVISION 2

Bob Gray 9-15-91

USE SULFUR BASED TAPPING, CUTTING
OPERATING ON.

AND DECREASE EACH UNIT WITHIN
UNIT'S AFTER EACH TIME IT IS REMOVED FROM
LITTING OPERATION. NO UNIT IS TO BE
LEFTLY MACHINED AND LEFT IN A SETUP
WITHOUT DECREASING

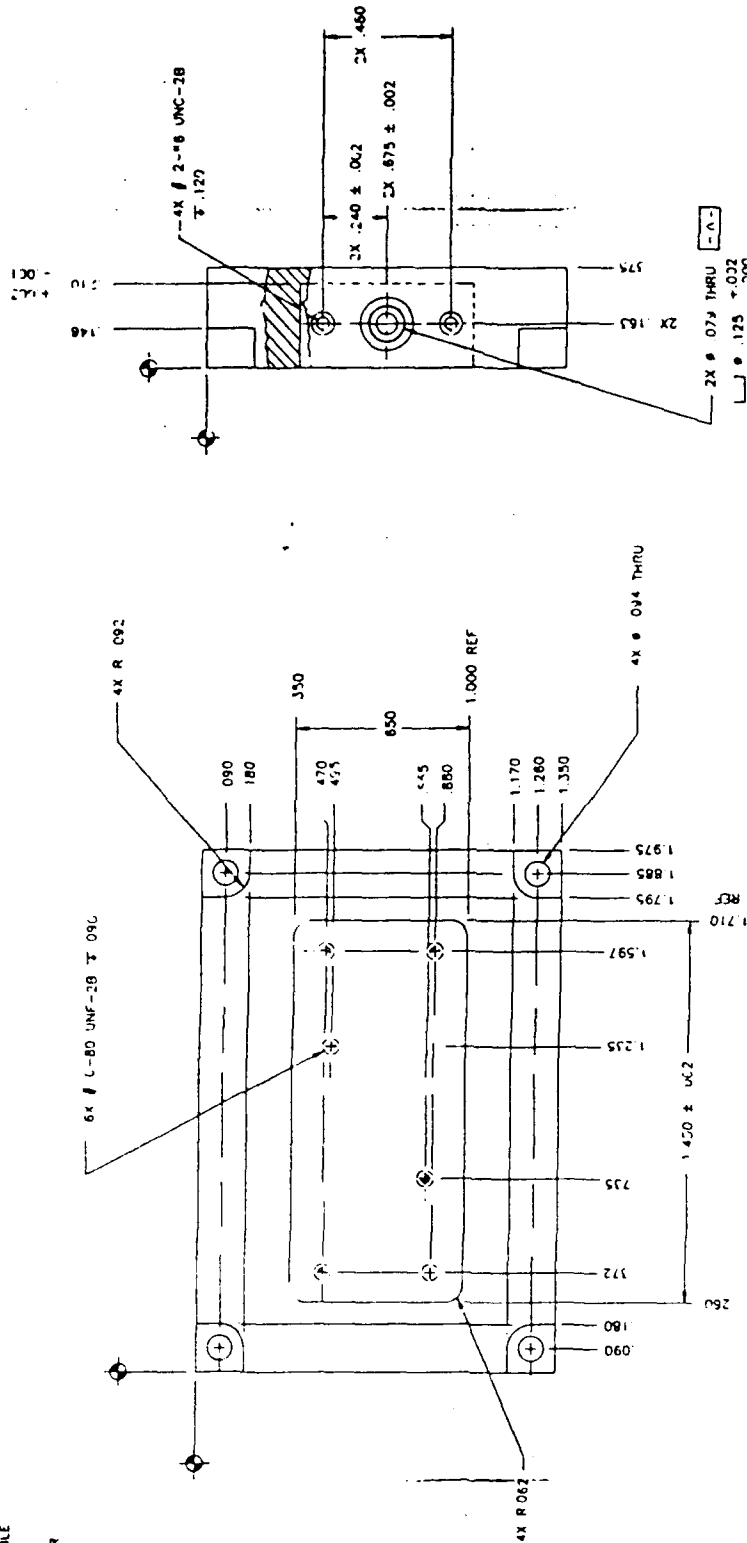
IN ALL SURFACE AND HOLES PERMISSIBLE
BREAK OFF MAX

CON BASE MATERIALS MAY BE U.C. FOR
MAX 2X DEBURRING

LE ROUGHNESS

1. BREAK THRU OR DIMPLE FAR SIDE
FEATURES

AND TAG WITH P/N 380-558372-001
CURRENT REVSLN LETTER



2X .075 THRU
1.125 ± .032
1.039 ± .001
1.165 ± .001
1.000 ± .000
1.130 x 130

SEP 19 1981

SK-CASE,
SCP-2000

380-558372

RON JONES 9/14/81

303 SST (304)
AS100 (100)

100 (100)

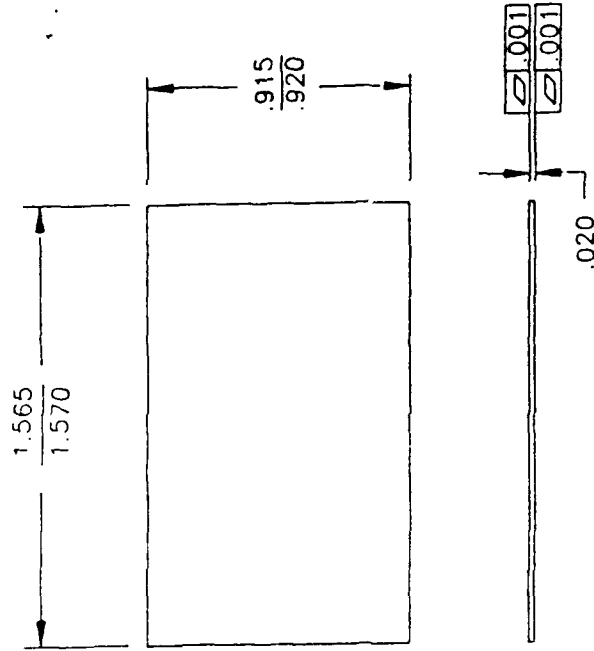
REV	DATE	BY	CHK	APP
1	9/14/81	RJ		
2	9/14/81	RJ		
3	9/14/81	RJ		
4	9/14/81	RJ		

NOTES: UNLESS OTHERWISE SPECIFIED.

1. DO NOT BREAK SHARP EDGES.

2. DO NOT CHEM FILM.

3. BAG AND TAG WITH AVANTEK P/N
380-558409-001 AND CURRENT REV. LETTER
PER MIL-STD-130.



SEP 19 1991

CONFIGURATION MANAGEMENT
PREPRODUCTION CONTROL FILE
AUTHORIZED BY: *[Signature]*
DATE INTO FILE: 09/19/91 REVISION: 02

RON JONES 91/9/16

1/64 .003 1'
CST 304
PEP 00-S-763

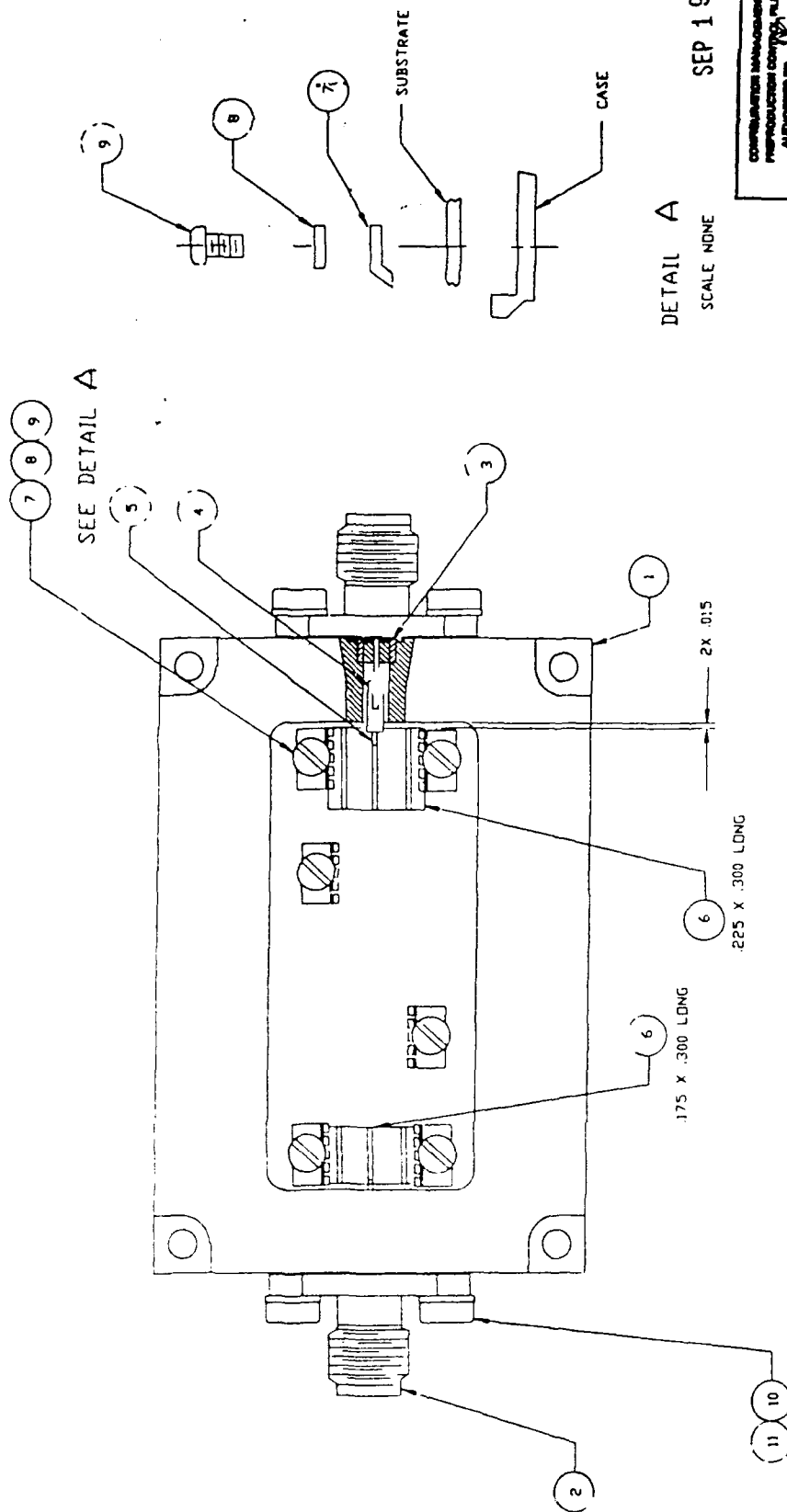
310-558374 3 -0000

APPROVED BY	
DESIGNER	MECH ENG
PROJECT ENG <i>[Signature]</i>	MFG ENG
PC	MFG ENG
	QUALITY ENG

SK L'D. S-P-2002

380-558409

NOTES: UNLESS OTHERWISE SPECIFIED
1: ASSEMBLE PER OPERATION SHEET.



DETAIL A
SCALE NONE

SEP 19 1991

COMBINATION MANAGEMENT
PRODUCTION CONTROL FILE
AUTHORISED BY: [Signature]
DATE INTO FILE 02/19/91 REVISION 02

SEE SEPARATE PARTS LIST 320-558373-001

DESIGNER	APPROVED BY	MECH ENG
[Signature]	[Signature]	MECH ENG
[Signature]	[Signature]	MECH ENG
[Signature]	[Signature]	QUALITY ENG

AMS

DATE YOUTIF 5/16/91

SK CASE ASSEMBLY,
SCP-2000

AD-558373
1 OF 1

SPC-1000

AMDP55R007
 PROFIT CENTER: DOC
 REQUESTOR : ANN
 PARENT PART: 310558128001 DESC: SK-SCP-1000 FSCM-24339 AVANTEK - DOCUMENTATION
 PRODUCTION BILL OF MATERIALS
 RUN-DATE 09/12/91 PAGE 1/1
 REPORT-DATE 09/12/91 SHOP 03967
 REV:02 STATUS:2 REV DATE:09/11/91

COMPONENT INFORMATION

RD REF DES	ITEM PART NUMBER	C DESCRIPTION	RV QTY	UM	C EFFECTIVITY	
					FROM	TO
/	0001 320558128001	2 SK-ASSY,CASE,SCP 02	1	EA	2	
/	0002 380028925001	5 OUTER LID X BAND B	1	EA	2	
/	9999 AD-358128000	2 SK-CASE ASSY SCP 2	0	RY	2	
/	9999 IN-358128000	INSTALLATION, SC	0	RY	2	

SEP 19 1991

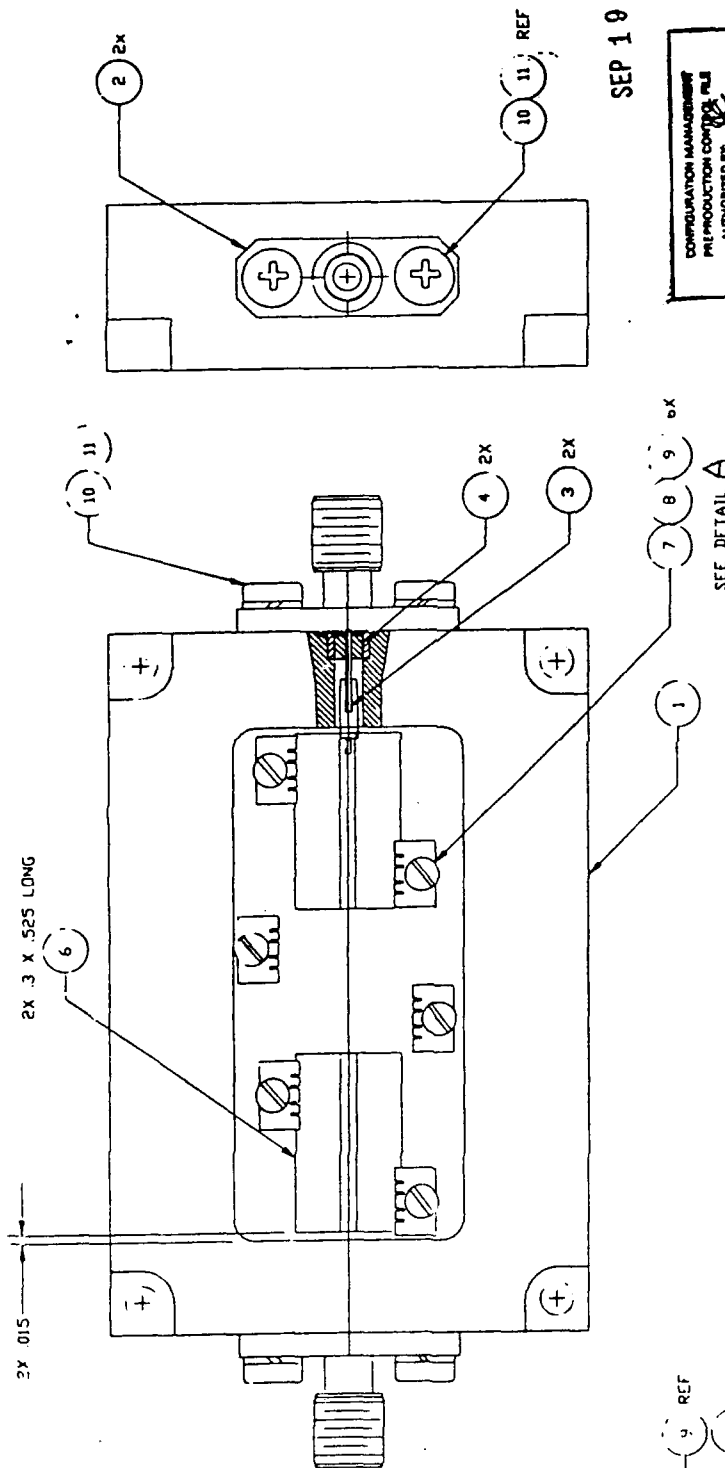
CONFIGURATION MANAGEMENT
 PREPRODUCTION CONTROL FILE
 AUTHORIZED BY: AC

DATE INTO FILE 091991 REVISION 02

OK
Bob Oly
9/16/91

NOTES UNLESS OTHERWISE SPECIFIED

1. ASSEMBLE PER OPERATION SHEET.
2. BAG AND TA' WITH P/N 320-558128 AND CURRENT REV LETTER PER MIL-STD-130



SEP 10 1991

CONFIGURATION MANAGEMENT
 PRE-PRODUCTION CONTROL FILE
 AUTHORIZED BY: [Signature]
 DATE INTO FILE: 09/10/91 REVISION: 02

SEE SEPARATE PARTS LIST 320-558128

DESIGNER	APPROVED BY	MECH ENG
PC	[Signature]	MECH ENG
		MECH ENG
		QUALITY ENG

SK-CASE ASSEMBLY,
 SCP-1000

RON JONES 9/8/10

SEC ABOVE

320-558128 SCP-1000

AD-558128

1:1

1 OF 1

DETAIL A
 SCALE NONE

R&D STATUS REPORT

DARPA Order No: 6268

Program Code No: 000008E20K43

Contractor: Hughes Aircraft Co. as a subcontractor to Superconductor Technologies Inc.

Contract No: N-00014-88-C-0713-S-HAC-1

Contract Amount: \$737,991.00

Effective Date of Contract: 01 Sept 88

Principal Investigator: Dennis Elwell

Telephone No: (714)759-7386

Report Title: The Processing of High Temperature Ceramic Superconducting Devices.

Reporting Period: 10/1/88 - 9/31/91

FINAL REPORT

SUMMARY

This report briefly summarizes work at Hughes Aircraft as subcontractors to Superconductor Technologies Inc. over the period of the contract. The aim of the investigation was to evaluate two areas of possible application for high-Tc superconductors- connecting cables for IR detectors and passive microwave devices- and to design, build and test a replacement device using STI's material. The most important contributions of this study have been the feedback of test data which helped STI in their outstanding improvements in material performance at microwave frequencies, and the development of an original method for testing microwave materials at cryogenic temperatures, which allows in-situ calibration. The PIN-diode switched superconducting phase shifter which was selected for evaluation does not appear to be manufacturable at the present time.

DESCRIPTION OF PROGRESS

IR FOCAL PLANE INTERCONNECT

IR detectors operate at cryogenic temperatures, and are connected to electronic circuitry at substantially higher temperatures by a flexible cable fabricated on polyimide (see Fig. 1). The advantages of using a superconducting material to carry signals from the detector to the signal processor are its low thermal conductivity combined with superior performance as an electrical conductor, including a relative absence of dispersion.

We selected a typical cable in order to compare the predicted heat loss of a superconducting equivalent with that of a cable using a conventional material. The device selected was from a program known as AOA and actually has three cables and operates in a temperature range from 15 to 90K. In the case of the superconductor, deposition on polyimide is still not feasible and so we assumed a requirement for a rigid substrate. The total heat load for the three conventional cables is around 60 mW for a temperature difference of 75K and a cable length of 5.5 inches. The dominant contributor to this heat load are the two copper power leads, since the Kapton base is a poor thermal conductor. The superconducting leads to carry the same current would impose a load of only about 0.3 mW and so the loading of a superconducting interconnect would be

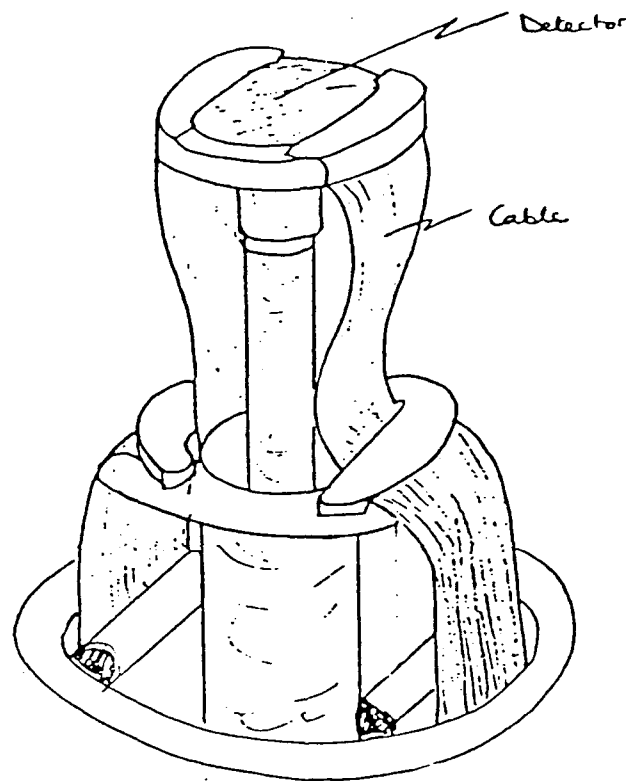


Fig. 1. Sketch of infra-red focal plane array assembly.

dominated by that of the substrate. An ideal substrate material would be fused silica, which would result in about 8 mW of heat leak. There has been progress in the deposition of high-Tc films on silica with barrier layers and the introduction of superconducting infra-red focal plane interconnects appears feasible and could be considered for new programs, especially those where power is of particular concern. Superconducting cables on substrates with higher thermal conductivity such as alumina would not be viable. There is a reluctance for IRFP device engineers to replace flexible with rigid cable, so the potential impact of superconducting cables would be particularly strong if they could be flexible. Deposition on polyimide is difficult, although not impossible since temperatures for in-situ deposition are comparable with the decomposition temperature of some polyimides. It is recommended to investigate the development of superconducting films on flexible polyimide cables as the technology for low-temperature (around 400 C) in-situ deposition matures. Such cables appear to have real potential in view of the extreme importance of reducing heat loss in satellite-based IR detectors.

MICROWAVE MEASUREMENT TECHNIQUES -

Ring Resonator

In the early phase of this investigation, the emphasis was on comparison of the properties at microwave frequencies of STI's thallium superconductor with those of conventional metals. A nominal goal for STI was the development of materials with X-band surface resistance an order of magnitude less than that of gold or silver at cryogenic temperatures. Sample size was limited to 0.5 x 0.5 inches, and the substrate was MgO.

Ring resonator was selected for these measurements on the basis of simplicity and the low radiative loss. Various arrangements were tried for launching the signals into the sample and minimizing the influence of a strap between the sample and the launcher pad on the fixture. Our development of cryogenic facilities for microwave measurements on ring resonator samples was mainly funded from our IR&D program and was described in a 1990 publication (D.J.Miehls, D.Elwell, P.S.Fleischner and A.A.Shapiro, Intl. J. Hybrid Microelectronics 13#4(1990)85).

Several assumptions are necessary in extracting surface resistance data from the microwave S parameter measurements. Among these are conversion from loaded to unloaded Q, subtraction of dielectric loss, and separation of microstrip from ground plane contributions. A standard sample was fabricated from gold by first sputtering a very thin Ti/W adhesion layer and then evaporating about a micron of gold. Gold was then plated to a total thickness of 9.5 microns, well above the skin depth at 4.6 GHz. Loaded Q measurements on this standard sample were 72.5 at room temperature and 193 at 33K. Our first TBCCO sample from STI had a Q of 39.6 at 75K, 56.7 at 50K and 64.8 at 25K. These data suggested a surface resistance for the superconductor of the same order as that of gold at room temperature, much higher than the value expected from extrapolation of STI's high frequency cavity measurements. This disappointing performance of the TBCCO film at lower microwave frequencies led STI to investigate the origins of the effect and to modify their film deposition process to remedy the problem.

The STI TBCCO film responded well to cycling between 20K and room temperature. There was no detectable degradation when a film was subjected to eight such cycles in an early test (Fig. 2). The variation in the resistivity near the transition temperature is within the error of measurement.

TRL Measurements

Following STI's breakthrough near the end of 1989 in producing greatly improved TBCCO films and the development of their own test facilities, our emphasis

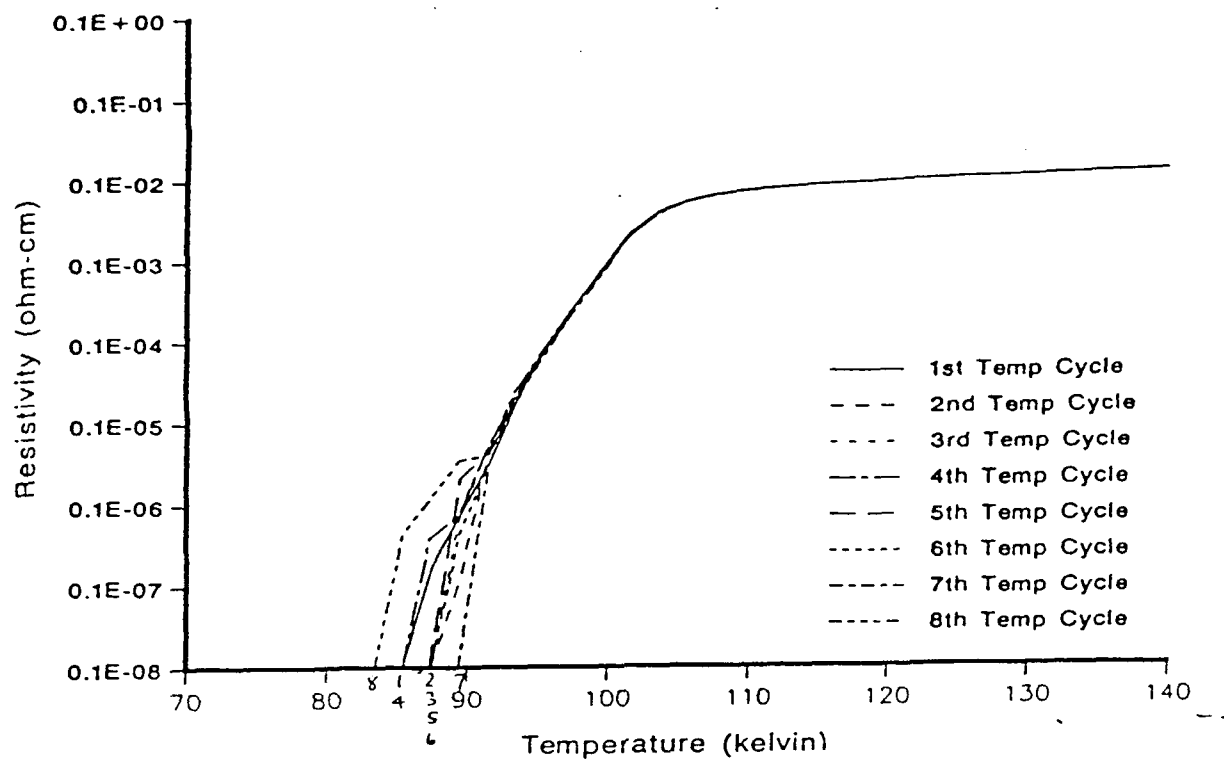


Figure 2. Resistivity vs. temperature data for TBCCO subjected to 8 cycles from 293 - 20K.

switched from characterizing materials towards the design and fabrication of a microwave device using the STI superconducting films. We selected a PIN-diode switched phase shifter which is the key component in airborne phased array radars. Insertion loss is of fundamental importance in respect both of the radar range and the power dissipated.

Because of the very small insertion loss which can be achieved even in conventional phase shifters, the introduction of replacement superconducting devices requires very sensitive and reliable measurement techniques for cryogenic temperatures at microwave frequencies. Our initial experience of X-band measurements on high-T_c materials convinced us that measurements which involved comparison between conventional and superconducting samples exchanged at room temperature would not be acceptable; allowing the chamber to warm to room temperature and then re-cooling would introduce uncertainties of the same order as the differences to be measured. A method of in-situ calibration of the measurement system, with immediate test of the superconductor at the cryogenic temperature, was therefore devised and a cryochamber modified to allow the introduction of this technique.

An important aspect of our measurement technique is the absence of direct contact between the microwave input and output signal carriers and the superconducting sample. RF coupling is achieved by a dipole/balun arrangement, with the RF energy entering the cryochamber via a ridged waveguide (See Fig. 3). Calibration is achieved by a TRL (thru reflect line) arrangement, the various elements in this array being moved into position at the measurement temperature by the use of a slider, as shown in Fig 3. Although the ridged guide in particular constitutes a significant heat sink, it was possible after careful modifications to reach temperatures as low as 29K. Precise location of the sample and standards in both horizontal and vertical directions is difficult to achieve to the required accuracy because of thermal expansion and contraction of the metal, but this was an important segment of our later work.

The system was validated using a thick film silver test part incorporating a standard mismatch circuit fabricated on an alumina substrate using thick film silver. This consisted of a microstrip impedance transformer with a return loss of about 10db. Fig. 4 shows scattering parameter data taken at room temperature. The data is all taken in a frequency range from 9.5 to 10.0 GHz. Fig. 4a shows insertion loss and return loss; both parameters show a small dependence on frequency. The markers are at values of 0.34 db for insertion loss and 14.35 db for return loss. In Fig. 4b we compare loss data for the Thru and Delay lines. The Thru line has lower loss, especially at the lower frequencies, but the return losses are well matched at reasonable values. Fig. 4c shows in the lower trace the return loss of the short circuit. The value at the marker is about 0.01 db which is considered acceptable. Also shown is the short to short isolation. We considered a value above 40 db to be acceptable and the measured values were around 60 db. There is a trend for the isolation to decrease slowly at the higher frequencies, the marker being at 53.9 db. In order to obtain the data of Fig. 4, we had to solve serious cryochamber moding problems. The use of absorbent materials in appropriate locations reduced this problem to a reasonable level, without seriously affecting vacuum or minimum achievable temperature.

Fig. 5 shows the data for the same standard mismatch circuit measured at 60K. Fig. 5a shows the insertion loss of the mismatch line and the data are generally similar to those at room temperature, with rather lower insertion loss at the higher frequencies. Fig. 5b compares the Thru and Delay lines and reveals a new problem, namely microphonics due to vibration of the compressor motor. This vibration has a strong influence on the return loss and has greatly contributed to the noise level in this figure. In our CTI cryochamber, the cold head is located directly above the compressor and it is impractical to insert

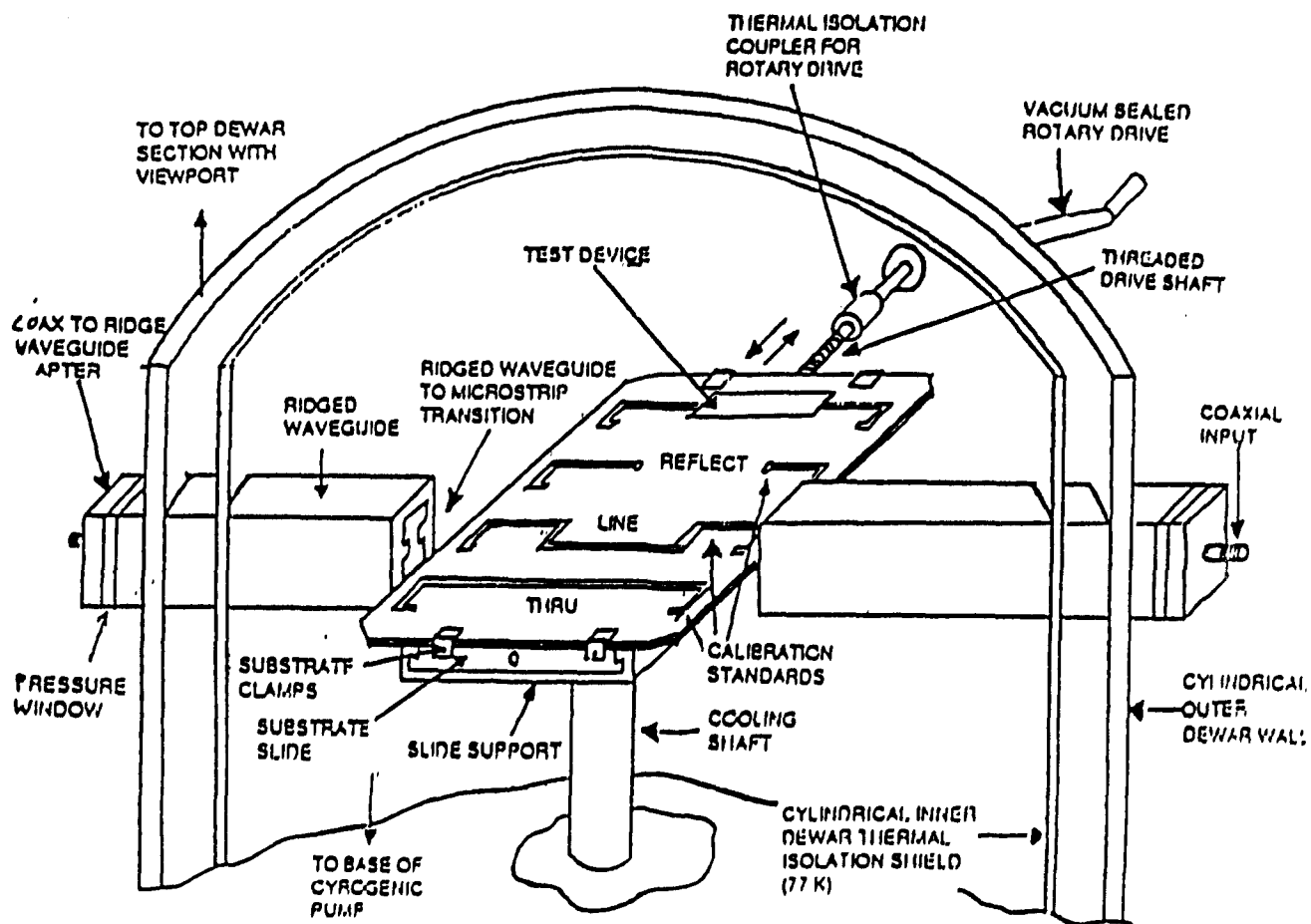
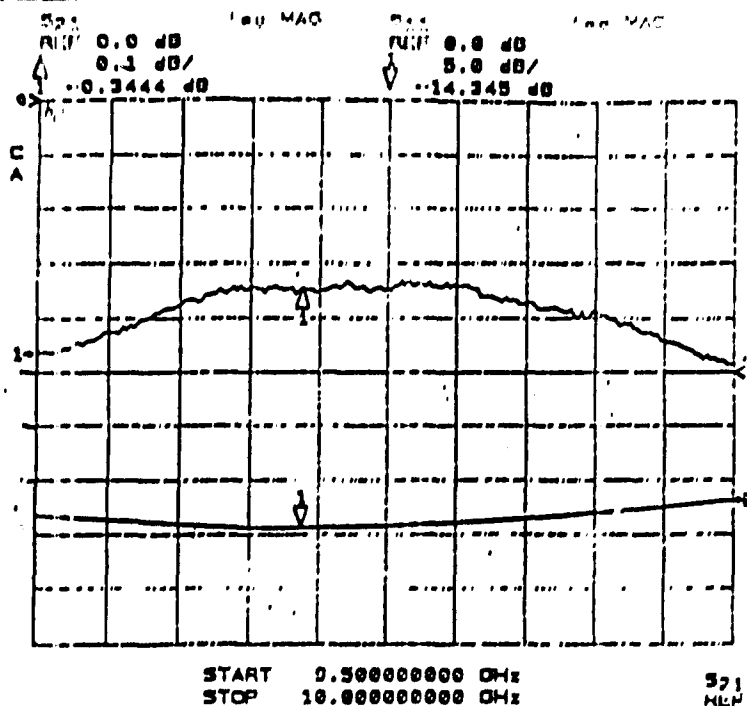
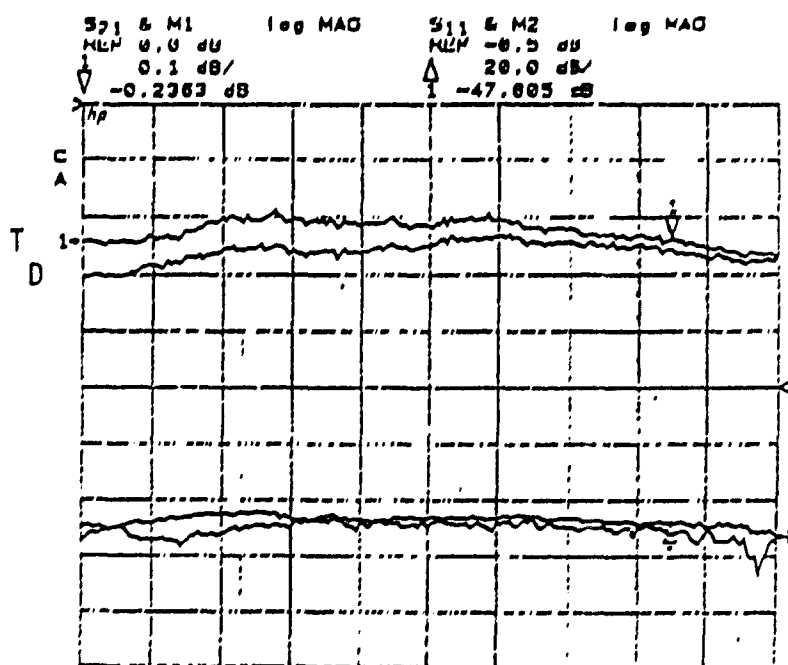


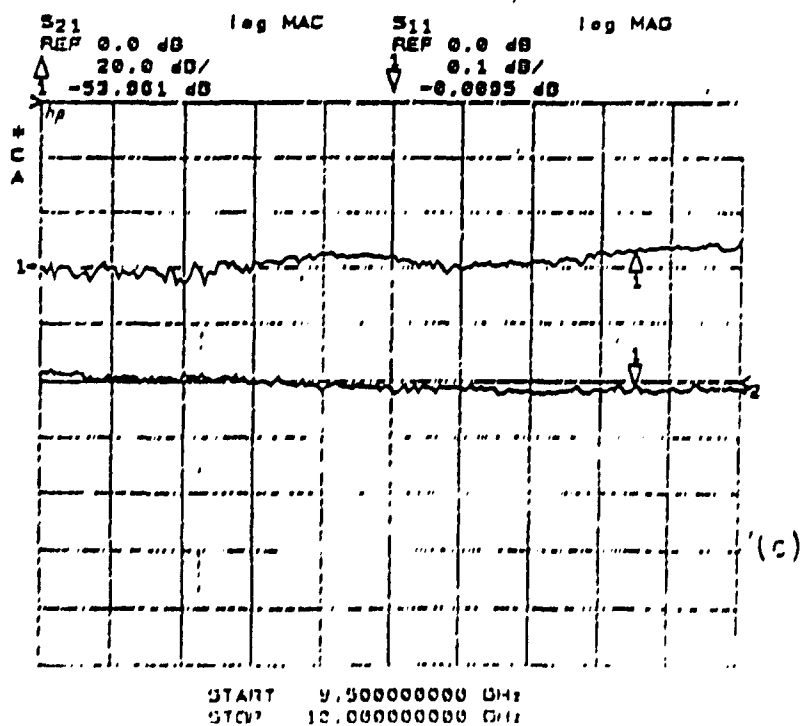
Fig. 3. Apparatus for microwave S parameter measurements at cryogenic temperatures using TRL calibration standards.



(a)



(b)



(c)

Fig. 4. Validation test fixture data: (a) Insertion loss and return loss for 10dB mismatch. (b) Insertion and return loss for Thru (T) and Delay (D) line. (c) Insertion loss and isolation for Short.

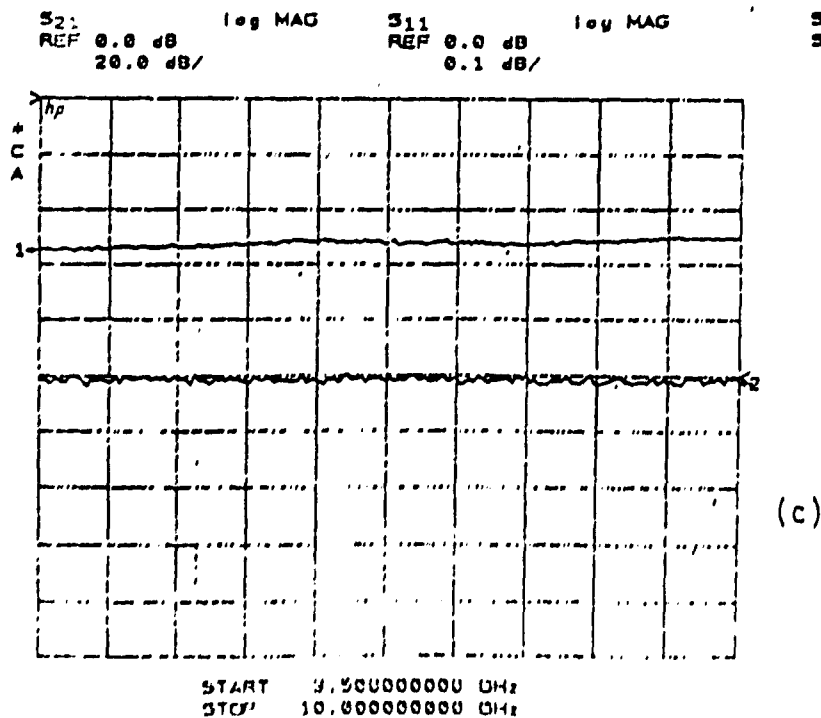
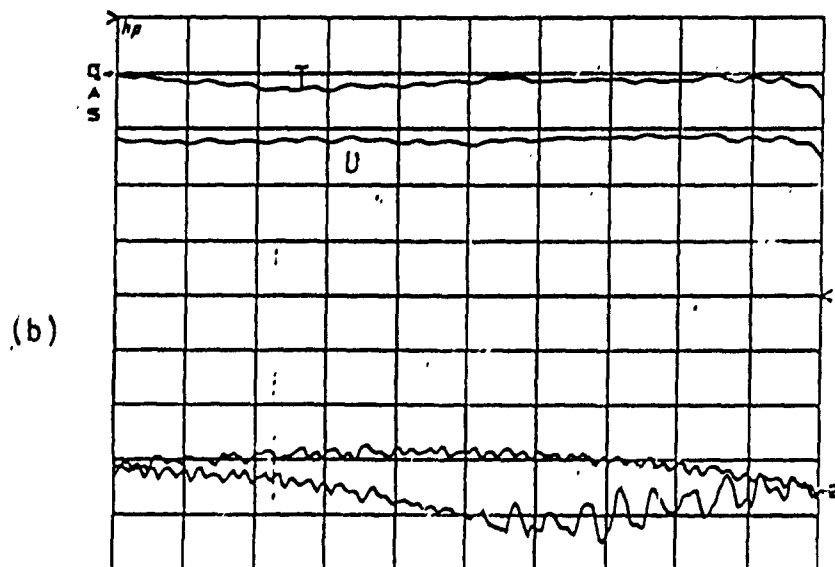
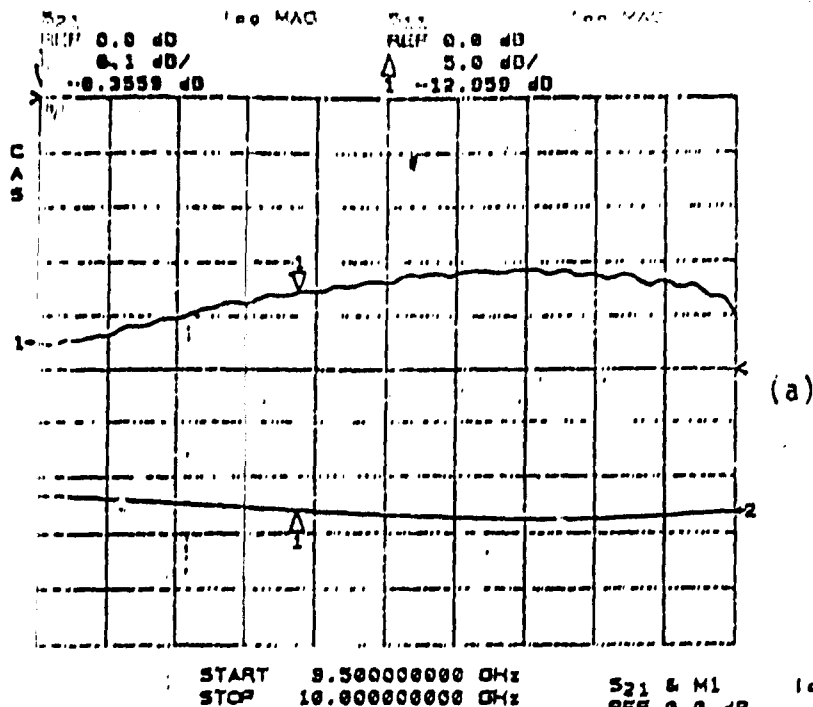


Fig. 5. Data for same sample as in Fig. 6 but at 60K.

vibration-damping material between the cold source and the sample. In cases where the duration of the measurement is short, the compressor can be switched off during measurement but the temperature then rises fairly rapidly. The S parameter measurements normally take too long (about 10 minutes) for this to be a practical solution, but we were able to reduce the noise by introducing additional smoothing of the data. The difference in insertion loss between thru and Delay lines was unreasonably high in this test. This difference was probably due to a positional error as described above. An additional source of error is that the dipoles may not be exactly similar in size and shape due to the manufacturing tolerances of thick film technology and this could lead to differences like that shown in Fig. 5b. This problem can be reduced by very careful processing and is probably not significant in this case since it does not show up in the room temperature comparison, but it must be considered in interpreting the data. Fig. 5c shows data for the Short, which is excellent for both insertion loss and isolation; both are very flat across the frequency range.

The reproducibility of the measurement system at 60K was checked by a series of six runs with the results plotted on the same graph. Fig. 6 shows this data. In each case the measurement was taken through the complete calibration procedure then the loss of the Delay line was measured and plotted. The sample was the same as discussed above. The reproducibility was generally very good except for the first run which showed rather higher loss at the lower frequencies.

Phase Bit

Since the main goal of this project was the comparison between normal metal and superconducting phase bits, the emphasis after the initial tests was to make and test a phase bit. Thin film gold was chosen for the standard sample. A 90 degree phase bit was designed on a substrate with dielectric constant $K=25$ (simulating lanthanum aluminate) and fabricated on a 1 cm square ceramic as shown in Fig. 7a. This phase bit is dropped into a hole in the TRL substrate (see Fig. 7b) for measurement, after connection to the conductor strips by bridging straps of minimal height.

The substrate fabrication technique is a multistep process using conventional thin film technology. The substrate surface is first coated with a thin layer of titanium/tungsten to give good adhesion. This is sputter-coated with gold and then electroplated to a thickness of about 3 microns, substantially thicker than the skin depth at X band. A 4210 photoresist is then used to pattern the metal coating by baking, exposure, development and etching, followed by cleaning to remove residual photoresist. A positive photoresist could be used as an alternative procedure. Connections to the back side of the substrate are preferably made by via connections through holes in the substrate. Ultrasonic drilling is a satisfactory method of putting via holes in LaAlO_3 substrates but the presence of the via holes complicates the film deposition process in the case where the sample is superconductor rather than gold.

Measurements on the standard phase bit at room temperature are shown in Fig. 8. Fig. 8a shows that the phase shift is around 94.5 degrees and has only a slight variation across the frequency band. This shift could be corrected and the frequency dependence removed by design iteration, but these performance figures are considered satisfactory for this initial demonstration. Figs. 8b and 8c are similar except that the signal is applied at opposite ends of the chamber, so that the data are a test of the reversibility of the arrangement. Both charts show similar behavior, with a tendency for the insertion losses to diverge with increasing frequency. This is typical behavior for this type of phase bit topology.

Fig. 9 shows data for the phase bit at 30K. The phase shift is rather higher

S21
REF 0.0 dB
0.1 dB/

log MAG

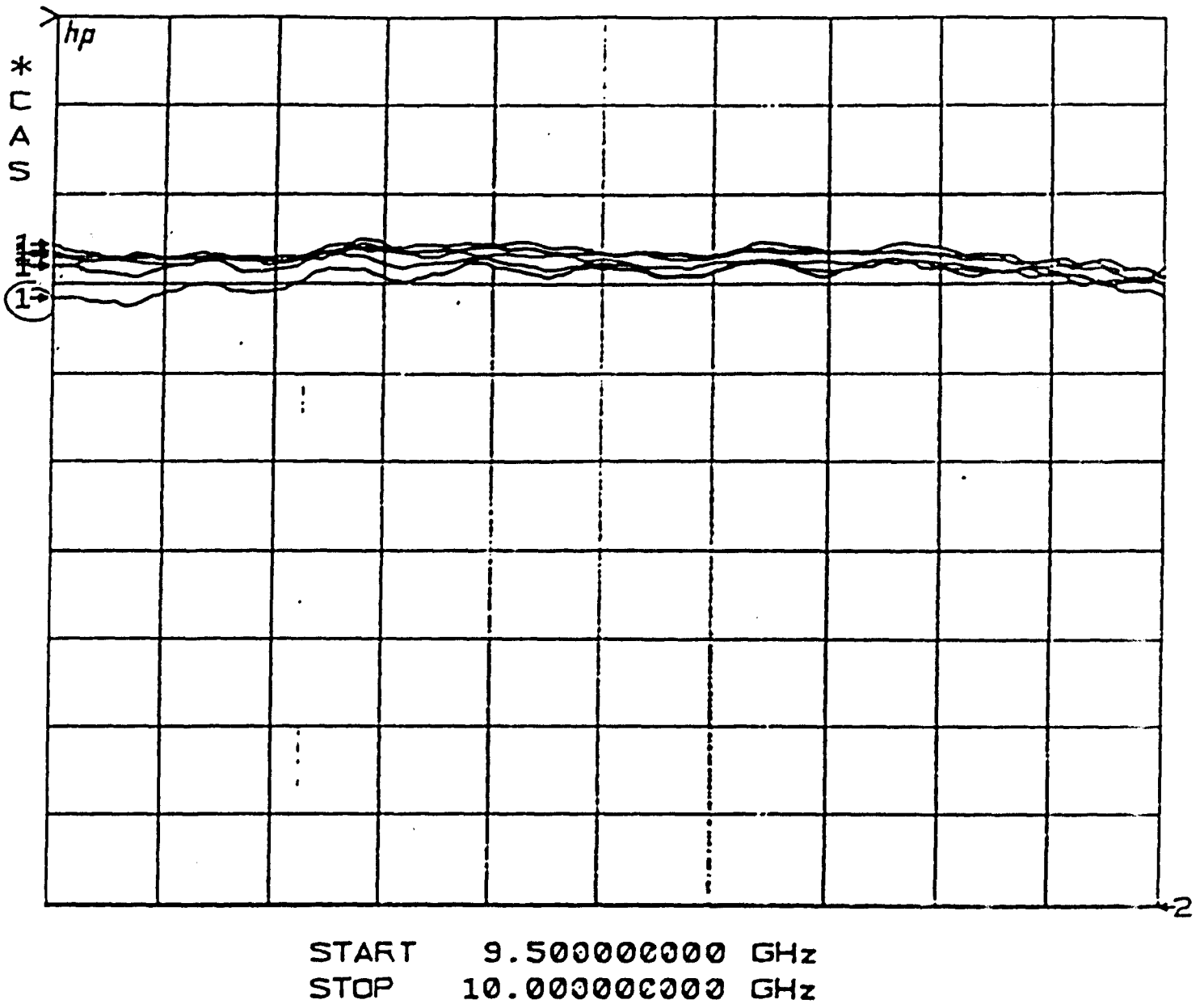


Fig. 6. Repeatability test data at 60K. Insertion loss of 10db mismatch repeated 6 times at 60K.

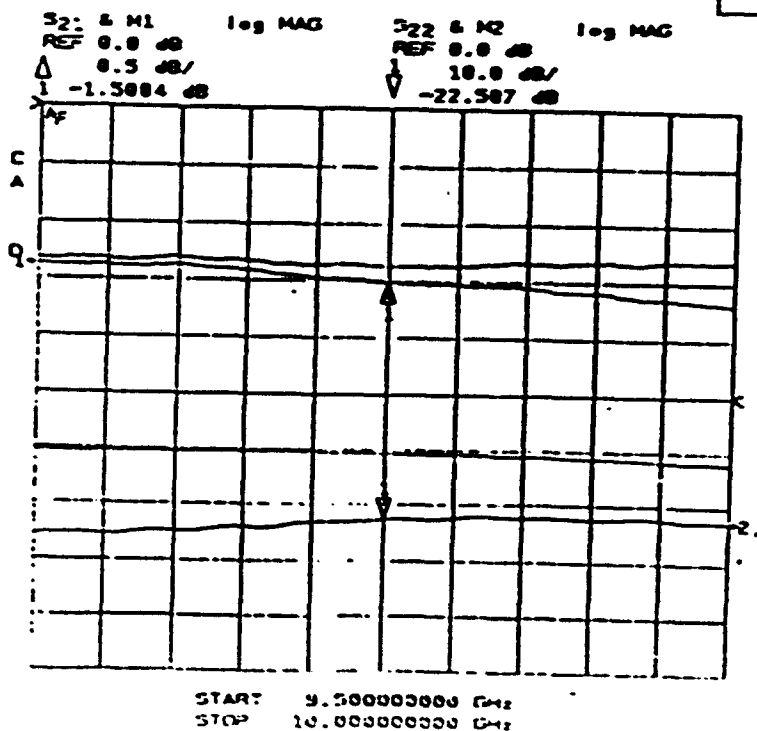
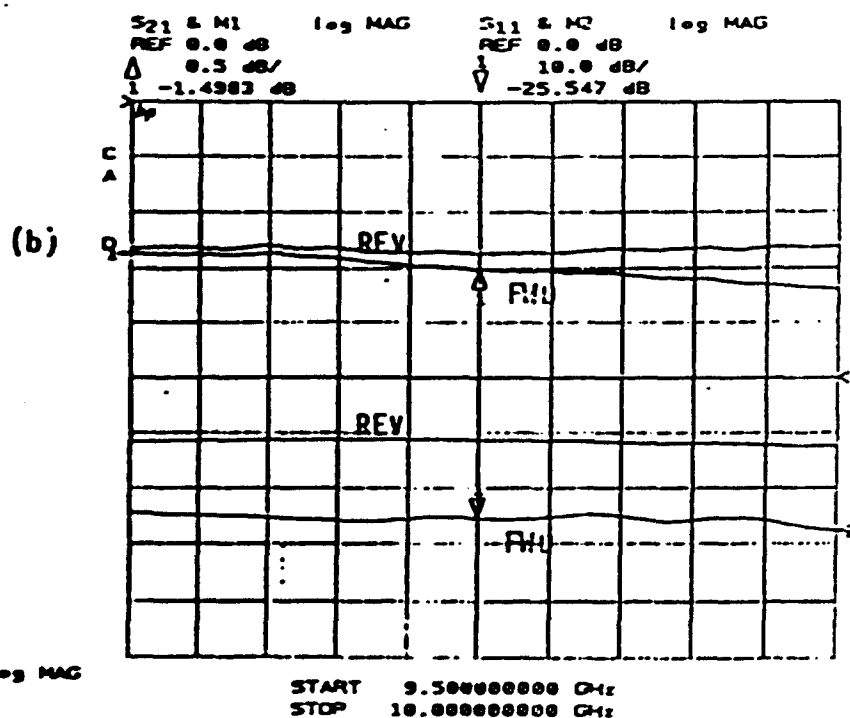
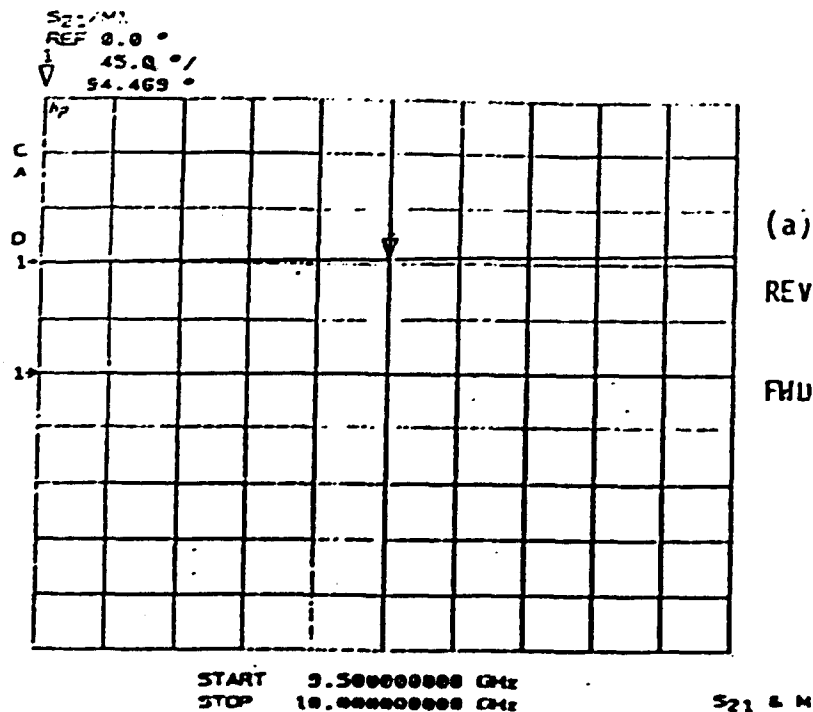


Fig.8 . Data for 9u degree phase bit at room temperature: (a) Phase snift; (b)Insertion and return loss; (c)Similar to (b) but with connections reversed.

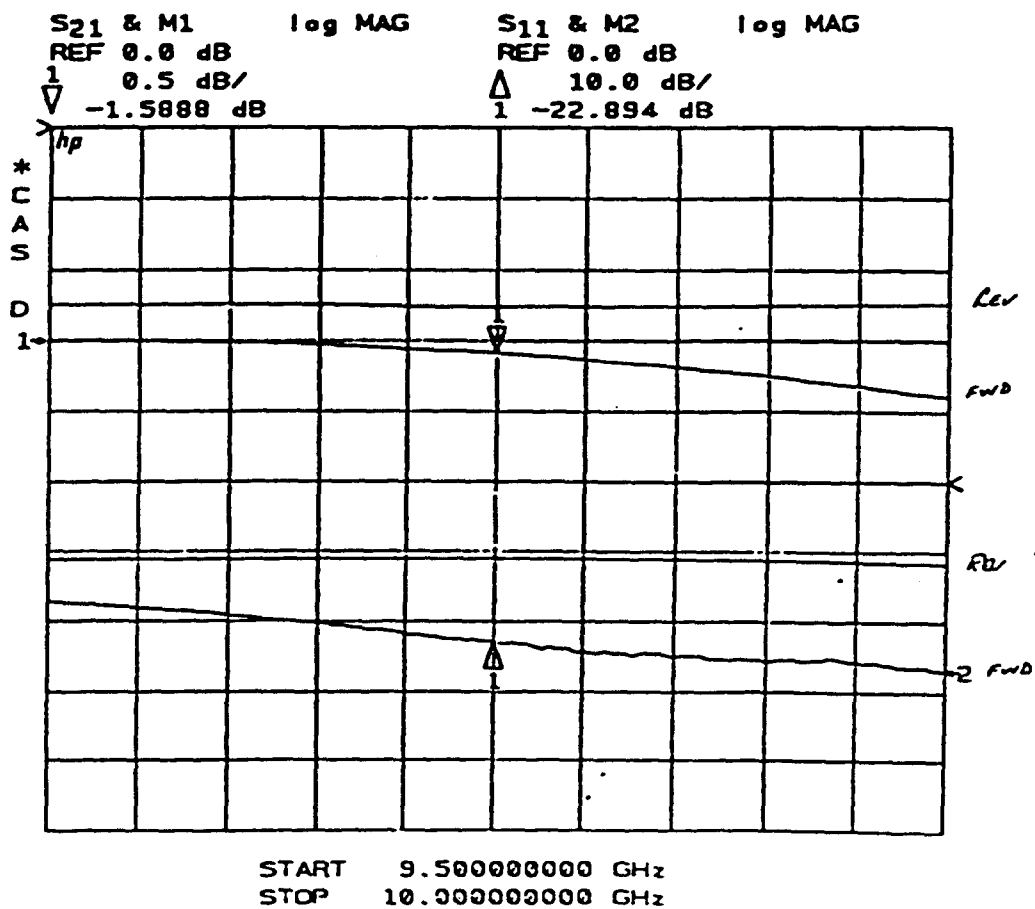
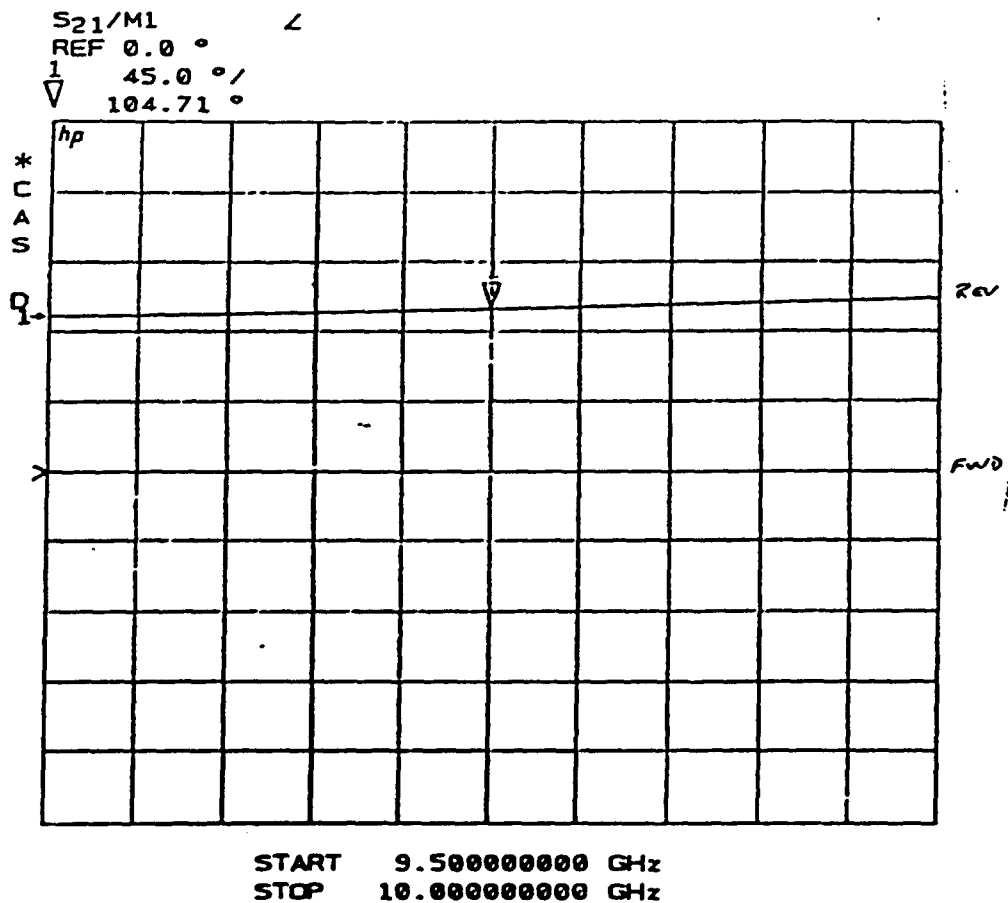


Fig. 9. (a) Phase Shift; (b) Insertion loss(upper data) and return loss (lower data) for standard gold phase bit at 30K.

than that at room temperature (104.7 degrees at center frequency) and the insertion loss is a little higher than at room temperature (1.59db versus 1.51db at room temperature). This appears an anomalous result since the conductivity of gold must increase at cryogenic temperatures. However the return loss of the cooled bit is less than the return loss of the room temperature bit so this would contribute to the loss. Some variability was experienced which was attributed to physical mismatch between the printed dipoles on the substrate and on the ridged waveguide. This problem could be reduced by the introduction of a sensitive position locator to check on small displacements on cooling so corrections could be made before measurements were taken. Unfortunately the program was terminated before this modification was complete.

SURVEYS OF HIGH-Tc APPLICATIONS

Over the course of the contract, there were three initiatives within Hughes Aircraft Company to seek promising applications for high-Tc materials in microwave systems, particularly radars. The microwave field was considered by Hughes to be the potentially the second most important applications area for the new superconductors, following data processing of IRFP array data using Josephson technology if this can be developed in these materials.

The first initiative was our survey which was reported in the Status Report of 2/28/89. A telephone survey of Radar Systems Group (RSG), Ground Systems Group (GSG) and Space and Communications Group (SCG) engineers found at that time the greatest interest from the latter group. Calculations had been performed at SCG of a narrow-band downconverter operating over a wide frequency range from a few MHz to 1.5 GHz, and substantial performance improvements coupled with weight reduction had been calculated. Unfortunately the device was for a classified application. We held a follow-up meeting at RSG and were encouraged to pursue superconducting phase shifters since reduced insertion loss would allow greater radar range and so provide an important tactical advantage which could more than compensate for the cryogenic cooling requirements.

As superconducting technology matured and material improvements approached even the more optimistic predictions of microwave performance, our systems colleagues took a harder look at their earlier projections and decided that a cooling system to maintain a phased array at 77K in a modern fighter was impractical in view of already severe power and weight restrictions.

Hughes carried out in May 1990 an applications study aimed primarily at ground-based applications of superconductors where power and weight considerations are not so severe. High sensitivity receivers were seen as the most likely application area, especially at the lower frequencies in view of the quadratic dependence of surface resistance on frequency. No single strong candidate for short-term HTS application was identified in this internal study.

In March 1991 a presentation of STI technology at RSG was arranged, and was attended by several senior engineers and managers. A low noise exciter was identified in this meeting as the leading candidate for replacement of a conventional by a superconducting device. This has the advantage over the phased array that only a single circuit is required per system, so greatly reducing cryogenic requirements. However this proposed application was identified too late to substitute for the phase shifter in this project.

CONCLUSIONS

This project was terminated by STI prematurely before the improved performance of a TBCCO superconducting phase bit could be quantified. Prior to this decision, progress both on our measurement facility and on superconducting

test samples was slow in comparison with our expectation. We underestimated the physical problems of implementing cryogenic measurements using the TRL method, and the presence of via holes in the substrates presented new challenges to STI's film deposition process that led to delays in sample preparation. In retrospect, an arrangement in which we relied on STI to provide samples in direct competition with their own internal requirements, at a time when the deposition process was in a phase of intense development and samples were scarce, was not a formula for the most rapid progress.

We recommend that the cryogenic TRL measurement system be optimized and will attempt to do this with internal Hughes funds.

We must reluctantly accept that substitution of HTS devices into major systems will be slower than we had expected, since the most important thrust within the systems houses is currently towards cost reduction. The cost of cryogenics in systems which have not previously required low temperature operation is a major hurdle, in spite of a slow expansion in cryoelectronics generally. A superconducting phased array radar now seems a very distant goal, but presumably one which will be realised at some point in the future. In the shorter term, we recommend that microwave HTS development be focussed on small components which can give substantial performance improvements with only local cooling, such as the low noise exciter referred to above.

FINAL REPORT

CONTRACT NO. N00019-88-C-0173-S-SA-1

15 NOVEMBER 1991



Lockheed Sanders, Inc

PROGRAM SUMMARY

Superconducting Technologies, Inc. and Lockheed Sanders are developing a passive microwave device incorporating high temperature superconducting (HTS) materials. The program includes development, characterization, lithography, and patterning of superconductor materials. An inverted microstrip HTS resonator is used to characterize a microwave oscillator.

ACCOMPLISHMENTS

The accomplishments over the life of the contract can be grouped into three areas: HTS characterization, oscillator development, and HTS lithography. The most significant advances were made in the processing techniques used to pattern HTS materials. The HTS characterization work was used to support the lithography effort in the early stages of the contract. The characterization was used to determine if a particular lithographic process was harmful to the HTS material. A 10 GHz oscillator using a half wavelength resonator was designed and tested with a gold resonator at both 298 K and 77 K. This work was transferred to STI before a working HTS resonator could be inserted into the oscillator.

HTS CHARACTERIZATION

In the early stages of the contract, the HTS films were characterized with a surface profilometer and a 10 GHz parallel plate cavity. The surface profilometer measurements gave an indication of the thickness uniformity of an HTS film. Early in the contract the surface of the HTS material varied by as much as $\pm 1 \mu\text{m}$. As the film quality improved, surface profilometry measurements were performed less frequently. The parallel plate cavity consisted of a copper ground plane, a 2 mil thick polyethylene dielectric, and a coaxial input probe. The HTS sample was placed faced down on the dielectric next to the coaxial input to form the cavity. The parallel plate cavity is shown in Figure 1. The cavity measurements were a easy, quick way to gauge the effect of process steps on the HTS material. A gold standard measured in the cavity produced a Q of ~ 80 while the best HTS films would produce a Q of ~ 400 .

HTS OSCILLATOR

A 10 GHz oscillator was designed using a half wavelength resonator as a stabilizing element which is shown in Figure 2. By using a high Q resonator, the performance of the oscillator would be improved. A resonator mask was designed and both gold and HTS resonators were fabricated. Because of the poor HTS film quality at the beginning of the contract the gold and HTS resonators had about the same Q. An oscillator using the gold resonator was tested at 298 K and 77 K and had performance as expected. Eventually STI supplied an HTS resonator and ground plane with a Q of 4000 to be used in the oscillator. These were installed but the oscillator did not fire off. Subsequently it was found the Q of the HTS resonator had fallen 150. The cause of the degradation was never determined and all the hardware was transferred back to STI to complete this task.

LITHOGRAPHY

Over the life of the contract many lithographic, passivation, and normal metal contact techniques were evaluated. In addition air bridges were developed and substrate thinning experiments were performed. After a series of materials evaluations, the wet etch technique chosen was a 1:200 HCl/H₂O solution at room temperature. Shipley 1375 was used as the photoresist with MF312 as the developer. Exposure was accomplished with 360 nm UV mask aligner. Two methods for bondable contacts were developed. The first was used for bonding on top of HTS material. A 5% bromine in methanol by volume solution was used to etch the surface of the HTS material. Sputtering 1 μ m of gold on the prepared surface will produce bond pull strengths exceeding 20 g. The second method was used for bonding to an isolated pad on LaAlO₃ which was then connected to the HTS material with a gold lift-off interconnect. The isolated pad consisted of an adhesion pad of sputtered TiW/Au followed by a 1 μ m evaporated Au layer. As an alternative to wet processing, ion beam milling experiments were also performed. A Commonwealth Scientific 3" Ion Mill System was used to pattern some test circuits. Typical parameters were 500 V accelerator voltage, 500 mA/cm² ion beam current, and $2 \cdot 10^{-4}$ Torr gas pressure using argon as the ion species. This produced circuits with improved edge definition but no discernable improvement in rf performance over wet etch techniques. The contrast between ion milling and

wet etching can be seen in Figure 3. Contacts electroplated directly to HTS material were also evaluated, but were discarded because the electroplating process dissolves the HTS material. Air bridge technology was also used and transferred to STI. Since part of the air bridge is electroplated, a 5 level mask scheme was developed to isolate the plated portion of the air bridge from the HTS material. The freestanding bridge is then connected to the HTS material. An example of a gold air bridge over HTS is shown in Figure 4. Finally thinning of LaAlO_3 substrates was performed. One square cm samples were successfully thinned from 20 mil to 5 and 4 mil thicknesses. A sample was thinned to 2 mil but the grinding induced a severe camber in the substrate.



 **Lockheed Sanders**

Figure 1. 10 GHz parallel plate cavity.

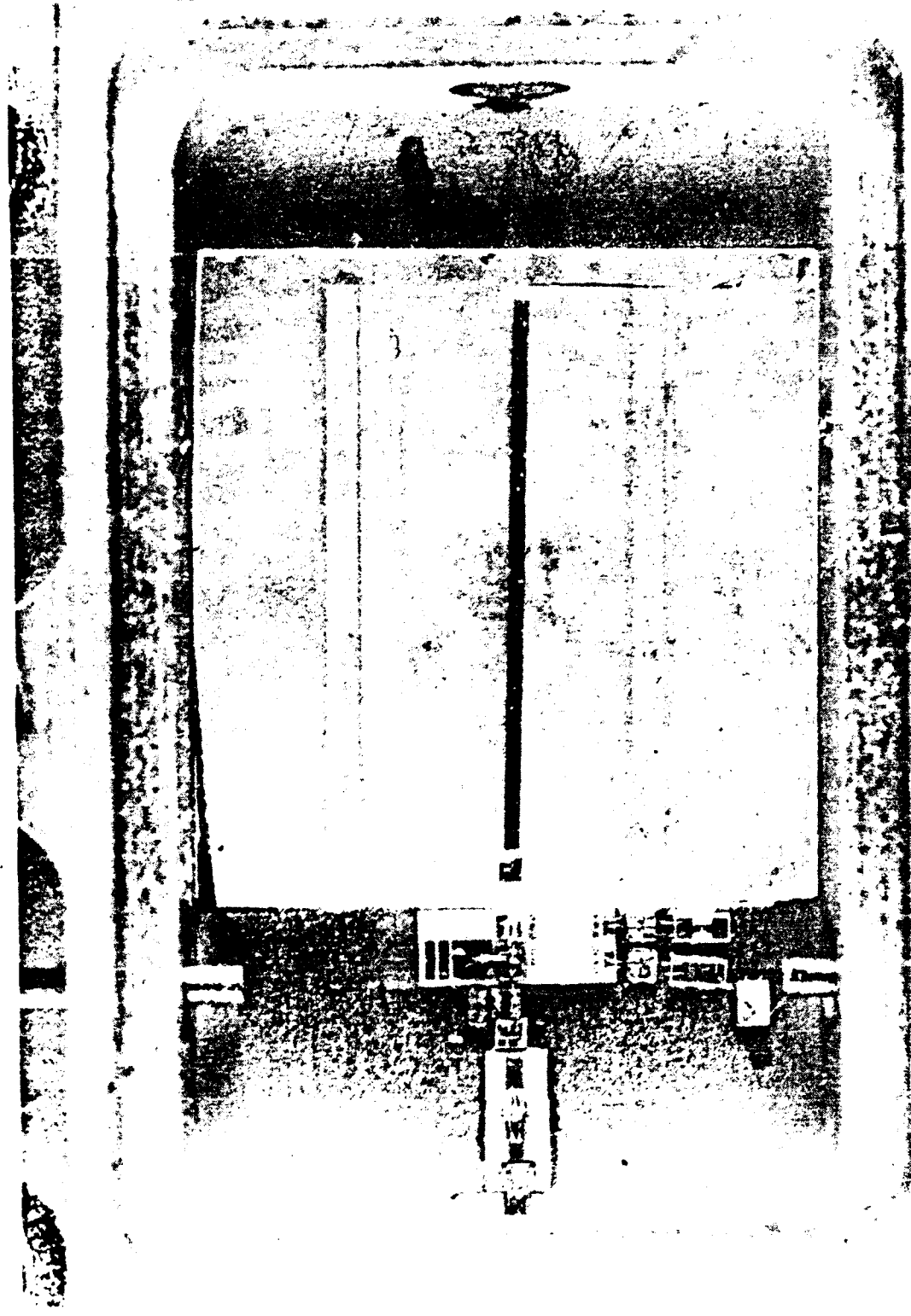


Figure 2. 10 GHz oscillator using half wavelength resonator.

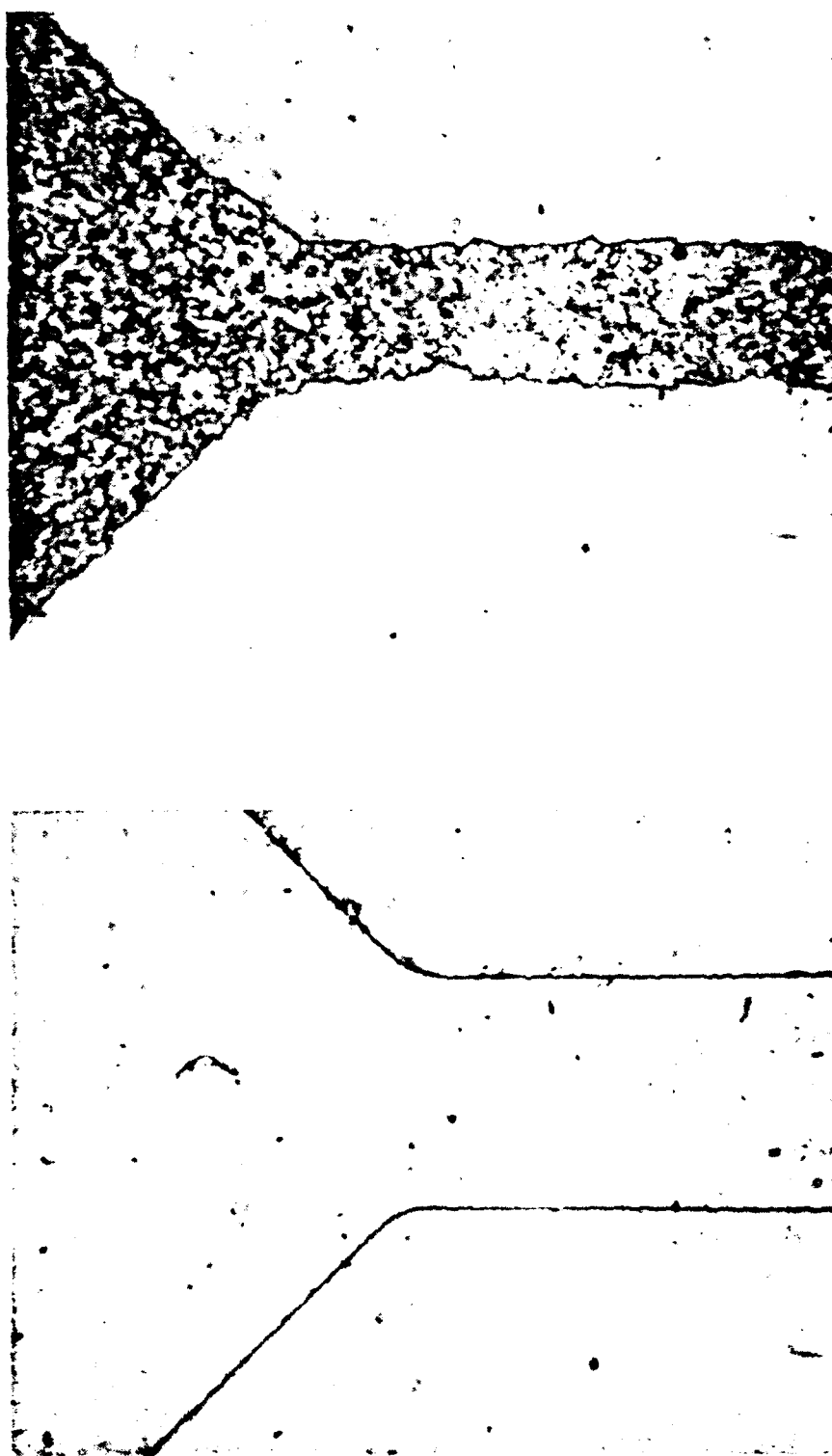


Figure 3. Wet etched thallium HTS (top), ion milled YBCO (bottom).

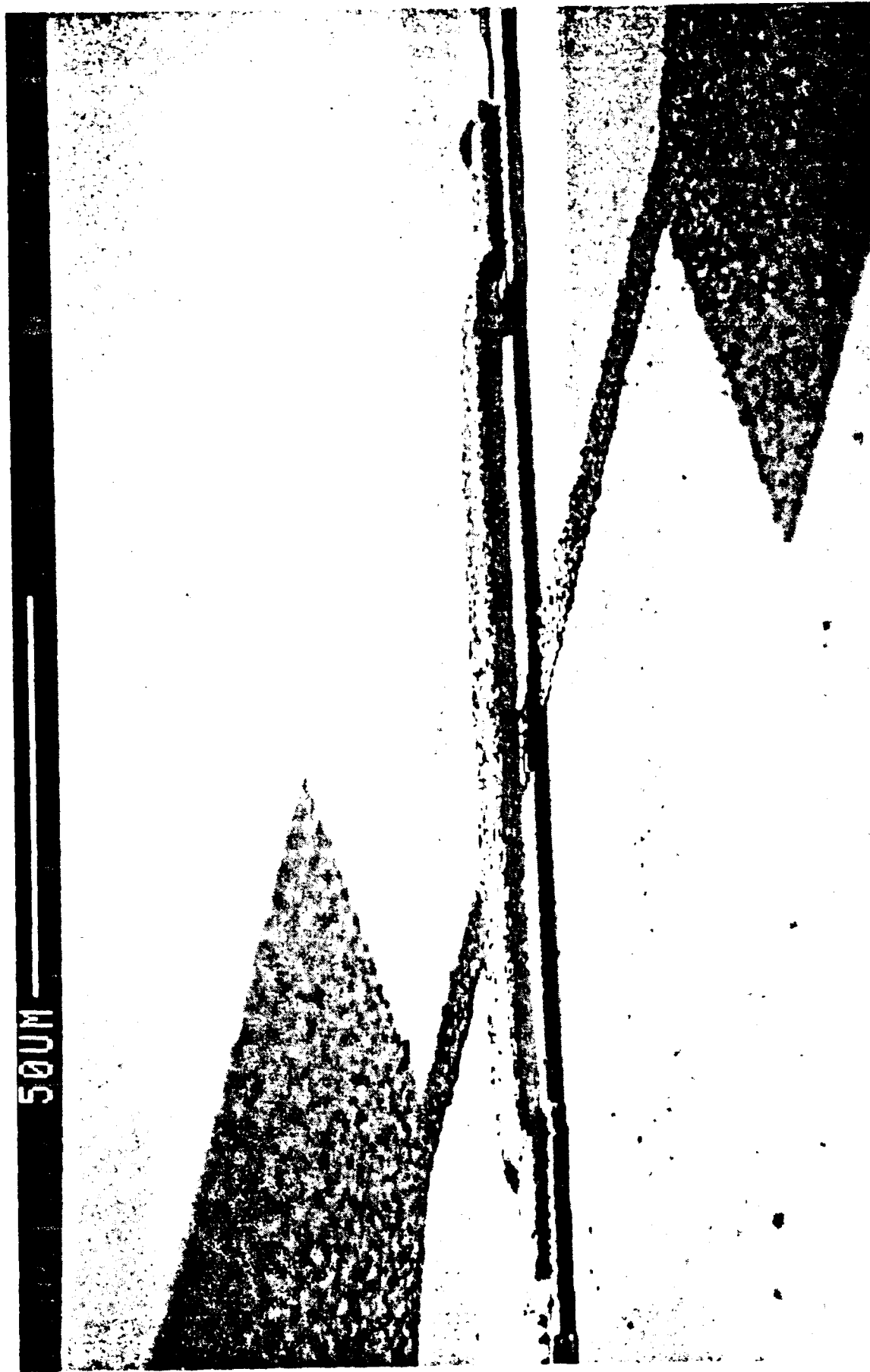


Figure 4. Gold air bridge over HTS material.

LMSC P008929

FINAL REPORT
SUPERCONDUCTOR APPLICATION RESEARCH

October 15, 1991

R. J. Adler and W. W. Anderson

Prepared for
SUPERCONDUCTOR TECHNOLOGIES, INC.
SANTA BARBARA, CA

Contract No. N00014-88-C-0713-S-LMSC-1

LOCKHEED RESEARCH & DEVELOPMENT DIVISION
LOCKHEED MISSILES & SPACE COMPANY, INC.
PALO ALTO, CALIFORNIA 94304

1. INTRODUCTION AND SUMMARY (PART I)

Heat leaking along the wiring into a low temperature satellite system, e.g. an infrared sensor at 10 K, can cause rapid loss of coolant or high refrigerator power consumption. This can shorten orbital lifetime and complicate the payload. If a set of high temperature superconductor (HTSC) leads is inserted between the cold system and the rest of the satellite, the heat leakage can be greatly reduced, while no extra electrical resistance is added. A superconducting thermal isolator device (STID) consists of a substrate of low thermal conductivity on which HTSC traces are deposited. A low thermal conductivity housing holds the assembly and provides electrical connections.

Five STID prototypes have been built and tested at LMSC using substrates and traces from STI. They use TlBaCaCuO traces on a polycrystalline zirconia substrate. Their thermal isolating performance is excellent, but their current carrying capacity is somewhat too small for practical applications: the traces carry a few hundreds of amps per cm^2 .

Five Mark I electrical test devices have also been built and tested. These use TlBaCaCuO traces on a LaAlO_3 substrate, which is not a good thermal insulating material; they are intended only for electrical testing. They have excellent electrical properties, with traces carrying hundreds of thousands of amps per cm^2 .

Finally two Mark II electrical test devices have been built and tested. These use TlBaCaCuO traces on substrates of single crystal ZrO_2 and polycrystalline ZrO_2 . The single crystal Mark II device is quite superior to the polycrystalline device, and has adequate electrical properties, with traces carrying about 5,000 amps per cm^2 . The single crystal Mark II test device was monitored over a period of about 5 weeks, and the trace quality deteriorated significantly over this time. This indicates that a passivation coating is probably necessary.

2. REQUIREMENTS BACKGROUND

2.1 The Problem

Figure 1 shows a schematic of a typical satellite low temperature system.

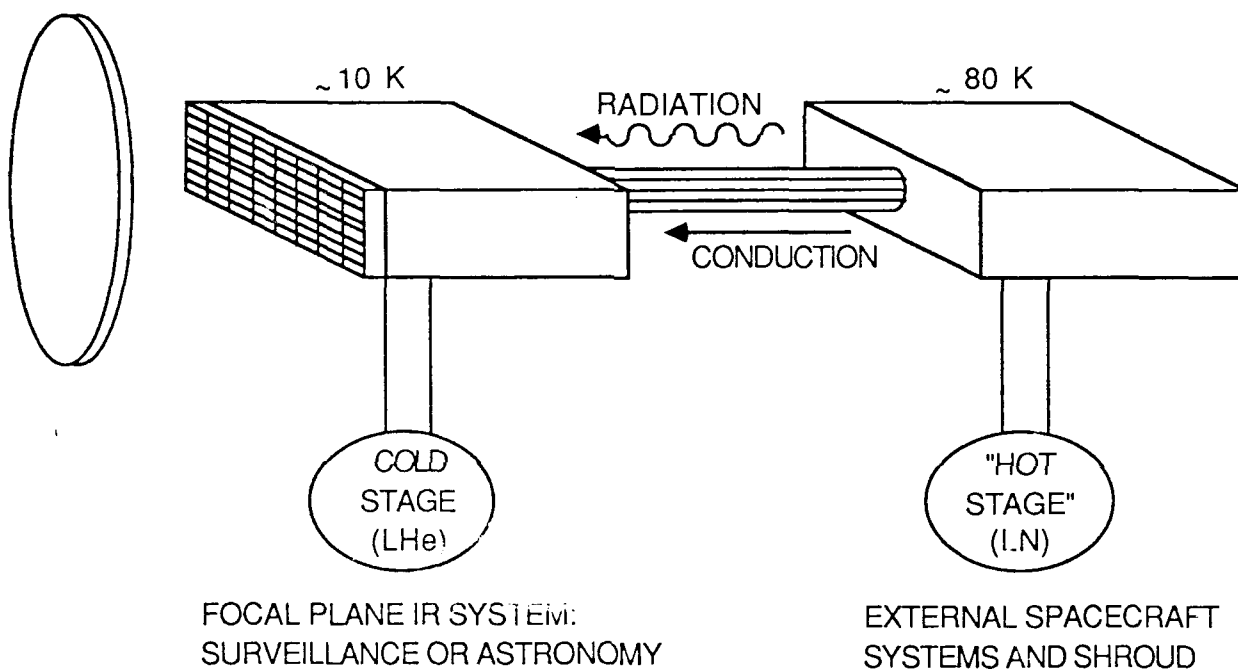


Figure 1. Schematic sketch of typical satellite low temperature system.

Examples might be an infrared surveillance sensor system, an infrared astronomical telescope, or a research spectrometer. The cold parts of such systems typically operate at under 10 K. They must communicate with the rest of the spacecraft, typically at about 77 K, through leads which pass power, command signals, and output signals. The leads inevitably leak some heat by conduction, and also generate some heat themselves due to their internal resistance, referred to as Joule heating. As a result there can be a serious loss of coolant in a stored cryogen system or power consumption in a mechanical cooler. This generally

translates into shortened orbital lifetime for a given weight in orbit, and a larger and a more complex payload. In turn this implies that megadollars may be wasted in space.

We might think to solve the problem by making a clever choice of metal for the wire leads, to pass electrical current but block heat flow. This cannot be done however, since normal metals which are good electrical conductors are also good heat conductors. This fact is embodied in the Weidemann-Franz relation, equation [1], which gives the ratio of thermal to electrical conductivity as a function of only the temperature T and two universal constants, the electron charge e , and Boltzmann's constant k .

$$\kappa_{th} / \kappa_{el} = (\pi k / e)^2 T / 3 \quad (\text{Weidemann-Franz relation}) \quad [1]$$

The Weidemann-Franz relation should hold reasonably well for any material in which electrical current and thermal energy are transported by *normal* electrons. It is reasonably accurate for most metals; for example around 0°C it holds to about 25%. (ref. 1)

2.2 The Conceptual Solution

Superconductors are not normal conductors and do not obey the Weidemann-Franz relation; electrical conduction is by condensed Cooper pairs, which behave like a condensed gas of bosons and do not transport entropy or heat (ref.s 2, 3). It is particularly fortunate that high temperature superconductors (HTSCs) can operate at the upper end of the temperature region desired, about 77 K, the boiling point of liquid nitrogen. By inserting a HTSC between the hot and cold parts of the system the heat leakage problem can be ameliorated. Unfortunately HTSCs cannot yet be made into usable flexible wires, so we need a device such as shown in Figure 2; this has HTSC traces on a dielectric substrate, which must be chosen to be a good match for the HTSC crystal structure, and also a good thermal insulating material. In addition the substrate and traces must be mounted in a low thermal conductivity housing.

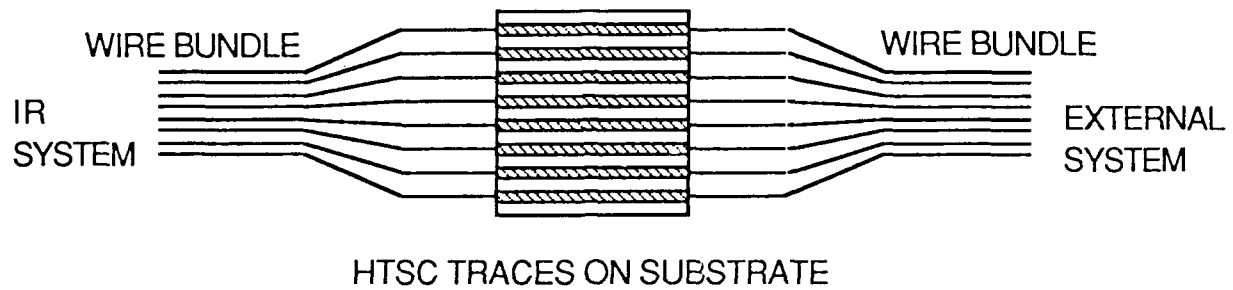


Figure 2. STID concept.

The detailed design for a STID will be discussed in section 6.

3. THERMAL CONDUCTIVITY OF SOME MATERIALS

The substrate material should be strong and have low thermal conductivity. Figure 3 compares the thermal conductivity of copper, ZrO_2 (zirconia), and the popular substrate material LaAlO_3 . At liquid nitrogen temperature, 77 K, the conductivity of ZrO_2 is 20 times less than that of LaAlO_3 and 300 times less than that of copper. At the low temperature of 10 K it is respectively 100 times and 30,000 times less.

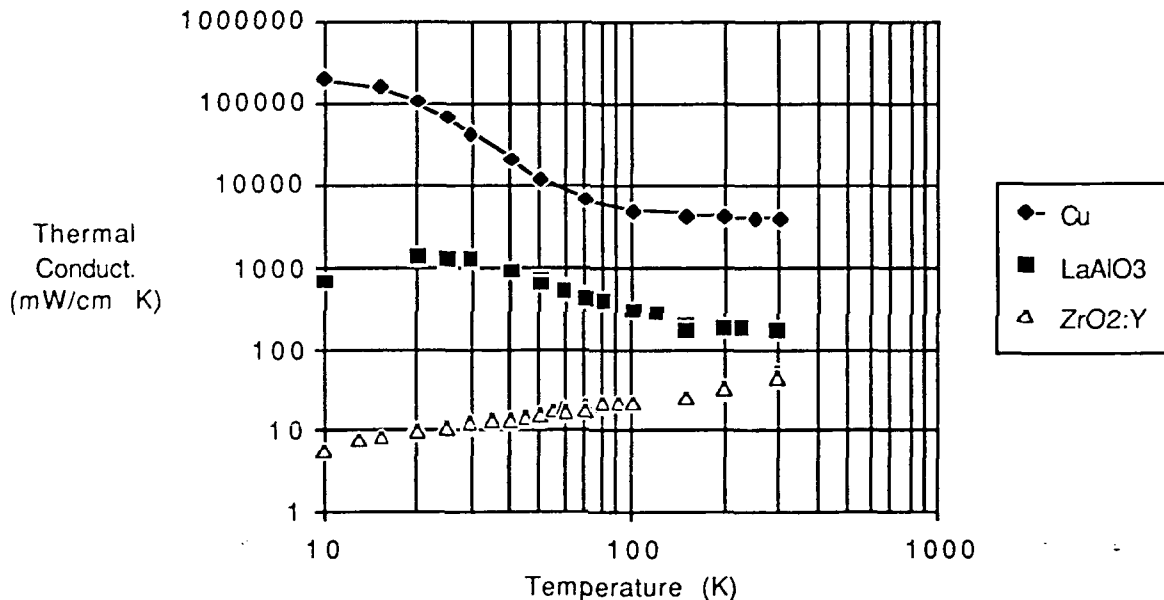


Figure 3. Thermal conductivity of copper, LaAlO_3 , and ceramic ZrO_2 .

We may conclude that ZrO_2 offers very low thermal conductivity. It is also a particularly hard and strong material and therefore offers an attractive substrate choice.

The data in Figure 3 are for polycrystalline or ceramic ZrO_2 , which was used in our prototype devices. We expect the thermal conductivity of single crystal ZrO_2 to be comparable to the polycrystalline material. This

should be true in particular at low temperatures where long wavelength phonons are most important, and grain boundaries offer less thermal impedance.

The conductivities of various HTSCs have been measured to be in the range 10 - 100 mW/cm K, comparable to ZrO_2 . The traces in a STID have a very small cross sectional area compared to the substrate since they are only about 1 μm thick. We may conclude that the heat leakage through the superconducting traces should be negligible.

4. HEAT LEAKAGE EXAMPLES

4.1 General

Each cryogenic space system has its own individual properties, so it is not reasonable to attempt a general analysis of heat leakage. We will instead consider some illustrative examples of the leakage of heat into a cold system via metallic wires compared to a STID structure. As noted above the HTSC leads should have negligible leakage compared to the substrate; we will assume that the housing for the STID can also be made with leakage that is negligible compared to the substrate

There are three sources of heat leakage into a cold system: (1) conduction from the hot exterior world which we take to be at about 77 K, (2) Joule heating due to current flowing in the metallic wires, and (3) radiation directly from the exterior world. Radiation will in general be rather small for a hot exterior at only 77 K, which is hot only by comparison with the cold system at about 10 K; the reason for this is that the radiation rate is proportional to T^4 (ref. 4). In any case the radiation leakage is common to the use of wires or a STID. We will thus consider only conduction and Joule heating in the following discussion.

The largest leads into a cold system generally provide power, and typically may carry about 500 mA. Other leads carry command and sensor signals into and out of the cold system, both at generally small currents, say of order 20 mA. For this reason the power leads are the most important source of Joule heating. A portion of the power carried by the leads will also be dissipated in the cold system itself, and the use of a STID clearly cannot prevent this.

The size of the signal leads is often not determined by the current they must carry but by mechanical strength considerations; that is they are the so-called minimum gauge, which is usually of order of 0.003 cm diameter.

Finally it is important to realize that all of the leads may have a short

duty cycle; that is they may carry current for only a small fraction of the time, but the leads must remain connected at all times. For these reasons the main source of heat leakage is generally conduction, and this is what we will illustrate below.

A further word about Joule heating is in order. A very thick wire will leak much heat by conduction, but will not produce much Joule heating because of its low resistance. A very thin wire will not leak much heat but will produce much Joule heating because of its high resistance. At some intermediate wire size the heat leakage should be a minimum, with not too much heating by either conduction or Joule heating. The determination of the optimum wire size is a straight-forward problem but depends on the temperature range and the wire materials, and usually must be done numerically.

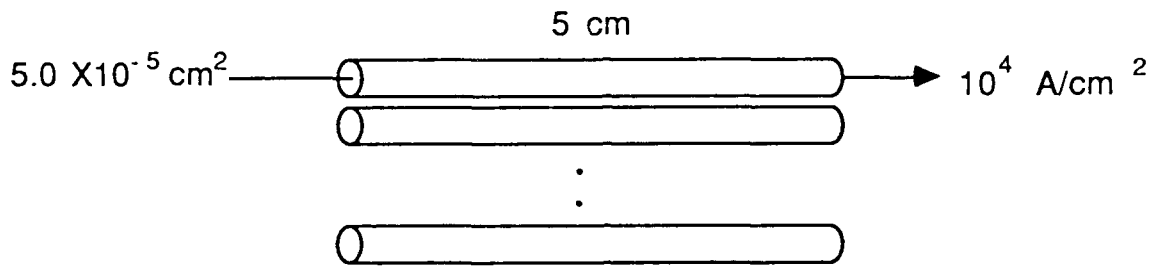
4.2 High Current Leads

Let us now consider some examples of how one estimates heat leakage by conduction and see why a STID should be expected to reduce it. First we will consider an example of high current carrying leads, a bundle of 10 copper wires able to carry 500 mA each, and about 5 cm long. We assume the cold system is at 6 K and the hot environment is at 77.5 K, which correspond to a laboratory test setup that we have used. Figure 4 shows a schematic of the wire bundle and the relevant numbers.

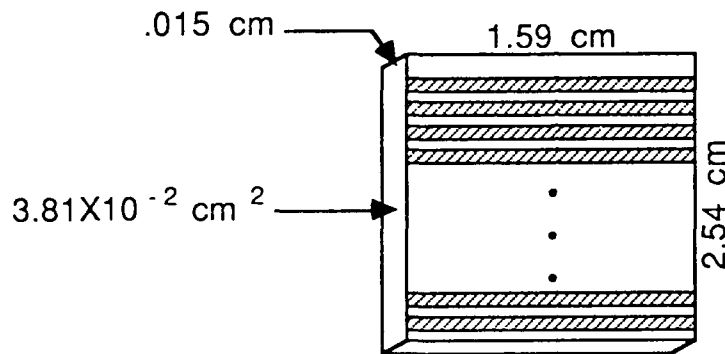
The only physics equation that we need is that giving heat flow in units of power as a function of the temperature difference (ref. 5).

$$P = \kappa_{th} (A/L) \Delta T \quad [2]$$

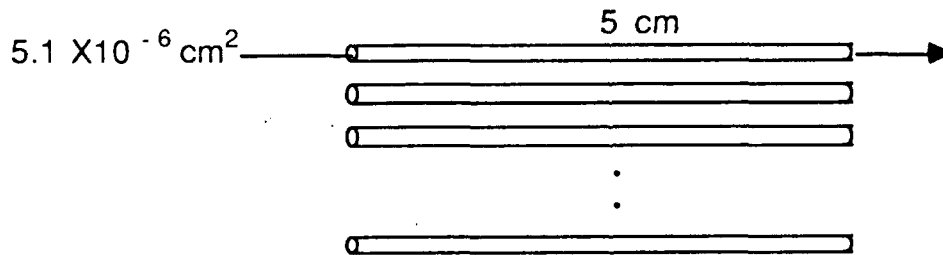
Here the power P has units of watts, A is the cross section of the wire, L is the length of the wire, ΔT is the temperature difference, and κ_{th} is the thermal conductivity. If the conductivity varies with temperature, as it usually does, the appropriate value to use is the average over the temperature range. (This is shown in Appendix A.)



(a) 10 Copper Wires @ 500 mA each



(b) STID Substrate and Traces



(c) 20 Copper Wires, 1 mil diameter

Figure 4. Schematic for heat leakage comparisons.

To determine the area of the wire needed for this example we use a fairly realistic rule-of-thumb, that the the current density in the wire should

not exceed about 5,000 to 10,000 A/cm². (We cannot apply a wire size optimization procedure since the duty cycle is not given.) By this current density criterion the area of each of the wires must be 5×10^{-5} cm². The average thermal conductivity of copper can be estimated from the curve in Figure 3 to be about 47×10^3 mW/cm K.

The heat leakage through 1 wire and the bundle of 10 are:

$$P(1) = 33.6 \text{ mW} \quad \text{and} \quad P(10) = 336 \text{ mW} \quad [3]$$

This rate of heat leakage implies that for each day in orbit about 29×10^3 J or 6.9×10^3 cal leak into the cold system, which is a sizeable amount.

4.3 STID

A STID could be constructed and inserted into the system of leads as indicated in Figure 4. The dimensions of the substrate shown in Figure 4 are those of our prototype design: 1.59 cm long by 2.54 cm wide by .015 cm thick. The average thermal conductivity of ZrO₂ is about 15 mW/cm K, as can be read from the graph in Figure 3. Ignoring the very small leakage through the traces themselves we obtain from equation [2].

$$P(S) = 25.7 \text{ mW} \quad [4]$$

The reduction from the 336 mW for the copper wire bundle is over an order of magnitude

4.4 Low Current Leads

Next we will consider an example with low current leads, a bundle of 20 copper wires to carry 20 mA input or output signals, about 5 cm in length. The size of such wires is not usually determined by considerations of current density but by mechanical strength. We will assume that 1 mil

copper wires are used, with a radius of 1.27×10^{-3} cm and an area of 5.1×10^{-6} cm². Again using equation [2] we obtain leakages through 1 wire and the bundle of 20.

$$P(1) = 3.4 \text{ mW} \text{ and } P(20) = 68 \text{ mW} \quad [5]$$

If a STID were inserted into the wire bundle the leakage would be the same as previously obtained in equation [4], or about 25.7 mW. Thus there is a reduction of leakage to be gained, but it is much less significant than for the heavier current leads first considered.

Table 1 gives a summary of the results of this section.

Table 1: Summary of Heat Leakage Examples

Specific Case	Thermal Conductivity (mW/cm K)	Area (cm ²)	Length (cm)	Power Leakage (mW)
High Current 10 Cu wires	47×10^3	5.0×10^{-4}	5.0	336
Low Current 20 Cu wires	47×10^3	5.1×10^{-6}	5.0	68
STID	15	3.81×10^{-2}	1.59	26

5. PAYOFFS

5.1 Orbital Lifetime Increase

To estimate heat leakages in real satellite systems one makes calculations like those illustrated above, but including Joule heating, variation of thermal conductivity with temperature, and a consideration of wire size optimization. Together with researchers in cryogenic spacecraft systems at LMSC under the leadership of T. Nast we have made estimates of heat leakage for 3 cryogenic spacecraft, and have thereby estimated the benefits in terms of orbital lifetime increase. We discuss these in the following paragraphs and summarize the results in table 2.

The spacecraft and systems studied were:

- (1) Cryogenic Limb Array Etalon Spectrometer
- (2) Advanced X-Ray Astronomical Facility Spectrometer
- (3) Spirit II cooler

We will discuss each in turn.

(1) Cryogenic Limb Array Spectrometer (CLAES):

CLAES is a satellite-borne instrument designed to study the atmosphere of the earth by detecting and measuring its gas composition. It is being flown on the Upper Atmosphere Research Satellite (UARS), launched in fall 1991. The CLAES device, including instrument and cryogenics, is about 2 m high by 1 m wide. The mass of the instrument is about 300 kg, and the mass of the cryogenic cooling system is about 900 kg. Note that the mass of the cooling system greatly exceeds the mass of the instrument, which is typical of cryogenic satellites. An array of semiconductor chips is used as a sensor, and is maintained at 15 K. Sensor cooling is by solid Ne at 13 K, while solid CO₂ at 125 K cools the optics and some peripheral equipment. Temperature of the instrument shell is about 200 K, and spacecraft temperature is about 300 K, which is typical for most

satellites. The present system has a heat load of 783 mW into the sensor package, and an expected useful lifetime in orbit of 1.8 years.

If CLAES were fitted with a STID we estimate that the heat load would be reduced to 614 mW and the useful lifetime in orbit would increase to 2.3 years. The benefit is thus about .5 year or 28% extended lifetime. (See Benefits Table.)

(2) Advanced X-Ray Astronomical Facility (AXAF) X-Ray Spectrometer:

The AXAF is designed to do basic X-Ray astronomy from orbit. It is in the preliminary proposal and contracting stage, and should fly in about 5 to 7 years. The X-ray spectrometer is the primary instrument on the satellite. With cryogenic system included the size of the instrument package is about 2 m by 1.7 m, and the mass is about 350 kg; the mass of the actual instrument is negligible compared to the cooling system.

Detectors are Si chips at .1 K. These are cooled with superfluid He to 1.5 K, then to .1 K by adiabatic demagnetization. A mechanical refrigerator cools the outer shell. The heat load of the spectrometer is about 6.2 mW, and the lifetime is about 6.1 years.

If the spectrometer were fitted with a STID we estimate that the heat load would decrease to 5.7 mW and the lifetime would increase to 6.6 years. The benefit is thus about .5 year, or 8%. (See Benefits Table.)

(3) Spirit III:

Spirit III involves an infrared telescope and a large cryogenic cooling system. The satellite will do a combination of surveillance and science missions. It is in the fabrication and assembly stage, and launch should be in about 1993. The detector is a semiconductor focal plane array maintained at 10 K. It is cooled by a 1000 liter tank of solid H₂ at about 20 K. The instrument and cooling system shell are maintained at about 200 K. Size and mass of the system are similar to the CLAES system discussed

above. Heat load of the instrument is about 694 mW, and lifetime is about 1.8 years.

If Spirit III were fitted with a STID we estimate that the heat load would decrease to 612 mW and the lifetime would increase to about 2.0 years. The benefit is thus about .2 years or 11%. (See Benefits Table.)

Table 2: Benefits Table

Program Name	Present Design		With STID		Benefit
	Heat Load	Life	Heat Load	Life	
Cryogenic Limb Array Etalon Spectrometer	783 mW	1.8 yr	614 mW	2.3 yr	.5 yr (28%)
AXAF X Ray Spectrometer	6.2 mW	6.1 yr	5.7 mW	6.6 yr	.5 yr (8%)
Spirit III	694 mW	1.8 yr	612 mW	2.0 yr	.2 yr (11%)

5.2 Benefits Table

The table summarizes the benefits of eliminating the heat load due to the presence of electrical lead wires for three projects that are being studied or developed at LMSC. The heat loads and lifetime numbers are based on detailed system analysis and include the benefits of thermal grounding and vapor cooling effects; that is full benefit has been taken of vapor cooling leads. Joule heating in the leads, thermal conduction through the leads, and the interaction of these effects has been included in the calculations.

5.3 Qualitative Design improvement

Some satellite systems would benefit from the use of a STID by having a qualitatively improved design, completely unlike present concepts. The astromag is such a system.

The astromag project involves a pair of low temperature superconducting toroidal magnets. These are to be used on the space station as part of the high energy physics instrumentation used in cosmic ray spectrometry. The current in the superconducting magnets is about 800 A. They are cooled by 4,000 liters of superfluid He at 1.5 K. A major problem involves disconnecting the high current Cu leads to the magnet after the persistent current has been started; the possibility of quenching of the supercurrent is a major reliability issue.

If the leads to the low temperature magnet contained a high current STID it should be possible to leave them connected during operation, so that quenching and explosive energy release would be much less likely. Such a system could be tested in the laboratory in the near future.

5.4 Simplicity and Convenience

Finally, the STID is a simple device. In present approaches to thermal isolation careful design is required. Thin delicate wires are often used, and these may even be tapered. This can lead to difficult installation and a mechanically weak system of kludges. By contrast a STID would be almost an off-the-shelf item, would be nearly as simple to install as a set of resistors, could be easily retrofitted, is mechanically robust, and should be very dependable.

6. STID DESIGN AND PROTOTYPE PROPERTIES

6.1 Design and Fabrication

The conceptual design of a STID is shown in figure 2. Realization of such a device requires a substrate with superconducting traces and a housing for the substrate. The housing must be mechanically strong, have high thermal impedance, and provide for electrical connections to the superconducting traces.

A preliminary housing design used a specially constructed fiberglass frame with low thermal conductivity connecting posts. A clamp arrangement secured the substrate to the housing and allowed small amounts of independent motion of the substrate within the housing for strain relief. Eight-pin connectors were provided at each end for attachment of thin connecting wires from the traces. The preliminary housing was rather bulky, about 5 cm by 5 cm by 1 cm, and the connecting wires were about 2 cm long.

While the preliminary housing served its purpose, it was difficult and expensive to construct and the long thin connecting wires were subject to damage. An improved version was therefore designed, based on experience with the preliminary housing. The improved version, the prototype design, was constructed from commercially available integrated circuit holders called flatpacks, was simple and cheap to construct, was only about 3 cm by 3 cm by .5 cm, and the thin wire interconnects were only about 2 cm long. Details and a photo of the prototype design are given below. The preliminary housing was only used for preliminary proof-of-concept measurements of thermal conductivity, while the prototype design was used for the definitive thermal and electrical testing as discussed below.

Figure 5 shows the prototype STID design. Ten of these were actually built and screened by electrical testing. Only the five best were tested in detail, and are discussed below. The other five were stored. The heart of the STID is the substrate holding the superconducting traces of TiBaCaCuO

(TBCCO). The innermost 22 traces, alternating wide and narrow, are the ones actually used. These are nominally $0.8\text{ }\mu\text{m}$ thick and $500\text{ }\mu\text{m}$ or $200\text{ }\mu\text{m}$ wide. Gold pads, about $0.5\text{ }\mu\text{m}$ thick, are deposited on the ends of the traces, to which 0.025 mm gold wires are attached by ultrasonic bonding. The other ends of the gold wires are ultrasonically bonded to the pads of the housing.

The superconducting traces of TBCCO are intended to carry at least $5,000\text{ A/cm}^2$. Thus the $200\text{ }\mu\text{m}$ traces should carry about 8 mA and the $500\text{ }\mu\text{m}$ traces should carry about 20 mA .

The substrate is polycrystalline ZrO_2 , 2.54 cm square by 0.15 mm thick. This material was chosen to provide a good surface for deposition of the traces, for low thermal conductance, and for strength. (As we will discuss below it does not appear to actually provide a good surface for deposition.) Note that the length of the substrate between the housing ends is somewhat reduced from 2.54 cm and is only 1.59 cm .

The housing is constructed by sawing the ends from a conventional flatpack designed for 1 inch square IC chips, then reconnecting them with 2 slabs of G10 fiberglass, about $.5\text{ cm}$ by $.1\text{ mm}$ thick. The thermal conductance of the fiberglass is quite low. The housing has a total of 22 leads on each side, as evident in the figure. The substrate with traces is attached to the housing at each end with epoxy. The substrate epoxy joint was tested by dipping the assembly from room temperature into liquid nitrogen at 77 K .

The device could be wrapped with aluminized mylar for thermal radiation shielding if desired. The overall dimensions, excluding the leads, are about 3.2 cm square by $.5\text{ cm}$ thick.

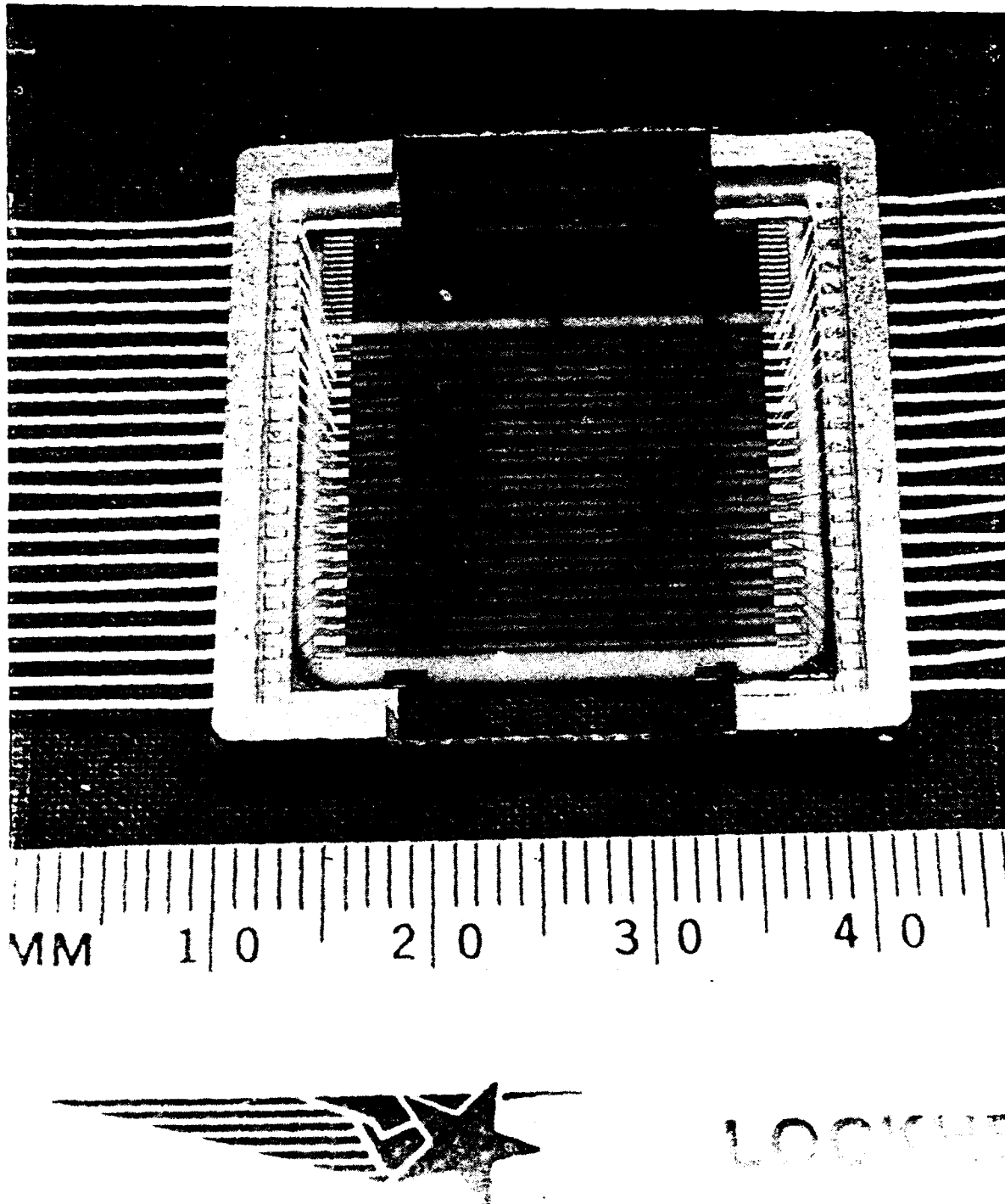


Figure 5. The LMSC STID prototype.

6.2 STID Thermal Properties

Thermal testing has been performed on the preliminary housing and one prototype STID mockup, and electrical testing on all of the 5 prototype STIDs

The thermal conductance of a STID can be estimated theoretically from the dimensions and the measured thermal conductivity of its materials. The main thermal leakage path is through the ZrO_2 substrate, which has an average thermal conductivity of about 15 mW/cm K in the range 10 to 100 K. The effective size of the substrate is 2.54 cm by 1.59 cm by 0.015 cm thick; in the test apparatus it sits between temperatures of 77.5 K and 6 K. From these numbers and equation [2] the heat leakage can be estimated to be

$$P(Z) = 25.7 \text{ mW} \quad (\text{leakage through zirconia substrate}) \quad [6]$$

The G10 fiberglass slabs leak very little heat since their thermal conductivity is only about 1.8 mW/cm K. For the 2 slabs of G10 which are 1.59 cm X .5 cm X .02 cm the heat leakage can be estimated as:

$$P(F) = 1.6 \text{ mW} \quad (\text{leakage through fiberglass slabs}) \quad [7]$$

Thus the estimated total heat leakage is:

$$P(T) = 27.3 \text{ mW} \quad (\text{total leakage by conduction}) \quad [8]$$

This should be considered as a rough upper limit since we have not included effects such as the thermal resistance of the epoxy joint between the substrate and the housing and the 2 dimensional nonuniformity of heat flow in the substrate.

The heat leakage of the device was measured as follows: one side was maintained at 6 K, and the other side was connected to a resistance

heater. The power to the heater was then adjusted to produce a temperature of 77.5 K at the hot side, and the power level measured. The measured heat flow, after correction for radiation, was found to be:

$$P(M) = 24.5 \pm 1 \text{ mW (measured leakage)} \quad [9]$$

This is in quite good agreement with the above theoretical estimate, so we may conclude that the thermal operation of the device is well understood. Table 3 summarizes the thermal conductivity results.

Table 3: STID Thermal Properties

Component	Area (cm ²)	Length (cm)	Conductivity (mW/cm K)	ΔT (K)	Power (mW)
Substrate	.038	1.59	15	71.5	25.7 (theory)
Fiberglass	.020	1.59	1.8	71.5	1.6 (theory)
Total Device	---	---	---	71.5	27 (theory)
Measured	---	---	---	71.5	24.5 \pm 1

6.3 STID Electrical Properties

The electrical properties of one of the STIDs (2L505.1) are shown in Figures 6 and 7. Figure 6 shows the measured resistance as a function of T for 6 of the traces. Note that the resistance of the gold connecting wires and other peripheral connections external to the traces is included, so the total resistance does not go to exactly zero. The resistance begins to rise at about 70 K, with the resistance of one of the traces remaining below 1 ohm up to about 78 K. The width of the transition is rather large, about 30 K. Figures 7a to 7f show the resistance as a function of current for all 22 of the connected traces at 40 K, 60 K and 80 K. In the 80 K curve the voltage begins to rise rapidly above about 1 ma (ref. 6). This corresponds to a current density of about 250 A/cm^2 , which is about an order of magnitude less than anticipated. In Appendix B similar curves for the other four devices are shown.

Note that there is a great deal of variation in the curves in both figures, with the resistance of the traces varying by about an order of magnitude. Since half of the traces are $500 \mu\text{m}$ and half are $200 \mu\text{m}$ some variation is to be expected. Variation between devices is even larger. Some display useful operating temperatures as low as 60 K, while the graphs for 2L505.1 show about 78 K. The variation of critical current (at which the voltage rises abruptly) is also very large.

6.4 STID Properties: Conclusions

The heat leakage allowed by the STIDs is quite low and in good agreement with theoretical estimates.

The current carrying ability however is over an order of magnitude lower than expected: whereas we expected at least $5,000 \text{ A/cm}^2$ when designing the device we found about 250 A/cm^2 when they were measured. In addition the expected T_c was about 100 K, whereas the measured values

THIS
PAGE
IS
MISSING
IN
ORIGINAL
DOCUMENT

2L505.1

(T=40K)

ODD # - 500um traces

EVEN # - 200um traces

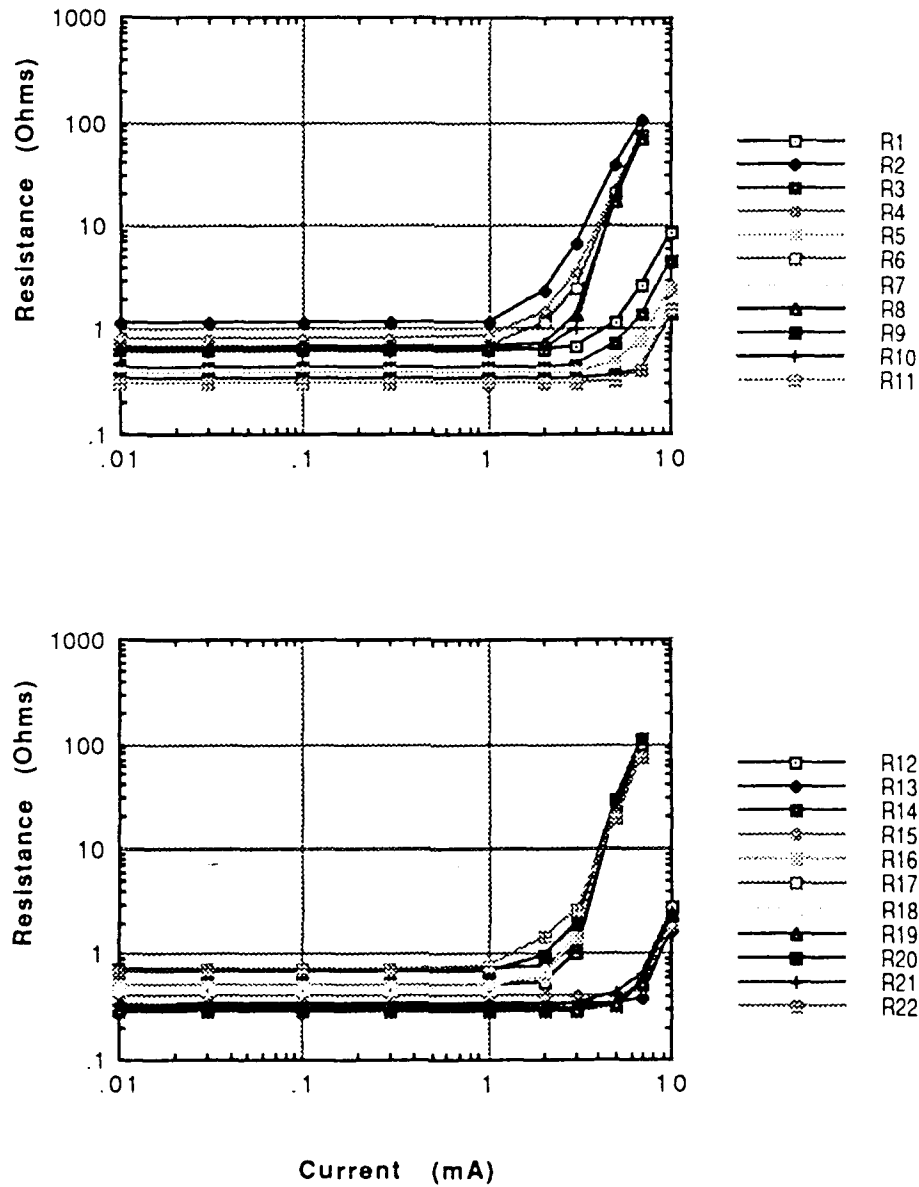


Figure 7a,b. Resistance of STID as function of current at 40 K.

2L505.1

(T=60K)

ODD # - 500um traces
EVEN # - 200um traces

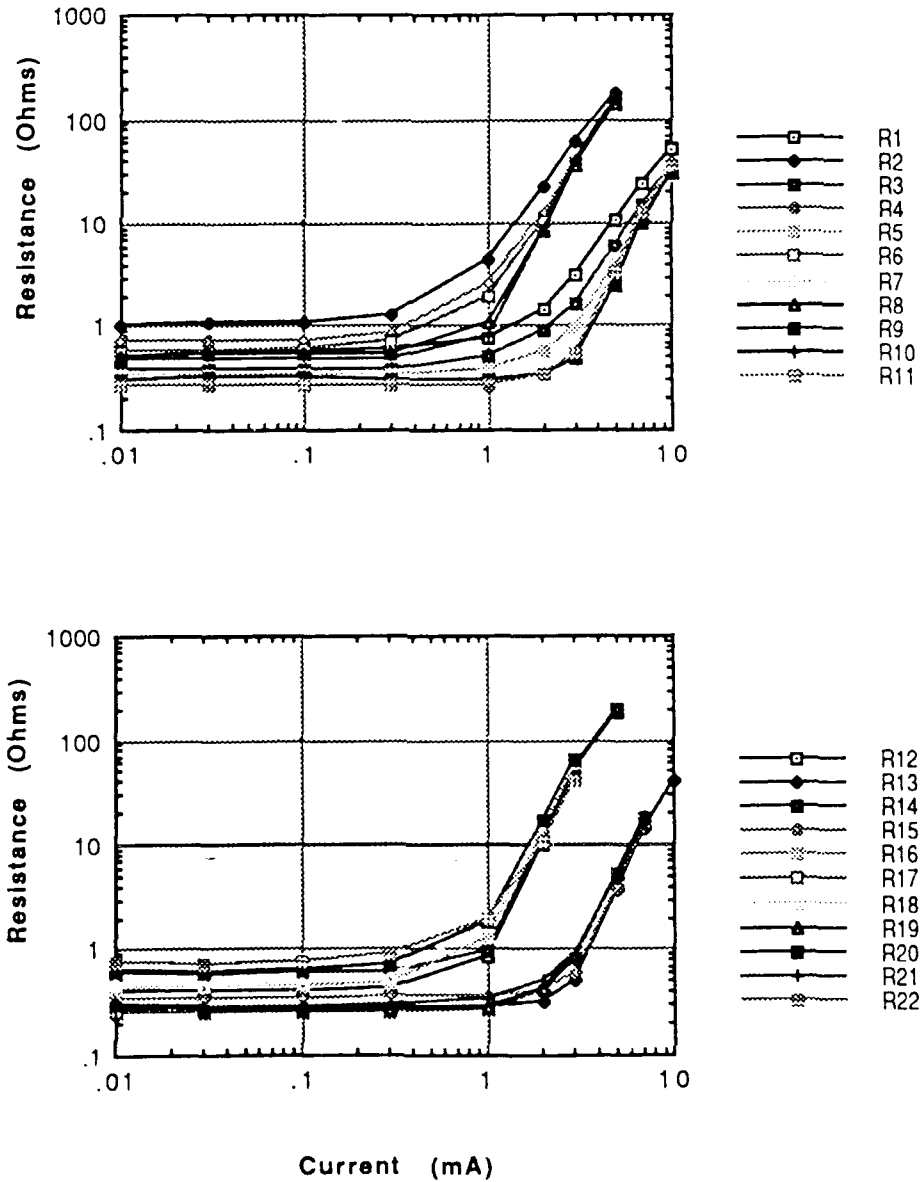


Figure 7c,d. Resistance of STID as function of current at 60 K.

2L505.1

(T=80K)

ODD # - 500um traces

EVEN # - 200um traces

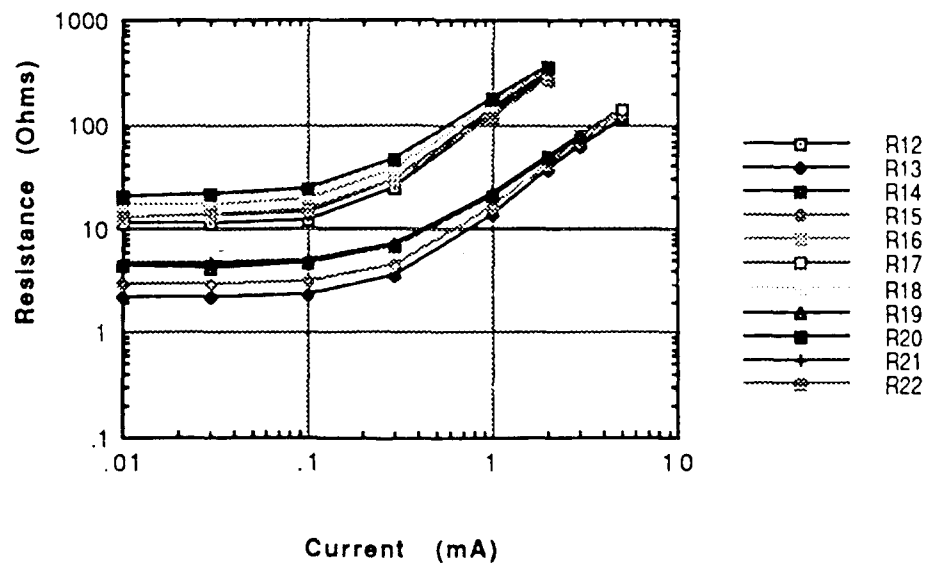
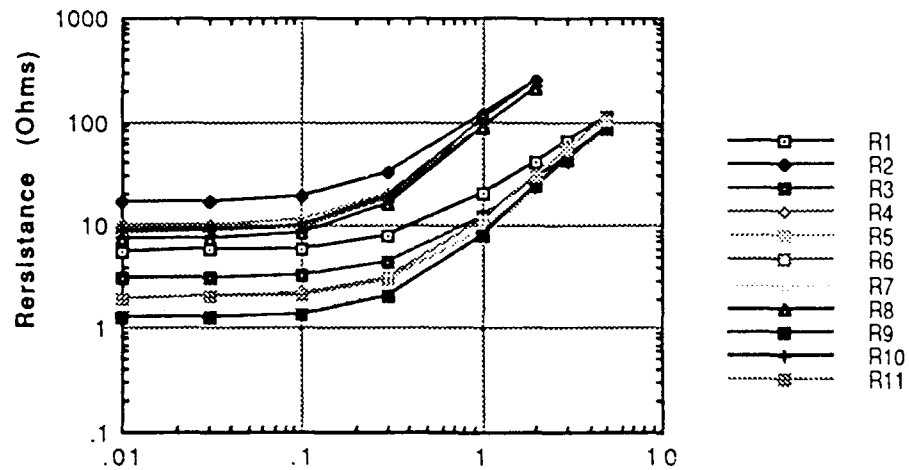


Figure 7e,f. Resistance of STID as function of current at 80 K.

varied between about 60 K and 80 K.

Thus the prototype STIDs function qualitatively as desired and are useful for testing. But they are not practical devices due to the low current capacity, and to a lesser extent due to the low transition temperature. The reasons for this will be discussed further in the next sections.

7. PROTOTYPE PROBLEMS AND SOLUTIONS

7.1 Design and Fabrication

Many minor problems were encountered in the design and fabrication of the STIDs, but all were eventually solved. Table 4 gives a summary of some of them.

Table 4: Design and Fabrication Problems and Solutions

Problem	Solution
Select thermally insulating substrate material	Zirconia (ZrO_2) strong and low conductivity
Obtain thin substrate	Zirconia ground down to .15 mm (6 mil) by STI
Deposit long TBCCO traces	1 inch traces produced by STI
Design simple strong thermal insulating housing (see Figure 6)	Cut ends from flatpack Fiberglass side strips Epoxy adhesive
Bond connecting wires (see Figure 7)	Pairs of 1 mil gold wire Ultrasonic wedge bonder Careful adjustment Expert operator

The wire bonding problem was the most chronic and difficult. Thermal compression bonding was tried, but the heat often destroyed the superconductor. Ultrasonic bonding often failed and sometimes lifted the gold layer. The problem was solved by testing different wire materials and sizes and bonding techniques. We finally settled on thin (1 mil) soft

gold wire in a carefully adjusted ultrasonic wedge bonder operated by an experienced expert operator. Figure 8 shows a typical wire bond made after the problem was solved.

7.2 Basic Physics

Two basic physics problems were encountered with the superconducting traces, as noted in section 6.4. The lesser problem was that the transition temperature was about 78 K or lower instead of the 100 K expected. One obvious solution is to select the STIDs with the best electrical properties out of those available. Appendix B shows the large variation in the electrical properties of the STIDs.

The major problem arose as noted in section 6.4, that the current capacity of the traces was over an order of magnitude less than expected. This prevents the STIDs from being practical, although they function qualitatively correctly and can be used for testing. This problem is certainly due to the poor morphology of the TBCCO traces on polycrystalline ZrO_2 , and is contrary to our expectation that polycrystalline ZrO_2 should be a good substrate. Figure 9 shows a SEM micrograph of the traces; the jumbled nature of the crystals shows that conduction must be via a torturous path of small cross sectional area through the logjam! Figure 10 shows TBCCO crystals on a substrate of LaAlO_3 , with greater smoothness and uniformity evident.

The trace quality problem appears to be due to a fundamental incompatibility of the ZrO_2 substrate with TBCCO. In the next sections we will discuss this further.

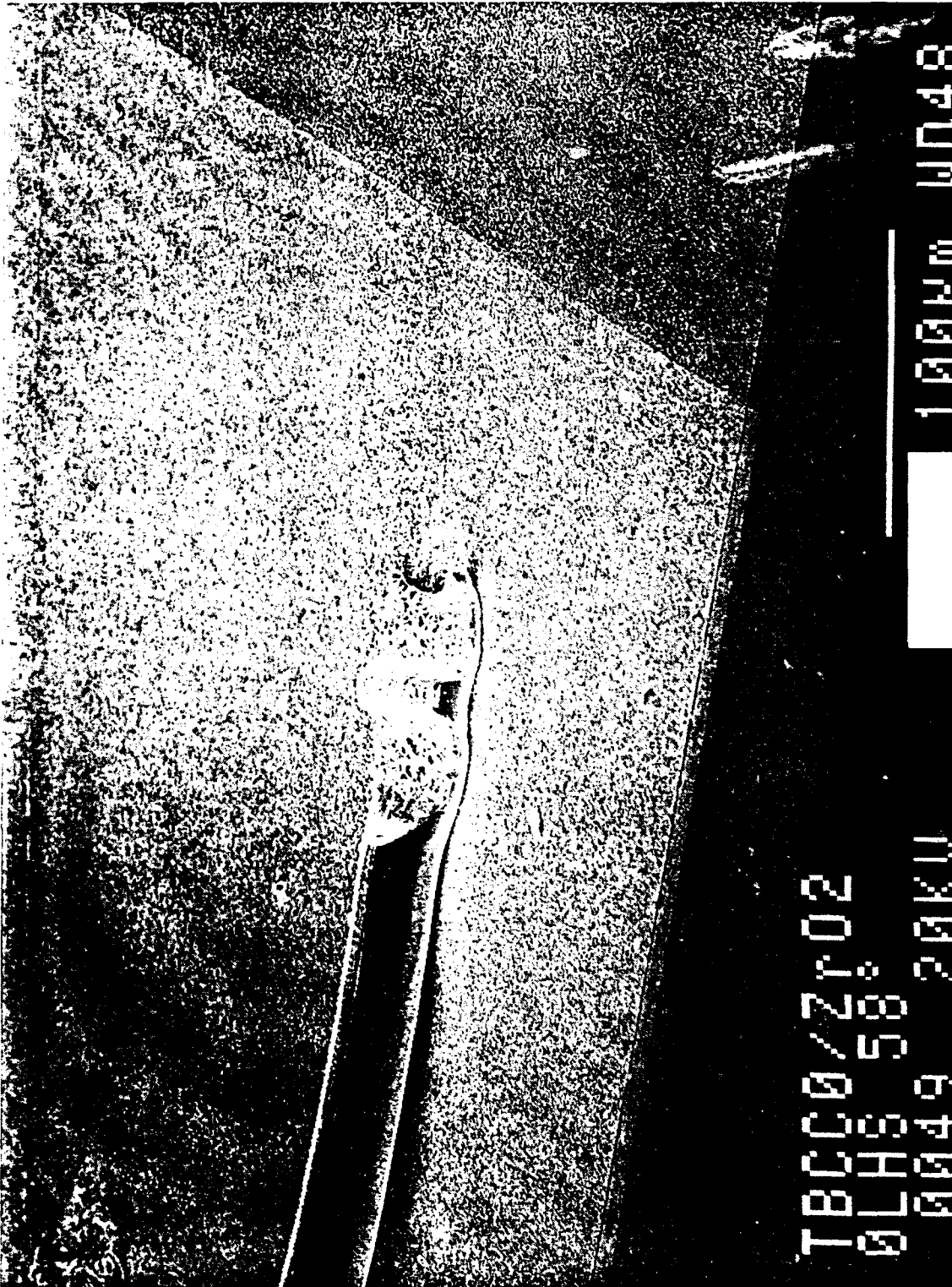


Figure 8. Gold wire ultrasonic bond to gold pad on superconductor



Figure 9. SEM photo of TBCCO traces on ZrO_2

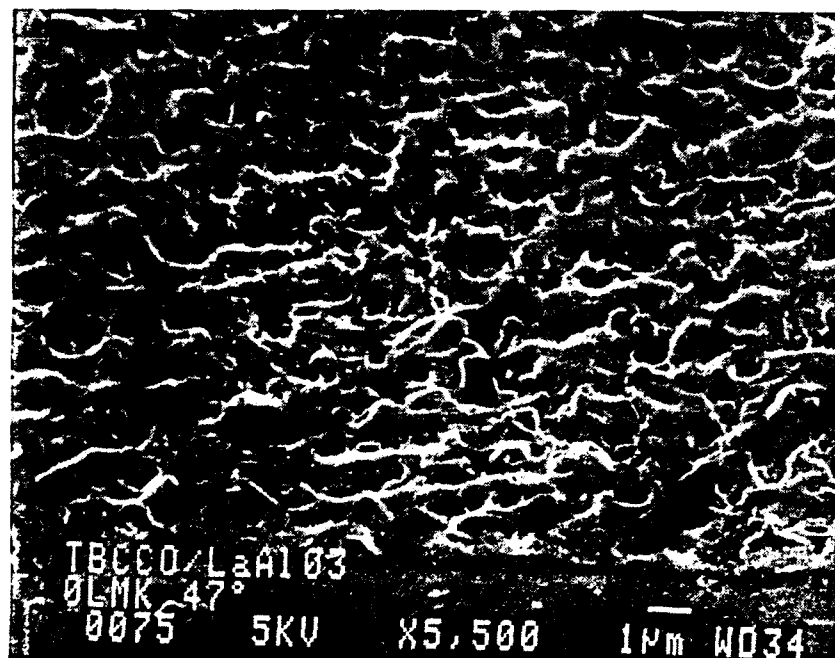
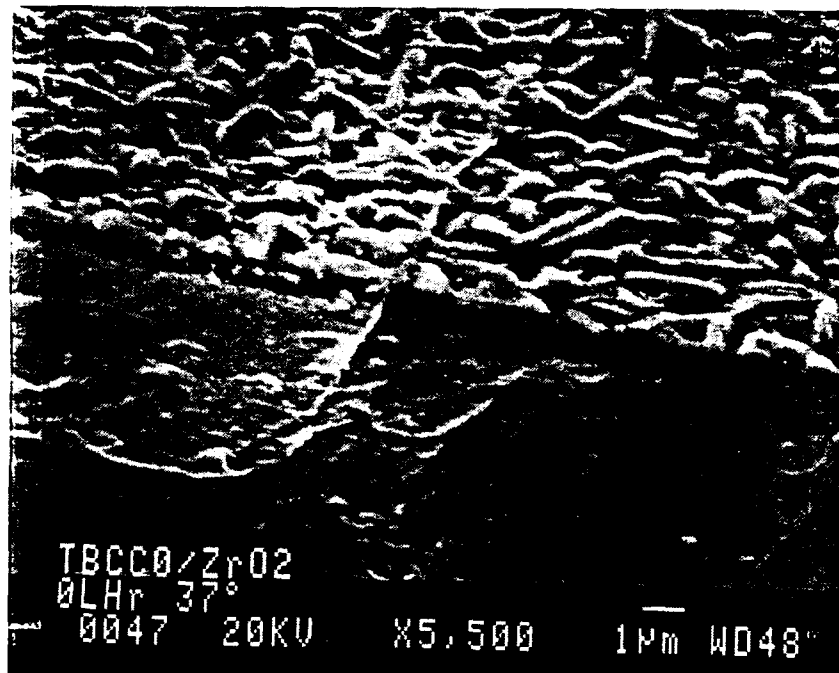


Figure 10. TBCCO traces on ZrO₂ (top) compared to LaAlO₃ (bottom).

8. MARK I TEST DEVICE

8.1 Intent

The next phase of the project was to design and fabricate 5 Mark I test devices with TBCCO traces on a LaAlO_3 substrate. The intent was to see what current capacity could be obtained in TBCCO traces. Since LaAlO_3 is a poor thermal insulator, evident from the thermal conductivity numbers in Figure 3, the devices were not intended to be thermal isolators.

8.2 Design and Fabrication

The design and fabrication of the Mark I test device are very similar to the STID. Superconducting traces of TBCCO are deposited on LaAlO_3 substrates by STI. These are nominally .8 μm thick and alternate 500 μm and 200 μm wide.

The expectation was that the traces should have a transition temperature of about 100 K and a current capacity in excess of about 10,000 A/cm². The actual values obtained equal or exceed these numbers.

The substrates are single crystals of 1 cm square LaAlO_3 , about half the size used in the STID. Substrate and traces are epoxied into a small standard flatpack with 11 leads. Electrical connections are made with gold wires as in the STID.

We emphasize that the test device is not intended or designed to be thermally isolating, since it is only an electrical test device. Five such test devices have been built and tested.

8.3 Electrical Properties

The electrical properties of the test device are extremely good, especially when compared with the STID. Figure 11 shows the resistance as a

function of temperature for test device 2L655.1; 4 leads are shown. The transition to superconducting at about 102 K is evident, and is only a few K wide. This is in agreement with the STI measurement using susceptibility, and is consistent with a large fraction of the bulk of the material being superconducting. Note also the low value of about .2 ohm for the residual resistance of connecting wires etc. It is impressive to compare Figure 11 for the Mark I test device with Figure 6 for the STID!

Figure 12 shows resistance as a function of current for the same test device. Figure 12a for 80 K indicates no sign of increasing resistance up to a current of 600 mA, corresponding to a current density of about $375,000 \text{ A/cm}^2$ in the 200 μm traces. The current capacity of the traces may be well above this, but we did not extend the measurements to higher current since the external connections are not expected to carry much more.

Figure 12b for 100 K shows a clear rise in resistance at about 100 mA for the 200 μm traces and about 300 mA for the 500 μm traces, corresponding to current capacity of about $60,000 \text{ A/cm}^2$. This also is remarkably large considering how close the temperature is to the transition temperature.

Some of the resistance measurements in Figure 12 were made using a short pulse technique instead of DC, due to the large currents involved. Figure 12a shows a small glitch at 20 mA where the pulse measurements

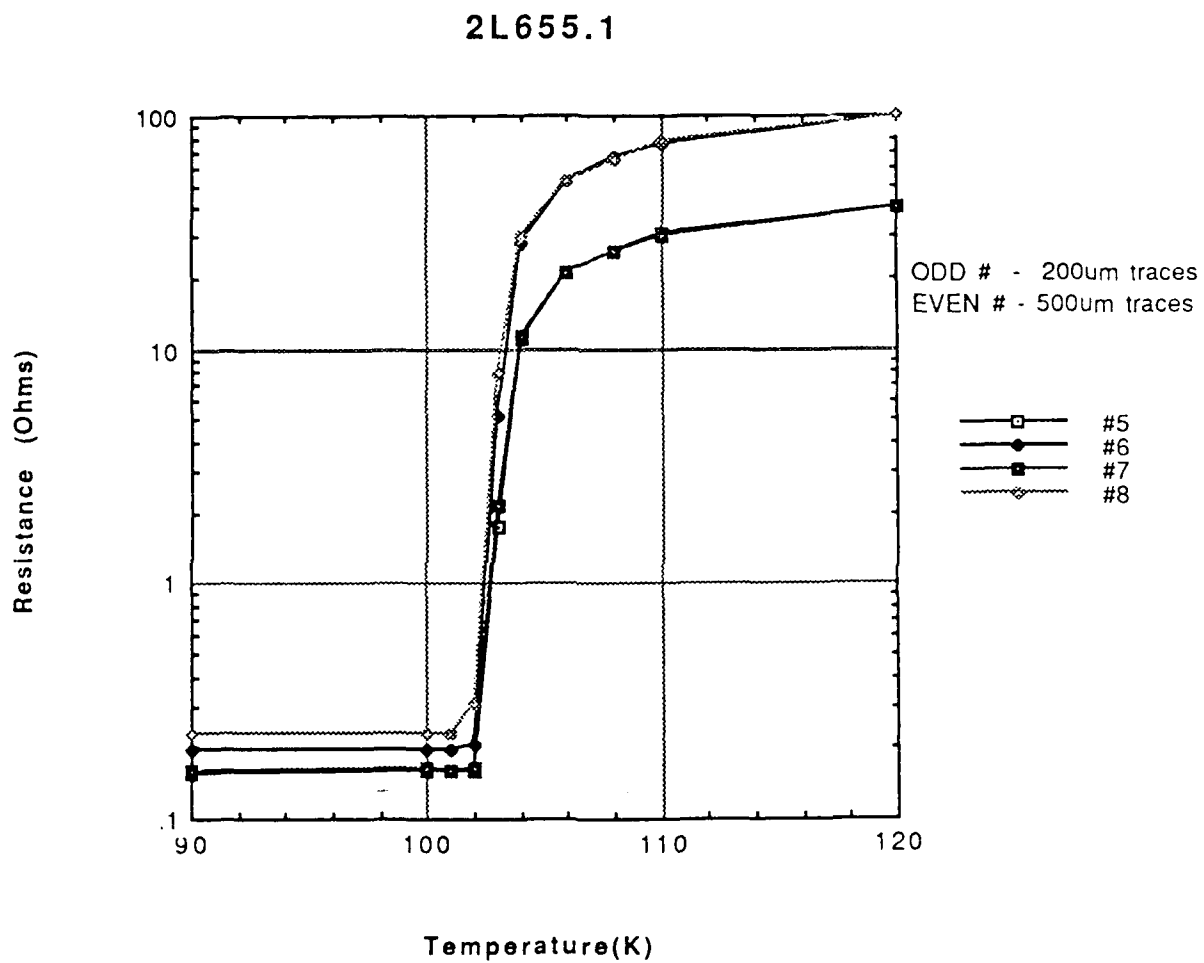


Figure 11. Resistance of M 1 test device as function of temperature

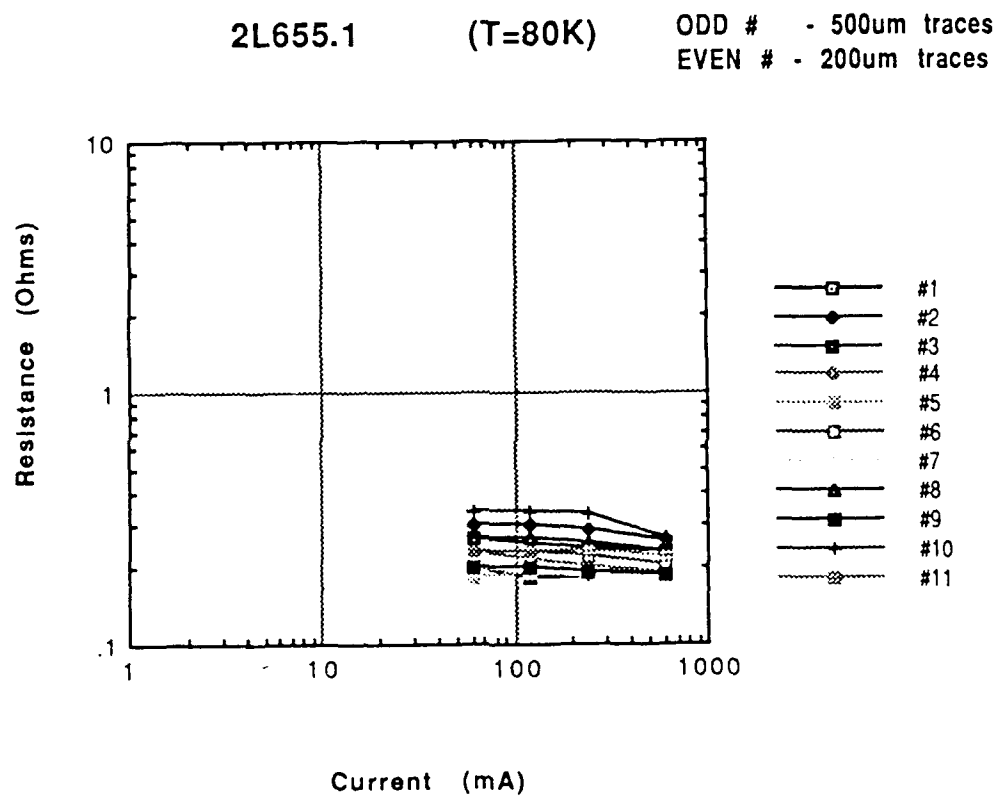


Figure 12a. Resistance of M 1 test device as function of current at 80 K

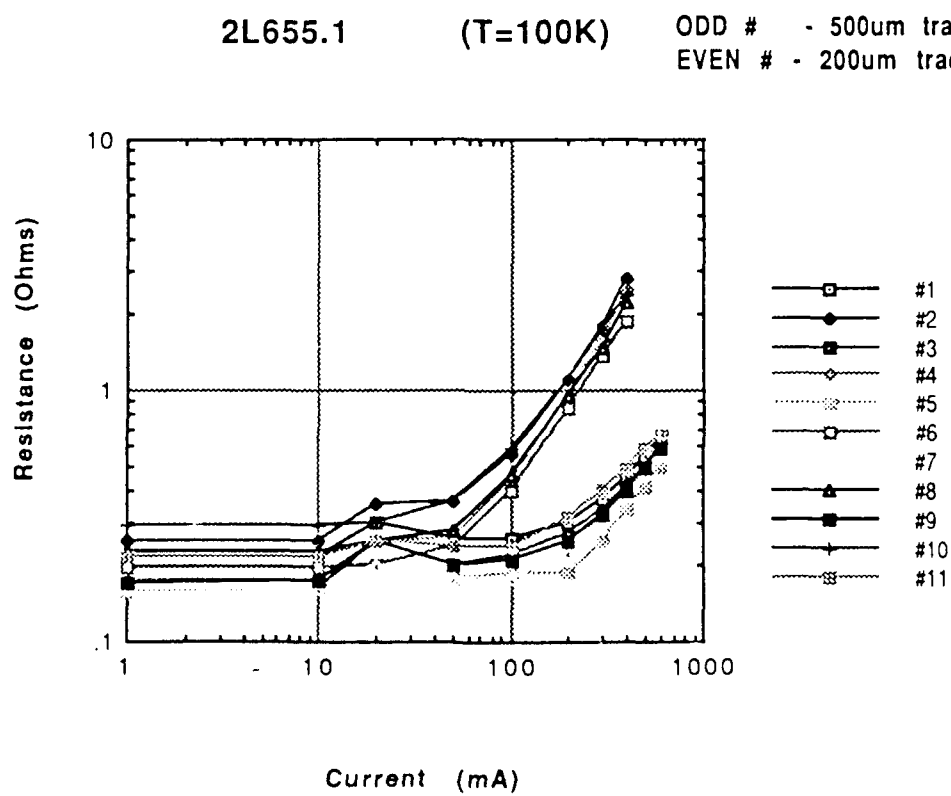


Figure 12b. Resistance of M 1 test device as function of current at 100 K

begin, and shows that the 2 measurement techniques are reasonably consistent.

Figure 10 is an SEM photo of the surface morphology of the TBCCO traces in the test device and also in a STID. Although rather irregular the structure of TBCCO on LaAlO_3 is much smoother than the TBCCO on ZrO_2 .

8.4 Mark I Test Device Properties: Conclusions

We conclude that the electrical properties of the test device are extremely good; the transition temperature equals that desired and expected, and the current capacity exceeds that expected by over an order of magnitude. Compared to the STID the transition temperature is over 20 K higher, and the current capacity is about 3 orders of magnitude greater.

9. MARK II TEST DEVICE

9.1 Intent

The final phase of the project was to design and fabricate two test devices, termed Mark II, with TBCCO traces, one on single crystal ZrO_2 and one on polycrystalline ZrO_2 . The intent was to find the reason for the low current capacity in the prototype STIDs, which all used polycrystalline material. Like the Mark I test devices the Mark IIs were not intended to be thermal isolators but strictly electrical test devices, specifically to determine if the current capacity problem was due to the use of polycrystalline substrate.

9.2 Design and Fabrication

The Mark II test devices use TBCCO traces of widths 200 μm and 500 μm like the prototype STIDs and the Mark I test devices. One Mark II device uses a 1 cm square substrate of polycrystalline ZrO_2 like the prototypes, and the other uses a 1 cm square substrate of single crystal ZrO_2 . Otherwise, construction is exactly like the Mark I test devices.

9.3 Electrical Properties

The current capacity of the traces on the polycrystalline substrate is only about 25 A/cm^2 , even lower than for the prototype STIDs; moreover the transition to superconductivity is quite wide, about 20 K or more.

The current capacity of the traces on the single crystal substrate is over two orders of magnitude larger, about 5,000 A/cm^2 , which is adequate for practical use.; moreover the transition to superconductivity is at about 100 K and very narrow.

Figure 13 shows the resistance as a function of temperature for both Mark II devices, 2L759.1 being single crystal and 2L759.3 being polycrystalline.

The transition to superconductivity begins at about 100 K for all traces shown, but is very much narrower and goes much lower for the single crystal device. In particular traces number 9 and 11 are especially good.

Figures 14a and 14b show resistance versus current for both devices at 77 K. Traces on the single crystal device carry about 20 mA before the resistance begins to rise, which corresponds to a current density of about 5,000 A/cm². By contrast traces on the polycrystalline device carry only about 0.1 mA, corresponding to only about 25 A/cm².

One serious problem was discovered with the single crystal device. Over the time period 5/17/91 to 6/25/91 the device degraded significantly. Figure 15 shows this clearly. Note in particular the increase in resistance for the best trace, number 9, at 30 mA; it increased from about 0.11 ohm to about .21 ohm. This indicates that a passivation coating is probably necessary

9.5 Mark II Test Device Properties: Conclusions

In summary it is clear that the poor electrical properties of the prototype STIDs are due to the polycrystalline substrates, and can be corrected with the use of a single crystal substrate. This is a straightforward if somewhat expensive solution. The degradation over time may be correctable with the use of a passivation coating.

2L759.1 (Single crystal zirconia)

2L759.3 (Polycrystalline zirconia)

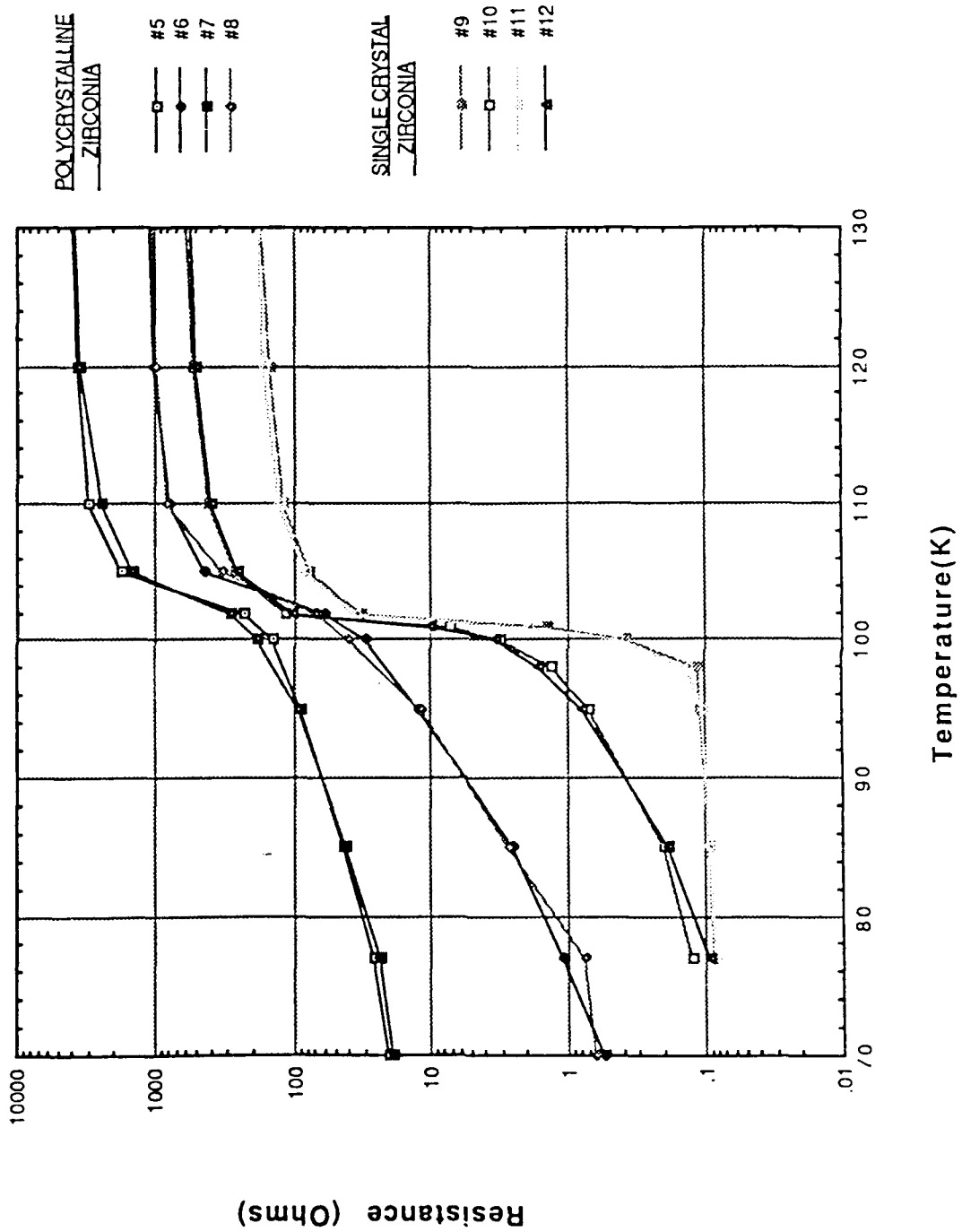
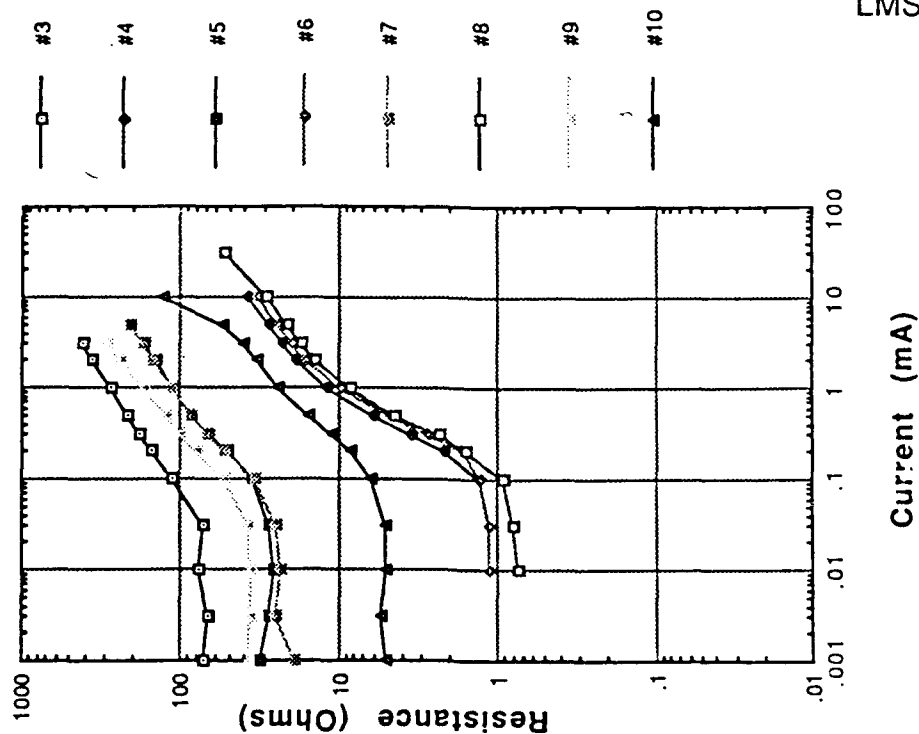
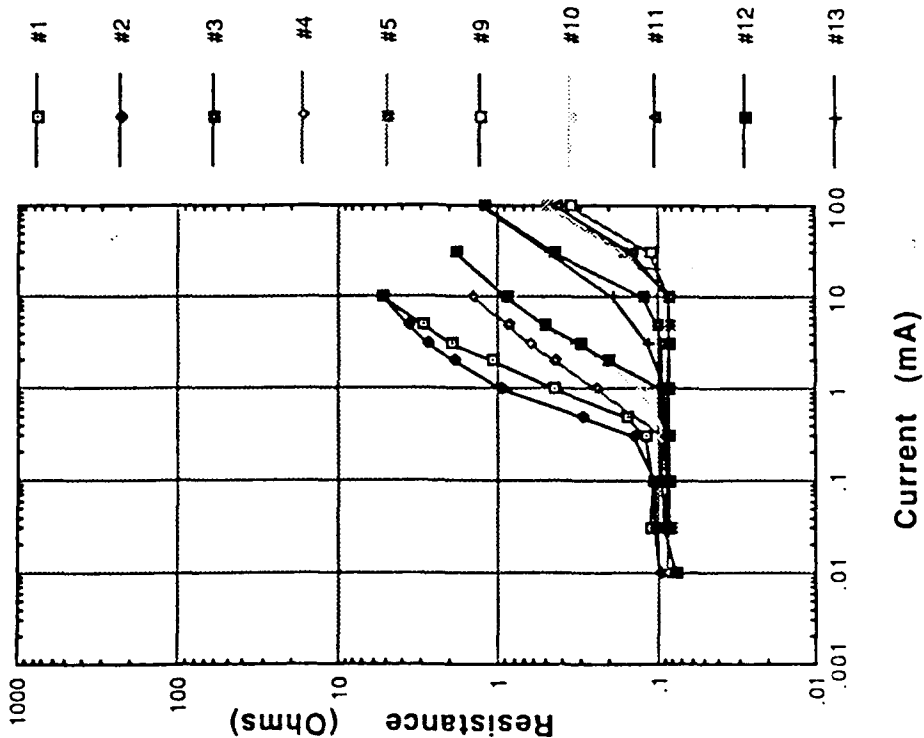


Figure 13. Resistance Versus Temperature for M 11 Test Devices

2L759.3 (T=77K)



2L759.1 (T=77K)



Figures 14a and 14b. Resistance Versus Current for M 11 Test Devices at 77 K

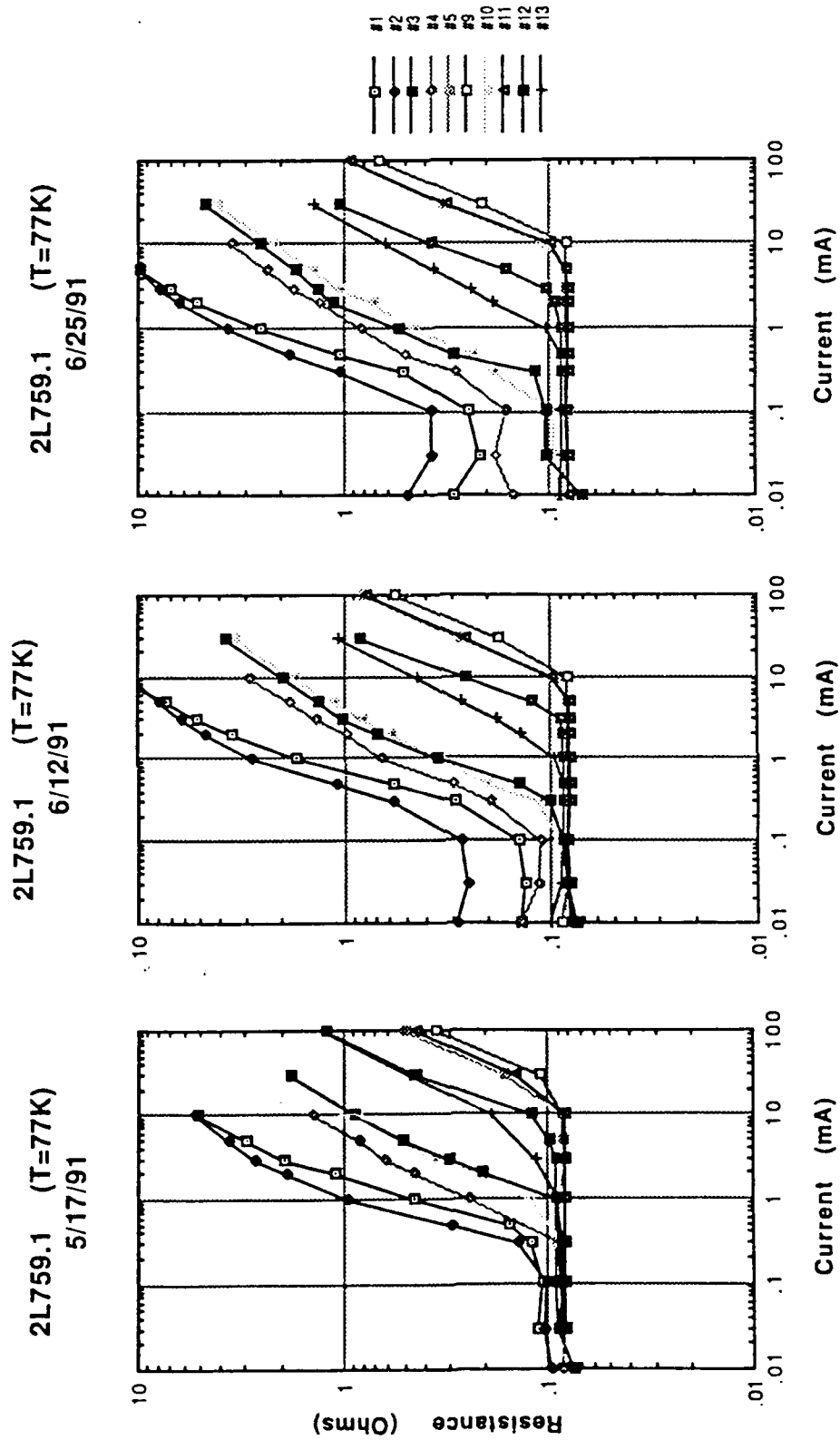


Figure 15. Change in Resistance Versus Current, Single Crystal M 11 Device

THIS
PAGE
IS
MISSING
IN
ORIGINAL
DOCUMENT

1. INTRODUCTION (PART II)

Passive microwave components made of patterned superconducting films on dielectric substrates have low resistance and generally high performance; they are thus of great interest. The patterning of such films is typically done by wet etching, but this entails a fundamental problem; considerable undercutting often results, leaving irregular edges in the pattern. One possible solution is to correct the undercutting with the use of a distorted initial profile. This, however, is not a very robust manufacturing approach, so other solutions are preferred.

The reason that wet etching undercuts TlBaCaCuO (TBCCO) films so badly is that the nominally isotropic etch in fact prefers the 'a' and 'b' directions to the 'c' direction. The film is oriented with the 'c' direction normal to the substrate, hence the undercutting. The basic task addressed in this study is to evaluate dry etching or ion milling as an alternative to wet etching in order to avoid the undercutting.

Ion milling is intrinsically highly anisotropic, and is known therefore to preserve lateral film dimensions very accurately. Thus there should be very little undercutting and distortion of thin film traces. However it is also known that ion milling produces a temperature rise that may degrade the superconducting properties of the TBCCO film. The solution explored in this project is to use active substrate cooling to protect the superconducting traces from the temperature rise.

2. TECHNICAL ACHIEVEMENTS

Argon milling should be capable of dry etching fine geometries in thin films with virtually no pattern undercutting, provided of course that the photoresist mask remains intact during etching. The main problem with the procedure is heating and ion bombardment damage to the film, which can degrade its superconducting properties.

We have reevaluated our original milling equipment, with regard to its effect on sample heating, and have changed to a 20 cm Technics Corp. mill which has much more efficient sample cooling at higher beam current densities. A recently deposited TBCCO sample (2L788.4) was coated with 1.5 μm of positive resist and patterned with the 6 mil resonator geometry from STI mask #23. It was then argon ion milled at 500 V with a current density of 0.32 mA/cm². The sample temperature did not exceed 60° C during the milling process as determined by an on-chip temperature monitor. Since the temperature remained well below the nominal upper bound of 120° C future milling may use a higher current density to increase the milling rate. The ion milling rate of the TBCCO film under these conditions was estimated to be about 100 Å/min. The milling time was extended to insure complete film removal in the area outside the 6 mil pattern. No residue of copper oxide remained after ion milling as has been observed with wet etching. The remaining pattern thickness was measured at 0.69 μm . The pattern width was measured as 152 μm versus a nominal 153 μm design value. Thus the expected accuracy was achieved.

After processing at LMSC the sample was returned to STI for resonator measurements. These indicated that there had been some degradation of the microwave characteristics during processing. It appears that the sample may have degraded due to exposure to the air for an extended time between process steps. Such exposure can easily be minimized in the future. The photoresist thickness should also be increased to eliminate actual contact between the ion beam and the active sample, while still permitting some over-milling to clear the unmasked area. This over-milling can be quantitatively verified by initially measuring the exact film thickness with a profilometer before attempting any active area processing.

APPENDIX A: THERMAL CONDUCTIVITY AVERAGES

In the basic thermal power equation [2] the appropriate value of the thermal conductivity to use is the average over temperature. This is intuitively reasonable and easy to demonstrate.

Consider a short segment of thermally conducting wire of length dx and area A , with a temperature difference of dT . The definition of thermal conductivity is

$$P = \kappa_{th}(T) A dT/dx \quad [a-1]$$

Power is understood to flow down the temperature gradient. Integrate this over the length of the wire, L , over which the temperature varies from T_i to T_f , to obtain

$$P L = A \int_{T_i}^{T_f} \kappa_{th}(T) dT \equiv A \langle \kappa_{th} \rangle \Delta T \quad [a-2]$$

where $\Delta T = T_f - T_i$. Thus:

$$P = A \langle \kappa_{th} \rangle \Delta T / L \quad [a-3]$$

This is the basic power equation used in the text, with $\langle \kappa_{th} \rangle$ denoted simply by κ_{th} .

APPENDIX B: ELECTRICAL DATA FOR PROTOTYPE STIDs

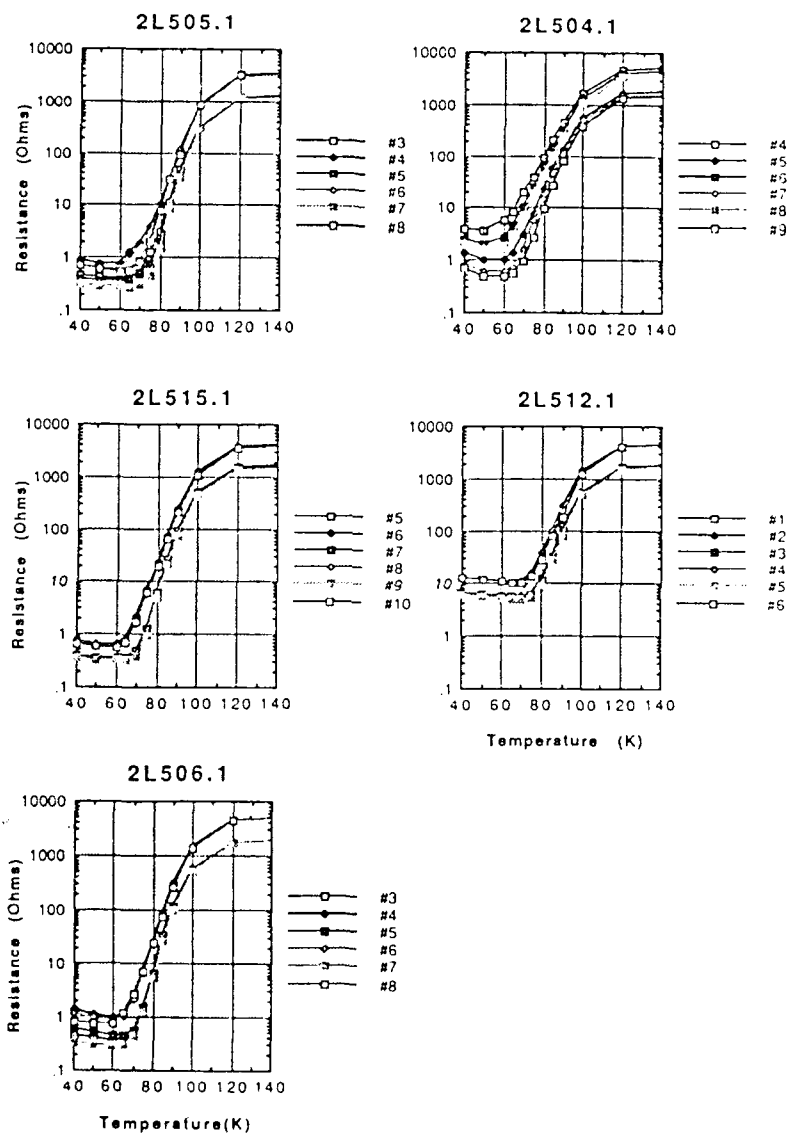


Figure b-1. Resistance of STIDs as function of temperature.

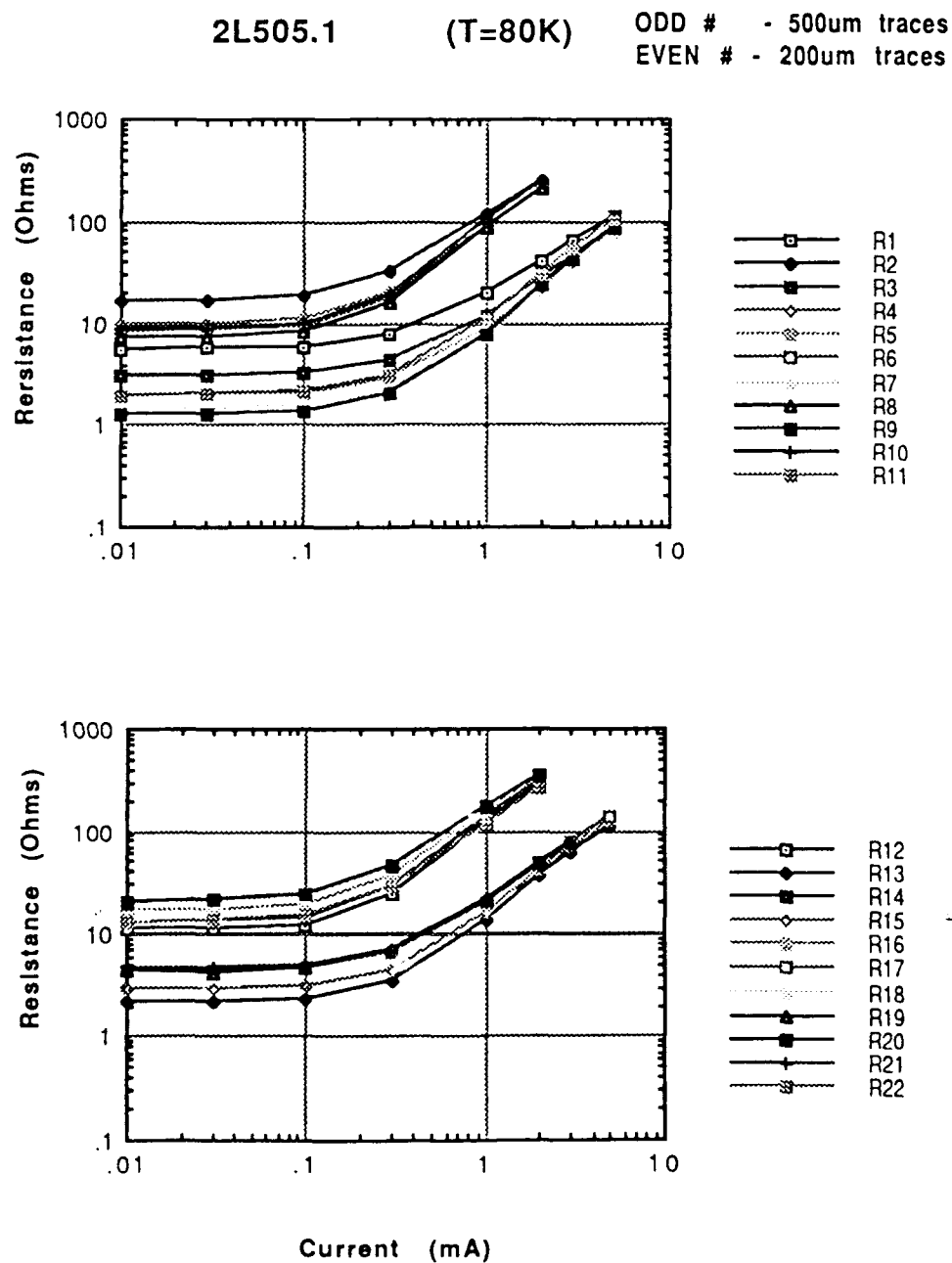


Figure b-2. Resistance of STID 2L505.1 as function of current at 80 K.

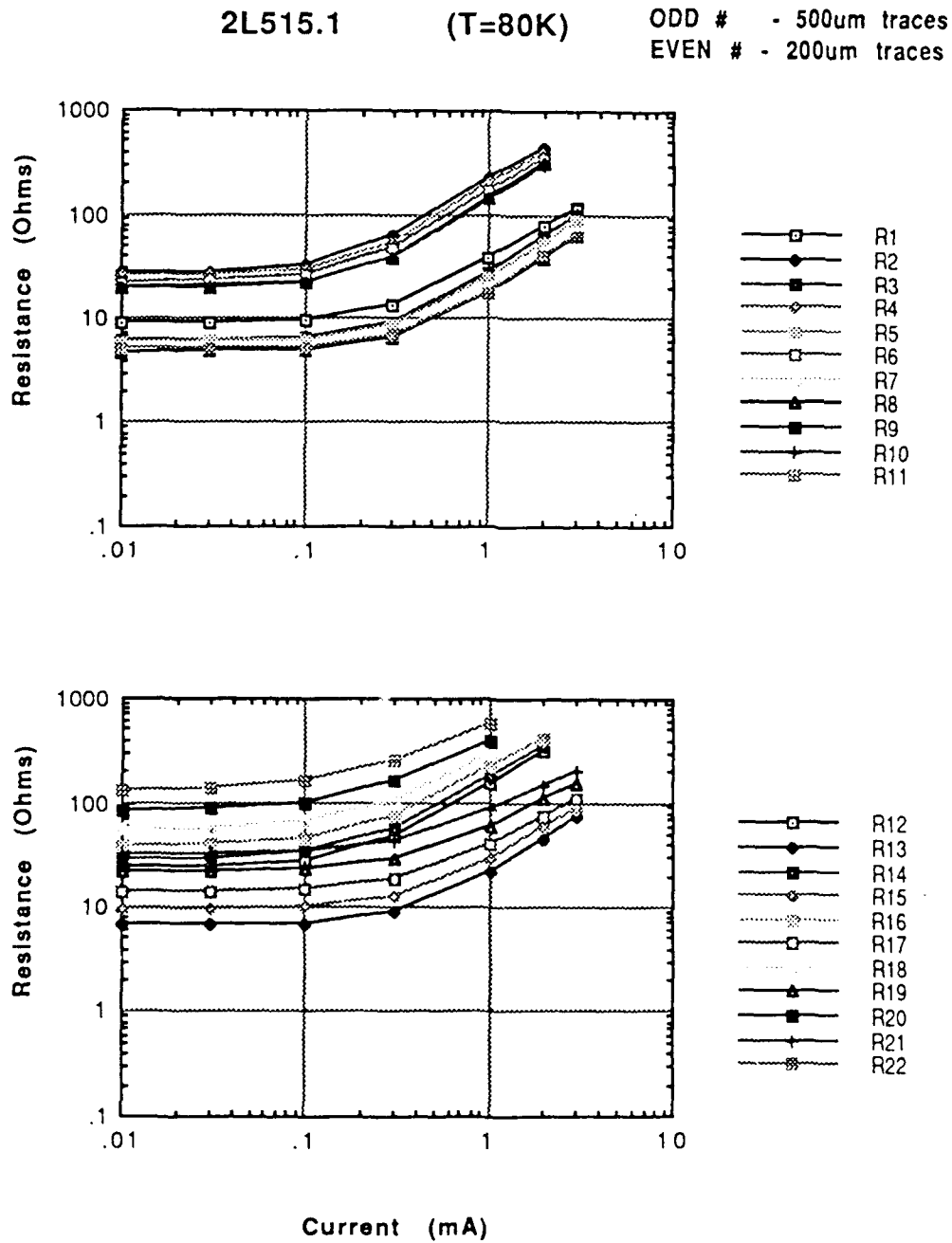


Figure b-3. Resistance of STID 2L515.1 as function of current at 80 K.

2L506.1

(T=80K)

ODD # - 500um traces

EVEN # - 200um traces

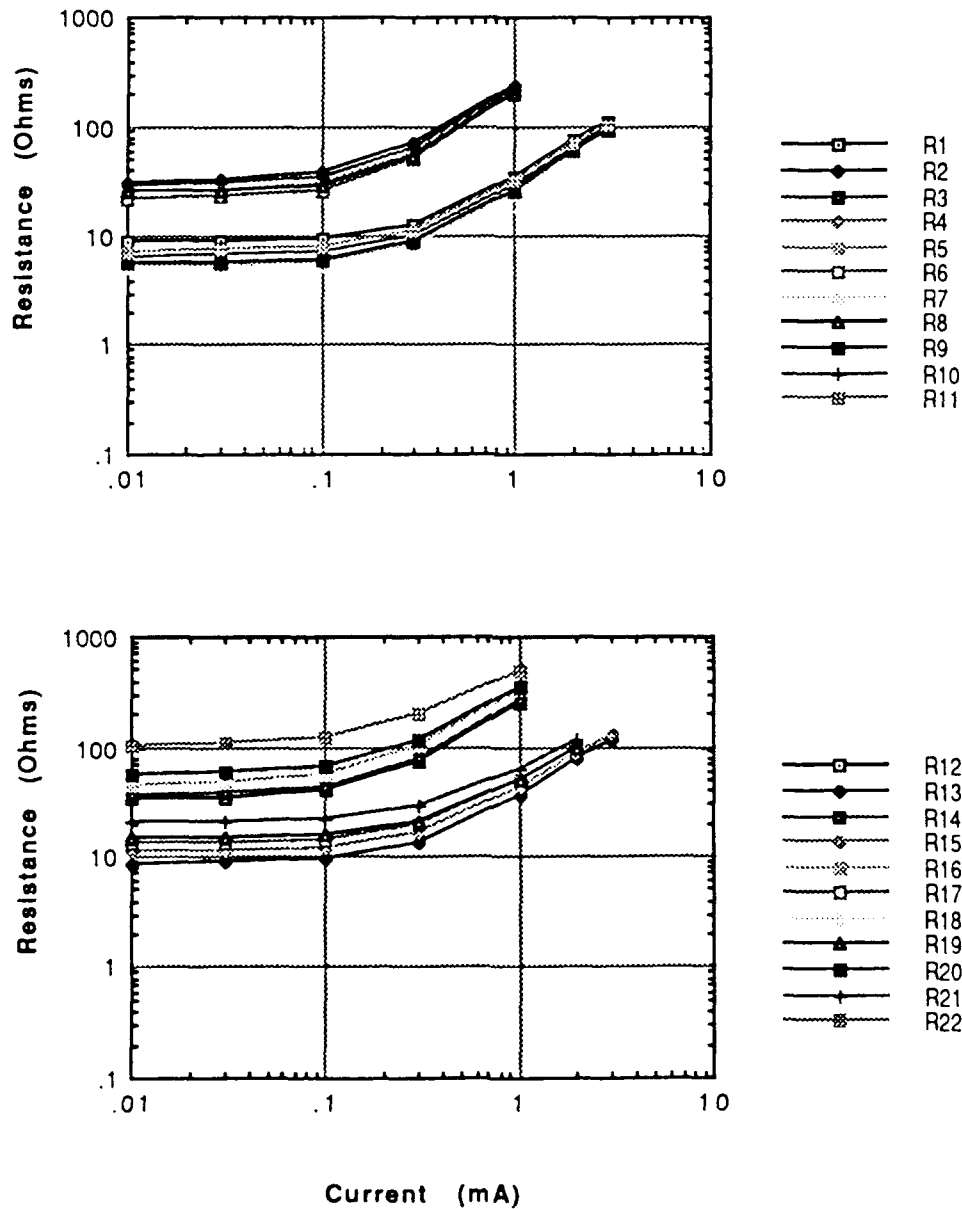


Figure b-4. Resistance of STID 2L506.1 as function of current at 80 K.

2L504.1

(T=80K)

ODD # - 500um traces

EVEN # - 200um traces

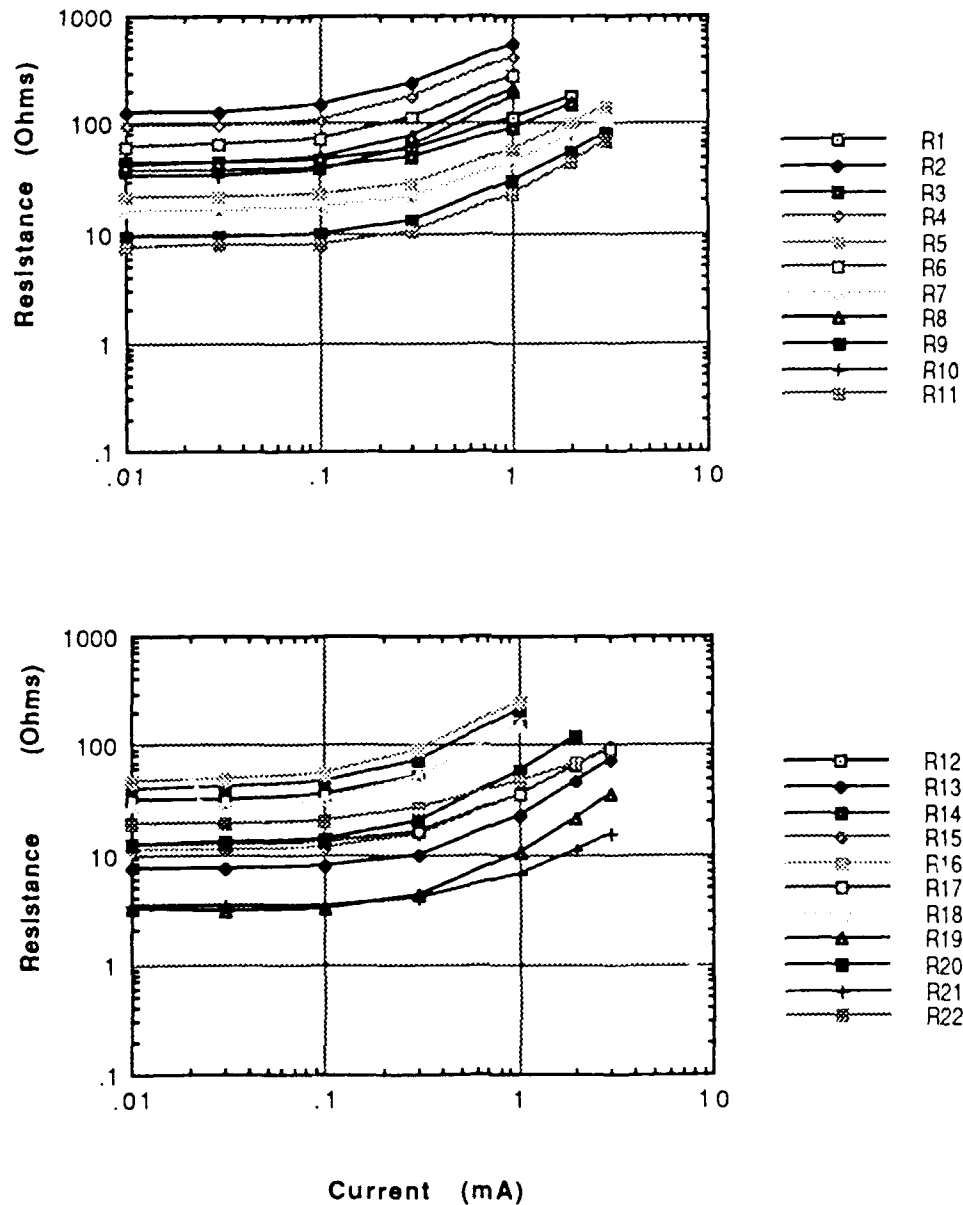


Figure b-5. Resistance of STID 2L504.1 as function of current at 80 K.

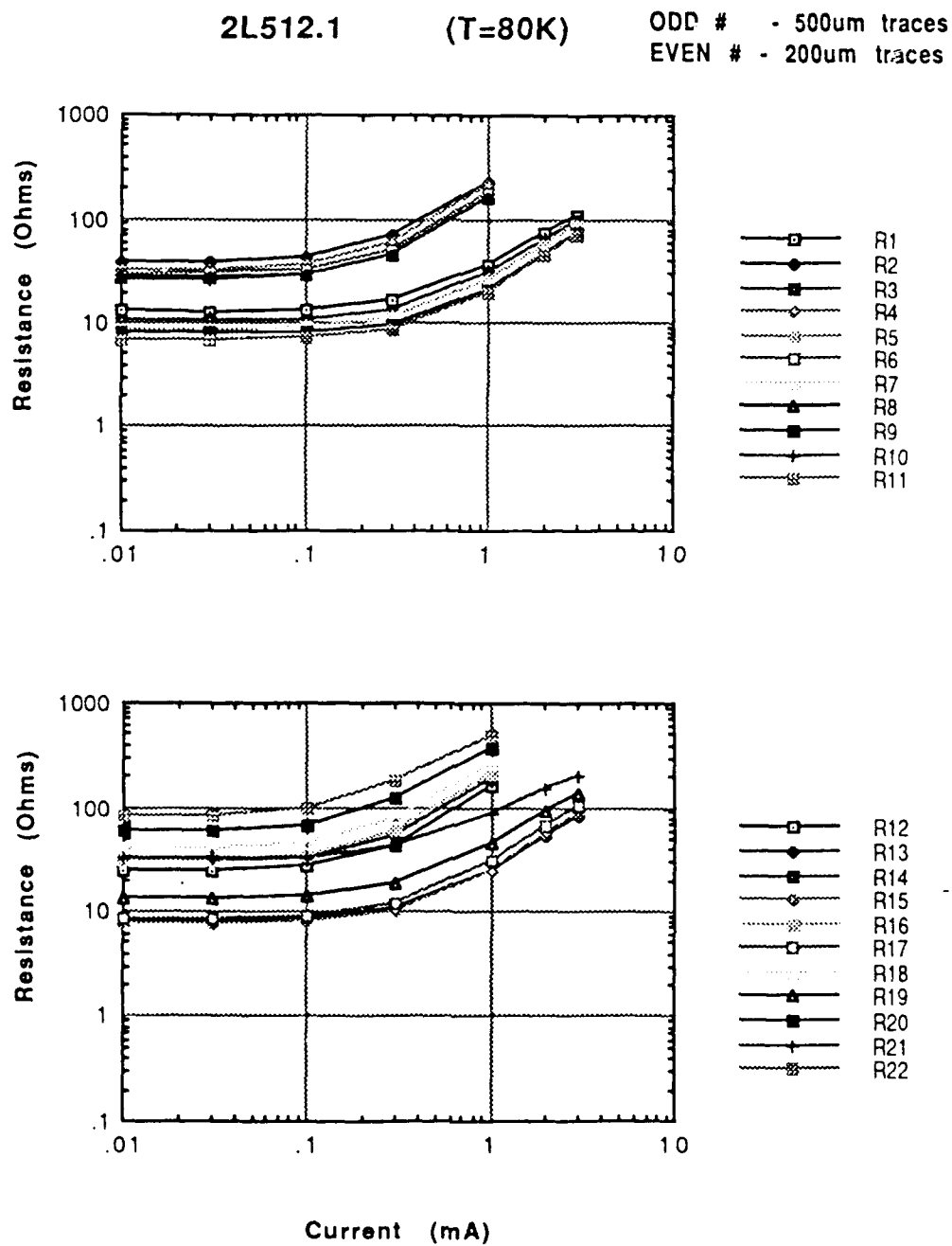


Figure b-6. Resistance of STID 2L512.1 as function of current at 80 K.

APPENDIX C: ELECTRICAL DATA FOR MARK I TEST DEVICE

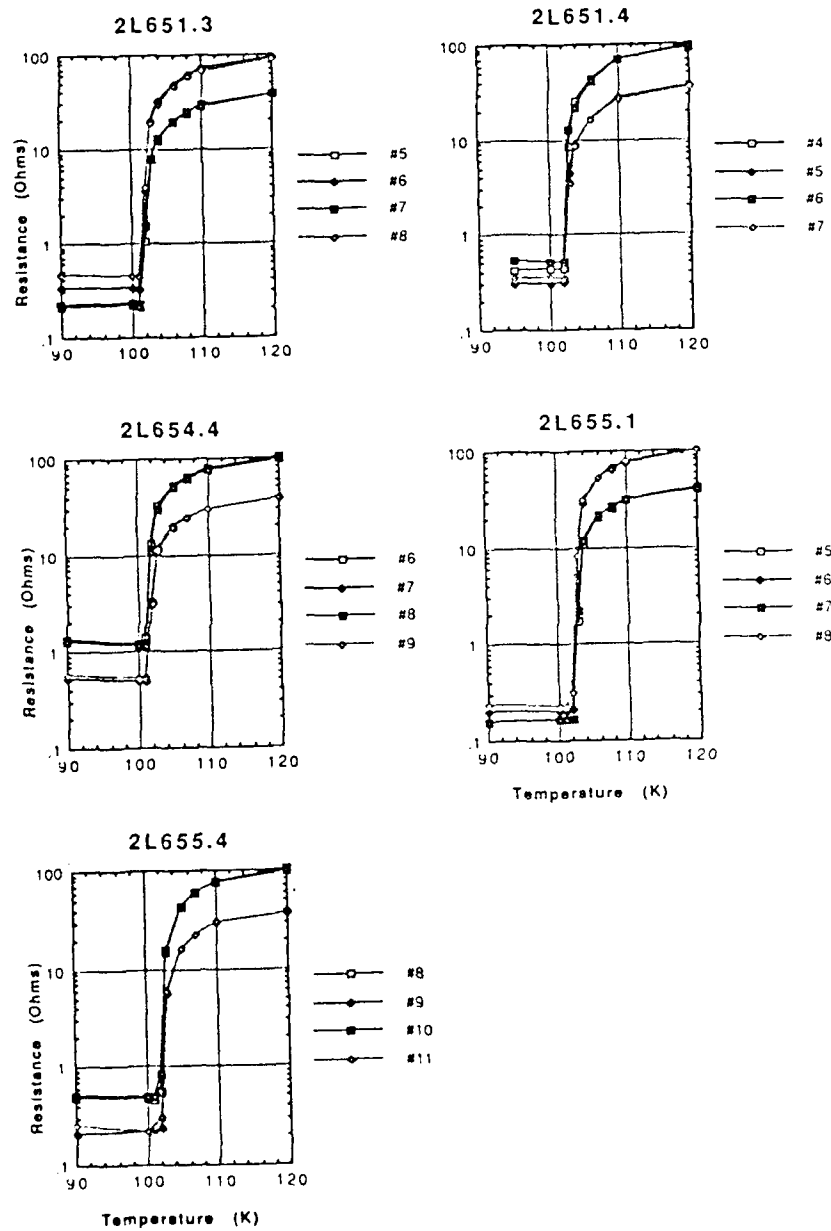


Figure c-1. Resistance of M I test devices as function of temperature.

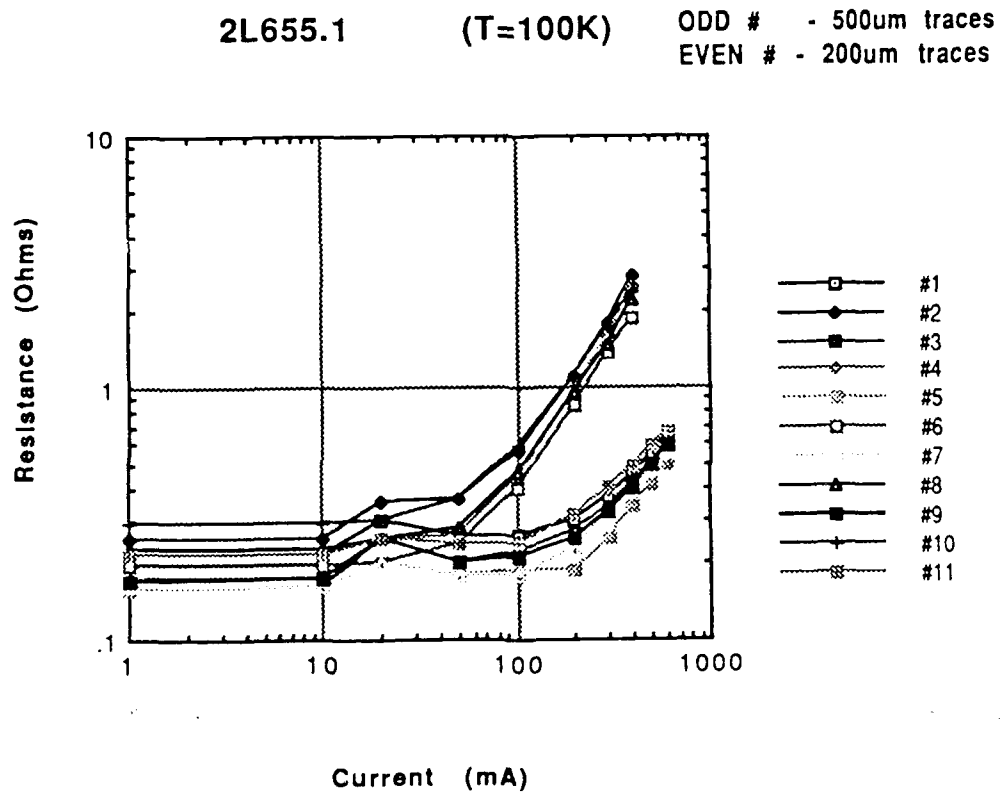


Figure c-2. Resistance of M I test device 2L655.1 vs. current at 100 K

2L651.4

(T=100K)

ODD # - 500um traces
EVEN # - 200um traces

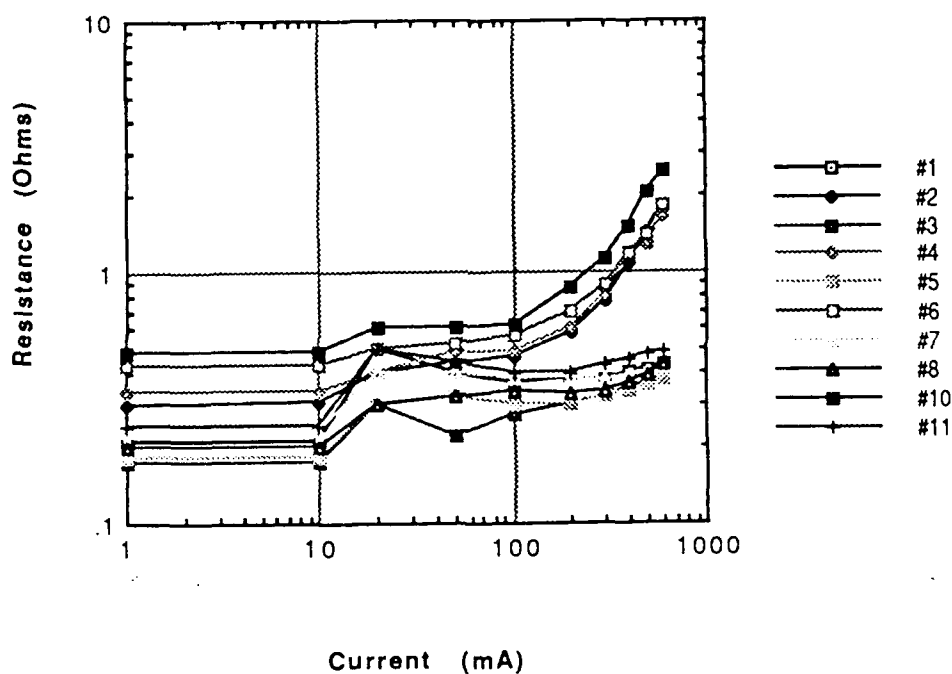


Figure c-3. Resistance of M I test device 2L651.4 vs. current at 100 K

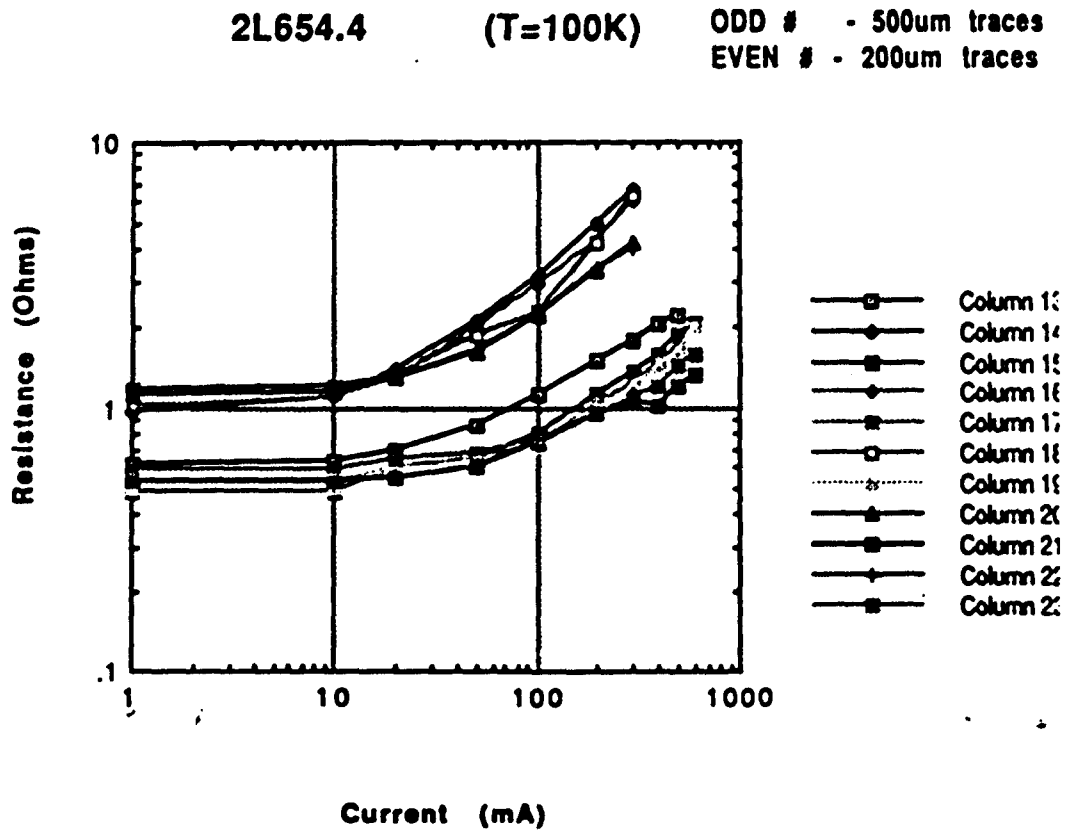


Figure c-4. Resistance of M I test device 2L654.4 vs. current at 100 K

2L655.4

(T=100K)

ODD # - 500um traces

EVEN # - 200um traces

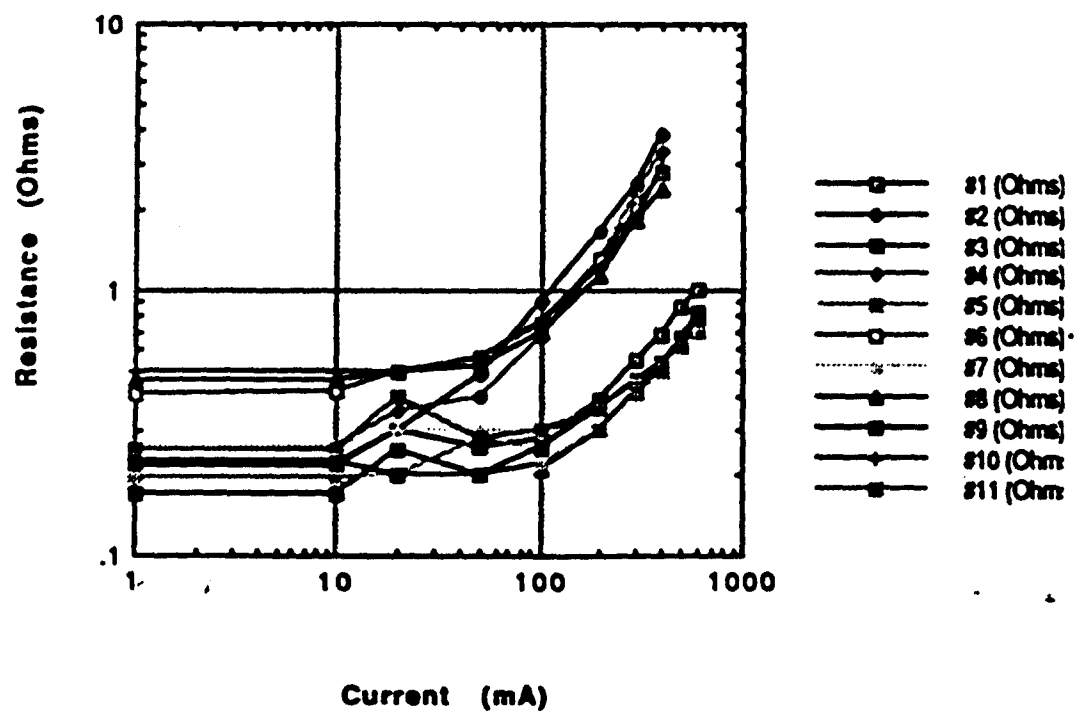


Figure c-5. Resistance of M I test device 2L655.4 vs. current at 100 K

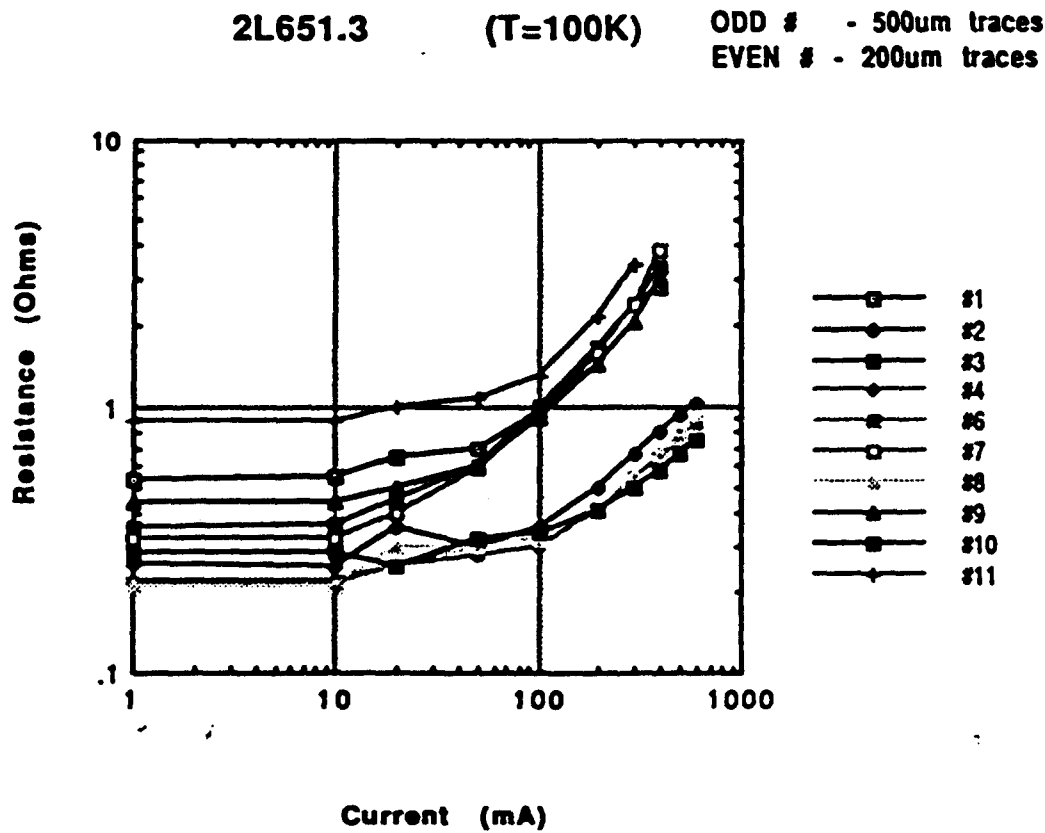


Figure c-6. Resistance of M I test device 2L651.3 vs. current at 100 K.